Robust decentralised output feedback control of interconnected grid system

Author:
Athanasius, Germane

Publication Date:
2008

DOI:
https://doi.org/10.26190/unsworks/19242

Robust Decentralised Output Feedback Control of Interconnected Grid System

Germane Xavier Athanasius
The University of New South Wales at The Australian Defence Force Academy

submitted in partial fulfillment of the requirements
for the PhD degree at the
School of Information Technology and Electrical Engineering
The University of New South Wales at The Australian Defence Force Academy

A thesis submitted for the degree of
Doctor of Philosophy

December 2008

I hereby declare that this submission is my own work and to the best of my knowledge it contains no material previously published or written by another person, nor material which to a substantial extent has been accepted for the award of any other degree or diploma at UNSW or any other educational institution, except where due acknowledgement is made in the thesis. Any contribution made to the research by others, with whom I have worked at UNSW or elsewhere, is explicitly acknowledged in the thesis.

I also declare that the intellectual content of this thesis is the product of my own work, except to the extent that assistance from others in the project's design and conception or in style, presentation and linguistic expression in acknowledged.

Germane Xavier Athanasius

Abstract

The novel contribution of the thesis is the design and implementation of decentralised output feedback power system controllers for power oscillation damping (POD) over the entire operating regime of the power system. The POD controllers are designed for the linearised models of the nonlinear power system dynamics. The linearised models are combined and treated as parameter varying switched systems. The thesis contains novel results for the controller design, bumpless switching and stability analysis of such switched systems.

Use of switched controllers against the present trend of having single controller helps to reduce the conservatism and to increase the uncertainty handling capability of the power system controller design. Minimax-LQG control design method is used for the controller design. Minimax-LQG control combines the advantages of both LQG and H^{∞} control methods with respect to robustness and the inclusion of uncertainty and noise in the controller design. Also, minimax-LQG control allows the use of multiple integral quadratic constraints to bound the different types of uncertainties in the power system application.

During switching between controllers, switching stability of the system is guaranteed by constraining the minimum time between two consecutive switchings. An expression is developed to compute the minimum time required between switchings including the effect of jumps in the states. Bumpless switching scheme is used to minimise the switching transients which occur when the controllers are switched.

Another contribution of the thesis is to include the effect of on load tap changing transformers in the power system controller design. A simplified power system model linking generator and tap changing transformer dynamics is developed for this purpose and included in the controller design.

The performance of the proposed linear controllers are validated by nonlinear computer simulations and through real time digital simulations. The designed controllers improve power system damping and provide uniform performance over the entire operating regime of the generator.

Acknowledgements

I begin my acknowledgement by thanking my supervisor, Associate Professor Hemanshu Roy Pota. He enthusiastically accepted me as his student and from the first day of my work, he was the pivotal person behind my research. He introduced me to the topic and guided me to the completion. There were many occasions, when I struggled for solutions, at those times he spent his precious time in helping me find solutions. His encouragements at despair moments were terrific, especially when my wife was seriously ill. He extended a helping hand to enable me to continue my research. I can only summarise his help as "without his support and help my thesis is impossible".

Next, I should thank Dr. Valeri Ugrinovskii who is my co-supervisor. His support in controller design is gratefully acknowledged. His critical comments at many times initially were painful but later it made me think a lot. I thank him for his open criticisms. I also thank him for the financial support provided to me from his research funds.

I thank Prof Rodrigo Andrade Ramos, Brazil, for his help in correcting my power system linearisation equations and for the discussions of power system modeling and simulations. I also thank Dr. Li Li for the technical help on controller design methodology and for reviewing the technical paper on controller design. My sincere thank goes to Dr. Shaiju for introducing me to switching stability concepts and for the long technical discussions I had with him on this topic. I also thank Prof Ian Peterson for his valuable comments on the work.

I thank Dr P. V Balasubramanium, Dr.Sujatha Subhash and other officials at Central Power Research Institute (CPRI), Bangalore, India for allowing me to test the controllers using the RTDS facility at CPRI. I thank them for providing necessary help and guidance to carry out the tests at CPRI.

I thank Dr. Anavatti G Sreenatha who helped me get the research opportunity at ADFA and to settle in Canberra. I would also like to thank Pam Giannakakis, Joan Woodward, and Elizabeth Carey, for the general administrative support provided to me. Software support from Jon Lowrey, Peter Boyland and Mike Wilson with computing issues were also invaluable. I also thank John Davis and the building officer who provided me day to day infrastructure support.

My appreciation also goes to fellow postgraduate students for making my journey a memorable experience and sharing friendship during the past few years.

I also wish to extend my warmest thanks to my friends, difficult to name all, in the University and community who have made my life in the Australian Capital fruitful and enjoyable. Moreover, I am grateful for enormous support and understanding from my loving wife and sons Arul and Paul.

Finally, I am indebted to the School of Information Technology and Electrical Engineering, the University of New South Wales, and Australian Research Council for financial support and the opportunity take up this PhD journey.

Dedicated to my parents, my wife and
my sons Arul and Paul

List of Publications

1. G. X. Athanasius, H. R. Pota, L. Li and V. Ugrinovski, "Robust Decentralized Control of Power Systems with OLTCs using MarkovJump Parameter Theory" *CPRI Power system Journal*, Vol.3 No.2. 2007.
2. G. X. Athansius, H. R. Pota, P.V. Balasubramanium and V. Ugrinovski, "Robust power system stabiliser design using minimax control approach: Validation using real time digital simulation" *46th IEEE Conference on Decision and Control*, 12-14 December 2007, New Orleans, Louisiana, USA. (pp. 2427-2432).
3. G. X. Athanasius, H. R. Pota, and V. Ugrinovski, "Robust Decentralized Output feed back controller for interconnected power system with bumpless switching" *International Conference on Power Systems (ICPS -2007).* 12-14th December 2007, Bangalore, India. (pp. 202-224). ISSN 0973-0338.
4. G. X. Athansius, H. R. Pota and V. Ugrinovski, "Robust Decentralized Switching Power System Stabilisers for Interconnected Power Grid: Stability using Dwell Time" *Proceedings of 17th IFAC world conference, July, 2008, Seoul.*(pp. 8419-8424)
5. H. R. Pota, G. X. Athanasius, V.Ugrinovski, and L. Li, "Control Design for Interconnected Power Systems with OLTCs via Robust Decentralized Control." *Proceedings of the American Control Conference*, 14-16 June 2006, Minneapolis, Minnesota USA. (pp. 3469-3474).
6. H. R. Pota, G. X. Athanasius, L. Li, and V. Ugrinovski, "Output Feedback Control Design for Interconnected Power Systems with OLTCs via Robust Decentralised Control." *Proceedings of the International Seminar on Power Transmission – Research Interests and Challenges.* 20-22 December 2005, Bangalore, India.
7. G. X. Athanasius, L. Li, H. R. Pota, and V. Ugrinovski, "Robust Decentralized Output feed back controller for interconnected power system - Theory and Design", *Journal paper under review.*
8. G. X. Athanasius, H. R. Pota, and V. Ugrinovski, "Robust Decentralized Power System Stabilisers for Interconnected Power Grid with OLTCs", *Journal paper under review.*

9. G. X. Athanasius, H. R. Pota, and V. Ugrinovski, "Decentralised Robust Switching Power System Controller Design and Validation through Simulations", *Journal paper under review.*
10. G. X. Athansius, H. R. Pota, P.V. Balasubramanium and V. Ugrinovski, "Robust parameter varying power system controller design and testing using RTDS", *Journal paper under review.*
11. G. X. Athanasius, H. R. Pota, and V. Ugrinovski, "Robust Decentralized Switching Power System Stabilisers for Interconnected Power Grids: Stability using Dwell Time", *Journal paper under review.*

Contents

List of Tables

List of Figures

List of Notations

Symbols

A_{ci}	state transition matrix of the i^{th} subsystem controller
A_i	state transition matrix of the i^{th} subsystem
A_{SYS}	state transition matrix of the multimachine system
B_{ci}	input matrix of the i^{th} subsystem controller
B_i	input matrix of the i^{th} subsystem
B_{SYS}	input matrix of the multimachine system
E_d	d-axis generated voltage of the synchronous machine
E_q	q-axis generated voltage of the synchronous machine
$\mathbf{F}$	transfer function of the bumpless compensator
$G_{ij} + jB_{ij}$	i^{th}, j^{th} element of the admittance matrix
H	inertia constant of the synchronous machine
i_a, i_b, i_c	three phase currents of the synchronous machine
I_0	zero sequence current of the synchronous machine
I_d	d-axis current of the synchronous machine
I_I	reference frame imaginary axis current of the synchronous machine
I_R	reference frame real axis current of the synchronous machine
I_q	q-axis current of the synchronous machine
J	moment of inertia of the rotor
K_{ci}	gain matrix of the i^{th} subsystem controller
L_i	interconnection effects matrix for i^{th} subsystem
M_{1i}, M_{2i}, M_{3i}	uncertainty bound constants of the i^{th} subsystem
P_e	electrical power generated by the rotor
P_i	real power flow at the i^{th} node of network
P_M	mechanical power input to the rotor
Q_i	imaginary power flow at the i^{th} node of network
r_{ai}	stator winding resistance of the synchronous machine
r_i	signal driving interconnection uncertainty of the i^{th} subsystem

T_R	terminal voltage sensor time constant
u_i	input vector of the i^{th} subsystem
V_d	d-axis terminal voltage of the synchronous machine
V_i	voltage at the i^{th} node of network
V_o	output voltage of the terminal voltage sensor
V_p	Lyapunov function of the system
V_q	q-axis terminal voltage of the synchronous machine
V_{ref}	reference voltage of the voltage regulator
V_t	terminal voltage of the synchronous machine
W_u, W_e	weighting constants of the cost function
x_{ci}	state vector of the i^{th} subsystem controller
x_d	unsaturated d-axis synchronous reactance of the synchronous machine
x'_d	d-axis transient reactance of the synchronous machine
x_i	state vector of the i^{th} subsystem
x_q	unsaturated q-axis synchronous reactance of the synchronous machine
x'_q	q-axis transient reactance of the synchronous machine
y_{ci}	input vector of the i^{th} subsystem controller
Y_{BUS}	admittance matrix of the network
Y_G	transient admittance matrix of the generators
Y_{LL}	equivalent load admittance matrix of the network
Y_{RED}	reduced admittance matrix of the network
z_i	controlled output of the i^{th} subsystem
α_i, β_i	parameter variation uncertainty magnitude constants of the i^{th} subsystem
δ	rotor angle of the synchronous machine
τ'_{do}	d-axis transient open circuit time constant of the synchronous machine
ω_m	angular velocity of the rotor
ξ_i	signal driving local perturbation of the i^{th} subsystem
ϕ_i	signal driving parameter uncertainty of the i^{th} subsystem
ζ_i	uncertainty output of the i^{th} subsystem
$\hat{\zeta}_i$	uncertainty output due to parameter variation of the i^{th} subsystem
τ_d	dwell time required for stable switching
Ψ	jump in system states during switching
σ	switching signal
τ_i, θ_i, η_i	scaling parameters of the i^{th} subsystem

Abbreviations and Acronyms

ANN	Artificial Neural Network
AVR	Automatic Voltage Regulator
$CPRI$	Central Power Research Institute
$EMTP$	Electro-Magnetic Transients Program
GA	Genetic Algorithm
$GARE$	Generalised Algebraic Riccati Equation
$HVDC$	High Voltage Direct Current
IQC	Integral Quadratic Constraints
LMI	Linear Matrix Inequality
LPV	Linear Parameter varying
LQG	Linear Quadratic Gaussian
LQR	Linear Quadratic Regulator
$OLTC$	On Load Tap Changing transformers
PSS	Power System Stabiliser
$RTDS$	Real Time Digital Simulation
SEP	Selected Equilibrium Point
$SMIB$	Single Machine on Infinite Bus
STR	Self Tuning Regulators

Chapter 1

Introduction

The primary task of the power system control is to provide reliable and secure electric power supply within a narrow band of voltage and frequency variation. As the demand for electric power is continuously increasing power systems are growing in size and complexity. Also, to meet the ever increasing demand, the system is forced to operate as close as possible to its maximum limit without sacrificing the reliability. The inherent damping of the system in most cases is low making the system marginally stable. These issues make the power system control task very difficult and challenging.

In an interconnected grid system, the rotor speed of all the machines connected to the grid must always be synchronised to the grid frequency and run at synchronised speed. When the steady state condition is disturbed due to load changes or fault in the system, the rotors of different machines start oscillating with respect to each other, exchanging energy between them. When these oscillations are allowed to grow, machines are pulled out of synchronisation. Small signal disturbances occur in a system continually because of small variations in load and generation. This can produce sustained oscillations in power angles and frequency and may disrupt the service [3]. There are several reasons for the dynamic instability in a power system. Among them, the weak couplings between interconnected systems which are randomly fluctuating, and a small group of machines with relatively low or negative damping against other machines in the system, are a couple of important factors which need to be considered. The work mentioned in [3] shows how the random fluctuations in the coupling between machines due to variations in load impedances and transmission line reactances can lead to instability. It also shows that such systems will be unstable for almost every sample path, the random variations can take, as time goes to infinity. Hence the power system should have proper control to ensure the stability of the system.

An interconnected power system is made up of different utilities. There is an agreement amongst the utilities on performance standards but each utility is free to choose the way in which to maintain the agreed performance. This style of operation

necessitates the decentralised control of the power system. Since the power system is interconnected in a complex manner, the controller providing damping control of the oscillations may require the knowledge of the states of the other machines connected to the grid in real time. However, because of the geographic separation of the location of the generating units, it is not always possible to transfer this information amongst machines in real time. Under these conditions a decentralised controller, which operates strictly based on the information of local states is desirable. However, the power system control should ensure that the power system is stable locally and globally. Global control is achieved through correct design and coordination of the local controls of the power system components [4].

Generator stability is achieved mainly through speed governor control and Automatic Voltage Regulator (AVR) control. Active power supplied by the generator is controlled by speed governor and reactive power supply through AVR. The response time of speed governor is usually slow when compared with local electromechanical swings, hence the speed governors are of little use in containing these modes. Fast operation of mechanical valves in steam turbines is found to cause torsional instabilities if the signals are not properly filtered. In the case of hydraulic turbines the droop characteristics and auxiliary controls need to be properly tuned to avoid instabilities [4]. Under these situations, power system relies upon improving damping through AVR control.

1.1 Power System Stabilisers

AVR plays an important role in keeping the generator in synchronism with other generators in the grid. To achieve this it should be fast acting. Using high AVR gains to increase the action time often lead to unstable and oscillatory responses. To increase the damping of the lightly damped mode AVR uses a signal proportional to rotor speed, although generator power and frequency also may be used [4, 5]. The dynamic compensator which is used to modify the input signal to AVR is commonly known as Power System Stabiliser (PSS). Most generators have a PSS to improve the stability and to damp out oscillations. The PSS design based on Single Machine on Infinite Bus (SMIB) model assumes that the grid to which the generator is connected has constant voltage and frequency. The power system model is linearised around a particular operating point and the design task is to synthesise the controller gain to meet the controller requirements. To improve the frequency response and mode

margins of the PSS, necessary tuned filters are also included. But in most situations, neither the SMIB nor a single operating mode assumptions are valid as systems undergo structural changes owing to large changes in load conditions. Also in an interconnected system each machine is affected by the changes happening elsewhere in the system.

1.1.1 Different design approaches

As the power systems grow in size, the complexities involved in the control design also increase. To meet the challenges posed, several new control techniques such as fuzzy control, adaptive control, control based on neural networks, LQR/LQG control, robust control and control based on genetic algorithms are investigated for the design of PSS [6–10] .

Fuzzy controllers

Fuzzy control is successfully applied in many practical applications. Power system controller design using fuzzy control is proposed in many works including [11–13]. In these works, PSSs are designed using fuzzy-logic and shown that the performance of the fuzzy controller is better than the conventional PSS. However, fuzzy-control method suffers from the well known phenomenon of rule explosion. Also for large scale systems, the number of linguistic variables and values become impractical to be implemented [14].

Artificial neural networks based controllers

Artificial Neural Networks (ANNs) are trained to map the complex systems without actually developing a mathematical model of those systems. Application of ANNs to tune PSS and also successfully replacing the PSS with trained ANNs are reported in many research works [6,15,16]. However, neural networks need to be trained with a sufficient number of samples or they should include online training architecture for successful implementation. Selection of a number of neurons and a number of neuron layers are current research topics. Also, establishing stability and robustness proofs is difficult on most situations [14].

Adaptive controllers

Conventional PSSs are designed using a power system model linearised around an operating point. If the system parameters vary as the operating point changes, the performance of the designed PSS degrades. Using adaptive control allows the controller parameter to be updated as the system parameters change. Successful

implementations of adaptive PSS are reported in [17,18]. In some works, Self Tuning Regulators (STRs) are proposed to replace PSS [14]. The model parameters are estimated based on the least square algorithm. However, it will be difficult to design full pole-placement STR for a multimachine power system. Adaptive controller performance during training is generally very poor and to overcome this solutions are proposed to use fuzzy controller or ANN to initialise the adaptive controller [14].

Controllers based on genetic algorithms

Application of Genetic Algorithms (GAs) to solve complex optimisation problems is a well established fact. Functioning of GA is based on the principle of natural evaluation mechanism. At each step of evolution, fitness values of each string is checked before allowing the next step. The cost function which needs to be minimised is assigned large fitness value. The process is repeated until maximum generation is reached which will lead to global or near global optimum solution. GAs are applied to PSS design successfully in many research works [8, 19, 20]. In [8], the PSS design problem is converted to an optimisation problem. The deviations of speeds, torque angles and control inputs from the nominal values are included in the performance cost to be minimised. The parameter variations during operating point changes are included by defining different performance indices corresponding to different operating points. For formulating optimisation problem, single performance index is defined with variation constraints to include parametric variations. Eigen value analysis and simulation results are used to validate the designed controller [8]. However with GAs, it is generally difficult to produce necessary proofs for stability and performance.

Robust Controllers

Apart from the above research, efforts were directed to improve upon the PSS design using classical methods such as root locus, Eigenvalue techniques, pole placement etc., but all these methods failed to address the model uncertainties in the controller design stage itself [21, 22]. In the later part of the eighties, robust control theory gained momentum as a control design tool to address the issue of model uncertainty. In robust control, robust stability and robust performance are given emphasis. A controller is said to be robust to a given set of system uncertainties if it provides stability and satisfactory performance for all system models considered in the design set [23]. Model uncertainties are usually bounded with the magnitude

of the frequency response of the nominal system and represented as additive or multiplicative uncertainties. When considering a multiplicative uncertainty, the actual plant model $G(s)$ can be represented in terms of nominal plant model $G_0(s)$ and uncertainty model $\Delta_m(s)$ as:

$$G(s) = [1 + \Delta_m(s)]\, G_0(s) \tag{1.1}$$

For the system shown in Figure 1.1 we can define the complementary sensitivity function (or the closed-loop transfer function) $T(s)$ the sensitivity function $S(s)$ as follows [23]:

$$T(s) = [G_0(s)K(s)]\,[I + G_0(s)K(s)]^{-1} \tag{1.2}$$

$$S(s) = [I + G_0(s)K(s)]^{-1} \tag{1.3}$$

The robust stability of the closed-loop system with the uncertainties, will be guaranteed if the following condition is satisfied [24]:

$$\|\Delta_m(s)T(s)\|_\infty = \sup\{\sigma_{max}\,[\Delta_m(s)T(s)]\} \leq 1 \tag{1.4}$$

where σ_{max} represents the maximum singular value and sup denotes the supremum or the least upper bound over all the frequency range considered. In Figure 1.1 $K(s)$ is the robust controller, $W_1(s)$ and $W_3(s)$ are the weighting function which are selected by the designer to achieve the control objectives. Choice of $W_1(s)$ affects the desired steady-state performance of the system and $W_3(s)$ affects the robustness property given by (1.4). Robust performance is achieved by synthesising $K(s)$ through optimisation of the following equation (1.5),

$$\min_{K(s)} \left\| \begin{matrix} W_1(s)S(s) \\ W_3(s)T(s) \end{matrix} \right\|_\infty = \min_{K(s)} \left\| \begin{matrix} W_1(s)\,[I + G_0(s)K(s)]^{-1} \\ W_3(s)\,[G_0(s)K(s)]\,[I + G_0(s)K(s)]^{-1} \end{matrix} \right\|_\infty \tag{1.5}$$

Robust control technique enabled the researchers to account for the uncertainties in the power system model to be included in the power system controller design. A considerable amount of research has been done from the early nineties till the present time to apply robust control techniques to address the issues faced by power system control and thereby to improve the controller performance [10, 25–37]. In these works, controllers are designed for multimachine power systems using robust

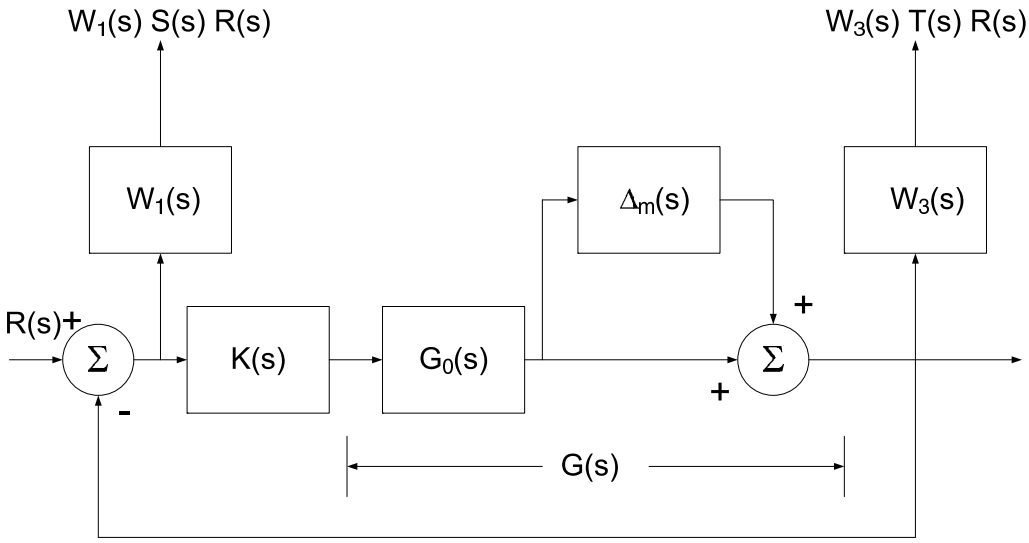

Figure 1.1. H^{∞} block diagram.

control techniques like H_{∞} optimisation, μ-synthesis and Linear Matrix Inequality (LMI) approach. Variations in system parameters and modeling errors are treated as uncertainties and included in the controller design [14,31]. In [31], a single controller is designed for the entire operating regime of the generator. This approach gives feasible controller solution only for systems having comparatively small uncertainty magnitude over the entire operating regime of the generator.

Using LMI approach, the solution for the Riccati equation to synthesise the controller is obtained by translating the quadratic matrix inequality representing Riccati equation into standard LMI framework through the Schur Complement method [38]. In [34], robust power system controllers are designed using LMI approach. In this work, the conventional PSS structure is assumed for the robust controller and the controller is synthesised using LMIs. LMIs can be used as an effective tool for solving robust controller optimisation problems [33].

As an alternative approach to control linearised power systems, one can consider the power system as an interconnected nonlinear system and much attention has been given to the design of nonlinear controllers using nonlinear system models [26, 29, 39]. Nonlinear feedback linearisation techniques are employed to linearise the power system models, thereby alleviating the operating point dependant nature of the linear designs [31]. Even though these controllers do improve the transient

stability of the system, their practical implementation is quite complicated and difficult due to their structures and often excessive control levels. Also, feedback linearisation schemes need exact plant parameters to cancel the inherent system nonlinearities and make the stability analysis a formidable task [31].

1.1.2 Parameter variation

Multimachine power system model is highly nonlinear and its parameters are subjected to wide variations when the load and generation varies. Power system controller design should be able to include these variations in the controller design stage. Different techniques are used to accomplish this, among these, use of gain scheduling and switching control are widely researched.

Gain scheduling

To tackle the problem of parameter variation, gain scheduled control offers an effective solution. Gain scheduling is successfully applied to many engineering applications including in aircrafts [40]. Generally, gain scheduling is done as follows [41]:*(i)* Several operating points are selected to cover the range of plant dynamics and these points are indexed by some scheduling variables. *(ii)* For each of these operating points a linearised plant model is constructed and a linear compensator is synthesised.*(iii)* In between the operating points, the parameters of the compensator are then interpolated or scheduled, thus resulting in a global compensator. Generally the scheduling variable should vary slowly and should be able to capture the plant's nonlinearities. In conventional gain scheduling, one cannot a priori assess stability, robustness and other performance properties of gain scheduled designs [41].

The lack of guaranteed stability property in gain scheduling is addressed through quasi-LPV scheduling [36,42] and by using LMI based designs [43,44]. In quasi-LPV scheduling the plant dynamics are rewritten to transform nonlinearities as time-varying parameters that are used as scheduling variables. Quasi-LPV approaches are computationally intensive, but offer guaranteed stability and performance properties [36, 42]. LMI based constructions of H_∞ optimal controllers can be adapted to compute gain scheduled controllers for LPV systems that guarantee stability and performance [42, 43].

Gain scheduling technique is applied successfully in power system control design [36, 45–47]. In [45, 46], robust controllers are designed at different operating points and the controller gain is interpolated to get continuous controller. In [47], linear

observer based controllers are designed for different operating points and Youla-Jahr-Bongiorno-Kucera parametrisation is used to schedule between the controllers. In [36], the plant model is linearised at different operating points and by using LMIs robust controller corresponding to these operating points are obtained. The curve fitting technique is used to obtain the controllers between the operating points.

However, it is worth noting the following points in relation to gain scheduling [42]: *(i)* Gain scheduling often involves several ad hoc steps, beginning with the problem formulation, which can be suitable in simple situations, but increasingly troublesome as more complex controllers are designed. *(ii)* The linearisation scheduling approach does not apply when little information is carried by plant linearisations about constant equilibria. The quasi-LPV approach, because of its conservative nature, may not yield controllers. *(iii)* Linearisation gain scheduling depends on rules of thumb and extensive simulation for the evaluation of stability and performance. Typically, stability can be assured only locally and in a "slow-variation" setting, and there are no performance guarantees. The quasi-LPV approach offers the potential of both stability and performance guarantees. But accurate continuous LPV modeling of the plant is required for successful implementation [48].

Switching controllers

Another approach to conquer wide variations in the plant parameter is to use switching controllers and suitably switching between them as the operating point shifts. Control techniques based on switching between different controllers have been applied extensively in recent years, particularly in the control of mechanical systems, the automotive industry, aircraft and air traffic control and switching power converters. In these applications it has been shown that switching control is capable of achieving stability and improve transient response. Different switching approaches are extensively researched and reported with regard to switching methodologies and switching stability proofs [49–62].

When two closed loop stable systems undergo switchings, we cannot guarantee the stability of the switched system [56] unless additional conditions are imposed on the switching frequency. Hence for systems undergoing switching, switching stability of the systems need to be established. Most of the proposed methods use Lyaponov function methods in some form or other to achieve switching stability. In [54, 62] a common Lyapunov function method switching rule is used. Some approaches [50, 54, 61] model the switching process as a stochastic process and develop the

necessary switching proofs. Preserving switching stability in the slow switchings is explored in detail in many works including [49,53,56]. Average dwell time approach for switching stability is established in [53, 54, 59].

Switching transients and bumpless compensator

One can design linear multiple controllers corresponding to different operating points to cover the entire operating regime of the plant. Controllers can then be suitably switched as the operating point changes. Switching stability can be preserved by employing some of the schemes mentioned above. However, if there is discontinuity in the output of the current controller and the new controller, it will lead to switching transients and create unwanted plant response.

The issue of switching between controllers with minimum transients was extensively studied by many researchers [48, 63–66]. In [63, 65] the problem of switching between two controllers is considered. The switching problem is formulated as a linear quadratic optimisation problem, to minimise the difference between the output of the online and to be switched offline controller is minimised at the time of switching. The solution to the problem gives a bumpless compensator which is used to drive the output of the offline controller to be equal to the online controller at the time of switching. Thus the bumpless compensator helps to initialise the offline controller states so that the jumps at the plant input is minimised at the switching instant. The bumpless compensator does not play any part after switching. However, in the scheme proposed in [65,66], the interest is to minimise the net transient including any further transients which may occur after switching.

1.1.3 Effect of on load tap changing transformers (OLTCs)

OLTCs are installed at many points in a power system to maintain the voltage at a preset level. OLTCs continuously respond to the changes in grid voltage. However, the action of OLTC after fault, is usually to weaken an already strained system [67]. This negative action of the OLTCs often leads to voltage collapse in the power system [67–69].

The small-signal stability of the interconnected system is affected by the dynamics of both the generators and the OLTCs. It is important to consider the interconnection effects due to OLTCs while designing PSS and also the interconnection effect of generators on OLTCs in the design of OLTC controllers. The effects of the dynamics of OLTC with respect to voltage collapse, stability and power transfer

ability are considered in [70–72]. In the works mentioned in [71, 72], the generators feeding the OLTCs are assumed as constant voltage sources but the secondary voltage of the OLTC is affected by the changes in the primary voltage as well as the load connected to the OLTC. Generally, the effects of OLTCs are not included while designing the PSS.

1.1.4 Motivation for current research

From the above discussion on the power system controller design, we can summarise the issues relating to the improvements in power system stability and power system controller design as follows:

- Each generator is affected by the dynamics of other generators connected in the grid. Therefore the interconnection effects from other machines need to be considered while designing the controllers.
- Power system parameters vary over a wide range due to changes in power generation and load in the grid. These parameter variations need to be included in the controller design.
- Designing a single controller for the entire operating range including the interconnection effects and parameter variation will make the controller design more conservative. This can be avoided by using swiching controllers.
- When using switching controllers, switching stability is to be ensured and the transients during switching are to be minimised.
- OLTCs form an important dynamical element in a grid system, so it is appropriate to include the effects of OLTCs in the controller design.

1.1.5 Contributions of the research

This research work is aimed to improve the present power system control design methodology. The proposed controller design is focussed upon to improve the damping and robustness provided by the power system controller. The major contributions of the thesis in this direction are summarised below:

1. The power system controllers are designed by treating the power system as a parameter varying switched system. The nonlinear power system model is linearised at different Selected Equilibrium Points (SEPs) covering the entire operating regime of the power system. Linear power system controllers are designed for these SEPs and the controllers are switched as the power system

operating point changes. Use of switched control helps to reduce the conservatism of the controller design. This approach also helps to increase the uncertainty handling capability of the design, as the net uncertainty is divided among different controllers.

2. Decentralised robust output feedback controllers are proposed. The design is based on the minimax LQG control design technique [22]. Minimax LQG methodology can be considered as a robust version of standard LQG controller design and it combines the advantages of both LQG control and H-infinity control [22]. Minimax LQG control provides a guaranteed cost controller enabling the inclusion of multiple uncertainties and noise depending upon the application.
3. The controller design takes into account the interconnection effects from other machines and the parameter variations due to generation and load changes by treating them as uncertainties and these effects are represented and bounded using Integral Quadratic Constraints (IQCs). Representing uncertainty using IQC has several advantages, among them the key feature of IQC is that the uncertainty is described purely in terms of bounds on the signals rather than bounding the magnitude of the uncertainty directly. To include the effect of parameter variations, the results and proofs in the work of [73] are extended in this research.
4. The stability of the switched system while switching among the controllers is preserved through dwell time constrained switchings. An expression has been developed to arrive at the dwell time required for stable switching, including the jump in system states, when the system jumps between different operating points during switchings.
5. The bumpless switching scheme was originally proposed in [74] for switching control in aerospace applications. We apply this scheme with necessary modifications for minimising the transients during controller switchings.
6. Power system controller design was extended to include the dynamics of OLTCs. For this purpose a simplified power system model was developed linking generator and OLTC dynamics. Robust output feedback controllers are designed using the power system model developed.

The proposed power system control methodologies are validated through simulations. Controllers are designed for test case power systems and simulations are

carried out under generation / load variations, fault conditions and reference voltage changes. Two types of simulations are included; computer simulations with nonlinear power system model and Real Time Digital Simulations (RTDSs) using the RTDS facility at CPRI, Bangalore, India.

1.2 Thesis chapters

The thesis consists of seven chapters excluding the chapter on introduction and the final conclusion chapter. The contents of each chapter are briefly introduced here.

Chapter 2: This chapter introduces the concepts of power system stability, power system network model and the multimachine power system model considered in this research. The dynamics of rotor swings and the effect of rotor dynamics are explained using a single machine on an infinite bus model system. The basic concepts of conventional PSS are also included.

The mathematical model of the power system network and the network model reduction are presented. This chapter also includes the network load flow analysis using the Newton-Raphson method.

The multimachine power system model considered in this work is presented in this chapter. A brief introduction to Park's transformation and common axis reference frame are given. The nonlinear multimachine power system model used for simulation studies and the linearisation of the nonlinear model are included. Linearisation steps and the state space representation of the power system which are used for controller design are also presented.

Chapter 3: The minimax LQG controller design methodology is explained in this chapter. The first part of the chapter is devoted to the basic concepts of minimax LQG design methodology and the uncertainty description using IQCs. A collection of important results and theorems used in the controller design are presented next. After this, the controller design is presented with controller stability proofs. The final part of the chapter consists of LMI optimisation procedure used in the synthesis of the controller.

Chapter 4: The dwell time switching scheme to preserve switching stability is presented in this chapter. The basic concepts of slow switching and dwell time are

given in the first part of the chapter. This is followed by the development of an expression and conditions for the dwell time required for stable switching. To validate the proposed scheme, a test case power system is selected and controllers are designed. Different controller switching scenarios are simulated and the results are presented.

Chapter 5: The bumpless switching scheme to reduce the switching transients is included in this chapter. The linear quadratic bumpless switching scheme and the bumpless compensator design are given in the first part of the chapter. In the second part, application of the scheme for power system controller switching is presented. The last part of the chapter consists of the validation of the bumpless switching scheme through simulations. The effectiveness of the scheme is demonstrated by comparing the simulation results with and without bumpless switchings.

Chapter 6: Validation of the controller design methodology through nonlinear computer simulations is presented in this chapter. The test case power system parameters, load flow results and state space representation of the system are given in the first part of the chapter. The controller design for different operating points, dwell time computations and bumpless compensator design are included in the following part. Simulation model, methodology and cases are given in the next part. The controllers are validated under different simulation cases involving load / generation variations, fault case and AVR reference voltage changes. The simulation responses are also compared with conventional PSS and the analysis of the simulation responses are also included.

Chapter 7: This chapter consists of the validation of the controller design using the RTDS facility. Introduction to the RTDS facility and the power system considered for validation are given in the first part of the chapter. In the next part, implementation details of the designed controllers are included. In the following part, simulation cases and results of the simulation are included. The simulation results are also compared with conventional PSS.

Chapter 8: Power system controller design including the dynamics of OLTCs is

presented in this chapter. In the first part of this chapter, a simplified multimachine power system model with OLTCs is included. The next part comprises the controller design, dwell time switching and bumpless switching methodologies. Simulation studies to validate the proposed controllers are included in the final part of this chapter.

Chapter 2

Power System Stability and Model

Interconnected power system is a complex nonlinear system. For satisfactory operation of the system and to meet the voltage and frequency requirements, maintaining the stability of the power system is crucial. In this chapter we introduce general power system stability and in particular rotor angle stability and the Power System Stabilisers (PSSs). Power generated from the generating station is transmitted and distributed to the load centers through power system networks. For power system studies, these networks and loads are represented using mathematical models. The network model description and the load flow analysis of the power system used in the research are included in the chapter. The dynamics of the power system consisting of many generating units are represented through a set of nonlinear equations. These equations are linearised for a particular equilibrium point to get the linearised power system model. The chapter discusses the nonlinear multimachine power system model and linear state space representation of the power system which are used in this research.

2.1 Power system stability

The demand for electricity in modern day living is ever increasing. More and more power stations are being continuously built and added to the grid. Thus grids grow in size and complexity posing many challenges for proper operation and control. The load connected to the grid is continuously changing so the generators in the grid need to have enough spinning reserve to cater for these changes. Also the system should meet constant voltage and frequency criteria in these circumstances and maintain the required reliability of service. To ensure reliable supply, co-ordinated power system control needs to be exercised at different levels. As a part of this, power systems have to maintain voltage and frequency stability at all times. The power system is highly complex and nonlinear, with dynamic responses influenced by a wide array of devices with different response rates and characteristics [2]. These issues make it difficult to maintain the power system stability.

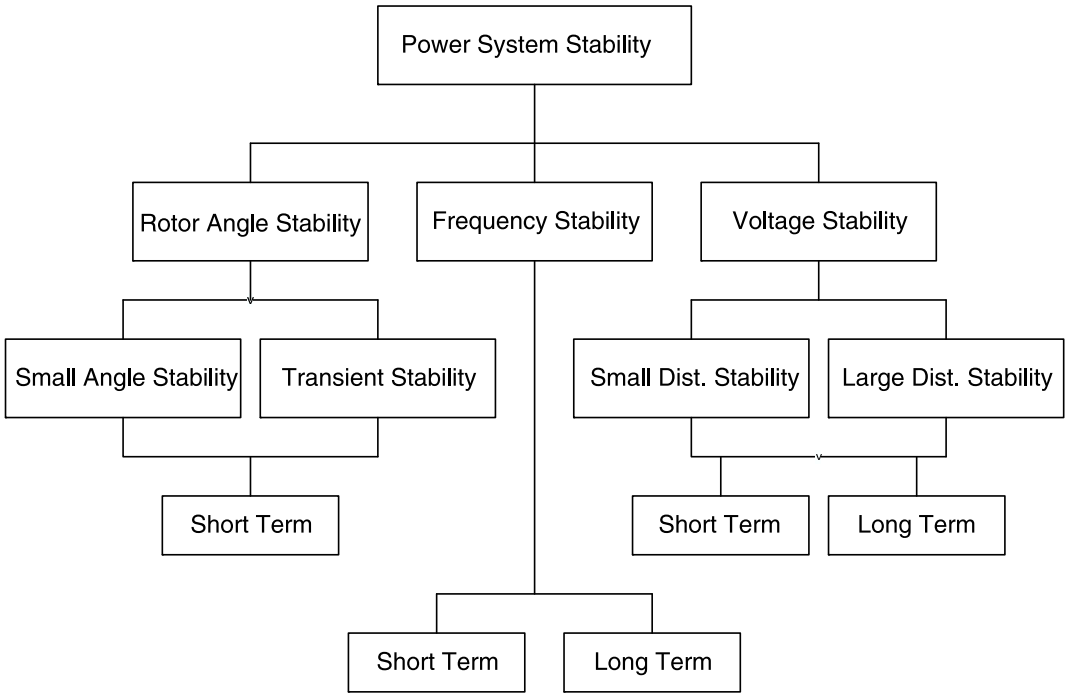

Figure 2.1. Power system stability classification [1]

Power system stability may be broadly defined as the ability of a power system, for a given initial operating condition, to regain a state of operating equilibrium after being subjected to a disturbance, with most system variables bounded so that practically the entire system remains intact [1], [2]. We can classify power system stability into three main classes as rotor angle stability, frequency stability and voltage stability. Depending on the nature of the disturbance to which the power system is subjected, stability is further classified as small disturbance or large disturbance. Again depending on the time period, stability is further divided as short term and long term stability. The power system stability classification is given in Figure 2.1 [1]. In this thesis work we are concerned about the small signal rotor angle stability of the power system.

2.1.1 Rotor angle stability

In an interconnected system, the frequencies of all the machines connected to the grid must be the same and the rotor speed of all the machines must always be synchronised to this frequency and run at the synchronised speed. The rotor angle

stability refers to the ability of the interconnected synchronous machines of the power system to remain in synchronism after being subjected to a disturbance. It depends on the ability to maintain or restore equilibrium between electromagnetic torque and mechanical torque of each synchronous machine in the system. Instability that may result, occurs in the form of increasing angular swings of some generators leading to their loss of synchronism with other generators [1].

Rotor angle

In a synchronous machine, the mechanical torque produced by the prime mover to drive the rotor is opposed by the electrical torque produced by the generator. Due to the spatial distribution of the windings in the stator of the generator, the magnetic field produced by the stator rotates at the same speed as the rotor under steady state conditions and the fields produced by stator and rotor align themselves. Depending upon the load delivered by the generator, the rotor field maintains a constant angle with the stator field; this angle is known as rotor angle (δ) Figure 2.2. To increase the power output of the generator more mechanical torque is applied and this advances the rotor with respect to the stator field increasing the rotor angle (δ) and conversely reduction of mechanical torque retards the rotor and reduces δ.

Swing equation

When the steady state condition is disturbed by either an increase or decrease in power, the rotor starts to oscillate about its equilibrium before settling to its new steady state rotor angle. The dynamics of these oscillations are represented mathematically by the equation (2.1) and generally known as the swing equation,

$$J\omega_m \frac{d^2\delta}{dt^2} = P_M - P_e, \tag{2.1}$$

where J is the moment of inertia of the rotor, ω_m the angular velocity of the rotor, P_M is the mechanical power, and P_e is the electrical power.

Under equilibrium conditions, mechanical power P_M balances the generated electrical power P_e. The electrical power P_e can change instantaneously, but it takes finite time to change the mechanical power P_M. This difference in power P_M - P_e is made up as the change in rotor kinetic energy. This stored energy is released during rotor oscillations before the rotor settles for new equilibrium conditions. For large synchronous machines the inherent mechanical damping of the rotor is negligible. Hence sufficient damping needs to be provided through electro-mechanical means

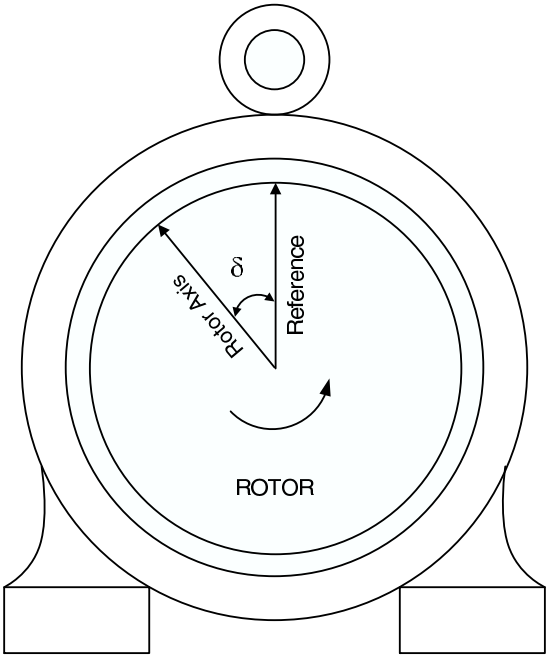

Figure 2.2. Rotor angle in a synchronous machine.

to damp out these oscillations. If these oscillations are allowed to grow, instability may result.

Single Machine on Infinite Bus (SMIB)

In a single machine on infinite bus model, it is assumed that the machine is connected to the grid with constant voltage and frequency as shown in Figure 2.3. The total reactance X_T is the sum of the transient reactance X'_d and the network reactance between the machine and the bus X_E; $E'_G\angle\delta$ the voltage behind X'_d, leads the reference bus voltage $E_B\angle 0$ by δ. The active power P_e transferred by the machine to the grid is given by [2],

$$P_e = \frac{E'_G\ E_B}{X_T}\sin\delta \tag{2.2}$$

From (2.2) it can be seen that power transferred by a machine to the grid is nonlinear and varies sinusoidally with δ. Maximum power is transferred when $\delta = 90^0$ and for stable operation $\delta < 90^0$ and for $\delta > 90^0$ the operation is unstable.

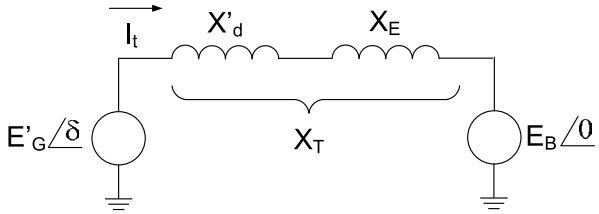

Figure 2.3. SMIB system

Effect of disturbance on rotor angle

Whenever the equilibrium between the mechanical power input and electrical power output is disturbed, oscillations are induced on the rotor. During disturbance if the mechanical power exceeds the electrical power the rotor accelerates, otherwise it decelerates. If one generator temporarily runs faster than the other, the angular position of its rotor relative to that of a slower machine will advance. Since the power-angle relationship is highly non-linear, beyond a certain limit, an increase in angular separation is accompanied by a decrease in power transfer such that angular separation is increased further. Instability results if the system cannot absorb the kinetic energy corresponding to these rotor speed differences. For any given situation, the stability of the system depends on whether or not the deviations in angular positions of the rotors result in sufficient restoring torques [1].

During a disturbance, the change in electromagnetic torque in a synchronous machine has two components [1]:

- Synchronising torque component, in phase with rotor angle deviation and lack of this component results in aperiodic or non-oscillatory instability.
- Damping torque component, in phase with speed deviation, and lack of this component results in oscillatory instability

Small disturbance (or small signal) rotor angle stability is concerned with the ability of the power system to maintain synchronism under small disturbances. The disturbances are considered to be sufficiently small that linearisation of the system equations are permissible for the purpose of analysis [2, 75, 76]. Two types of instabilities may arise:

- Increase in rotor angle through a non-oscillatory or aperiodic mode due to lack of synchronising torque.
- Rotor oscillations of increasing amplitude due to lack of sufficient damping torque.

Generally small disturbance rotor angle instability occurs due to lack of sufficient damping of oscillations [1].

Large disturbance rotor angle stability or transient stability is concerned with the ability of the power system to maintain synchronism after a severe disturbance such as short circuit on a transmission line is cleared. The resulting system response involves large excursions of generator rotor angles and is influenced by the nonlinear power-angle relationship. Transient stability depends on both initial conditions and severity of the disturbance. Instability is usually in the form of aperiodic angular separation due to insufficient synchronising torque manifesting as first swing instability [1].

2.1.2 Conventional Power System Stabiliser

Synchronous machines connected to the grid employ Power System Stabilisers to enhance the damping of the rotor oscillations. PSS uses the change in speed $\Delta\omega$ as the feedback variable and its output V_s is mixed with the reference voltage V_{ref} to produce the excitation signal. The block diagram in Figure 2.4 shows the excitation system with Automatic Voltage Regulator (AVR) and PSS [2]. The amount of damping provided by PSS depends on the value of the gain block K_{STAB}. The phase compensation block introduces phase lead necessary to compensate for the phase lag that is introduced between the exciter input and the generator electrical torque. The wash out block serves as a high-pass filter, with the time constant T_W high enough to allow signals associated with oscillations in ω_r to pass unchanged and block slowly varying speed changes. It allows the PSS to respond only to the fast changes in speed.

2.2 Network Model

We need a mathematical representation of electrical grid in order to study and analyse the system. The electrical network consists of generators, transformers, transmission lines, compensators, load etc., and these elements are to be included in the mathematical model. After suitable representation of these elements we can arrive at the network model of the system in terms of its admittance matrix.

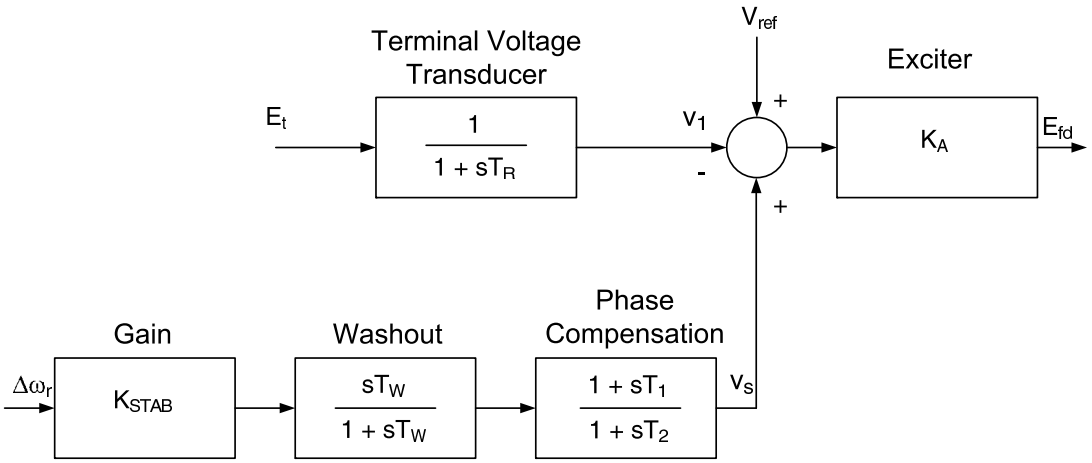

Figure 2.4. PSS with AVR Block diagram [2].

Generally because of a large number of nodes in the system, this matrix will be of large size, which can be reduced in size for constant impedance loads.

Load flow analysis using Newton-Raphson (NR) method is used to solve the power flow across various nodes of the system. Using the solutions of the power flow equations we can determine the voltage and current flow at nodes. We briefly describe the network representation and the load flow analysis used in this work.

2.2.1 Network Representation

We shall consider a network consisting of $m + n$ buses with n generator buses and m load buses. We can write the network equation for this grid system using node admittance matrix as follows:

$$\begin{bmatrix} I_1 \\ \dots \\ I_n \\ I_{n+1} \\ \dots \\ I_{n+m} \end{bmatrix} = \begin{bmatrix} Y_{11} & \dots & Y_{1n} & Y_{1(n+1)} & \dots & Y_{1(n+m)} \\ \dots & \dots & \dots & \dots & \dots & \dots \\ Y_{n1} & \dots & Y_{nn} & Y_{n(n+1)} & \dots & Y_{n(n+m)} \\ Y_{(n+1)1} & \dots & Y_{(n+1)n} & Y_{(n+1)(n+1)} & \dots & Y_{(n+1)(n+m)} \\ \dots & \dots & \dots & \dots & \dots & \dots \\ Y_{(n+m)1} & \dots & Y_{(n+m)n} & Y_{(n+m)(n+1)} & \dots & Y_{(n+m)(n+m)} \end{bmatrix} \begin{bmatrix} V_1 \\ \dots \\ V_n \\ V_{n+1} \\ \dots \\ V_{n+m} \end{bmatrix} \tag{2.3}$$

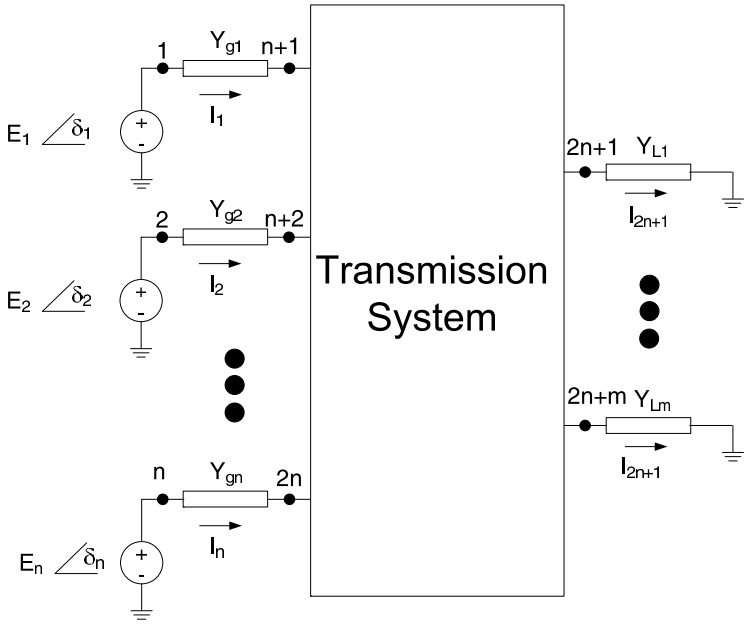

Figure 2.5. Network augmented with voltage behind syn.reactance.

The above equation (2.3) can be represented in short as,

$$I_{\text{bus}} = Y_{\text{bus}} V_{\text{bus}} \tag{2.4}$$

and the admittance matrix Y_{bus} can be partitioned as,

$$Y_{\text{bus}} = \begin{bmatrix} Y_1 & Y_2 \\ Y_3 & Y_4 \end{bmatrix} \tag{2.5}$$

where Y_1 is $(n \times n)$, Y_2 is $(n \times m)$, Y_3 is $(m \times n)$ and Y_4 is $(m \times m)$ matrices.

We can represent the i^{th} synchronous machine connected to the grid as a voltage source $E_i \angle \delta_i$, connected behind a transient reactance $1/Y_{gi}$. Using this representation we can augment the network by including the generator reactance as shown in Figure 2.5. The augmented network can be renumbered with generator internal nodes from 1 to n and original network buses from $n+1$ to $2n+m$.

In the augmented network, we can represent the transient admittances of the generators as matrix $Y_G = \text{diag}\ (Y_{gi})$ of size $n \times n$. Now the admittance matrix of

the network becomes,

$$\hat{Y}_{\text{bus}} = \begin{bmatrix} Y_G & -Y_G & 0 \\ -Y_G & Y_1 + Y_G & Y_2 \\ 0 & Y_3 & Y_4 \end{bmatrix} \tag{2.6}$$

We assume the loads as constant impedances and the value of the equivalent load admittances can be obtained from the load flow results as follows [77]:

$$Y_{Li} = \frac{P_{Li} - j\ Q_{Li}}{|V_i|^2} \quad \text{where } i = n+1, \ldots, 2n+m \tag{2.7}$$

where $P_{Li} - j\ Q_{Li}$ is the power flow and $|V_i|$ is voltage at i^{th} bus. We can represent the load admittance at generator buses $n+1$ to $2n$ as matrix $Y_{LG} = \text{diag}\ (Y_{Li})$ where $i = n+1$ to $2n$ and the load admittance at load buses $2n+1$ to $2n+m$ as matrix $Y_{LL} = \text{diag}\ (Y_{Li})$ where $i = 2n+1$ to $2n+m$.

Now by including the load admittance into the network admittance matrix, we have:

$$\tilde{Y}_{\text{bus}} = \begin{bmatrix} Y_G & -Y_G & 0 \\ -Y_G & (Y_1 + Y_G + Y_{LG}) & Y_2 \\ 0 & Y_3 & Y_4 + Y_{LL} \end{bmatrix} \tag{2.8}$$

2.2.2 Network Reduction

To obtain the dynamic model we can simplify the network admittance matrix by eliminating all buses except the generator buses 1 to n. This reduction can be achieved as follows [77]:

We can partition the admittance matrix $\tilde{Y}_{\text{bus}}$ into generator node elements and the remaining node elements. Now $\tilde{Y}_{\text{bus}}$ becomes,

$$\tilde{Y}_{\text{bus}} = \begin{bmatrix} Y_A & Y_B \\ Y_C & Y_D \end{bmatrix} \tag{2.9}$$

where Y_A is $(n \times n)$, Y_B is $(n \times n+m)$, Y_C is $(n+m \times n)$ and Y_D is $(n+m \times n+m)$ matrices. Now we can rewrite the network equations corresponding to the

admittance matrix given by (2.9) as,

$$\begin{bmatrix} I_A \\ 0 \end{bmatrix} = \tilde{Y}_{\text{bus}} \begin{bmatrix} V_A \\ V_D \end{bmatrix} \tag{2.10}$$

We can obtain the reduced admittance matrix Y_{RED} by eliminating the $n+m$ buses as,

$$I_A = [Y_{RED}]\ V_A, \quad \text{where } Y_{RED} = \left[Y_A - Y_B Y_D^{-1} Y_C\right] \tag{2.11}$$

We use the reduced admittance matrix in (2.11) in the multimachine power system model. We represent the $\left(i^{th}, j^{th}\right)$ element of the admittance matrix as $G_{ij} + jB_{ij}$ and we use this notation in formulating the power system model.

2.2.3 Load flow by Newton-Raphson method

The real and reactive power flows at i^{th} node of a power system with n nodes are given by (2.12). To solve power flow at each node, we solve the set of equations for these nodes. Since these equations are highly nonlinear, we can use Newton-Raphson's iterative technique for solving nonlinear equations to solve these power flow equations [2]. The real and reactive power flows at the i^{th} node are given by:

$$\begin{aligned} P_i &= |V_i| \sum_{j=1}^{n} |V_j| \left[G_{ij} \cos(\theta_i - \theta_j) + B_{ij} \sin(\theta_i - \theta j)\right] \\ Q_i &= |V_i| \sum_{j=1}^{n} |V_j| \left[G_{ij} \sin(\theta_i - \theta_j) - B_{ij} \sin(\theta_i - \theta j)\right] \end{aligned} \tag{2.12}$$

where P is the real power, Q the reactive power, V the voltage and θ voltage angle at the respective node of the power system. It can be seen from (2.12), that the real power P and the reactive power Q at each node are the functions of voltage magnitude V and angle θ of all nodes.

Let us designate the generator bus as PV bus and the load bus as PQ bus. Generally we specify active power and voltage for PV buses and active and reactive power for PQ buses. If we denote the specified values using superscript sp, then we

can write the load flow equations for a power system with n buses as [2]:

$$\begin{aligned}
P_1(\theta_1,\ldots,\theta_n,V_1,\ldots,V_n) &= P_1^{sp}\\
\ldots\quad\ldots\quad\ldots\quad\ldots\quad\ldots\quad\ldots&\\
P_n(\theta_1,\ldots,\theta_n,V_1,\ldots,V_n) &= P_n^{sp}\\
Q_1(\theta_1,\ldots,\theta_n,V_1,\ldots,V_n) &= Q_1^{sp}\\
\ldots\quad\ldots\quad\ldots\quad\ldots\quad\ldots\quad\ldots&\\
Q_n(\theta_1,\ldots,\theta_n,V_1,\ldots,V_n) &= Q_n^{sp}
\end{aligned} \tag{2.13}$$

To solve the above equation iteratively, we make initial estimates for voltage and angles, and denote them as V^0 and θ^0. With these initial estimates, we can apply Newton-Raphson method and rewrite the load flow equations as [2]:

$$\begin{bmatrix}
P_1^{sp}-P_1(\theta_1^0,\ldots,\theta_n^0,V_1^0,\ldots,V_n^0)\\
\ldots\quad\ldots\quad\ldots\quad\ldots\quad\ldots\quad\ldots\\
P_n^{sp}-P_n(\theta_1^0,\ldots,\theta_n^0,V_1^0,\ldots,V_n^0)\\
Q_1^{sp}-Q_1(\theta_1^0,\ldots,\theta_n^0,V_1^0,\ldots,V_n^0)\\
\ldots\quad\ldots\quad\ldots\quad\ldots\quad\ldots\quad\ldots\\
Q_n^{sp}-Q_n(\theta_1^0,\ldots,\theta_n^0,V_1^0,\ldots,V_n^0)
\end{bmatrix} =
\begin{bmatrix}
\frac{\partial P_1}{\partial\theta_1}\cdots\frac{\partial P_1}{\partial\theta_n}\frac{\partial P_1}{\partial V_1}\cdots\frac{\partial P_1}{\partial V_n}\\
\ldots\quad\ldots\quad\ldots\quad\ldots\\
\frac{\partial P_n}{\partial\theta_1}\cdots\frac{\partial P_n}{\partial\theta_n}\frac{\partial P_n}{\partial V_1}\cdots\frac{\partial P_n}{\partial V_n}\\
\frac{\partial Q_1}{\partial\theta_1}\cdots\frac{\partial Q_1}{\partial\theta_n}\frac{\partial Q_1}{\partial V_1}\cdots\frac{\partial Q_1}{\partial V_n}\\
\ldots\quad\ldots\quad\ldots\quad\ldots\\
\frac{\partial Q_n}{\partial\theta_1}\cdots\frac{\partial Q_n}{\partial\theta_n}\frac{\partial Q_n}{\partial V_1}\cdots\frac{\partial Q_n}{\partial V_n}
\end{bmatrix}
\begin{bmatrix}
\Delta\theta_1\\ \ldots\\ \Delta\theta_n\\ \Delta V_1\\ \ldots\\ \Delta V_n
\end{bmatrix} \tag{2.14}$$

which can be written as,

$$\begin{bmatrix}\Delta P\\ \Delta Q\end{bmatrix} = \begin{bmatrix}\frac{\partial P}{\partial\theta} & \frac{\partial P}{\partial V}\\ \frac{\partial Q}{\partial\theta} & \frac{\partial Q}{\partial V}\end{bmatrix}\begin{bmatrix}\Delta\theta\\ \Delta V\end{bmatrix} \tag{2.15}$$

where the first matrix on the right hand side of equation (2.15) is called Jacobian matrix. In (2.15), we assume all buses to be PQ buses, but for each PV bus, terms corresponding to ΔQ and ΔV would be absent. At each step of the iteration, $\Delta\theta$ and ΔV are computed and the initial estimates are updated. This process is carried out until the errors in $\Delta\theta$ and ΔV falls below the specified tolerance.

2.3 Power system model

To develop a mathematical model for a multimachine system, each machine connected to the grid is to be represented by a set of dynamic equations. Using Park's transformation, for a balanced operation, the three phase time varying currents can

be expressed as two components. With this representation, it is possible to represent the time varying inductance as constant inductances making the dynamical representation of the machine simple. Another simplification is achieved by adopting a common reference frame and transferring the variables of all machines to this reference frame. After transferring the variables to the common reference frame, the system can be represented by a set of nonlinear equations. These nonlinear equations are linearised around an operating point to get a linear model which is used for controller design and analysis.

2.3.1 Park's transformation

Park's transformation defines a new set of stator variables such as currents, voltages or flux linkages in terms of the actual winding variables [78]. The new quantities are obtained from the projection of the actual variables on to three axes; one along the direct axis of the rotor field winding, called the direct axis (d-axis); a second along the neutral axis of the field winding, called the quadrature axis (q-axis); and the third on a stationary axis as shown in Figure 2.6.

With reference to Figure 2.6, let us define the d-axis of the rotor at some instant of time to be at an angle θ with respect to the fixed reference frame. The three phase stator currents i_a, i_b and i_c are transformed as direct axis current I_d, quadrature axis current I_q and zero sequence current I_0 using Park's transformation as:

$$\begin{bmatrix} I_d \\ I_q \\ I_0 \end{bmatrix} = \frac{2}{3} \begin{bmatrix} \cos\theta & \cos\left(\theta - \frac{2\pi}{3}\right) & \cos\left(\theta + \frac{2\pi}{3}\right) \\ -\sin\theta & -\sin\left(\theta - \frac{2\pi}{3}\right) & -\sin\left(\theta + \frac{2\pi}{3}\right) \\ \frac{1}{2} & \frac{1}{2} & \frac{1}{2} \end{bmatrix} \begin{bmatrix} i_a \\ i_b \\ i_c \end{bmatrix} \tag{2.16}$$

when i_a, i_b and i_c are balanced, I_d, I_q and I_0 are constant for all θ.

Then we can write the dynamic equations of the i^{th} synchronous machine as follows [78]:

$$\dot{\delta}_i = \omega_0 \omega_i \tag{2.17}$$

$$\dot{\omega}_i = \frac{1}{2H_i}\left[P_{m_i} - E'_{qi} I_{qi} - (x'_{di} - x'_{qi}) I_{di} I_{qi}\right] \tag{2.18}$$

$$\dot{E}'_{qi} = \frac{1}{\tau'_{doi}}\left[E_{FDi} - E'_{qi} - (x_{di} - x'_{di}) I_{di}\right] \tag{2.19}$$

$$V_{qi} = E'_{qi} - r_{ai} I_{qi} + x'_{di} I_{di} \tag{2.20}$$

$$V_{di} = -r_i I_{di} + x'_{qi} I_{qi} \tag{2.21}$$

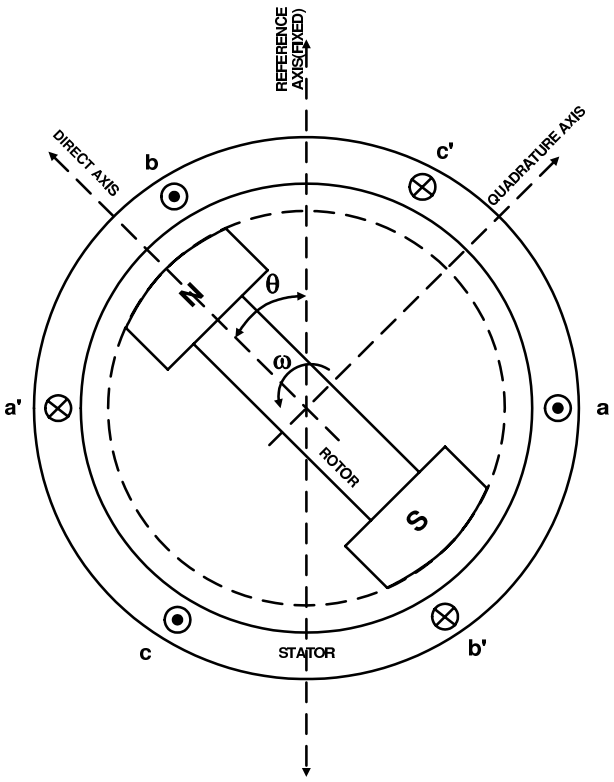

Figure 2.6. Synchronous Machine d-q axis representation

where E'_{qi}, I_{qi} and x'_{qi} are the stator voltage, current and reactance projected on q-axis and I_{di} and x'_{di} are the current and reactance projected on d-axis using Park's transformation, r_{ai} is the stator resistance and E_{FDi} is the field voltage. In the above expressions normally r_i is neglected and $x'_{qi} = x'_{di}$.

Terminal voltage sensor model

The terminal voltage measurement sensor dynamics is expressed as:

$$\dot{V}_{oi} = \frac{1}{T_{ri}} \left(V_{oi} - |V_{ti}| \right) \tag{2.22}$$

where $|V_{ti}|$ is the magnitude of synchronous machine terminal voltage, V_{oi} is the output of the transducer and T_{ri} is the sensor time constant.

2.3.2 Common axis reference frame

In order to analyse the voltages and currents of different machines in a grid system it is necessary that these quantities are expressed in a common reference frame. Generally the terminal voltage of the swing bus is chosen as the reference axis and

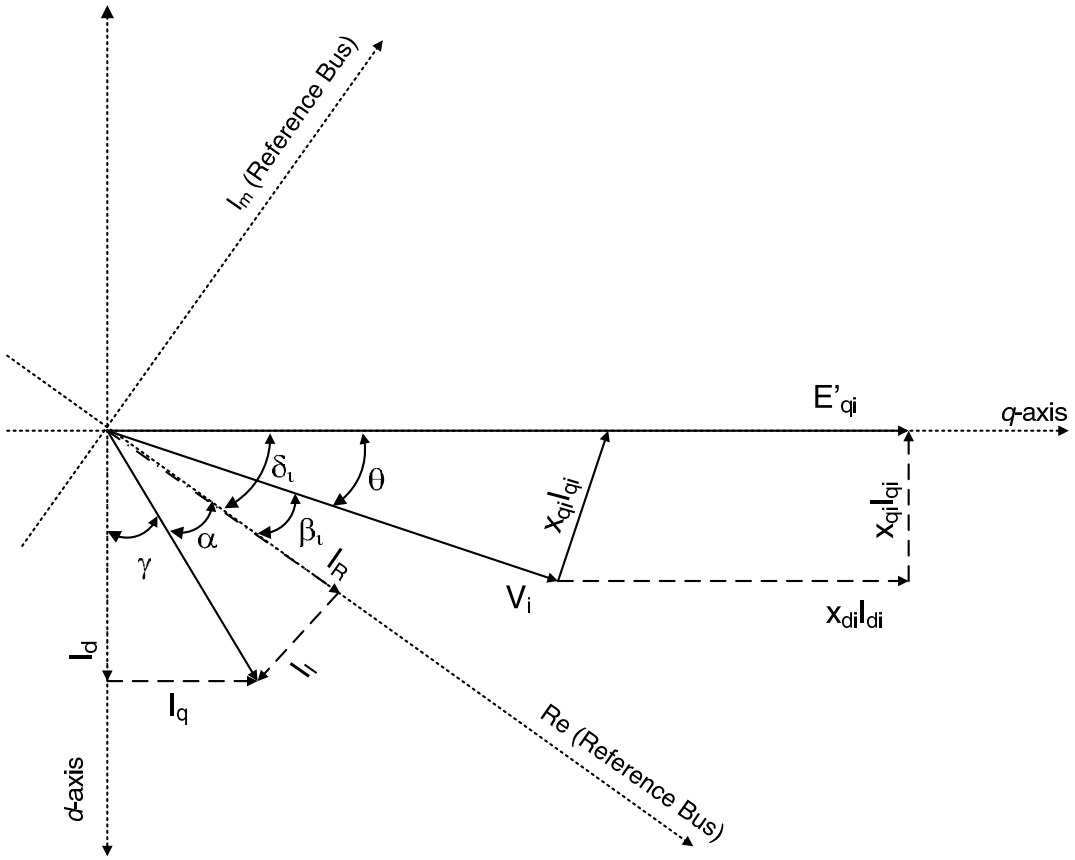

Figure 2.7. Reference frame vector representation

all other quantities are expressed with reference to this axis. In Figure 2.7, the voltages and currents of i^{th} generator are referred to the reference frame and this is carried out as follows:

V_i and β_i are the terminal voltage and angle obtained from the load flow. Generator current I_i can be obtained using the expression, $I = YV$ where I and V are the vector array of currents and voltages of all nodes and Y is the admittance matrix of the network. The value of θ is obtained from, $\theta = \tan^{-1}\left(\frac{x_{qi}I_i}{V_i}\right)$. The generator load angle δ_i is given by $\delta_i = \theta + \beta_i$.

Using the above data, generator current I_i can be resolved into direct and quadrature axis currents as $I_{di} = I_i \cos\gamma$ and $I_{qi} = I_i \sin\gamma$ where $\gamma = 90 - (\alpha + \delta)$. The quadrature axis emf is given by $E'_{qi} = V_i + x_{di}I_{di} + x_{qi}I_{qi}$.

The transformation matrix between dq-axis and the reference frame is given by,

$$\Pi = \begin{bmatrix} \cos\delta_i & \sin\delta_i \\ -\sin\delta_i & \cos\delta_i \end{bmatrix} \tag{2.23}$$

The dq-axis currents are expressed in reference axis as,

$$\begin{bmatrix} I_{qi} \\ I_{di} \end{bmatrix} = \Pi \begin{bmatrix} I_{Ri} \\ I_{Ii} \end{bmatrix} \tag{2.24}$$

2.3.3 Synchronous Machine Model

The following set of equations [78] can be used to describe the behavior of an i^{th} generator in a multimachine power system consisting of n generators:

$$\dot{\delta}_i = \omega_s\omega_i - \omega_s \tag{2.25}$$

$$\dot{\omega}_i = \frac{1}{2H_i}\left(P_{mi} - E'_{qi}I_{qi}\right) \tag{2.26}$$

$$\dot{E}'_{qi} = \frac{1}{\tau'_{do}}\left[K_{ai}(V_{oi} - V_{refi} + V_{si}) - E'_{qi} + (x_{di} - x'_{di})I_{di}\right] \tag{2.27}$$

$$\dot{V}_{oi} = \frac{1}{T_{ri}}\left(V_{oi} - |V_{ti}|\right) \tag{2.28}$$

where

$$I_{qi} = I_{Ri}\cos\delta_i + I_{Ii}\sin\delta_i \tag{2.29}$$

$$I_{di} = -I_{Ri}\sin\delta_i + I_{Ii}\cos\delta_i \tag{2.30}$$

With respect to the reference axis, the generator currents are given by,

$$I_{Ri} = \sum_{k=1}^{n} |E'_{qk}|\left(G_{ik}\cos\delta_k - B_{ik}\sin\delta_k\right) \tag{2.31}$$

$$I_{Ii} = \sum_{k=1}^{n} |E'_{qk}|\left(G_{ik}\sin\delta_k + B_{ik}\cos\delta_k\right) \tag{2.32}$$

2.3.4 Linearised Synchronous Machine Model

The nonlinear synchronous machine model described in Section 2.3.3 are linearised about an equilibrium point to get a linear synchronous machine model. We can

linearise the model (2.25)-(2.28) as follows: On linearising (2.25) we get $\dot{\Delta\delta}_i$ as,

$$\dot{\Delta\delta}_i = \omega_s^0 \Delta\omega_i \tag{2.33}$$

When equations (2.31) and (2.32) are linearised we get ΔI_{Ri} and ΔI_{Ii} as,

$$\begin{aligned}\Delta I_{Ri} = &\sum_{k=1}^{n} |E_{qk}^{'0}| \left(G_{ik}\cos\delta_k^0 - B_{ik}\sin\delta_k^0\right)\Delta E_{qk}^{'} \\ &- \sum_{k=1}^{n} |E_{qk}^{'0}| \left(G_{ik}\sin\delta_k^0 + B_{ik}\cos\delta_k^0\right)\Delta\delta_k\end{aligned} \tag{2.34}$$

$$\begin{aligned}\Delta I_{Ii} = &\sum_{k=1}^{n} |E_{qk}^{'0}| \left(G_{ik}\cos\delta_k^0 + B_{ik}\sin\delta_k^0\right)\Delta E_{qk}^{'} \\ &+ \sum_{k=1}^{n} |E_{qk}^{'0}| \left(G_{ik}\cos\delta_k^0 - B_{ik}\sin\delta_k^0\right)\Delta\delta_k\end{aligned} \tag{2.35}$$

When equations (2.29) and (2.30) are linearised we get ΔI_{qi} and ΔI_{di} as,

$$\Delta I_{qi} = \cos\delta_i^0 \Delta I_{Ri} - I_{Ri}^0 \sin\delta_i^0 \Delta\delta_i + \sin\delta_i^0 \Delta I_{Ii} + I_{Ii}^0 \cos\delta_i^0 \Delta\delta_i \tag{2.36}$$

$$\Delta I_{di} = -\sin\delta_i^0 \Delta I_{Ri} - I_{Ri}^0 \cos\delta_i^0 \Delta\delta_i + \cos\delta_i^0 \Delta I_{Ii} - I_{Ii}^0 \sin\delta_i^0 \Delta\delta_i \tag{2.37}$$

ΔI_{Ri} and ΔI_{Ii} can be eliminated from (2.36) and (2.37) by substituting equations (2.34) and (2.35) into equations (2.36) and (2.37).
To get $\Delta\dot{\omega}_i$, we linearise (2.26),

$$\Delta\dot{\omega}_i = \frac{1}{2H_i}(\Delta P_{mi} - I_{qi}^0 \Delta E_{qi}^{'} - E_{qi}^{'0} \Delta I_{qi}) \tag{2.38}$$

When we linearise (2.27), we get $\Delta\dot{E}_{qi}^{'}$ as,

$$\Delta\dot{E}_{qi}^{'} = \frac{1}{\tau_{doi}^{'}}\left[K_{ai}(\Delta V_{oi} + \Delta V_{si}) - \Delta E_{qi}^{'} + (x_{di} - x_{di}^{'})\Delta I_{di}\right] \tag{2.39}$$

From equations (2.38) and (2.39), ΔI_{qi} and ΔI_{di} can be eliminated by using equations (2.34) to (2.37).

The terminal voltage V_{ti} is given by,

$$\begin{aligned} |V_{ti}| &= \left(V_{qi}^2 + V_{di}^2\right)^{\frac{1}{2}} \\ &= \left[(E_{qi} + x'_{di}I_{di})'^2 + (-x^{'}_{di}I_{qi})^2\right]^{\frac{1}{2}} \\ &= \left[E_{qi}^{'2} + 2E^{'}_{qi}x'_{di}I_{di} + x^{'2}_{di}(I_{qi}^2 + I_{di}^2)\right]^{\frac{1}{2}} \end{aligned} \tag{2.40}$$

By eliminating I_{di} from equation (2.40) using equation (2.30) we get,

$$V_{ti} = \left[E_{qi}^{'2} + 2E'_{qi}x'_{di}(I_{Ii}\cos\delta_i - I_{Ri}\sin\delta_i) + x^{'2}_{di}(I_{Ri}^2 + I_{Ii}^2)\right]^{\frac{1}{2}} \tag{2.41}$$

To linearise (2.41), we make the following substitution. Let $V_{ti} = y_i^{\frac{1}{2}}$, then,

$$\begin{aligned} \Delta V_{ti} &= \frac{1}{2}\left(\frac{1}{y_i^{\frac{1}{2}}}\right)\Delta y_i \\ &= \frac{1}{2}\left(\frac{1}{V_{ti}^0}\right)\Delta y_i \end{aligned} \tag{2.42}$$

where Δy_i is given by,

$$\begin{aligned} \Delta y_i = {} & 2E_{qi}^{'0}\Delta E'_{qi} + 2x'_{di}(I_{Ii}^0\cos\delta_i^0\Delta E'_{qi} + E_{qi}^{'0}\cos\delta_i^0\Delta I_{Ii} - \\ & E_{qi}^{'0}I_{Ii}^0\sin\delta_i^0\Delta\delta_i - I_{Ri}^0\sin\delta_i^0\Delta E'_{qi} - E_{qi}^{'0}\sin\delta_i^0\Delta I_{Ri} - \\ & E_{qi}^{'0}I_{Ri}^0\cos\delta_i^0\Delta\delta_i) + 2x^{'2}_{di}\left(I_{Ri}^0\Delta I_{Ri} + I_{Ii}^0\Delta I_{Ii}\right) \end{aligned} \tag{2.43}$$

Finally to get $\Delta\dot{V}_{oi}$, we linearise (2.28) as,

$$\Delta\dot{V}_{oi} = \frac{1}{T_{ri}}\left(\Delta V_{oi} - \Delta|V_{ti}|\right) \tag{2.44}$$

From the above discussion, we define the state vectors for the linearised synchronous machine as,

$$\Delta x_i = \left[\Delta\delta_i, \Delta\omega_i, \Delta E'_{qi}, \Delta V_{oi}\right]' \tag{2.45}$$

$$\text{and input vector,} \quad \Delta u_i = [0, \Delta V_{si}, 0, 0]' \tag{2.46}$$

2.3.5 Synchronous Machine Model for Interconnected System

For a power system consisting of n generators, using the linearised equations given in Section 2.3.4, the state vectors and input vectors of all generators can be lumped together as follows:

$$\Delta x = [\Delta\delta x_1, \Delta\delta x_2, \cdots, \Delta\delta x_n]' \tag{2.47}$$

$$\Delta u = [\Delta\delta u_1, \Delta\delta u_2, \cdots, \Delta\delta u_n]' \tag{2.48}$$

Using equations in Section 2.3.4, we can write,

$$\begin{aligned} \dot{x} &= f(x,u) \\ \dot{\Delta}x &= A_{SYS}\Delta x + B_{SYS}\Delta u \\ \text{where } A_{SYS} &= \frac{\partial f}{\partial x}\Big|_{x=x_0,u=u_0} \text{ and } B_{SYS} = \frac{\partial f}{\partial u}\Big|_{x=x_0,u=u_0} \end{aligned} \tag{2.49}$$

where matrix A_{SYS} is the system transition matrix of size $(4n \times 4n)$ and B_{SYS} is the system input matrix of size $(4n \times 1)$

2.4 Chapter summary

Power system stability and classification are briefly presented in this chapter. The concepts of rotor angle stability and the dynamics of rotor swings are explained. The dynamics of rotor swings of a single machine connected to SMIB system is analysed. The structure of the conventional PSS is also briefed.

This chapter describes the network model used for the controller design and simulation studies. It also details the load flow analysis that needs to be carried out to determine the power flow across the network and the voltage vectors at various buses in the network. The mathematical model of the power system network and admittance matrix of the network are presented. Simplification of the network by eliminating all the nodes except the ones with generator is also included. Load flow analysis of the network using Newton-Raphson method is explained.

The linearised power system model and its state space representation which are used in power system controller design are explained. The nonlinear multimachine power system model using Park's transformation is presented. Steps involved in

obtaining the linearised multimachine model from the set of the nonlinear equations defining the system are given in detail. The state space representation of the linearised power system model is included.

Chapter 3

Decentralised Robust Controller Design

3.1 Introduction

Classical controller design methodologies such as pole placement technique were successfully applied to single input and single output systems. It became very difficult to design controllers for multi-input and multi-output systems using classical design methods. This prompted the need to develop optimal control design and also aero-space applications demanded optimal control to optimise the use of propellant to maximise the payload delivered to orbit. Optimal control techniques such as linear quadratic regulator (LQR) gave systematic steps to design optimal controllers for multi input-output systems by minimising the performance cost function.

To design controllers for systems with partial information and affected by sensor noises, linear quadratic Gaussian (LQG) stochastic optimal control was developed. LQG design techniques provided multivariable output feedback control. But these design methods failed to address robustness of control which is the fundamental requirement of any control system. Indeed, the enhancement of robustness is one of the main reasons for using feedback [79]. Robustness is the property of a control system, whereby it maintains specified performance and stability, in the presence of variations in the plant dynamics and errors in the plant model used in the controller design. To overcome the lack of robustness in the above mentioned control methods, robust control technique was developed. Among the robust control techniques, minimax LQG is a recently developed robust control methodology. We use minimax LQG approach to design the power system controllers. In this research, we extend the results and stability proofs proposed in [73], to include the uncertainties arising due to parameter variations around the Selected Equilibrium Point (SEP) when the load and generation changes in the controller design.

Minimax LQG controller design methodology can be considered as a robust version of standard LQG controller design methodology [80], [81]. It involves finding a controller to minimise the worst case of a quadratic cost functional. The worst case is taken over all admissible uncertainties in a given stochastic uncertain system

model [82]. Synthesising the minimax LQG controller involves solving two algebraic Riccati equations dependent on scaling parameters.

To solve the optimisation problem to synthesise the minimax LQG controller, we first convert it to an parameterised unconstrained optimisation problem using S-procedure. Then we express this parameterised objective function as linear matrix relation. This representation enables us to use the rank constrained optimisation solution proposed in [73], to solve the problem of optimising the performance bound.

The chapter is organised as follows: The first part gives a general introduction to the uncertainty model used. The main theorems and results referred to in the controller stability proof are given in the next part. The following part consists of the proposed controller design and stability proofs. In the final part of the chapter, the rank constrained LMI optimisation approach to synthesise the controller is presented.

3.2 Uncertainty Description

To apply minimax LQG methodology for the control system design, we should specify the uncertain system model against which the control system has to be robust.

Uncertainty arising over the nominal plant model can be modeled in different ways depending on the nature of the uncertainty expected and the type of the problem. By including all the possible uncertainties, the robustness of the system could be improved but this would lead to conservative design and increased complexity in the control design procedure and implementation. Thus, there is a trade off between the conservatism of the uncertain model used and the tractability of the corresponding robustness analysis and robust controller synthesis problem [83], [22].

Some of the common sources of uncertainty in a plant model are:

(i) Uncertainty in parameter values in the system model, which may be either constant or time varying.

(ii) Uncertainty due to unmodeled system dynamics.

(iii) Uncertainty due to the effect of neglecting nonlinearities in the system.

3.2.1 Uncertain system with norm bounded uncertainty

Let us consider a nominal linear system of the form,

$$\begin{aligned} \dot{x}(t) &= Ax(t) + B_1 u(t) \\ y &= C_2 x(t) \end{aligned} \tag{3.1}$$

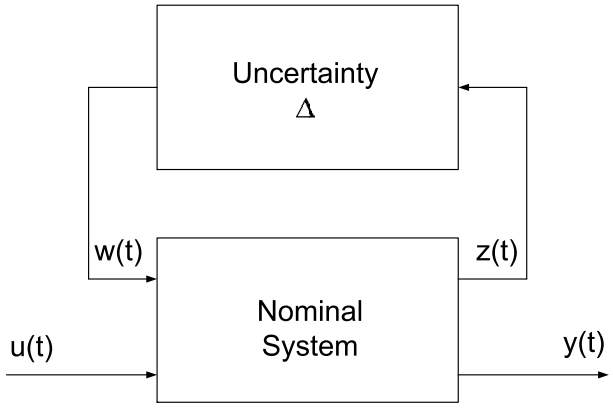

Figure 3.1. Nominal and uncertainty model

An important class of uncertain models involves separating the nominal system model from the uncertainty in the system in a feedback interconnection as shown in Figure 3.1. Such a feedback interconnection between the nominal model and uncertainty is sometimes referred to as Linear Fractional Transformation (LFT) [83]. In this model, uncertainty operator Δ is bounded as follows:

$$\|\Delta(t)\| \leq 1, \quad \forall t \quad \rightarrow \text{Norm bounded time varying uncertainty}$$
$$\|\Delta(j\omega)\| \leq 1, \quad \forall \omega \quad \rightarrow \text{Norm bounded uncertainty at all frequencies.}$$

Let us consider an uncertain system with norm bounded uncertainty. We can describe such a system using the state equations as [22]:

$$\dot{x}(t) = [A + B_2\Delta(t)C_1]\,x(t) + [B_1 + B_2\Delta(t)D_1]\,u(t) \tag{3.2}$$
$$y(t) = [C_2 + D_2\Delta(t)C_1]\,x(t) + D_2\Delta(t)D_1u(t) \tag{3.3}$$

where $x(t) \in \mathbf{R}^n$ is the state, $u(t) \in \mathbf{R}^m$ is the control input, $y(t) \in \mathbf{R}^l$ is the measured output and $\Delta(t) \in \mathbf{R}^{p\times q}$ is a time varying matrix of uncertainty parameters satisfying the bound

$$\Delta(t)'\Delta(t) \;\leq\; I \tag{3.4}$$

Equation (3.4) can be equivalently re-written as,

$$\|w(t)\| \;\leq\; \|z(t)\| \tag{3.5}$$

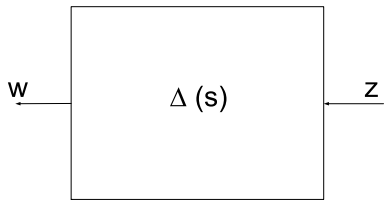

Figure 3.2. Uncertainty transfer function

Even though the uncertainty bound description given by (3.5) allows for time-varying uncertain parameters, it does not allow for dynamic uncertainties which may arise from unmodeled dynamics. Along with some other reasons [22], which lead to the representation of uncertainties using Integral Quadratic Constraints (IQCs).

3.2.2 Uncertain system with IQCs

An uncertain model should be capable of capturing the features of the real system and uncertainty in the system. The uncertainty model should also allow us to get a tractable solution to the control problem under consideration. There are number of advantages in using IQC representation. This class of uncertainties satisfying an IQC is richer than the class of uncertainties satisfying norm bound condition. It also allows us to model structured uncertain dynamics in systems subject to stochastic noise processes. Another key feature of IQC is that, the uncertainty is described purely in terms of bounds on the signals rather than bounding the uncertainty Δ directly [22].

Let us consider an uncertainty block as shown in Figure 3.2. Using Parseval's theorem, it follows that the frequency bound,

$$\|\Delta(j\omega)\| \leq 1, \quad \forall \quad \omega > 0$$

is equivalent to the time bound

$$\int_0^\infty \|w(t)\|^2 \mathrm{d}t \leq \int_0^\infty \|z(t)\|^2 \mathrm{d}t \tag{3.6}$$

for all signals $z(t)$, provided these integrals exist. The time domain uncertainty bound (3.6) is called an IQC [83]. Alternatively, if we are only interested in a finite

horizon control problem, we can have the following IQC (3.7), [83]:

$$\int_0^T \|w(t)\|^2 \mathrm{d}t \leq \int_0^T \|z(t)\|^2 \mathrm{d}t \tag{3.7}$$

The IQC uncertainty description can be extended to include energy bounded noise acting on the system. This situation is shown in Figure 3.3. Here $\tilde{w}(t)$ is the

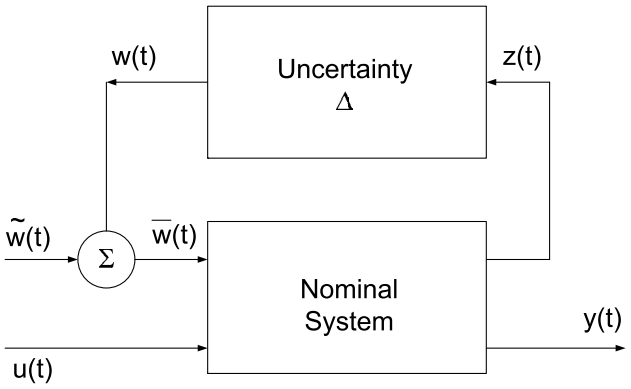

Figure 3.3. Uncertainty system with noise inputs.

energy bounded noise acting on the system. To model the uncertainty with noise, we can modify the IQC given by (3.6) as follows:

$$\int_0^\infty \|\bar{w}(t)\|^2 \mathrm{d}t \leq d + \int_0^\infty \|z(t)\|^2 \mathrm{d}t \tag{3.8}$$

The presence of the term d in equation (3.8) can allow for nonzero initial condition on the uncertainty conditions [22]. This property will be used in our controller design later.

3.2.3 Systems with multiple uncertainty blocks

In some systems, it may be necessary to model several uncertainty sources which are acting independently. We shall define a structured uncertainty in which multiple uncertainty blocks can be admitted [22]. Consider such a system with multiple

uncertainties as below:

$$\begin{aligned}
\dot{x}(t) &= Ax(t) + B_1 u(t) + \sum_{j=1}^{k} B_{2j}\xi_j(t);\\
z_1(t) &= C_{11}x(t) + D_{11}u(t);\\
z_2(t) &= C_{12}x(t) + D_{12}u(t);\\
&\vdots\\
z_k(t) &= C_{1k}x(t) + D_{1k}u(t);\\
y(t) &= C_2 x(t) + \sum_{j=1}^{k} D_{2j}\xi_j(t);
\end{aligned} \tag{3.9}$$

where $x(t) \in \mathbf{R}^n$ is the state, $u(t) \in \mathbf{R}^m$ is the control input, $\xi_1(t) \in \mathbf{R}^{q1}$, $\xi_2(t) \in \mathbf{R}^{q2}$, $\cdots$, $\xi_k(t) \in \mathbf{R}^{qk}$ are the uncertainty inputs, $z_1(t) \in \mathbf{R}^{q1}$, $z_2(t) \in \mathbf{R}^{q2}$, $\cdots$, $z_k(t) \in \mathbf{R}^{qk}$ are the uncertainty outputs, $y(t) \in \mathbf{R}^l$ is the measured output. Also in the above equations, $A, B_1, B_2, C_{11}, \cdots, C_{1k}, C_2, D_{11}, \cdots, D_{1k}$ and D_2 are constant matrices of suitable sizes. The uncertainty in the above system can be described by equations of the following form:

$$\begin{aligned}
\xi_1(t) &= \phi_1\left[t, x(\cdot), u(\cdot)\right];\\
\xi_2(t) &= \phi_2\left[t, x(\cdot), u(\cdot)\right];\\
&\vdots\\
\xi_k(t) &= \phi_k\left[t, x(\cdot), u(\cdot)\right];
\end{aligned} \tag{3.10}$$

For the uncertain system (3.9) and uncertainties (3.10), a bound on the uncertainty is determined by the following IQC condition [22]:

Definition 1 *An uncertainty of the form* (3.10)*, is an admissible uncertainty for the system* (3.9)*, if the following conditions hold: Given any locally square integrable control input u(·) and any corresponding solution to equations* (3.9)*,* (3.10) *defined on an existence interval (0,t*$_*$*), where t*$_*$ *is the upper limit of the time interval over which the solution exists, then there exists a sequence* $\{t_i\}_{i=1}^{\infty}$ *and constants* $d_1 \geq 0, \cdots, d_k \geq 0$ *such that* $t_i \to t_*, t_i \geq 0$ *and*

$$\int_0^{t_i} \|\xi_j(t)\|^2 dt \leq d_j + \int_0^{t_i} \|z_j(t)\|^2 dt \tag{3.11}$$

for all i and for $j = 1, 2, \cdots, k$. Also note that t_* and t_i may be equal to infinity.

It may also be noted that the class of uncertainties satisfying an IQC of the form (3.11) includes norm bounded uncertainties as particular case.

3.3 Collection of results referred in the thesis

The thesis uses several results from different sources to develop the controller design and stability proofs. Some of these results are included here for ready reference.

3.3.1 H^∞ norm

The H^∞ norm of the transfer function for a linear time invariant (LTI) system can be defined as follows [22]. Consider the LTI system,

$$\begin{aligned} \dot{x} &= Ax + Bw \\ z &= Cx, \end{aligned} \tag{3.12}$$

where A is a stable matrix and B, C are real constant matrices of appropriate dimensions. Also, $x \in \mathbf{R}^n$ is the state, $w \in \mathbf{R}^p$ is the disturbance input and $z \in \mathbf{R}^q$ is the uncertainty output. Suppose that the disturbance input satisfies $w(\cdot) \in L_2[0, +\infty)$. Let $\mathfrak{W}_{wz}$ denote the linear operator which maps $w(\cdot)$ to $z(\cdot)$ for this system. Furthermore, let $\|\mathfrak{W}_{wz}\|_\infty$ denote the induced norm of this linear operator:

$$\|\mathfrak{W}_{wz}\|_\infty := \sup_{w(\cdot)\in L_2[0,+\infty), \|w(\cdot)\|_2 \neq 0} \frac{\|z(\cdot)\|_2}{\|w(\cdot)\|_2} \tag{3.13}$$

where $z(\cdot)$ is the output of the system (3.12) corresponding to the disturbance input $w(\cdot)$ and the initial condition, $x(0) = 0$. The H^∞ norm of the corresponding transfer function $H_{wz}(s) = C(sI - A)^{-1}B$ is defined as follows:

$$\|H_{wz}(s)\|_\infty := \sup_{w\in\mathbf{R}} \sigma\left[C(sI - A)^{-1}B\right] \tag{3.14}$$

where $\sigma(\cdot)$ denotes the maximum singular value of a matrix. It then follows that $\|H_{wz}(s)\|_\infty = \|\mathfrak{W}_{wz}\|_\infty$ [84]. This fact motivates the notion $\|\mathfrak{W}_{wz}\|_\infty$ in (3.13).

3.3.2 Strict bounded real lemma

With reference to the H^∞ control theory and the associated Riccati equations following conditions are stated [22]:

Lemma 1 *(Strict bounded real lemma) The following statements are equivalent:*

(i) *A is stable and $\|C(sI - A)^{-1}B\|_\infty < 1$;*

(ii) *There exists a matrix $\tilde{P} > 0$ such that*

$$A'\tilde{P} + \tilde{P}A + \tilde{P}BB'\tilde{P} + C'C < 0; \tag{3.15}$$

(iii) *The Riccati equation*

$$A'P + PA + PBB'P + C'C = 0; \tag{3.16}$$

has a stabilising solution $P \geq 0$.

Furthermore, if these statements hold then $P < \tilde{P}$.

3.3.3 S-procedure

The robust control problems involving constrained optimisation can be converted to an intermediate unconstrained minimax optimisation problem and solved. In convex optimisation theories, this is achieved through Lagrange multipliers [85]. Another method similar to Lagrange multipliers is known as S-procedure which allows one to convert the constrained optimisation problem to unconstrained game type problem. S-procedure method converts the constrained optimisation problem to unconstrained minimax optimisation problem involving a number of "scaling" parameters which are analogous to Lagrange multipliers. In fact, the S-procedure converts robust control problems involving structured uncertainty into parameter dependent unstructured uncertainty and also leads to non conservative results for control problems [22]. A general and systematic description of the S-procedure can be found in [86].

Let the real-valued functionals $\mathfrak{g}_0(x)$, $\mathfrak{g}_1(x)$, $\cdots$, $\mathfrak{g}_k(x)$ be defined on an abstract space χ. Also, let $\tau_1, \cdots, \tau_k$ be a collection of real numbers and $\tau = [\tau_1, \cdots, \tau_k]'$, let

$$\mathrm{S}(\tau, x) := \mathfrak{g}_0(x) - \sum_{j=1}^{k} \tau_j \mathfrak{g}_j(x) \tag{3.17}$$

We consider the following conditions on the functionals $\mathfrak{g}_0(x)$, $\mathfrak{g}_1(x)$, $\cdots$, $\mathfrak{g}_k(x)$:

(i) $\mathfrak{g}_0(x) \geq 0$ for all x such that $\mathfrak{g}_1(x) \geq 0, \cdots, \mathfrak{g}_k(x) \geq 0$.

(ii) There exists a collection of constants $\tau_1 \geq 0, \cdots, \tau_k \geq 0$, such that $\mathrm{S}(\tau, x) \geq 0$ for all $x \in \chi$.

In general, condition (ii) implies condition (i). The term S-procedure refers to the procedure of replacing condition (i) by the stronger condition (ii). In a typical application of the S-procedure, the functionals $\mathfrak{g}_0(x)$, $\mathfrak{g}_1(x)$, $\cdots$, $\mathfrak{g}_k(x)$ depend on physical parameters [22].

Now let us consider a S-procedure result for a quadratic functional and k quadratic constraints [22]. Consider a linear system of the following form:

$$\begin{aligned} \dot{\eta}(t) &= \Phi\eta(t) + \Lambda\mu(t); \\ \sigma(t) &= \Pi\eta(t) \end{aligned} \tag{3.18}$$

where Φ is a stability matrix. For this system with a given initial condition $\eta(0) = \eta_0$, a corresponding set $\mathfrak{L} \subset L_2[0, +\infty)$ is defined as follows:

$$\mathfrak{L} := \left\{ \lambda(\cdot) = \begin{bmatrix} \sigma(\cdot) \\ \mu(\cdot) \end{bmatrix} : \mu(\cdot) \in L_2[0, +\infty) \text{ and } \eta(0) \ = \ \eta_0 \right\} \tag{3.19}$$

Also, we consider the following set of integral functionals mapping from $\mathfrak{L}$ into $\mathbf{R}$:

$$\begin{aligned} \mathfrak{g}_0(\lambda(\cdot)) &:= \int_0^\infty \lambda(t)' M_0 \lambda(t) \mathrm{d}t + \gamma_0; \\ \mathfrak{g}_1(\lambda(\cdot)) &:= \int_0^\infty \lambda(t)' M_1 \lambda(t) \mathrm{d}t + \gamma_1; \\ &\vdots \\ \mathfrak{g}_k(\lambda(\cdot)) &:= \int_0^\infty \lambda(t)' M_k \lambda(t) \mathrm{d}t + \gamma_k; \end{aligned} \tag{3.20}$$

where M_0, M_1, $\cdots$, M_k are given matrices and γ_0, γ_1, $\cdots$, γ_k are given constants.

Theorem 1 *Consider a system of the form* (3.18)*, a set* $\mathfrak{L}$ *of the form* (3.19) *and a set of functionals of the form* (3.20)*. Suppose that these functionals have the following properties:*

(i) $\mathfrak{g}_0(\lambda(\cdot)) \leq 0$ *for all* $\lambda(\cdot) \in \mathfrak{L}$ *such that*

$$\mathfrak{g}_1(\lambda(\cdot)) \geq 0, \mathfrak{g}_2(\lambda(\cdot)) \geq 0, \cdots, \mathfrak{g}_k(\lambda(\cdot)) \geq 0; \tag{3.21}$$

(ii) there exists a $\lambda(\cdot) \in \mathfrak{L}$ *such that*

$$\mathfrak{g}_1(\lambda(\cdot)) > 0, \mathfrak{g}_2(\lambda(\cdot)) > 0, \cdots, \mathfrak{g}_k(\lambda(\cdot)) > 0; \tag{3.22}$$

Then there will exist constants $\tau_1 \geq 0$, $\tau_2 \geq 0$, $\cdots$, $\tau_k \geq 0$ *such that*

$$\mathfrak{g}_0(\lambda(\cdot)) + \sum_{j=1}^{k} \tau_j \mathfrak{g}_j(\lambda(\cdot)) \leq 0 \tag{3.23}$$

for all $\lambda(\cdot) \in \mathfrak{L}$.

3.3.4 Collection of Definitions and Prepositions

Consider the uncertain system described by (3.9), associated with the system, is the following cost functional of the form;

$$J = \int_0^\infty [x(t)'Rx(t) + u(t)'G(u)]\, \mathrm{d}t \tag{3.24}$$

where $R = R' > 0$ and $G = G' > 0$ are given weighting matrices [87]. The uncertainties described by (3.10) are said to be admissible uncertainties if satisfying the following definition [22].

Definition 2 *Let* $S_1 > 0$, $S_2 > 0$, $\cdots$, $S_k > 0$, *be given positive-definite matrices. Then an uncertainty of the form* (3.10) *is an admissible uncertainty for the system* (3.9), *if the following conditions hold: Given any locally square integrable control input* $u(\cdot)$ *and any corresponding solution to equations* (3.9), (3.10) *with an interval of existence (0,*t_**) (that is* t_* *is the upper time limit for which the solution exists), then there exists a sequence* $\{t_i\}_{i=1}^{\infty}$ *such that* $t_i \to t_*, t_i \geq 0$ *and*

$$\int_0^{t_i} \left[\|z_j(t)\|^2 - \|\xi_j(t)\|^2\right] dt \geq -x(0)'S_j x(0) \tag{3.25}$$

for all i *and for* $j = 1, 2, \cdots, k$. *Also note that* t_* *and* t_i *may be equal to infinity.*

We shall consider a problem of optimizing of the worst case of the cost functional (3.24) via a linear state feedback controller of the form,

$$\begin{aligned} \dot{x}(t) &= A_c x_c(t) + B_c x(t); \quad x_c(0) = 0; \\ u(t) &= C_c x_c(t) + D_c x(t) \end{aligned} \tag{3.26}$$

When the controller of the form (3.26) is applied to the uncertain system then the resulting closed loop system can be described as,

$$\begin{aligned} \dot{h}(t) &= \hat{A}h(t) + \hat{B}_2\xi(t); \\ z(t) &= \hat{C}h(t); \\ u(t) &= \hat{K}h(t) \end{aligned} \tag{3.27}$$

where

$$h(t) = \begin{bmatrix} x(t) \\ x_c(t) \end{bmatrix}; \quad \xi(t) = \begin{bmatrix} \xi_1(t) \\ \vdots \\ \xi_k(t) \end{bmatrix}; \quad z(t) = \begin{bmatrix} z_1(t) \\ \vdots \\ z_k(t) \end{bmatrix}; \quad \hat{A} = \begin{bmatrix} A + B_1 D_c & B_1 C_c \\ B_c & A_c \end{bmatrix};$$

$$\hat{B}_2 = \begin{bmatrix} B_{21} \dots B_{2k} \\ 0 \quad \dots \quad 0 \end{bmatrix}; \quad \hat{C} = \begin{bmatrix} C_{11} + D_{11} D_c & D_{11} C_c \\ \vdots & \vdots \\ C_{1k} + D_{1k} D_c & D_{1k} C_c \end{bmatrix} \quad \hat{K} = \begin{bmatrix} D_c & C_c \end{bmatrix}.$$

Definition 3 *The controller* (3.26) *is said to be a guaranteed cost controller for the uncertain system* (3.9), (3.10) *with cost functional* (3.24) *and initial condition x(0) = x_0 if the following conditions hold [22]:*

(i) The matrix $\hat{A}$ defined in (3.27) *is stable.*

(ii) There exists a constant $c_0 > 0$ such that the following conditions hold: For all admissible uncertainties, the solution to the closed loop system (3.25), (3.27) *corresponding to the initial condition h(0) = $[x_0', 0]'$ satisfies*

$$[x(\cdot), u(\cdot), \xi_1(\cdot), \cdots, \xi_k(\cdot)] \in L_2[0, +\infty) \tag{3.28}$$

and hence, $t_* = \infty$. Also, the corresponding value of the cost functional (3.24) *satisfies the bound $J \leq c_0$.*

An uncertain system (3.9), (3.10) *with the cost function* (3.24) *which admits a guaranteed cost controller* (3.26) *with initial condition x(0) = x_0 is said to be guaranteed cost stabilisable with this initial condition.*

The absolute stability of the closed loop system (3.27) can be defined as follows [22]:

Definition 4 *The closed loop uncertain system* (3.27), (3.25) *is said to be absolutely stable if there exists a constant $c > 0$ such that the following conditions hold:*

(i) For any initial condition h(0) = h_0 and any uncertainty inputs $\xi_j(\cdot) \in L_2[0, +\infty)$, the system (3.27) *has a unique solution defined on $[0, +\infty)$.*

(ii) Given any admissible uncertainty for the uncertain system (3.27) *then all corresponding solutions to equations* (3.27), (3.25) *satisfy $[h(\cdot), \xi(\cdot), \cdots, \xi_k(\cdot)] \in L_2[0, +\infty)$ (hence, $t_* = \infty$) and*

$$\|h(\cdot)\|_2^2 + \sum_{j=1}^{k} \|\xi_j(\cdot)\|_2^2 \leq c\|h_0\|^2. \tag{3.29}$$

The required guaranteed cost controller can be constructed by solving a parameter dependant Riccati equation. This Riccati equation can be defined as follows [22]: Let $\tau_1 > 0, \cdots, \tau_k > 0$ be given constants and consider the following Riccati equation

$$\begin{aligned} &\left(A - B_1 G_\tau^{-1} D_\tau' C_\tau\right)' X_\tau + X_\tau \left(A - B_1 G_\tau^{-1} D_\tau' C_\tau\right) - X_\tau B_1 G_\tau^{-1} B_1 X_\tau \\ &+ X_\tau \tilde{B}_2 \tilde{B}_2' X_\tau + C_\tau' \left(I - D_\tau G_\tau^{-1} D_\tau'\right) C_\tau = 0 \end{aligned} \tag{3.30}$$

where

$$C_\tau := \begin{bmatrix} R^{\frac{1}{2}} \\ 0 \\ \sqrt{\tau_1} C_{11} \\ \vdots \\ \sqrt{\tau_k} C_{1k} \end{bmatrix}; \quad D_\tau := \begin{bmatrix} 0 \\ G^{\frac{1}{2}} \\ \sqrt{\tau_1} D_{11} \\ \vdots \\ \sqrt{\tau_k} D_{1k} \end{bmatrix};$$

$$G_\tau := D_\tau' D_\tau; \quad \tilde{B}_2 := \left[\tfrac{1}{\sqrt{\tau_1}} B_{21} \cdots \tfrac{1}{\sqrt{\tau_k}} B_{2k} \right].$$

The parameter $\tau_1 > 0, \cdots, \tau_k > 0$ are to be chosen so that this Riccati equation has a positive-definite solution $X_\tau > 0$. Hence we can consider a set $\mathfrak{T}_0 \subset \mathbf{R}^k$ defined

as follows:

$$\mathfrak{T}_0 := \left\{ \begin{array}{c} \tau = [\tau_1, \cdots, \tau_k] \in \mathbf{R}^k : \tau_1 > 0, \cdots, \tau_k > 0 \\ \text{and Riccati equation (3.30) has a solution } X_\tau > 0 \end{array} \right\} \tag{3.31}$$

If X_τ is the minimal positive-definite solution to Riccati equation (3.30), then the corresponding guaranteed cost controller to be considered is given by

$$u(t) = -G_\tau^{-1} \left(B_1' X_\tau + D_\tau' C_\tau \right) x(t) \tag{3.32}$$

In the above context, the following Theorem 2, [22], gives the bound on the cost function.

Theorem 2 *Consider the uncertain system* (3.9), (3.10) *with cost function* (3.24). *Then for any* $[\tau_1, \cdots, \tau_k]' \in \mathfrak{T}_0$, *the corresponding controller* (3.32) *is a guaranteed cost controller for this uncertain system with any initial condition* $x_0 \in \mathbf{R}^n$. *Furthermore, the corresponding value of the cost function* (3.24) *satisfies the bound*

$$J \leq x_0' X_\tau x_0 + \sum_{j=1}^{k} \tau_j x_0' S_j x_0 \tag{3.33}$$

for all admissible uncertainties and moreover, the closed loop uncertain system (3.9), (3.10), (3.32) *is absolutely stable.*

The following Theorem 3, [22], shows that the controller construction given in Theorem 2 can be used to construct a controller which approaches the minimax optimum.

Theorem 3 *Consider the uncertain system* (3.9), (3.10) *with cost function* (3.24) *with and suppose that* $B_{21} \neq 0, \cdots, B_{2k} \neq 0$. *Then:*

(i) Given a non-zero initial condition $x_0 \in \mathbf{R}^n$, *the uncertain system* (3.9), (3.10) *will be guaranteed cost stabilisable with initial condition x(0) =* x_0 *if and only if the set* $\mathfrak{T}_0$ *defined in* (3.31) *is not empty.*

(ii) Suppose the set $\mathfrak{T}_0$ *is not empty and let* Ξ *be the set of all admissible uncertainties for the uncertain system* (3.9), (3.10). *Also for any initial condition* $x_0 \neq 0$, *let* Θ *denote the set of all guaranteed cost controllers of the form* (3.26) *for the uncertain*

system with this initial condition. Then

$$\inf_{u(\cdot)\,\in\,\Theta}\ \sup_{\xi(\cdot)\,\in\,\Xi} J = \inf_{\tau\,\in\,\mathfrak{T}_0}\left[x_0' X_\tau x_0 + \sum_{j=1}^{k}\tau_j x_0' S_j x_0\right]. \tag{3.34}$$

3.4 Controller Design

Our aim is to design a robust output feedback controller which includes parameter variations, interconnection effects and any other local uncertainties as the admissible uncertainties in the controller design. Recent work by Li Li et al [73], describes the methodology to design decentralised robust output feedback control for large interconnected systems. In [73], a controller design scheme is proposed to design controllers for systems with randomly varying operating point; each operating point is considered as a mode and the jumping process from one mode to another is modeled as Markov jump parameter process. In [73], IQCs are used to describe the uncertainties and Linear Matrix Inequality (LMI) solution technique is used to solve the optimisation problem. Two classes of uncertainties are considered in [73], which are uncertainties in local subsystem model and uncertainties in interconnection signals from other subsystems and these uncertainties are defined using IQCs.

The results in [73] are extended in this thesis: We consider a deterministic system as compared to the randomly varying system in [73]. Also, we include the parameter variations around the model corresponding to the selected equilibrium point due to generation and load changes as additional uncertainty along with local and interconnection uncertainties. In this section complete problem formulation, stability proofs and optimisation procedure are given for the interconnected power system controller design method.

Let us consider a generator in a power system with variable power output $\rho(\cdot)$ In [88]. Each generator connected to the grid is treated as a subsystem and formulated as a system affected by parameter variations and by the interconnection effects. Effects due to parameter variations around the operating point and interconnection effects are treated as uncertainties on the subsystem. IQCs are used to describe the uncertainties and LMI optimisation technique is used to solve the optimisation problem.

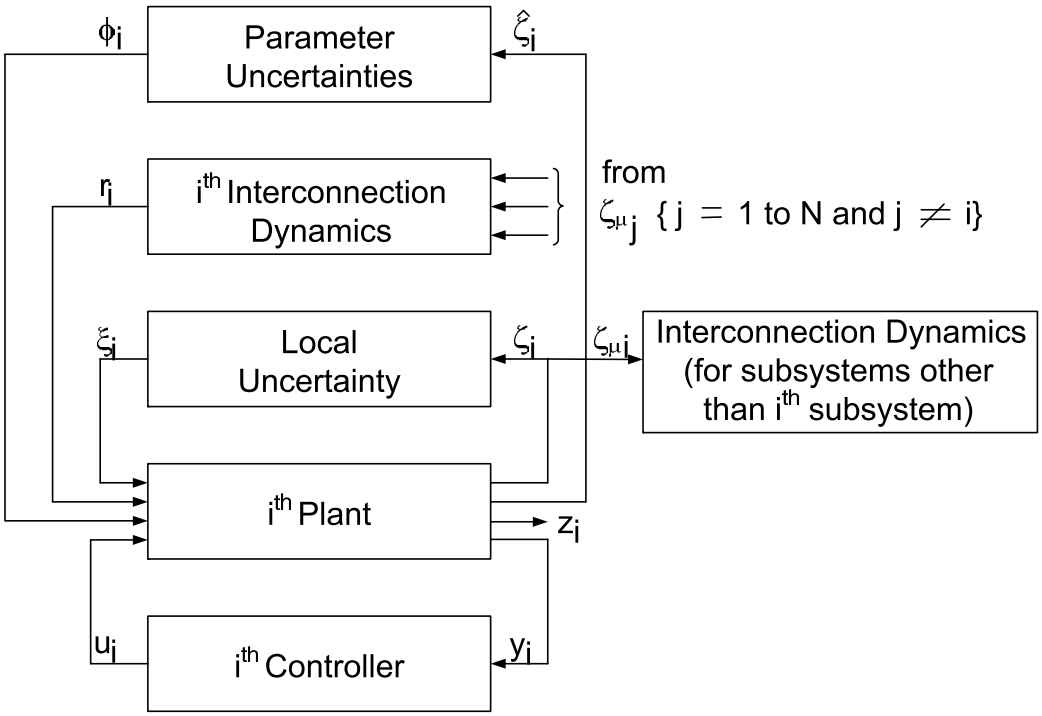

Figure 3.4. Subsystem configuration

We consider a large scale system $\mathbb{S}$ comprising of N subsystems $\mathbb{S}_i$, as shown in Figure 3.4, of the following form [89], [90] and [88]:

$$\begin{aligned}
\mathbb{S}_i : \dot{x}_i(t) &= A_i(\gamma)x_i(t) + B_i u_i(t) + E_i\xi_i(t) + \beta_i\phi_i(t) + L_i r_i(t),\\
z_i(t) &= C_i x_i(t) + D_i u_i(t),\\
\zeta_i(t) &= H_i x_i(t) + G_i u_i(t),\\
\hat{\zeta}_i(t) &= \alpha_i I x_i(t),\\
y_i &= C_{y,i}x_i(t) + D_{y,i}\xi_i(t),
\end{aligned} \tag{3.35}$$

where $A_i(\gamma)$ is the system matrix corresponding to the SEP with power output $\rho(\cdot) = \gamma$, x_i is the state vector and in the case of generators, it is obtained from the SEP (2.25) to (2.28), $x_i = [\Delta\delta_i, \Delta\omega_i, \Delta E_{qi}, \Delta V_{oi}]'$, u_i the control inputs which are the PSS outputs ΔV_{si}, $\xi_i \in \mathbf{R}^{p_i}$ is the perturbation, $\zeta_i \in \mathbf{R}^{h_i}$ is the uncertainty output (made up of both the system states, and the control inputs), $\hat{\zeta}_i$ is the uncertainty output due to parameter variation around operating point, $z_i \in \mathbf{R}^{q_i}$ is the controlled output of the subsystem which consists of both the subsystem states and control

inputs, and y_i is output of the system which is $\Delta\omega_i$ feedback to the controller. The input r_i is the interconnection signals from the other subsystems S_j, $j \neq i$, on the subsystem S_i. The input ξ_i describes the effect of local uncertain modeling errors in this subsystem and α_i and β_i are constants and will be defined later.

For the interconnected power system, the subsystem matrices A_i, B_i and L_i can be obtained from the system matrices A_{SYS} and B_{SYS} defined by (2.49) as follows:

$$
\begin{aligned}
A_i &= A_{SYS}\,[4i-3:4i, 4i-3:4i] && (3.36)\\
B_i &= B_{SYS}\,[4i-3:4i] && (3.37)\\
L_{iA1} &= A_{SYS}\,[4i-3:4i, 1:4(i-1)]\\
&\qquad \text{for } i = 2,\cdots,n \text{ and for } i = 1, L_{iA1}\text{is vacuous}\\
L_{iA2} &= A_{SYS}\,[4i-3:4i, 4(i+1)-3:4n]\\
&\qquad \text{for } i = 2,\cdots,n-1 \text{ and for } i = n, L_{iA2}\text{is vacuous}\\
L_{iA} &= [L_{iA1}, L_{iA2}]\\
L_{iB} &= [B_1,\cdots,B_{i-1},B_{i+1},\cdots,B_n]\\
L_i &= [L_{iA}, L_{iB}] && (3.38)
\end{aligned}
$$

where n is the number of subsystems.

The variations in $A_i(\cdot)$ due to load and generation changes are treated as an additional disturbance and the system is regarded as a perturbation of a linear fixed parameter system. The variations in the matrix $A_i(\cdot)$ can be regarded as modeling uncertainty and driven by $\phi_i(t)$, [91], where

$$\phi_i(t) := \frac{1}{\beta_i}\left[A_i(\gamma+\Delta\gamma) - A_i(\gamma)\right] x_i(t) \tag{3.39}$$

The designed controller will stabilize the nominal plant corresponding to the SEP with the specified parameter variations around the SEP provided, the constraint (3.39) is satisfied. The size of neighborhood is determined by the choice of α_i and β_i where positive real numbers α_i, β_i and $\gamma \in \Gamma$ be so chosen that

$$\sup_{\rho\in\Omega_\gamma} \|A_i(\rho) - A_i(\gamma)\| < \alpha_i\beta_i \tag{3.40}$$

where $\|\cdot\|$ in (3.40) denotes the largest singular value.

System $\mathbb{S}$ satisfies the following assumptions [73]:

Assumption 1 *For each $i = 1, \cdots, N$, given locally square integrable signals $[u_i(\cdot), r_i(\cdot), \xi_i(\cdot), \phi_i(\cdot)]$ for any initial condition $x_i(0) = x_{i0}$, the solution to the subsystem (3.35) exists on any finite time interval [0,T] of the interval [0, $+\infty$) and is locally square integrable i.e, $\int_0^T \|x_i(\cdot)\|^2 dt | x_{i0} < \infty$*

Assumption 2 *For all $i = 1, \cdots, N \quad D_i' D_i + G_i' G_i > 0, \quad D_{yi} D_{yi}' > 0.$*

Assumption 3 *The pair $(A_i, C_i' C_i)$, $i = 1, \cdots, N$, is observable.*

Assumption 4 *The pair (A_i, B_i), $i = 1, \cdots, N$, is stabilisable.*

Assumption 5 *For all $i = 1, \cdots, N$, $C_i' D_i = 0$, $H_i' G_i = 0$, $E_i D_{yi}' = 0$.*

Assumption 6 *For all $i = 1, \cdots, N$, $[E_i \; L_i] \neq 0$.*

The above assumptions are standard assumptions used in H_∞ type of problems. Assumption 1 states that the plant under consideration is well defined on each finite time sub interval $[0, T]$. Assumptions 2 to 4 are technical assumptions which will be used to prove the feasibility of the coupled Riccati equations and inequalities arising in the necessary part of Theorem 4; these assumptions formulate the basic controllability and observability properties of the uncertain system $\mathbb{S}$. They are often used in Riccati approach to robust control design [92] and [93]. Typically, these assumptions allow one to infer that the corresponding Riccati equations have positive definite and minimal solutions [92] and [94]. Assumptions 5 and 6 are made for convenience; they are not restrictive and are often made to simplify the derivation of robust control solutions.

3.4.1 Uncertainty Description

The uncertainties, in (3.35), are driven by signals $\xi_i(t), r_i(t)$ and $\phi_i(t)$ and their corresponding outputs are $\zeta_i(t), \zeta_\mu(t)$ and $\hat{\zeta}_i(t)$. We shall use the IQC description given by Definition 2 to characterise the uncertainties. Let M_{1i}, M_{2i}, M_{3i}, $i = 1, \cdots, N$ be three collections of positive definite symmetric matrices. The following definitions describe the three kinds of feasible uncertainty sets considered in this work.

Definition 5 *A collection of uncertainty inputs $\xi_i(\cdot), i = 1, \cdots, N$, represents an admissible uncertainty for the large scale system $\mathbb{S}$ if the following conditions hold:*

Given locally square integrable control inputs $u_i(\cdot)$, locally square integrable parameter variation inputs $\phi_i(\cdot)$,and locally square integrable interconnection inputs $r_i(\cdot), i = 1, \cdots, N$ there exists a sequence$\{t_l\}_{l=1}^{+\infty}, t_l \to +\infty$, such that

$$\int_0^{t_l} \left(\|\zeta_i(t)\|^2 - \xi_i(t)\|^2 \right) dt \geq -x'_{i0} M_{1i} x_{i0}, M_{1i} = M'_{1i} > 0, \quad \forall i = i = 1, \cdots, N \tag{3.41}$$

The set of all such admissible uncertainties is denoted by Ξ.

Definition 6 *A collection of uncertainty inputs $\phi_i(\cdot), i = 1, \cdots, N$ represents an admissible parameter variation for the large scale system $\mathbb{S}$ if the following conditions hold: Given any locally square integrable control inputs $u_i(\cdot)$, locally square integrable local uncertainty inputs $\xi_i(\cdot)$, and locally square integrable interconnection inputs $r_i(\cdot), i = 1, \cdots, N$ there exists a sequence$\{t_l\}_{l=1}^{+\infty}, t_l \to +\infty$, such that*

$$\int_0^{t_l} \left(\|\hat{\zeta}_i(t)\|^2 - \|\phi_i(t)\|^2 \right) dt \geq -x'_{i0} M_{2i} x_{i0}, M_{2i} = M'_{2i} > 0, \quad \forall i = i = 1, \cdots, N \tag{3.42}$$

The set of all such admissible parameter variation uncertainties is denoted by Ψ.

Definition 7 *The subsystem $\mathbb{S}_i$ of the large scale system $\mathbb{S}$ is said to have admissible interconnections to other subsystems of this large-scale system, if the following hold: Given any locally square integrable control inputs $u_i(\cdot)$, locally square integrable local uncertainty inputs $\xi_i(\cdot)$ and locally square integrable parameter variation inputs $\phi_i(\cdot), i = 1, \cdots, N$ there exists a sequence$\{t_l\}_{l=1}^{+\infty}, t_l \to +\infty$, such that*

$$\int_0^{t_l} \left(\sum_{\mu \neq i} \|\zeta_\mu(t)\|^2 - \|r_i(t)\|^2 \right) dt \geq -x'_{i0} M_{3i} x_{i0}, M_{3i} = M'_{3i} > 0, \quad \forall i = 1, \ldots, N; \tag{3.43}$$

The corresponding uncertain interconnection input $r_i(\cdot)$ is referred to as an admissible uncertain interconnection input. The set admissible interconnection inputs is denoted by Π.

With the uncertainties defined, we shall proceed to describe the decentralised robust controller.

3.4.2 Robust Decentralised Control

For uncertain large scale system $\mathbb{S}$ comprising subsystems $\mathbb{S}_i$ of the form (3.35) and subject to the constraints (3.41), (3.42) and (3.43), we consider the problem of decentralised absolute stabilisation by means of decentralised linear output feedback controllers of the form,

$$\begin{aligned} \dot{x}_{c,i}(t) &= A_{c,i}x_{c,i}(t) + B_{c,i}y_i(t); \\ u_i(t) &= K_{c,i}x_{c,i}(t), \end{aligned} \tag{3.44}$$

where $x_{ci} \in \mathbb{R}^{n_{ci}}$ is the i^{th} controller state vector.

We can define the absolute stability achieved through the decentralised linear output feedback controllers (3.44) using Definition 4, as follows:

Definition 8 *The large scale system $\mathbb{S}$ subject to perturbations and interconnections satisfying the constraints* (3.41), (3.42) *and* (3.43) *is said to be absolutely stabilisable via decentralised output feedback control if there exists a decentralised output feedback controller of the form* (3.44) *and a constant $C_1 > 0$ such that for any initial conditions $[x_i'(0), x_{ci}'(0)]$, any local uncertainty inputs $\xi_i(\cdot)$, parameter variation uncertainty inputs $\phi_i(\cdot)$, and any admissible interconnection inputs $r_i(\cdot)$ subject to constraints* (3.41), (3.42) *and* (3.43), *the signals $x_i(\cdot)$, $x_{ci}(\cdot)$, $u_i(\cdot)$, $\xi_i(\cdot)$, $\phi_i(\cdot)$ and $r_i(\cdot)$ belong to $L_2[0, +\infty)$ and are uniformly bounded.*

$$\begin{aligned} &\sum_{i=1}^{N} \left[\| x_i(\cdot) \|_2^2 + \| x_{ci}(\cdot) \|_2^2 + \| u_i(\cdot) \|_2^2 + \| \xi_i(\cdot) \|_2^2 + \| \phi_i(\cdot) \|_2^2 + \| r_i(\cdot) \|_2^2 \right] \leq \\ C_1 &\sum_{i=1}^{N} \left[\| x_i(0) \|_2^2 + \| x_{ci}(0) \|_2^2 \right] \end{aligned} \tag{3.45}$$

The stability property (3.45) provides a bound on the norm of closed loop transients, which is uniform with respect to admissible uncertainties and interconnections satisfying the magnitude constraints (3.41), (3.42) and (3.43). This justifies referring to this property as an absolute stability property.

One common approach to achieve robust stabilisation is via evaluation of the worst case performance of uncertain system. The idea is to seek a controller of the form (3.44), which achieves a bounded system performance measured in terms of

the performance cost,

$$\sup_{\Xi,\Psi,\Pi} \int_0^\infty \sum_{i=1}^N \|z_i\|^2 dt \tag{3.46}$$

where Ξ, Ψ and Π are admissible set of uncertainties and interconnection inputs given in Definitions 5, 6 and 7 respectively. Once such a controller is found, it is often possible to show that this controller is also absolutely stabilising in the sense of Definition 8. We note that in some problems given a set $\mathcal{U}$ of allowable controllers, it is possible to find a controller which attains a optimal system performance given by,

$$\inf_{\mathcal{U}} \sup_{\Xi,\Psi,\Pi} \int_0^\infty \sum_{i=1}^N \|z_i\|^2 dt \tag{3.47}$$

For other problems such as the one considered here, it is only possible to obtain a controller of the form (3.44) which guarantees a bound on the optimal system performance (3.47).

3.4.3 Controller Design and Stability Conditions

Let $\tau_i > 0, \eta_i > 0, \theta_i > 0, i = 1, \cdots, N$, be given constants, and $\bar{\theta}_i = \sum_{j=1, j\neq i}^N \theta_j$. We consider a collection of the coupled generalized algebraic Riccati equations (GAREs) [73]:

$$A_i' X_i + X_i A_i + \bar{C}_i' \bar{C}_i - X_i \left(B_i R_i^{-1} B_i' - \bar{B}_{2,i} \bar{B}_{2,i}' \right) X_i + \eta_i \alpha_i^2 I + X_i \left(\eta_i^{-1} \beta_i^2 \right) X_i = 0, \tag{3.48}$$

$$A_i' Y_i + Y_i A_i + Y_i \bar{B}_{2,i} \bar{B}_{2,i}' Y_i - \left(C_{y,i}' W_i^{-1} C_{y,i} - \bar{C}_i' \bar{C}_i \right) + \eta_i \alpha_i^2 I + Y_i \left(\eta_i^{-1} \beta_i^2 \right) Y_i = 0 \tag{3.49}$$

where $R_i = \bar{D}_i' \bar{D}_i, \quad W_i = \bar{D}_{y,i} \bar{D}_{y,i}'$ and

$$\begin{aligned}
\bar{C}_i &= \begin{bmatrix} C_i \\ (\tau_i + \bar{\theta}_i)^{1/2} H_i \end{bmatrix}, \\
\bar{D}_i &= \begin{bmatrix} D_i \\ (\tau_i + \bar{\theta}_i)^{1/2} G_i \end{bmatrix}, \\
\bar{B}_{2,i} &= \begin{bmatrix} \tau_i^{-1/2} E_i & \theta_i^{-1/2} L_i \end{bmatrix}, \\
\bar{D}_{y,i} &= \begin{bmatrix} \tau_i^{-1/2} D_{y,i} & 0 \end{bmatrix}.
\end{aligned} \tag{3.50}$$

Then associated with (3.48) and (3.49) is a collection of decentralized dynamic output feedback controllers of the form

$$\begin{aligned}\dot{x}_{c,i} &= \left[A_i - \left(B_i R_i^{-1} B_i' - \bar{B}_{2,i}\bar{B}_{2,i}' - \eta_i^{-1}\beta_i^2 I\right) X_i\right] x_{c,i}(t) \\ &\quad + \left(Y_i - X_i\right)^{-1} C_{y,i}' W_i^{-1}\left[y_i(t) - C_{y,i} x_{c,i}(t)\right], \\ u_i &= \left(-R_i^{-1} B_i' X_i\right) x_{c,i}(t). \end{aligned} \tag{3.51}$$

Furthermore, consider a set of vectors,

$$\begin{aligned}\mathcal{T} = \{\{\tau_i, \eta_i, \theta_i\}_{i=1}^N \in \mathbf{R}^{3N}, \tau_i > 0, \eta_i > 0, \theta_i > 0 : \text{ the set of coupled GAREs (3.48),} \\ \text{admits a set of solutions } X_i \geq 0 \text{and the set of coupled GAREs (3.49)} \\ \text{admits a set of solutions } Y_i \geq 0 \text{ such that } Y_i > X_i\}\end{aligned} \tag{3.52}$$

Note that the minimal positive definite solutions X_i to the coupled equations (3.48) as well as solutions Y_i to the GAREs (3.49) depending upon the chosen $\{\tau_i, \eta_i, \theta_i\}_{i=1}^N \in \mathcal{T}$ and this dependance is assumed throughout.

We can state the following Theorems 4 and 5 using the results of [73] and Theorem 3. Necessary and sufficient conditions for the uncertain interconnected system $\mathbb{S}$ to be robustly stabilisable by means of the controller (3.44) is given in the Theorem 4. Theorem 5 characterises guaranteed robust performance achievable by means of such controller.

Theorem 4 *Consider a large scale system* $\mathbb{S}$ *in which the uncertainties and interconnections satisfy the constraints* (3.41), (3.42) *and* (3.43). *This system is absolutely stabilisable via a decentralised dynamic output feedback controller of the form* (3.44) *if and only if the set* $\mathcal{T}$ *is non-empty.*

Theorem 5 *Given a vector of initial conditions* $x_i(0) = x_{i0}$, *consider a* $\mathcal{U}$ *of decentralised controllers* (3.44). *The optimal worst case performance achievable via decentralised controllers of the class* $\mathcal{U}$ *is upper bounded as follows:*

$$\inf_{\mathcal{U}} \sup_{\Xi,\Psi,\Pi} \int_0^\infty \sum_{i=1}^N \|z_i\|^2 dt \leq \inf_{\mathcal{T}} J(\tau, \eta, \theta) \tag{3.53}$$

where Ξ, Ψ *and* Π *are the sets of admissible uncertainties and admissible interconnection inputs given in Definitions 5, 6 and 7 respectively and*

$$J(\tau,\eta,\theta) \triangleq \sum_{i=1}^{N} x_{i0}' \left(X_i + \tau_i M_{1i} + \eta_i M_{2i} + \theta_i M_{3,i}\right) x_{i0}. \tag{3.54}$$

Suppose $\{\tau_i^*, \eta_i^*, \theta_i^*\}_{i=1}^N$ *attains the infimum on the right-hand side of* (3.53). *Then a decentralized controller satisfying this upper-bound is given by* (3.51) *in which* $\tau_i = \tau_i^*$,, $\eta_i = \eta_i^*$, *and* $\theta_i = \theta_i^*$, $i = 1, \cdots, N$ *with initial condition* $x_{c,i}(0) = x_i(0)$.

Remark 1 To achieve the claimed bound on the worst case performance, the optimisation problem defined on the right hand side of (3.53) must be solved, which requires the knowledge of plant initial states $x_i(0)$. When the plant's initial states are completely known, it is natural to pass that knowledge on to the controller by setting $x_{ci}(0) = x_i(0)$. In practice however, the initial state of the plant may not be known. As will be seen from the proof of Theorem 5, in that case an alternative stabilising controller can be obtained by letting $x_{ci}(0) = 0$. However, this controller will generally guarantee a higher bound on the system performance. Specifically in this case the bound on the performance is given by the quantity on the right hand side of (3.53) in which the matrices X_i is replaced with Y_i.

3.4.4 Proof of the "only if" part of Theorem 4: Necessary condition for absolute stability

Suppose given large scale system $\mathbb{S}$ is stabilisable via decentralised output feedback and condition (3.45) holds. That is, there exists a linear decentralised output feedback controller of the form (3.44), such that the corresponding closed loop system with uncertainty perturbations and interconnections of the sets Ξ, Ψ and Π satisfies (3.45). Then we conclude that there exists a decentralised controller of the form (3.44) and finite constant $c > 0$ such that,

$$\sup_{\Xi,\Psi,\Pi} \int_0^\infty \sum_{i=1}^{N} \|z_i\|^2 dt \;<\; c \tag{3.55}$$

Our objective is to infer from (3.55) that the set $\mathcal{T}$ is not empty. The proof of the statement will proceed as follows. First using the general S-procedure results of Section 3.3.3 and [22], we will show that condition (3.55) implies the solvability

of certain family of scaled H_∞ control problems. Each problem is formulated for a subsystem of an uncertain system (3.35), and involves some scaling parameters τ_i, η_i and θ_i. The next step will be to use the existing results of H_∞ control to establish that the vector of scaling parameters $\{\tau_i, \eta_i, \theta_i\}_{i=1}^N$ belongs to the set $\mathcal{T}$.

For an arbitrary pair of elements of Ξ, Ψ and Π, let us rewrite the corresponding closed loop system in the form,

$$\dot{\bar{x}}_i(t) = \bar{A}_i \bar{x}_i(t) + \tilde{B}_{2i} w_i(t) \tag{3.56}$$

where

$$\begin{aligned}
\bar{A}_i &= \begin{bmatrix} A_i & B_i K_{ci} \\ B_{ci} C_{yi} & A_{ci} \end{bmatrix}, \qquad \tilde{B}_{2i} = \begin{bmatrix} E_i & L_i & \beta_i I \\ B_{ci} D_{yi} & 0 & 0 \end{bmatrix} \\
\bar{x}_i(t) &= \begin{bmatrix} x_i' & x_{ci}' \end{bmatrix}', \\
w_i &= \begin{bmatrix} \xi_i'(t) & r_i'(t) & \phi_i'(t) \end{bmatrix}', \quad w = [w_1'(t) \cdots w_N'(t)]'
\end{aligned} \tag{3.57}$$

In view of (3.55), one can choose a sufficiently small constant $\varepsilon > 0$ such that,

$$(1+\varepsilon) \int_0^\infty \sum_{i=1}^N \|z_i\|^2 dt \;<\; c - \varepsilon \tag{3.58}$$

Let us define the following quadratic functionals,

$$\begin{aligned}
\mathfrak{g}_0(w) &= (1+\varepsilon) \int_0^\infty \sum_{i=1}^N \|z_i\|^2 dt - c + \varepsilon \\
\mathfrak{g}_{i,1}(w) &= \int_0^\infty \left(\|\zeta_i(t)\|^2 - \|\xi_i(t)\|^2 \right) dt + x_{i0}' M_{1i} x_{i0} \\
\mathfrak{g}_{i,2}(w) &= \int_0^\infty \left(\|\hat{\zeta}_i(t)\|^2 - \|\phi_i(t)\|^2 \right) dt + x_{i0}' M_{2i} x_{i0} \\
\mathfrak{g}_{i,3}(w) &= \int_0^\infty \left(\sum_{\mu \neq i} \|\zeta_\mu(t)\|^2 - \|r_i(t)\|^2 \right) dt + x_{i0}' M_{3i} x_{i0}
\end{aligned} \tag{3.59}$$

Now we consider a set of inputs $w \in L_2[0, +\infty)$ for which

$$\mathfrak{g}_{i,1}(w) \geq 0, \mathfrak{g}_{i,2}(w) \geq 0 \text{ and } \mathfrak{g}_{i,3}(w) \geq 0 \tag{3.60}$$

Condition (3.60) implies that each such input satisfies the constraints (3.41), (3.42) and (3.43) with $t_l = +\infty$. Therefore in view of the assumption that the chosen controller guarantees the satisfaction of the condition (3.55), inequality (3.60) implies that $\mathfrak{g}_0(w) < 0$ (follows from (3.58)). Further more since $M_{1i} > 0$, $M_{2i} > 0$ and $M_{3i} > 0$, one can choose an input w to satisfy the results of [22]. According to the S-procedure results in Theorem 1 and [22], these facts imply that one can find the constants $\tau_i \geq 0, \eta_i \geq 0, \theta_i \geq 0, i = 1, \cdots, N$ such that,

$$\mathfrak{g}_0(w) + \sum_{i=1}^{N} [\tau_i \mathfrak{g}_{i,1}(w) + \eta_i \mathfrak{g}_{i,2}(w) + \theta_i \mathfrak{g}_{i,3}(w)] \leq 0 \tag{3.61}$$

for any input $w \in L_2[0, +\infty)$. Using the notation $I(w) = \int_0^\infty \sum_{i=1}^N \|z_i\|^2 dt$, and substituting in (3.61)

$$\begin{aligned} I(w)(1 \ +\varepsilon) + \varepsilon - c + \sum_{i=1}^{N} \left[\tau_i \int_0^\infty \left(\|\zeta_i(t)\|^2 - \|\xi_i(t)\|^2 \right) dt + \tau_i \left(x_{i0}' M_{1i} x_{i0} \right) \right] \\ + \sum_{i=1}^{N} \left[\eta_i \int_0^\infty \left(\|\hat{\zeta}_i(t)\|^2 - \|\phi_i(t)\|^2 \right) dt + \eta_i \left(x_{i0}' M_{2i} x_{i0} \right) \right] \\ + \sum_{i=1}^{N} \left[\theta_i \int_0^\infty \left(\sum_{\mu \neq i} \|\zeta_\mu(t)\|^2 - \|r_i(t)\|^2 \right) + \theta_i \left(x_{i0}' M_{3i} x_{i0} \right) \right] dt \leq 0 \end{aligned} \tag{3.62}$$

on simplification we can write,

$$\begin{aligned} I(w) + \int_0^\infty \left[\left(\sum_{i=1}^{N} \left(\tau_i + \bar{\theta}_i \right) \|\zeta_i(t)\|^2 + \eta_i \|\hat{\zeta}_i(t)\|^2 \right) - \|\bar{w}_i(t)\|^2 \right] dt \leq \\ -\varepsilon I(w) + c - \varepsilon - \sum_{i=1}^{N} x_{i0}' \left(\tau_i M_{1i} + \eta_i M_{2i} + \theta_i M_{3i} \right) x_{i0} \end{aligned} \tag{3.63}$$

where

$$\bar{w}_i = \left[\tau_i^{\frac{1}{2}} \xi_i'(t), \quad \theta_i^{\frac{1}{2}} r_i'(t), \quad \eta_i^{\frac{1}{2}} \phi_i'(t) \right], \qquad \bar{w} = [\bar{w}_1, \cdots, \bar{w}_N]$$

In view of (3.63), a scaled subsystem can be written as,

$$\begin{aligned}
\dot{x}_i(t) &= A_i x_i(t) + B_i u_i(t) + \tau_i^{-\frac{1}{2}} E_i \tau_i^{\frac{1}{2}} \xi_i(t) + \eta_i^{-\frac{1}{2}} \beta_i \eta_i^{\frac{1}{2}} \phi_i(t) + \theta_i^{-\frac{1}{2}} L_i \theta_i^{\frac{1}{2}} r_i(t), \\
z_i(t) &= C_i x_i(t) + D_i u_i(t), \\
\left(\tau_i + \bar{\theta}_i\right)^{\frac{1}{2}} \zeta_i(t) &= \left(\tau_i + \bar{\theta}_i\right)^{\frac{1}{2}} H_i x_i(t) + \left(\tau_i + \bar{\theta}_i\right)^{\frac{1}{2}} G_i u_i(t), \\
\eta_i^{\frac{1}{2}} \hat{\zeta}_i(t) &= \eta_i^{\frac{1}{2}} \alpha I x_i(t), \\
y_i(t) &= C_{y,i} x_i(t) + D_{y,i} \xi_i(t),
\end{aligned} \tag{3.64}$$

The above equations can be written in a compact form as,

$$\begin{aligned}
\dot{x}_i(t) &= A_i x_i(t) + B_i u_i(t) + \hat{B}_{2,i} \bar{w}_i(t) \\
\bar{z}_i(t) &= \hat{C}_i x_i(t) + \hat{D}_i u_i(t), \\
y_i(t) &= C_{y,i} x_i(t) + \hat{D}_{y,i} \bar{w}_i(t),
\end{aligned} \tag{3.65}$$

where

$$\hat{B}_{2,i} = \begin{bmatrix} \bar{B}_{2,i} & \eta_i^{-\frac{1}{2}} \beta_i I \end{bmatrix}, \quad \bar{B}_{2,i} = \begin{bmatrix} \tau_i^{-\frac{1}{2}} E_i & \theta_i^{-\frac{1}{2}} L_i \end{bmatrix}, \quad \bar{z}_i = \begin{bmatrix} z_i & (\tau_i + \bar{\theta}_i)^{\frac{1}{2}} \zeta_i'(t) & \eta_i^{\frac{1}{2}} \hat{\zeta}_i'(t) \end{bmatrix}'$$

$$\hat{C}_i = \begin{bmatrix} \bar{C}_i \\ \eta_i^{\frac{1}{2}} \alpha_i I \end{bmatrix}, \quad \bar{C}_i = \begin{bmatrix} C_i \\ (\tau_i + \bar{\theta}_i)^{\frac{1}{2}} H_i \end{bmatrix}, \quad \hat{D}_i = \begin{bmatrix} \bar{D}_i \\ 0 \end{bmatrix}, \quad \bar{D}_i = \begin{bmatrix} D_i \\ (\tau_i + \bar{\theta}_i)^{\frac{1}{2}} G_i \end{bmatrix},$$

and $\hat{D}_{y,i} = \begin{bmatrix} \tau_i^{-\frac{1}{2}} D_{yi} & 0 & 0 \end{bmatrix}$

System (3.65) is similar to the systems described by (3.9) and (3.27). We can now use the results concerning the controller design of Section 3.3.4 and the relevant results of [22]. Using the Preposition 3 of Section 5.3.1 of [22], it can be shown that condition (3.63) implies that $\tau_i > 0, \eta > 0, \theta_i > 0$. We also note that in case of zero initial conditions $x_i(0) = 0$, $x_{c,i}(0) = 0$, in (3.63) we can use Preposition 2 of Section 5.3.1 of [22] and we can write,

$$c - \varepsilon - \sum_{i=1}^{N} x_{i0}' \left(\tau_i M_{1i} + \eta_i M_{2i} + \theta_i M_{3i}\right) x_{i0} \leq 0; \tag{3.66}$$

Substituting (3.66) in (3.63) we get,

$$I(w)+ \int_0^{\infty} \left[\left(\sum_{i=1}^{N} \left(\tau_i + \bar{\theta}_i\right) \|\zeta_i(t)\|^2 + \eta_i \|\hat{\zeta}_i(t)\|^2 \right) - \|\bar{w}_i(t)\|^2 \right] dt \leq -\varepsilon I(w)$$
$$\forall w \in L_2[0, +\infty); \tag{3.67}$$

We can write,

$$I(w) + \int_0^{\infty} \left[\left(\sum_{i=1}^{N} \left(\tau_i + \bar{\theta}_i\right) \|\zeta_i(t)\|^2 + \eta_i \|\hat{\zeta}_i(t)\|^2 \right) - \|\bar{w}_i(t)\|^2 \right] dt \geq$$
$$I(w) - \int_0^{\infty} \|\bar{w}_i(t)\|^2 dt \tag{3.68}$$

Using (3.67) and (3.68) we can write,

$$\begin{aligned} I(w) - \int_0^{\infty} \|\bar{w}_i(t)\|^2 dt &\leq -\varepsilon I(w) \\ (1+\varepsilon)\, I(w) &\leq \int_0^{\infty} \|\bar{w}_i(t)\|^2 dt \\ \frac{I(w)}{\int_0^{\infty} \|\bar{w}_i(t)\|^2 dt} &\leq \frac{1}{1+\varepsilon} \end{aligned} \tag{3.69}$$

Condition (3.69) implies that the closed loop augmented system corresponding to the chosen controller (3.44),

$$\begin{aligned} \dot{\bar{x}}(t) &= \bar{A}\bar{x}(t) + \tilde{B}_2 \bar{w}(t) \\ \bar{z}(t) &= \tilde{C}\bar{x}(t) \end{aligned} \tag{3.70}$$

where

$$A = diag\left\{\bar{A}_i\right\}_{i=1}^{N}, \quad \bar{x} = \left[\bar{x}_1', \cdots, \bar{x}_N'\right]',$$
$$\bar{B}_2 = diag\left\{ \begin{bmatrix} \tau_i^{-\frac{1}{2}} E_i & \theta_i^{-\frac{1}{2}} L_i & \eta_i^{-\frac{1}{2}} \beta_i I \\ \tau_i^{-\frac{1}{2}} B_{c,i} D_{yi} & 0 & 0 \end{bmatrix} \right\}_{i=1}^{N} \text{ and}$$
$$\tilde{C} = diag\left\{ \begin{bmatrix} \hat{C}_i & \hat{D}_i K_{c,i} \end{bmatrix} \right\}_{i=1}^{N}$$

satisfies the following H_∞ type condition given by (3.13)

$$\sup_{\bar{w}\neq 0, \bar{w}\in L_2[0,+\infty]} \frac{\int_0^{+\infty} \|\bar{z}\|^2 dt}{\int_0^{+\infty} \|\bar{w}\|^2 dt} < 1 \tag{3.71}$$

Here, $\bar{z}$ is the output of the system (3.70) corresponding to the initial condition $\bar{x}(0)$. Condition (3.71) implies that for each $i = 1, \cdots, N$,

$$\sup_{\bar{w}_i\neq 0, \bar{w}_i\in L_2[0,+\infty]} \frac{\int_0^{+\infty} \|\bar{z}_i\|^2 dt}{\int_0^{+\infty} \|\bar{w}_i\|^2 dt} < 1 \tag{3.72}$$

where $\bar{w}_i$ is the disturbance input of the closed loop subsystem corresponding to the open loop subsystem,

$$\begin{aligned} \dot{x}_i(t) &= A_i x_i(t) + B_i u_i(t) + \hat{B}_{2,i}\bar{w}_i(t) \\ \bar{z}_i(t) &= \hat{C}_i x_i(t) + \hat{D}_i u_i(t), \\ y_i(t) &= C_{y,i} x_i(t) + \hat{D}_{y,i}\xi_i(t), \quad x_i(0) = 0 \end{aligned} \tag{3.73}$$

and the i^{th} entry of the considered controller (3.44) with initial condition $x_{c,i} = 0$. To verify this fact, it is sufficient to let $\bar{w}_j(\cdot) = 0, j \neq i$, in (3.71) and (3.70). Indeed all entries $\bar{z}_j(\cdot), j \neq i$ of the corresponding output vector of the system (3.70) will be equal to zero, hence (3.72) follows from (3.71).

Condition (3.72) and the internal stability of the closed loop system imply that the entry u_i of the given controller of the form (3.44) solves the H_∞ disturbance attenuation problem. Now we can apply the results of [22] to each system (3.73). The satisfaction of (3.72) for the internally stable closed loop system consisting of (3.73) and the controller (3.44) is equivalent to the following conditions [22]: The GAREs (3.48) admit a set of minimal positive definite solutions $X_i > 0$ and GAREs (3.49) admit a set of positive definite solutions $Y_i > 0$ such that $Y_i > X_i$. That is the selected collection of the constants τ_i, η_i, θ_i belong to the set $\mathcal{T}$, hence this set is not empty. Also the system (3.65) is in similar form of the system mentioned in [22] (3.2.1), hence we can apply Lemma 3.2.3 of [22] to (3.65) and considering the GAREs in [22] and [73] we can write,

$$A_i' X_i + X_i A_i + \hat{C}_i'\hat{C}_i - X_i \left(B_i R_i^{-1} B_i' - \hat{B}_{2,i}\hat{B}_{2,i}' \right) X_i = 0, \tag{3.74}$$

$$A_i'Y_i + Y_iA_i + Y_i\hat{B}_{2,i}\hat{B}_{2,i}'Y_i - \left(C_{y,i}'W_i^{-1}C_{y,i} - \hat{C}_i'\hat{C}_i\right) = 0, \tag{3.75}$$

from (3.74) and (3.75) the GAREs mentioned in (3.48) and (3.49) are obtained.

3.4.5 Proof of the "if" statement of Theorem 4: The sufficient condition for absolute stabilisability

Suppose the set $\mathcal{T}$ defined in (3.52) is not empty. To prove the condition of absolute stabilisability, we wish to show that the set $\mathcal{T}$ being non empty implies the absolute stabilisability of the uncertain system (3.35) subject to the uncertainty constraints (3.41), (3.42) and (3.43) using Theorem 3.

To prove this claim, we select a collection $\{\tau_i, \eta_i, \theta_i\}_{i=1}^N \in \mathcal{T}$ and show that the decentralised controller (3.51) defined using this collection solves a H_∞ control problem for an aggregated system comprising scaled subsystems of the system (3.35) and driven by arbitrary square integrable interconnection and local uncertainty inputs. In particular, this will imply that this controller is an internally stabilising controller. Then we will show that, this fact and assumption of the theorem that the admissible uncertainty and interconnections of the system (3.35) satisfy IQCs (3.41), (3.42) and (3.43) together imply absolute stability of the corresponding uncertain closed loop system consisting of the plant (3.35) and the decentralised controller (3.51).

Let us choose a collection $\{\tau_i, \eta_i, \theta_i\}_{i=1}^N \in \mathcal{T}$. Associated with this collection of constants, consider the system

$$\begin{aligned}
\dot{x}(t) &= Ax(t) + Bu(t) + \hat{B}_2\bar{w}(t)\\
\bar{z}(t) &= \hat{C}x(t) + \hat{D}u(t),\\
y(t) &= C_yx(t) + \hat{D}_y\bar{w}(t),
\end{aligned} \tag{3.76}$$

where

$$\begin{aligned}
&x = [x_1', \cdots, x_N']', \quad u = [u_1', \cdots, u_N']', \quad A = diag\,(A_i)_{i=1}^N\\
&B = diag\,(B_i)_{i=1}^N, \quad \hat{B}_2 = diag\left(\hat{B}_{2,i}\right)_{i=1}^N, \quad \hat{C} = diag\left(\hat{C}_i\right)_{i=1}^N\\
&\hat{D} = diag\left(\hat{D}_i\right)_{i=1}^N, \quad C_y = diag\,(C_{y,i})_{i=1}^N, \quad \hat{D}_y = diag\left(\hat{D}_{y,i}\right)_{i=1}^N
\end{aligned}$$

in which $\hat{C}_i$, $\hat{D}_i$, $\hat{B}_{2,i}$ and $\hat{D}_{y,i}$ were defined in (3.50) and (3.65) and the input $\bar{w} \in L_2[0, +\infty)$. Also consider the matrices $X = diag\{X_i\}_{i=1}^N$ and $Y = diag\{Y_i\}_{i=1}^N$

whose entries X_i, Y_i satisfy the conditions described in the definition of set $\mathcal{T}$. Then we conclude that $X \geq 0$, $Y \geq 0$ solve the GAREs:

$$A'X + XA + \hat{C}'\hat{C} - X\left(BR^{-1}B' - \hat{B}_2\hat{B}_2'\right)X = 0, \tag{3.77}$$

$$A'Y + YA + Y\hat{B}_2\hat{B}_2'Y - \left(C_y'W^{-1}C_y - \hat{C}'\hat{C}\right) = 0, \tag{3.78}$$

$$Y > X, \qquad R := diag\{R_i\}_{i=1}^N, \quad W := diag\{W_i\}_{i=1}^N$$

Further more the pair (A, B) is stabilisable since the pair (A_i, B_i) corresponding to each subsystem of the system (3.76) are stabilisable by Assumption 4. Similarly the pairs $(A, \hat{C}'\hat{C})$ is observable through Assumption 3.

Consider the augmented controller (A_c, B_c, K_c) with state vector $x_c = [x_{c1}', \cdots, x_{cN}']'$ where $A_c = diag\,(A_{c,i})_{i=1}^N$, $B_c = diag\,(B_{c,i})_{i=1}^N$ and $K_c = diag\,(K_{c,i})_{i=1}^N$ and $A_{c,i}, B_{c,i}$ and $K_{c,i}$ are given by (3.51). Then it follows from the H_∞ control theory [22], that the controller (A_c, B_c, K_c) solves the output feedback H_∞ control problem defined by the system (3.76) and the H_∞ norm bound (3.71).

Write the closed loop system as,

$$\begin{aligned}
\dot{\tilde{x}}(t) &= \begin{bmatrix} A & BK_c \\ B_cC_y & A_c \end{bmatrix}\tilde{x}(t) + \begin{bmatrix} \hat{B}_2 \\ B_c\hat{D}_y \end{bmatrix}\bar{w}(t) \\
&\triangleq A_{cl}\tilde{x}(t) + B_{cl}\bar{w}(t), \\
\bar{z}(t) &= \begin{bmatrix} \hat{C} & \hat{D}K_c \end{bmatrix}\tilde{x}(t)
\end{aligned} \tag{3.79}$$

where $\tilde{x}(t) = (x', x_c')'$, then $\|T_{\bar{z}\bar{w}}\|_\infty < 1$; here $T_{\bar{z}\bar{w}}$ denotes the closed loop system mapping from $\bar{w}$ to $\bar{z}$. Because the chosen controller (3.51) solves the H_∞ problem, this fact implies internal stability of the closed loop system (3.79). Then $\|\tilde{x}\|_2^2 < \infty$, and hence there exists a sufficiently small $\epsilon > 0$ such that $\tilde{z} = \left[\epsilon^{\frac{1}{2}}\tilde{x}', \bar{z}'\right]'$ and $\|T_{\tilde{z}\bar{w}}\|_\infty < 1$.

Let,

$$\begin{aligned}
\bar{z} &= \begin{bmatrix} \hat{C} & \hat{D}K_c \end{bmatrix}\tilde{x}(t) \\
&= \check{C}\tilde{x}(t)
\end{aligned} \tag{3.80}$$

then,

$$\begin{aligned}\check{C}'\check{C} &= \begin{bmatrix} \hat{C}'\hat{C} & \hat{C}'\hat{D}K_c \\ K_c'\hat{D}'\hat{C} & K_c'\hat{D}'\hat{D}K_c \end{bmatrix} \\ &= \begin{bmatrix} \hat{C}'\hat{C} & 0 \\ 0 & XBR^{-1}\hat{D}'\hat{D}R^{-1}B'X \end{bmatrix} \\ &= \begin{bmatrix} \hat{C}'\hat{C} & 0 \\ 0 & XBR^{-1}B'X \end{bmatrix} \end{aligned} \tag{3.81}$$

In (3.81), $\hat{C}'\hat{D}K_c = 0$, using Assumption 5 and $K_c = -R^{-1}B'X$ and $R = \hat{D}'\hat{D}$, using equations (3.48), (3.48) and (3.51).

Applying the strict bounded real lemma conditions by Lemma 1 and equation (3.15), there exist $\check{P} > 0$, such that

$$\check{P}A_{cl} + A_{cl}'\check{P} + \check{P}B_{cl}B_{cl}'\check{P} + \begin{bmatrix} \hat{C}'\hat{C} & 0 \\ 0 & XBR^{-1}B'X \end{bmatrix} + \epsilon I < 0 \tag{3.82}$$

Using (3.80) and (3.81) we have,

$$\int_0^T \|\tilde{z}(t)\|^2 dt \leq \int_0^T \tilde{x}'(t) \left(\begin{bmatrix} \hat{C}'\hat{C} & 0 \\ 0 & XBR^{-1}B'X \end{bmatrix} + \epsilon I \right) \tilde{x}(t) dt$$

Let $\tilde{x}'\check{P}\tilde{x}$ be a Lyaponov function associated with the system (3.79). We have,

$$\begin{aligned}\frac{\mathrm{d}}{\mathrm{d}t}\left(\tilde{x}'\check{P}\tilde{x}\right) &= 2\tilde{x}'\check{P}\left(A_{cl}\tilde{x} + B_{cl}\bar{w}\right) \\ &= \tilde{x}'\left(\check{P}A_{cl} + A_{cl}'\check{P}\right)\tilde{x} + 2\tilde{x}'\check{P}B_{cl}\bar{w}\end{aligned} \tag{3.83}$$

Since the closed loop system is internally stable, then for each $\bar{w} \in L_2[0, +\infty)$ and any initial condition $\tilde{x}(0)$, we have $\tilde{z} \in L_2[0, +\infty)$. Let $T > 0$ be a time constant. Since $\check{P} > 0$ from Lemma 1, it is easy to establish by completing the squares that for any $\bar{w} \in L_2[0, +\infty)$ and any initial condition $\tilde{x}(0)$ and using equation (3.83), the

trajectories of the closed loop system (3.76) satisfy,

$$\begin{aligned}
\int_0^T \|\tilde{z}(t)\|^2 dt &\leq \int_0^T \|\tilde{z}(t)\|^2 dt + \tilde{x}(T)'\check{P}\tilde{x}(T) \\
&\leq \int_0^T \|\tilde{z}(t)\|^2 dt + \tilde{x}(T)'\check{P}\tilde{x}(T) - \tilde{x}'(0)\check{P}\tilde{x}(0) + \tilde{x}'(0)\check{P}\tilde{x}(0) \\
&\leq \int_0^T \|\tilde{z}(t)\|^2 dt + \tilde{x}'(0)\check{P}\tilde{x}(0) + \int_0^T \frac{\mathrm{d}}{\mathrm{d}t}\left[\tilde{x}'(t)\check{P}\tilde{x}(t)\right] dt \\
&= \int_0^T \tilde{x}'(t)\left(\begin{bmatrix} \hat{C}'\hat{C} & 0 \\ 0 & XBR^{-1}B'X \end{bmatrix} + \epsilon I\right)\tilde{x}(t)dt \\
&+ \int_0^T \tilde{x}'(t)\left(\check{P}A_{cl} + A_{cl}'\check{P}\right)\tilde{x}(t)dt + \int_0^T 2\tilde{x}'(t)\check{P}B_{cl}\bar{w}(t)dt + \tilde{x}'(0)\check{P}\tilde{x}(0) \\
&= \int_0^T \tilde{x}'(t)\left(\check{P}A_{cl} + A_{cl}'\check{P} + \begin{bmatrix} \hat{C}'\hat{C} & 0 \\ 0 & XBR^{-1}B'X \end{bmatrix} + \epsilon I\right)\tilde{x}(t)dt \\
&+ \int_0^T 2\tilde{x}'(t)\check{P}B_{cl}\bar{w}(t)dt + \tilde{x}'(0)\check{P}\tilde{x}(0) \\
&\leq \tilde{x}'(0)\check{P}\tilde{x}(0) - \int_0^T \left[\tilde{x}'(t)\check{P}B_{cl}B_{cl}'\check{P}\tilde{x}(t) - 2\tilde{x}'(t)\check{P}B_{cl}\bar{w}(t)\right] dt \\
&= \tilde{x}'(0)\check{P}(0)\tilde{x}(0) + \int_0^T \|\bar{w}(t)\|^2 dt - \int_0^T \|\bar{w}(t) - B_{cl}'\check{P}\tilde{x}(t)\|^2 dt \\
&\leq \|\bar{w}(t)\|_2^2 + \tilde{x}'(0)\check{P}(0)\tilde{x}(0)
\end{aligned} \tag{3.84}$$

Now, let $\{t_l\}_{l=1}^{+\infty}$ be a sequence of times as in Definitions 5, 6 and 7. Let us fix a time t_l and choose an arbitrary collection of admissible local uncertainty inputs $\xi_1(\cdot), \cdots, \xi_N(\cdot)$ and $\phi_1(\cdot), \cdots, \phi_N(\cdot)$ and admissible interconnection inputs $r_1(\cdot), \cdots, r_N(\cdot)$. Based on the chosen admissible uncertainties, we define the following uncertainty input $\bar{w}^l$ for the system (3.79):

$$\bar{w}^l(\cdot) = \left[\tau_1^{\frac{1}{2}}\xi_1^{l'}(\cdot), \eta_1^{\frac{1}{2}}\phi_1^{l'}(\cdot), \theta_1^{\frac{1}{2}}r_1^{l'}(\cdot), \cdots, \tau_N^{\frac{1}{2}}\xi_N^{l'}(\cdot), \eta_N^{\frac{1}{2}}\phi_N^{l'}(\cdot), \theta_N^{\frac{1}{2}}r_N^{l'}(\cdot)\right]' \tag{3.85}$$

where ξ_i^l, ϕ_i^l and r_i^l are obtained by extending the chosen admissible uncertainty inputs $\xi_i(\cdot)$ and $\phi_i(\cdot)$ and interconnections $r_i(\cdot)$ to have the value zero in the interval $[t_l, +\infty]$. Then, $\bar{w}^l(\cdot) \in L_2[0, +\infty)$ and hence condition (3.84) holds for this particular uncertainty input and for any $T = t_l$. From (3.41), (3.42), (3.43), (3.63), (3.65)

and (3.84) we have that,

$$\int_0^{t_l} \sum_{i=1}^{N} \left[\epsilon \|\tilde{x}_i\|^2 + \|z_i\|^2 + \| \left(\tau_i + \bar{\theta}_i\right) \zeta_i \|^2 + \|\eta_i \hat{\zeta}_i\|^2 \right] dt \leq \tilde{x}'(0) \check{P} \tilde{x}(0)$$
$$+ \int_0^{t_l} \sum_{i=1}^{N} \|\tau_i \xi_i\|_2^2 + \|\theta_i r_i\|_2^2 + \|\eta_i \phi_i\|_2^2$$
$$\int_0^{t_l} \sum_{i=1}^{N} \left(\epsilon \|\tilde{x}_i\|^2 + \|z_i\|^2 \right) dt \leq \tilde{x}'(0) \check{P} \tilde{x}(0)$$
$$+ \sum_{i=1}^{N} x_i'(0) \left(\tau_i M_{1i} + \eta_i M_{2i} + \theta_i M_{3i} \right) x_i(0) \tag{3.86}$$

Here $z_i(\cdot)$ are the outputs of (3.35) corresponding to the state trajectory of the closed loop system (3.79) driven by the input $\bar{w}^l(\cdot)$. By definition, we can choose $t_l \to +\infty$. Then (3.86) implies $x_i(\cdot), x_{c,i}(\cdot), u_i(\cdot) \in L_2[0, +\infty)$. Consequently $\xi_i(\cdot), \phi_i(\cdot), r_i(\cdot), \zeta_i(\cdot), \hat{\zeta}_i(\cdot) \in L_2[0, +\infty)$. Then condition (3.45) follows from (3.86), (3.41), (3.42) and (3.43). This proves absolute stability of the closed loop system as formulated in Definition 8.

3.4.6 Proof for Theorem 5

Let us write the GAREs for the aggregated system using (3.74) and (3.75) as,

$$\mathfrak{P}(X) := A'X + XA + \hat{C}'\hat{C} - X \left(BR^{-1}B' - \hat{B}_2 \hat{B}_2' \right) X = 0, \tag{3.87}$$

$$\mathfrak{Q}(Y) := A'Y + YA + Y\hat{B}_2\hat{B}_2'Y - \left(C_y' W^{-1} C_y - \hat{C}'\hat{C} \right) = 0, \tag{3.88}$$

Let $\Sigma = \begin{bmatrix} Y & X - Y \\ X - Y & Y - X \end{bmatrix}$ then we can show that the matrix Σ satisfy the following GAREs:

$$\Sigma A_{cl} + A_{cl}'\Sigma + \Sigma B_{cl} B_{cl}' \Sigma + \begin{bmatrix} \hat{C}'\hat{C} & 0 \\ 0 & XBR^{-1}B'X \end{bmatrix} = \begin{bmatrix} \mathfrak{Q}(Y) & \mathfrak{P}(X) - \mathfrak{Q}(Y) \\ \mathfrak{P}(X) - \mathfrak{Q}(Y) & \mathfrak{Q}(Y) - \mathfrak{P}(X) \end{bmatrix} = 0 \tag{3.89}$$

We shall evaluate the terms on the left hand side of the equation (3.89) as follows:

$$\begin{aligned}\Sigma A_{cl} + A_{cl}'\Sigma &= \begin{bmatrix} Y & X-Y \\ X-Y & Y-X \end{bmatrix}\begin{bmatrix} A & BK_c \\ B_cC_y & A_c \end{bmatrix} \\ &+ \begin{bmatrix} A' & C_y'B_c' \\ K_c'B' & A_c' \end{bmatrix}\begin{bmatrix} Y & X-Y \\ X-Y & Y-X \end{bmatrix} \\ &= \begin{bmatrix} YA+(X-Y)B_cC_Y & YBK_c+(X-Y)A_c \\ (X-Y)A+(Y-X)B_cC_Y & (X-Y)BK_c+(Y-X)A_c \end{bmatrix} + \\ &\quad \begin{bmatrix} A'Y+C_y'B_c'(X-Y) & A'(X-Y)+C_y'B_c'(Y-X) \\ K_c'B'Y+A_c'(X-Y) & K_c'B(X-Y)+A_c'(Y-X) \end{bmatrix} \end{aligned} \tag{3.90}$$

$$\begin{aligned}\Sigma B_{cl}B_{cl}'\Sigma &= \begin{bmatrix} Y & X-Y \\ X-Y & Y-X \end{bmatrix}\begin{bmatrix} \hat{B}_2 \\ B_c\hat{D}_y \end{bmatrix}\begin{bmatrix} \hat{B}_2' & \hat{D}_y'B_c' \end{bmatrix}\begin{bmatrix} Y & X-Y \\ X-Y & Y-X \end{bmatrix} \\ &= \begin{bmatrix} Y\hat{B}_2+(X-Y)B_c\hat{D}_y \\ (X-Y)\hat{B}_2+(Y-X)B_c\hat{D}_y \end{bmatrix} \times \\ &\quad \begin{bmatrix} \hat{B}_2'Y+\hat{D}_y'B_c'(X-Y) & \hat{B}_2'(X-Y)+\hat{D}_y'B_c'(Y-X) \end{bmatrix} \\ &= \begin{bmatrix} a_{11} & a_{12} \\ a_{21} & a_{22} \end{bmatrix} \end{aligned} \tag{3.91}$$

where

$$\begin{aligned} a_{11} &= \left[Y\hat{B}_2+(X-Y)B_c\hat{D}_y\right]\left[\hat{B}_2'Y+\hat{D}_y'B_c'(X-Y)\right], \\ a_{12} &= \left[Y\hat{B}_2+(X-Y)B_c\hat{D}_y'\right]\left[\hat{B}_2'(X-Y)+\hat{D}_y'B_c'(Y-X)\right] \\ a_{21} &= \left[(X-Y)\hat{B}_2+(Y-X)B_c\hat{D}_y\right]\left[\hat{B}_2'Y+\hat{D}_y'B_c'(X-Y)\right] \\ a_{22} &= \left[(X-Y)\hat{B}_2+(Y-X)B_c\hat{D}_y\right]\left[\hat{B}_2'(X-Y)+D_y'B_c'(Y-X)\right] \end{aligned}$$

Let

$$\Sigma A_{cl} + A_{cl}'\Sigma + \Sigma B_{cl}B_{cl}'\Sigma + \begin{bmatrix} \hat{C}'\hat{C} & 0 \\ 0 & XBR^{-1}B'X \end{bmatrix} = \begin{bmatrix} \lambda_{11} & \lambda_{12} \\ \lambda_{21} & \lambda_{22} \end{bmatrix} \tag{3.92}$$

Using equation (3.51) we have,

$$\begin{aligned} A_c &= A - BR^{-1}B'X + \hat{B}_2\hat{B}_2'X - (X-Y)^{-1}C_y'W^{-1}C_y \\ K_c &= -R^{-1}B'X \quad \text{and} \quad B_c = (Y-X)^{-1}C_y'W^{-1} \end{aligned} \tag{3.93}$$

From (3.49), (3.75), (3.90), (3.91), (3.92) and (3.93) we have,

$$\begin{aligned} \lambda_{11} &= [YA + (X-Y)B_cC_Y] + \left[A'Y + C_y'B_c'(X-Y)\right] \\ &\quad + \left\{\left[Y\hat{B}_2 + (X-Y)B_c\hat{D}_y\right]\left[\hat{B}_2'Y + \hat{D}_y'B_c'(X-Y)\right]\right\} + \hat{C}'\hat{C} \\ &= YA - C_y'W^{-1}C_y + A'Y - C_y'C_yW^{-1} + Y\hat{B}_2\hat{B}_2'Y - Y\hat{B}_2\hat{D}_y'C_yW^{-1} - C_y'W^{-1}\hat{D}_y\hat{B}_2'Y \\ &\quad + C_y'W^{-1}C_y + \hat{C}'\hat{C} \\ &= A'Y + YA + Y\hat{B}_2\hat{B}_2'Y - \left(C_y'W^{-1}C_y - \hat{C}'\hat{C}\right)\mathfrak{Q}(Y) = 0 \end{aligned} \tag{3.94}$$

$$\begin{aligned} \lambda_{12} &= [YBK_c + (X-Y)A_c] + \left[A'(X-Y) + C_y'B_c'(Y-X)\right] \\ &\quad + \left\{\left[Y\hat{B}_2 + (X-Y)B_c\hat{D}_y'\right]\left[\hat{B}_2'(X-Y) + \hat{D}_y'B_c'(Y-X)\right]\right\} \\ &= -YBR^{-1}B'X + XA - XBR^{-1}B'X + X\hat{B}_2\hat{B}_2'X - X(Y-X)^{-1}C_y'W^{-1}C_y - YA \\ &\quad + YBR^{-1}B'X - Y\hat{B}_2\hat{B}_2'X + Y(Y-X)^{-1}C_y'W^{-1}C_y + A'X - A'Y + C_y'C_yW^{-1} \\ &\quad + Y\hat{B}_2\hat{B}_2'X - Y\hat{B}_2\hat{B}_2'Y + Y\hat{B}_2\hat{D}_y'C_yW^{-1} + C_y'W^{-1}\hat{D}_y\hat{B}_2'(X-Y) + C_y'W^{-1}C_y \\ &= A'X + AX - A'Y - YA - XBR^{-1}B'X + X\hat{B}_2\hat{B}_2'X - Y\hat{B}_2\hat{B}_2'Y + C_y'W^{-1}C_y \\ &= \mathfrak{P}(X) - \mathfrak{Q}(Y) = 0 \end{aligned} \tag{3.95}$$

$$\lambda_{21} = \lambda_{12} = 0 \tag{3.96}$$

$$
\begin{aligned}
\lambda_{22} &= [(X-Y)BK_c + (Y-X)A_c] + [K_c'B(X-Y) + A_c'(Y-X)] \\
&+ \left\{ \left[(X-Y)\hat{B}_2 + (Y-X)B_c\hat{D}_y \right] \left[\hat{B}_2'(X-Y) + D_y'B_c'(Y-X) \right] \right\} \\
&= -XBR^{-1}B'X + YBR^{-1}B'X + YA - YBR^{-1}B'X + Y\hat{B}_2\hat{B}_2'X \\
&- Y(Y-X)^{-1}C_y'W^{-1}C_y - XA + XBR^{-1}B'X - X\hat{B}_2\hat{B}_2'X \\
&+ X(Y-X)^{-1}C_y'W^{-1}C_y - XBR^{-1}B'X + YBR^{-1}B'X + A'Y - XBR^{-1}B'X \\
&+ X\hat{B}_2\hat{B}_2'Y - C_y'W^{-1}C_y(X-Y)^{-1}Y - A'X + XBR^{-1}B'X - X\hat{B}_2\hat{B}_2'X \\
&+ C_y'W^{-1}C_y(X-Y)^{-1}X + X\hat{B}_2\hat{B}_2'X - X\hat{B}_2\hat{B}_2'Y - Y\hat{B}_2\hat{B}_2'X + Y\hat{B}_2\hat{B}_2'Y \\
&+ (X-Y)\hat{B}_2\hat{D}_y'C_yW^{-1} + C_y'W^{-1}\hat{D}_y\hat{B}_2'(X-Y) - C_y'W^{-1}C_y + XBR^{-1}B'X \\
&= A'Y + YA - A'X - XA + y\hat{B}_2\hat{B}_2'Y - C_y'W^{-1}C_y + XBR^{-1}B'X - X\hat{B}_2\hat{B}_2'X \\
&= \mathfrak{P}(Y) - \mathfrak{Q}(X) = 0
\end{aligned} \tag{3.97}
$$

Equations (3.94) to (3.97) show that Σ satisfies GAREs (3.89). Now choose $\tilde{x}'(t)\Sigma\tilde{x}(t)$ as candidate Lyapunov function similar to (3.83), (3.84) and (3.86) we have,

$$
\int_0^{t_l} \|\bar{z}\|^2 dt \leq \|\bar{w}\|^2 + \tilde{x}'(0)\Sigma\tilde{x}(0) \tag{3.98}
$$

$$
\int_0^{t_l} \sum_{i=1}^{N} \|z_i\|^2 dt \leq \tilde{x}'(0)\Sigma\tilde{x}(0) + \sum_{i=1}^{N} x_i'(0) \left(\tau_i M_{1i} + \eta_i M_{2i} + \theta_i M_{3i}\right) x_i(0) \tag{3.99}
$$

where $\bar{z}$ is the output of the closed loop system (3.79) and $z_i(\cdot)$ are the outputs of (3.35) corresponding to the state trajectory of the closed loop system (3.79) driven by the input $\bar{w}^l(\cdot)$ in (3.85). Therefore

$$
\sup_{\Xi,\Psi,\Pi} \int_0^{+\infty} \sum_{i=1}^{N} \|z_i\|^2 dt \leq \tilde{x}'(0)\Sigma\tilde{x}(0) + \sum_{i=1}^{N} x_i'(0) \left(\tau_i M_{1i} + \eta_i M_{2i} + \theta_i M_{3i}\right) x_i(0) \tag{3.100}
$$

We have

$$\begin{aligned}
\tilde{x}'\Sigma\tilde{x} &= \begin{bmatrix} x & x_c \end{bmatrix} \begin{bmatrix} Y & X-Y \\ X-Y & Y-X \end{bmatrix} \begin{bmatrix} x \\ x_c \end{bmatrix} \\
&= x'Yx + x_c'(X-Y)x + x'(X-Y)x_c + x_c'(Y-X)x_c \\
&= x'Yx - x_c'(Y-X)x - x'(Y-X)x_c + x_c'(Y-X)x_c \\
&= x'Yx + (x_c'-x)'(Y-X)x_c - x_c'(Y-X)x + x'(Y-X)x - x'(Y-X)x \\
&= x'Xx + (x_c-x)'(Y-X)x_c - (x_c'-x)(Y-X)x \\
&= x'Xx + (x_c-x)'(Y-X)(x_c-x) \qquad (3.101)
\end{aligned}$$

Using (3.101) in (3.100), we can write,

$$\begin{aligned}
\sup_{\Xi,\Psi,\Pi} \int_0^{+\infty} \sum_{i=1}^{N} \|z_i\|^2 dt \leq\ & x'(0)Xx(0) + [x_c(0)-x(0)]'(Y-X)[x_c(0)-x(0)] \\
& + \sum_{i=1}^{N} x_i'(0)\left(\tau_i M_{1i} + \eta_i M_{2i} + \theta_i M_{3i}\right) x_i(0) \\
=\ & \sum_{i=1}^{N} x_i'(0)\left(X_i + \tau_i M_{1i} + \eta_i M_{2i} + \theta_i M_{3i}\right) x_i(0) \qquad (3.102)
\end{aligned}$$

by letting $x_c(0) = x(0)$. It is obvious from (3.102) that (3.53) holds and provides the smallest bound over all $x_c(0)$. This concludes the proof.

3.4.7 Rank Constrained LMI Realisation

LMIs in robust control

We can reduce a very wide variety of problems arising in system and control theory to a few standard convex or quasi-convex optimisation problems involving linear matrix inequalities (LMIs). In comparison with the conventional approach to seek an analytic or frequency-domain solution to the matrix inequalities, in certain situations numerical solutions to matrix inequalities can be obtained more efficiently using LMIs, [95]. The robust control analysis and design generally involves the solution of Lyaponov and Riccati equations. Using LMIs, solutions for the robust control and optimisation problem can be achieved quite easily [38, 96].

Let us consider a system with rational transfer function matrix $G(s)$ and described by (3.103):

$$\begin{aligned} \dot{x}(t) &= Ax(t) + Bu(t) \\ y(t) &= Cx(t) + Du(t) \end{aligned} \tag{3.103}$$

If all the poles of $G(s)$ are in the left half of the s-plane then,

$$\|G(s)\|_\infty := \sup_{\omega \in \mathbf{R}} \{\sigma\left[G(j\omega)\right]\} \tag{3.104}$$

The transfer function of the system (3.103) will satisfy (3.104) if and only if, the Riccati equation (3.105),

$$A^T P + PA + C^T C + \left(PB + C^T D\right)\left(I - D^T D\right)\left(PB + C^T D\right)^T \tag{3.105}$$

has a positive solution, $P = P^T > 0$ [38]. Here, equation (3.105) is a Quadratic Matrix Inequality (QMI). We can convert the solvability of the QMI (3.105) into a LMI condition as follows [38]. The solvability of (3.105) is equivalent to

$$P > 0, \quad \begin{bmatrix} A^T P + PA + C^T CPB + C^T \\ B^T P + D^T CD^T D - I \end{bmatrix} \leq 0 \tag{3.106}$$

The above equation is a standard LMI with positive matrix P and solution of the LMI equation (3.105) can be used to solve the control problem [38].

Solution to optimisation problem through rank constrained LMIs

Optimisation algorithm proposed by [97], has been used to solve the optimisation problem on the right hand side of (3.53). Here, the idea is to replace the optimisation problem $\inf_{\mathcal{T}} J(\tau, \eta, \theta)$ with an equivalent optimisation problem involving rank constrained LMIs.

To introduce the rank constrained LMI optimisation problem related to the optimisation problem stated in Theorem 5, consider the following matrix inequalities, instead of the Riccati equations (3.48), (3.74)

$$A_i' X_i + X_i A_i + \hat{C}_i' \hat{C}_i - X_i \left(B_i R_i^{-1} B_i' - \hat{B}_{2,i} \hat{B}_{2,i}'\right) X_i < 0, \tag{3.107}$$

by left and right multiplying (3.107) with $\tilde{X}_i = X_i^{-1}$, we get,

$$\tilde{X}_i A_i' + A_i \tilde{X}_i + \tilde{X}_i \hat{C}_i' \hat{C}_i \tilde{X}_i - \left[B_i R_i^{-1} B_i' - \hat{B}_{2,i} \hat{B}_{2,i}' \right] < 0, \tag{3.108}$$

Introducing matrices F_i of appropriate dimensions, without changing the feasibility of (3.108), we add a quadratic term of F_i to the left-hand side of (3.108) as follows,

$$\tilde{X}_i A_i' + A_i \tilde{X}_i + \tilde{X}_i \hat{C}_i' \hat{C}_i \tilde{X}_i + \hat{B}_{2,i} \hat{B}_{2,i}' + F_i' R_i F_i + B_i F_i + F_i' B_i' < 0, \tag{3.109}$$

Using (3.50), the terms of (3.109) can be represented as follows,

$$\begin{aligned} \hat{B}_{2,i} \hat{B}_{2,i}' &= \tau_i^{-1} E_i E_i' + \theta_i^{-1} L_i L_i' + \eta_i^{-1} \beta_i^2 I \\ \tilde{X}_i \hat{C}_i' \hat{C}_i \tilde{X}_i &= \tilde{X}_i \left[C_i' C_i + (\tau_i + \bar{\theta}_i) H_i' H_i + \eta_i \alpha_i^2 I \right] \tilde{X}_i \\ F_i' R_i F_i &= F_i' \left[D_i' D_i + (\tau_i + \bar{\theta}_i) G_i' G_i \right] F_i \end{aligned} \tag{3.110}$$

Let $\tilde{\tau}_i = \tau_i^{-1}, \tilde{\eta}_i = \eta_i^{-1}, \tilde{\theta}_i = \theta_i^{-1}$. By combining (3.109), (3.110) and applying Schur complement, we obtain the following LMIs with variables $\tilde{X}_i, F_i, \tilde{\tau}_i, \tilde{\theta}_i, \tilde{\eta}_i$:

$$\begin{bmatrix} N_i & \alpha_i \tilde{X}_i & F_i' D_i' + X_i C_i' & Q_i \\ \star & -\tilde{\eta}_i I & 0 & 0 \\ \star & \star & -I & 0 \\ \star & \star & \star & -\Theta_i \end{bmatrix} < 0 \tag{3.111}$$

where

$$\begin{aligned} N_i &= \tilde{X}_i A_i' + A_i \tilde{X}_i + \tilde{\tau}_i E_i E_i' + \tilde{\theta}_i L_i L_i' + \tilde{\eta}_i \beta_i^2 I + B_i F_i + F_i' B_i' \\ Q_i &= \left[F_i' G_i' + \tilde{X}_i' H_i', \cdots, F_i' G_i' + \tilde{X}_i' H_i' \right] \quad (N\text{entries}) \\ \Theta_i &= diag \left[\tilde{\tau}_i I, \tilde{\theta}_1 I, \cdots, \tilde{\theta}_{i-1} I, \tilde{\theta}_{i+1} I, \cdots, \tilde{\theta}_N I \right]. \end{aligned}$$

Similarly, by substituting (3.50), into (3.49) and applying the Schur complement, we obtain following LMIs with variables $Y_i, \tau_i, \eta_i, \theta_i$:

$$\begin{bmatrix} M_i & \beta_i Y_i & Y_i E_i & Y_i L_i \\ \star & -\eta_i I & 0 & 0 \\ \star & \star & -\tau_i I & 0 \\ \star & \star & \star & -\theta_i I \end{bmatrix} < 0 \tag{3.112}$$

where

$$M_i = A_i'Y_i + Y_iA_i - \tau_i C_{y,i}'[D_{y,i}D_{y,i}']^{-1}C_{y,i} + C_i'C_i + (\tau_i + \bar{\theta}_i)H_i'H_i + \eta_i\alpha_i^2 I$$

The coupling condition $Y_i > X_i > 0$ is equivalent to

$$\begin{bmatrix} \tilde{X}_i & I \\ I & Y_i \end{bmatrix} > 0 \tag{3.113}$$

Now consider the performance upper bound on the right hand side of (3.53). Note that minimizing $J(\tau, \eta, \theta)$ is equivalent to minimizing $W_1 + \cdots + W_N$ subject to

$$W_i > x_{i0}' \left[X_i + \tau_i M_{1i} + \eta_i M_{2i} + \theta_i M_{3i}\right] x_{i0}. \tag{3.114}$$

Using Schur complement again, (3.114) is equivalent to following LMIs:

$$\begin{bmatrix} W_i & x_{i0}' & x_{i0}'M_{1i}^{\frac{1}{2}} & x_{i0}'M_{2i}^{\frac{1}{2}} & x_{i0}'M_{3i}^{\frac{1}{2}} \\ \star & \tilde{X}_i & 0 & 0 & 0 \\ \star & \star & \tilde{\tau}_i I & 0 & 0 \\ \star & \star & \star & \tilde{\eta}_i I & 0 \\ \star & \star & \star & \star & \tilde{\theta}_i I \end{bmatrix} > 0 \tag{3.115}$$

The conditions $\tilde{\tau}_i > 0, \tau_i > 0, \tilde{\tau}_i\tau_i = 1,$, $\tilde{\eta}_i > 0, \eta_i > 0, \tilde{\eta}_i\eta_i = 1, \tilde{\theta}_i > 0, \theta_i > 0$ and $\tilde{\theta}_i\theta_i = 1$ are equivalent to

$$\begin{aligned} &\begin{bmatrix} \tilde{\tau}_i & 1 \\ 1 & \tau_i \end{bmatrix} \geq 0, \quad rank \begin{bmatrix} \tilde{\tau}_i & 1 \\ 1 & \tau_i \end{bmatrix} \leq 1, \\ &\begin{bmatrix} \tilde{\eta}_i & 1 \\ 1 & \eta_i \end{bmatrix} \geq 0, \quad rank \begin{bmatrix} \tilde{\eta}_i & 1 \\ 1 & \eta_i \end{bmatrix} \leq 1, \\ &\begin{bmatrix} \tilde{\theta}_i & 1 \\ 1 & \theta_i \end{bmatrix} \geq 0, \quad rank \begin{bmatrix} \tilde{\theta}_i & 1 \\ 1 & \theta_i \end{bmatrix} \leq 1, \end{aligned} \tag{3.116}$$

Consider the following optimisation problem in the variables $W_i, \tilde{X}_i, F_i, Y_i, \tilde{\tau}_i, \tilde{\eta}_i, \tilde{\theta}_i, \tau_i, \eta_i$ and θ_i:

$$\inf (W_1 + \cdots + W_N) \text{ subject to (3.111), (3.112), (3.113), (3.115) and (3.116)} \tag{3.117}$$

This problem is a problem of minimizing a linear cost subject to rank constrained LMIs. The proof showing equivalence between the optimisation problem (3.117) and optimisation on the right hand side of (3.53) is established in [97].

3.4.8 Controller design steps

The controller design steps corresponding to a SEP can be summarised as follows:

(i) Using the load flow results corresponding to the SEP, the system matrices A_{SYS} and B_{SYS} can be found using (2.33), (2.38), (2.39), (2.44) and (2.49).

(ii) From the system matrices A_{SYS} and B_{SYS}, the subsystem matrices and uncertainty definitions are obtained using (3.36), (3.37), (3.38) and (3.40).

(iii) With the subsystem matrices and uncertainties defined, the rank constrained LMI problem (3.117) is solved, to a desired accuracy, obtaining a collection of $\theta_i, \tau_i, \eta_i, \tilde{X}_i, Y_i$.

(iv) Substituting the found θ_i, τ_i, η_i into GAREs (3.48) and solving (3.48) to obtain X_i. Note that Y_i can be selected from the found feasible solution the problem (3.117) (refer the proof of Theorem 3 of [97]).

(v) The robust stabilising controller can be constructed (3.51) using the computed θ_i, τ_i, η_i, X_i and Y_i.

3.5 Chapter summary

The proposed controller design methodology and stability proofs are given in this chapter. The basics of minimax LQG control and the representation of the uncertainties using IQCs are given in detail. Important results and theorems used in the control design development are also included for reference. The proposed decentralised control with subsystem representation, uncertainty description and stability theorems used are stated in detail. The proofs for the stability theorems are derived step by step. The LMI optimisation method to synthesise the controller and the steps involved in the controller design for a SEP are also included.

Chapter 4

Switching Stability Through Dwell Time

4.1 Introduction

In this research, we design power system controllers which provide robust performance over the entire operating regime of the power system. To achieve this, we treat the power system as parameter varying switched system. We divide the entire operating regime of the generator into several zones with respect to power output of the generator and each zone consisting of one Stable Equilibrium Point (SEP). We design a decentralised output feedback controller as explained in Chapter 3, for the power system linearised around each such SEPs and capable of providing robust performance within the zone with admissible uncertainties considered. When the power output of the generator changes from one zone to another, the controller corresponding to the new zone has to be selected and switched.

Even though the controllers and plant are closed loop stable, we need to ensure that the switched system is stable. One method of achieving the switching stability is through slow switching. For the power system considered here the dynamics of power variation can be treated as a slow process and the corresponding switching stability during controller switching can be achieved by allowing dwell time between consecutive switchings.

Switching stability through slow switching is established in many works including [98] and [64]. Generally, these works assume that the states are continuous during switching and individual switching systems have their origin as common equilibrium point. In our work, we switch controllers with power system corresponding to different SEPs. This will lead to jumps in states at the switching instants. In this thesis, the work in [56] is extended to system states which jump at switching instances.

The first section of this chapter gives a brief introduction to switched systems and need for switching stability. In the next section, we develop the stability criteria and an expression for dwell time. Determination of dwell time is given in the following section. Finally we illustrate this theory by selecting a test case power system and computing at the required dwell time and simulation results are presented.

Simulation cases which are related to dwell time study are included in this chapter and detailed simulations are given in Chapter 6.

4.2 Switching system and stability

Switching control finds many applications in different fields. In complex control situations, often control objectives and plant models are subjected to changes. To meet the control requirements, it may not be always possible, by employing a single controller. In such scenarios, it is usual to design multiple linear controllers corresponding to the linearised operating points of the nonlinear plant and then these controllers are switched properly to meet the design objectives.

When switching control is used, stability of the switched systems need to be established apart from individual systems stability. Even though the individual systems are closed loop stable it is not necessary that when switching takes place between these systems, the resulting system will be stable. It is shown with numerical example in [64], when switching was done between two stable systems this can lead to unstable state trajectories.

There are many methods available to deal with the stability issue arising due to controller switchings [98–100]. Sufficient conditions for uniform stability, uniform asymptotic stability, exponential stability and instability are established in [101]. Stability analysis of switched systems is usually carried out using a Lyapunov function for each subsystem [99]. These Lyapunov functions are connected together in some manner, in order to compose a Lyapunov function that guarantees that the energy of the overall system decreases to zero along the state trajectories of the system.

If the dynamics of the switching systems are of slow varying nature, we can introduce a number $\tau > 0$ and restrict the class of admissible switching signals to signals with the property that the interval between any two consecutive switching is greater than τ. This time τ is usually referred as "dwell time" [98]. If all the linear systems under consideration for switching are globally asymptotically stable, then the switched linear system also will be globally asymptotically stable [98], if the dwell time τ is sufficiently large enough. The required lower bound on τ can be explicitly calculated from the parameters of the individual subsystems. The procedure to arrive at the lower bound on τ is established in [56, 98]. The systems considered in [56, 98] have the assumptions that the states are continuous during

switching and individual switching systems have the origin as common equilibrium point. In the switching of power system controllers corresponding to the different SEPs using dwell time, we consider the effect of different equilibria and the jumps in the state trajectory at switching instants. We extend the results of [56, 98] to include these additional complexities during switching. In the following section, we develop the conditions for switching stability and arrive at lower bound on the dwell time required for stable switching.

4.3 Algebraic constraints on dwell time for stable switching

Now we discuss the stability of a switched system made up of two systems P_1 and P_2:

$$P_1 : \dot{x} = A_1 x, \tag{4.1}$$

$$P_2 : \dot{x} = A_2 x - A_2 \Psi, \tag{4.2}$$

where $x \in R^n$ is the state-vector and $\Psi \in R^n$ is a constant vector; the equilibrium point for P_1 is 0 and that of P_2 is Ψ; matrices A_1 and A_2 are stable matrices and further, there exist Lyapunov functions $V_1(x)$ and $V_2(x - \Psi)$ for P_1 and P_2 respectively.

We look at the configuration where the system is continuously switching between P_1 and P_2 and determine the stability of this system. The first question is: if both P_1 and P_2 are stable then how is it that switching between the two will make the overall system unstable? For finite number of switchings, stability is guaranteed but the same cannot be said of infinite number of switchings.

Formally we define stability as follows:

Definition 9 *Given systems P_1 and P_2 and an infinite switching sequence $P_1 \rightarrow P_2 \rightarrow P_1$, the system is stable if there exists a r-ball*

$$B_r = \{z : V_1(z) \leq r\}$$

such that for every P_1-state $x(t_0) \notin B_r$, where t_0 $\{t_{01}, t_{02}, t_{03}, \cdots\}$ is the instance when the system switches from P_1 to P_2, there exists a τ_d^{12} such that when the system switches back to P_1 from P_2, at time $t_0 + \tau_d^{12}$, P_1-state $x(t_0 + \tau_d^{12})$ approaches B_r as

the number of switching goes to infinity. We can similarly define stability for the switching sequence $P_2 \rightarrow P_1 \rightarrow P_2$.

Let the system states at the switching instances be denoted as follows (see Figure 4.1 and 4.2):

$$x_1 = x(t_0) \quad \text{and} \quad x_2 = x_1 - \Psi \tag{4.3}$$

$$y_1 = x(t_1) \quad \text{and} \quad y_2 = y_1 - \Psi \tag{4.4}$$

where the system switches from P_1 to P_2 at t_0 and back to P_2 at t_1.

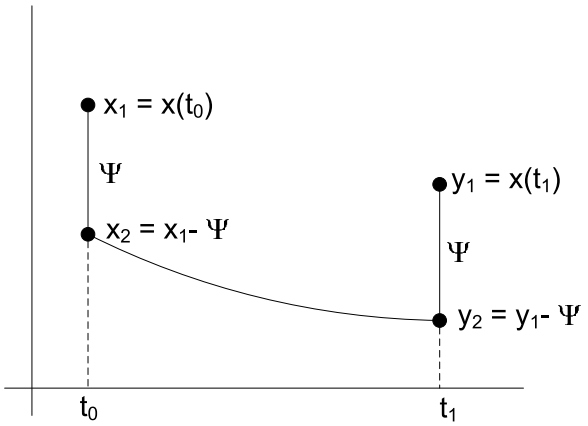

Figure 4.1. Representation of system states at switching instances.

Note that the definition of stability is satisfied, once the system reaches inside a ball and not necessarily as it approaches the origin. There is a good reason for this. Systems P_1 and P_2 have different equilibrium points and when the system switches to P_2, the state approaches Ψ, the equilibrium point of P_2. This means that the ball B_1 has to be large enough to include both equilibrium points (0 and Ψ) (see Figure 4.2).

To see the motivation for the above stability definition, we define balls B_0 B_1, and B_2, shown in Figure 4.2:

$$B_0 = \{z : V_1(z) \leq V_1(x(t_0))\} \tag{4.5}$$

$$B_1 = \{z : V_1(z) \leq V_1(x(t_1))\} \tag{4.6}$$

$$B_2 = \{z : V_2(z - \Psi) \leq V_2(x(t_0) - \Psi)\} \tag{4.7}$$

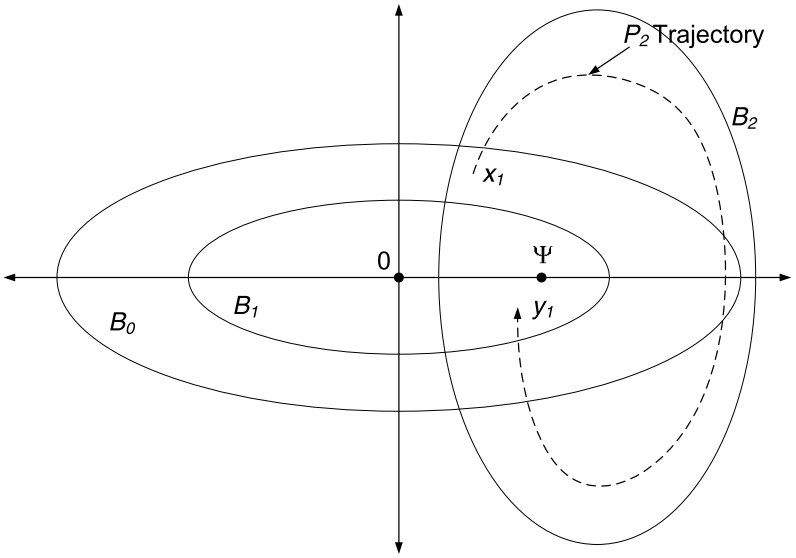

Figure 4.2. Balls B_0 and B_1 and system trajectory (dashed)

The interpretation of what these balls are is simple. (Please note that since $V_1(x)$, $V_2(x-\Psi)$ are positive-definite, balls B_0, B_1, and B_2 define closed volumes.) Let t_0 be the time at which the system switches from P_1 to P_2 and then at time t_1, switches back from P_2 to P_1; the two balls B_0 and B_1 correspond to the bound on system states at time instants t_0 and t_1. Ball B_2 gives the bound on the trajectory when the system is switched to P_2.

Our notion of stability is that if $B_1 \subset B_0$, for all switchings $P_1 \to P_2 \to P_1$, then the infinite switchings result in a stable system. If such is not the case then every switching may push the state into a larger and larger ball leading to instability.

The condition that B_1 be a subset of B_0 can be ensured by imposing a condition on the minimum time spent in P_2 during every $P_1 \to P_2 \to P_1$ cycle. This time is called the dwell time, denoted as τ_d^{12}, and our final result is that if the time spent in P_2 is greater than the dwell time, i.e., $t_1 - t_0 \geq \tau_d^{12}$, then the switched system is stable.

Next, we obtain an expression for the dwell time to ensure the stability of the switched system. Let Lyapunov functions V_1 and V_2 satisfy the following inequalities for some positive constants a_1, a_2, b_1, b_2, c_1 and c_2:

$$a_1 |x|^2 \leq V_1(x) \leq b_1 |x|^2 \tag{4.8}$$

$$a_2 \left|x-\Psi\right|^2 \leq V_2(x-\Psi) \leq b_2 \left|x-\Psi\right|^2 \tag{4.9}$$

$$\frac{\partial V_1}{\partial x} A_1 x \leq -c_1 \left|x\right|^2 \tag{4.10}$$

$$\frac{\partial V_2}{\partial x} \left(A_2 x - A_2 \Psi\right) \leq -c_2 \left|x-\Psi\right|^2 \tag{4.11}$$

From equation (4.8),

$$\frac{V_1(x)}{b_1} < \left|x\right|^2,$$

substituting this in (4.10),

$$\frac{\partial V_1}{\partial x} A_1 x \leq -2\lambda_1 V_1(x) \tag{4.12}$$

where $\lambda_1 = \frac{c_1}{2b_1}$. This implies that for any positive τ,

$$V_1\left(x\left(t_0+\tau\right)\right) \leq e^{-2\lambda_1 \tau} V_1\left(x\left(t_0\right)\right) \tag{4.13}$$

since $\frac{dV_1(x)}{dt} \leq -2\lambda_1 V_1(x)$ and V_1 decays exponentially. Similarly we have

$$V_2\left(x\left(t_0+\tau\right)-\Psi\right) \leq e^{-2\lambda_2 \tau} V_2\left(x\left(t_0\right)-\Psi\right).$$

From (4.8) and definitions (4.3) and (4.4) we have:

$$a_1 \left|x_1\right|^2 \leq V_1(x_1) \leq b_1 \left|x_1\right|^2 \tag{4.14}$$

$$a_2 \left|x_2\right|^2 \leq V_2(x_2) \leq b_2 \left|x_2\right|^2 \tag{4.15}$$

We find the dwell time, τ_d^{12}, by showing that when $t_1 - t_0 \geq \tau_d^{12}$ then, there exists a ν such that (for x_1 and y_1 defined in (4.3), (4.4))

$$V_1(y_1) - V_1(x_1) \leq -\nu \left|x_1\right|^2 \tag{4.16}$$

Since V_1 is a positive definite function, we can substitute an upper bound for $V_1(y_1)$ and lower bound for $V_1(x_1)$ and obtain,

$$b_1 \left|y_1\right|^2 - a_1 \left|x_1\right|^2 \leq -\nu \left|x_1\right|^2 \tag{4.17}$$

Next we get a bound on $|y_1|$; we know that,

$$V_2(y_2) \leq e^{-2\lambda_2 \tau_d^{12}} V_2(x_2) \tag{4.18}$$

$$\implies a_2 |y_2|^2 \leq b_2 e^{-2\lambda_2 \tau_d^{12}} |x_2|^2 \tag{4.19}$$

$$\implies a_2 |y_1 - \Psi|^2 \leq b_2 e^{-2\lambda_2 \tau_d^{12}} |x_1 - \Psi|^2 \tag{4.20}$$

Fact:

$$\begin{aligned} (a+b-b)^2 &= (a-b)^2 + b^2 + 2(a-b)b \\ &\leq (a-b)^2 + b^2 + (a-b)^2 + b^2 \\ \therefore (a-b)^2 > 0 &\implies 2ab < a^2 + b^2 \implies 2(a-b)^2 \geq a^2 - 2b^2 \end{aligned} \tag{4.21}$$

Using the fact that $2(a-b)^2 \geq a^2 - 2b^2$ with (4.20), we have,

$$\begin{aligned} -a_2 |\Psi|^2 + \frac{a_2}{2} |y_1|^2 &\leq e^{-2\lambda_2 \tau_d^{12}} b_2 |x_1 - \Psi|^2 \\ &\leq e^{-2\lambda_2 \tau_d^{12}} b_2 \left(|x_1|^2 + |\Psi|^2 \right) \end{aligned} \tag{4.22}$$

Substituting the upper bound on $|y_1|^2$ from (4.22) into (4.17) we have,

$$\begin{aligned} 4\frac{b_1 b_2}{a_2} e^{-2\lambda_2 \tau_d^{12}} |x_1|^2 + 2\frac{b_1}{a_2} |\Psi|^2 \left(2e^{-2\lambda_2 \tau_d^{12}} b_2 + a_2 \right) \\ - a_1 |x_1|^2 \leq -\nu |x_1|^2 \end{aligned} \tag{4.23}$$

The middle term in the left-hand-side of the above equation (4.23) is independent of $|x_1|$ and unless x_1, the state at which the system switches from P_1 to P_2, is outside of some region, inequality (4.23) cannot be satisfied. We ensure that x_1 is outside of some region by constraining it as follows:

$$|x_1|^2 \geq 2\frac{b_1}{a_1} K_\Psi^{12} |\Psi|^2 \quad \text{where} \quad K_\Psi^{12} > 1. \tag{4.24}$$

Substituting (4.24) in (4.23) we have,

$$4\frac{b_1 b_2}{a_2} e^{-2\lambda_2 \tau_d^{12}} |x_1|^2 + \frac{a_1}{a_2 K_\Psi^{12}} |x_1|^2 \left(2e^{-2\lambda_2 \tau_d^{12}} b_2 + a_2 \right) - a_1 |x_1|^2 \leq -\nu |x_1|^2 \tag{4.25}$$

From (4.25) we have the condition that τ_d^{12} should be such that,

$$4\frac{b_1 b_2}{a_2}e^{-2\lambda_2\tau_d^{12}} + \frac{a_1}{a_2 K_\Psi^{12}}\left(2e^{-2\lambda_2\tau_d^{12}}b_2 + a_2\right) - a_1 < 0 \tag{4.26}$$

Thus for stable switching τ_d^{12} should satisfy,

$$\begin{aligned} 2e^{-2\lambda_2\tau_d^{12}}\left(\frac{2b_1b_2K_\Psi^{12} + a_1b_2}{a_2K_\Psi^{12}}\right) &< a_1\left(\frac{K_\Psi^{12}-1}{K_\Psi^{12}}\right) \\ 2e^{-2\lambda_2\tau_d^{12}} &< \frac{a_1a_2\left(K_\Psi^{12}-1\right)}{2\left(2b_1b_2K_\Psi^{12}+a_1b_2\right)} \\ \tau_d^{12} &> \frac{1}{2\lambda_2}\log\left[\frac{a_1a_2\left(K_\Psi^{12}-1\right)}{2\left(2b_1b_2K_\Psi^{12}+a_1b_2\right)}\right] \end{aligned} \tag{4.27}$$

In the above, we have proved that the r-ball into which system trajectories converge is given by:

$$B_r^{12} = \{z : V_1(z) \leq 2b_1K_\Psi^{12}|\Psi|^2\} \tag{4.28}$$

From this, it can be seen that there is a trade-off between K_Ψ^{12} and τ_d^{12}.

So far we have only considered the $P_1 \to P_2 \to P_1$ cycle but the development for the $P_2 \to P_1 \to P_2$ cycle is symmetrical to this and the dwell time τ_d^{21} required for dwelling in P_1 can be obtained by replacing $a_1 \to a_2$, $b_1 \to b_2$, $c_1 \to c_2$, $\lambda_2 \to \lambda_1$ and $K_\Psi^{12} \to K_\Psi^{21}$ constants in the above expression (4.27) and is given by,

$$\tau_d^{21} > \frac{1}{2\lambda_1}\log\left[\frac{a_1a_2\left(K_\Psi^{21}-1\right)}{2\left(2b_1b_2K_\Psi^{21}+a_2b_1\right)}\right] \tag{4.29}$$

The corresponding r-ball into which system trajectories converge is given by:

$$B_r^{21} = \{z : V_2(z) \leq 2b_2K_\Psi^{21}|\Psi|^2\} \tag{4.30}$$

From the above discussions we conclude that for any switching sequence $P_1 \to P_2 \to P_1 \to P_2 \to P_1 \cdots$ satisfying the corresponding dwell time conditions given by inequalities (4.27) and (4.29), the state x reaches the region $B_r = B_r^{12} \cup B_r^{21}$

4.4 Determination of dwell time

To estimate the dwell time τ_d, the constants a_p, b_p, c_p, λ_p and K_Ψ are evaluated. Let the system under consideration be $\dot{x} = A_p x$ and the corresponding Lyapunov function $V_p(x)$ of the system is given by,

$$V_p(x) = x' M_p x \tag{4.31}$$

where M_p satisfies,

$$A_p' M_p + M_p A_p < 0 \tag{4.32}$$

M_p can be evaluated by solving the Riccati equation (4.32). Equation (4.8) will be satisfied if,

$$\begin{aligned} a_p &= \text{minimum Eigen value of } M_p \\ b_p &= \text{maximum Eigen value of } M_p \end{aligned} \tag{4.33}$$

From equations (4.9) and (4.31), we can write,

$$\begin{aligned} 2M_p x A_p x &\leq -c_p \left|x\right|^2 \\ < Ap' M_p x, x > + < x, M_p A_p x > &\leq -c_p \left|x\right|^2 \\ < (M_p Ap + A_p' M_p) x, x > &\leq -c_p \left|x\right|^2 \end{aligned} \tag{4.34}$$

The above inequality will hold if,

$$c_p = \text{maximum Eigen value of } < A_p' M_p + M_p A_p > \tag{4.35}$$

now $\lambda_p = \frac{c_p}{2b_p}$. The value of K_Ψ should be depending on the system under consideration, taking any practical limitations into account so that it satisfies the inequality $K_\Psi > 1$.

4.5 Validation of switching with dwell time

In order to demonstrate the practical implementation of the dwell time switching scheme for a power system, we consider a test case power system. We design the controllers corresponding to the SEPs and arrive at the dwell time required for different controller switching combinations. Simulations are carried out under different scenarios for validation.

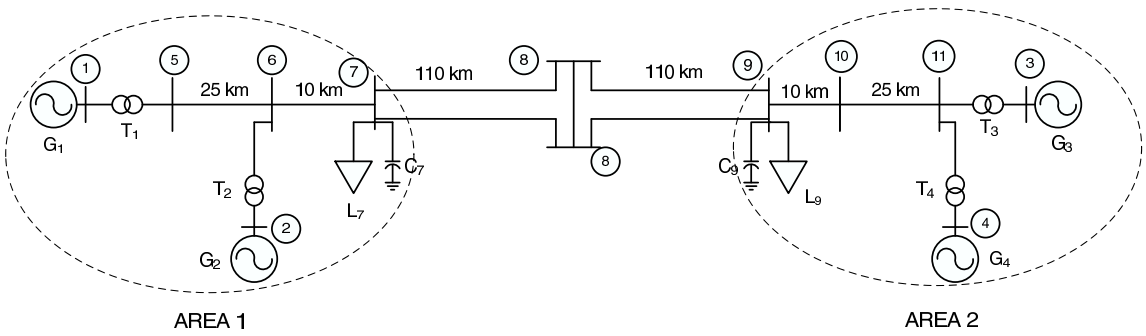

Figure 4.3. Two area four machine system.

4.5.1 Simulation setup

To demonstrate dwell time switching scheme through simulations, the grid system shown in Figure 4.3 is used. The system consists of two power system areas Area 1 and Area 2 connected through a twin circuit tie line of 220 km in length. The transmission system nominal voltage is 400 kV. Generation voltages are stepped up by the transformers connected to the generators. Load centers are located at buses 7 and 9. The buses 7 and 9 have shunt capacitors. Generators 1 to 4 and transformers 1 to 4 are identical and their parameters are given in Appendix A, Table A.1 and A.3. The generator AVR parameter are given in Table A.2. Transmission line parameters are given in 400 kV, 100 MVA base in Table A.4. For the analysis of the system, 400 kV and 100 MVA are chosen as base quantities.

Controllers for the considered system are designed as explained in Section 3.4.8. The generators G_1, G_3 and G_4 operate as base generators and deliver 400 MW. Single controller is designed for generators G_1, G_3 and G_4 corresponding to this SEP. Generator G_2 takes up the variations in the power demand by the load. The operating range of G_2 is from 0 to 400 MW. We divide the operating range of G_2 into 16 equal power zones of 25 MW each. We have one SEP corresponding to each power zone. We design 16 controllers for G_2 corresponding to each SEP providing robust stabilisation for a power variation of $\pm$ 25 MW within the zone. Generators G_1, G_3 and G_4 have single controller corresponding to 400 MW SEP. Different SEP identification numbers are given in Table 4.1.

SEP 1	SEP 2	SEP 3	SEP 4	SEP 5	SEP 6	SEP 7	SEP 8
25 MW	50 MW	75 MW	100 MW	125 MW	150 MW	175 MW	200 MW
SEP 9	SEP 10	SEP 11	SEP 12	SEP 13	SEP 14	SEP 15	SEP 16
225 MW	250 MW	275 MW	300 MW	325 MW	350 MW	375 MW	400 MW

Table 4.1. Identification of different the SEPs of generator G_2.

4.5.2 Stability conditions and dwell time computation

As the generation of G_2 varies from one zone to another, we select the suitable controller and switch in. While switching, the stability of the switched system are preserved through dwell time. We arrive at the dwell time required for different possible switching combinations. As the first step for the computation of satisfying dwell time, we work out the closed loop system matrices corresponding to each SEP. Next, to check wether the SEPs satisfy our stability conditions, we verify following. Let us consider two switching sequences, $P_i \rightarrow P_j \rightarrow P_i$ and $P_j \rightarrow P_i \rightarrow P_j$. To meet switching stability as per Definition 9, inequalities (4.36) should be met,

$$\begin{aligned} V_i(\Psi^{ij}) &< r^{ij} = 2b_i K_\Psi^{ij} |\Psi^{ij}|^2 \\ V_j(\Psi^{ji}) &< r^{ji} = 2b_j K_\Psi^{ji} |\Psi^{ji}|^2 \end{aligned} \tag{4.36}$$

The values of Ψ^{ij} and Ψ^{ji} are given by the difference between the steady state vectors corresponding to the closed loop system of i^{th} and j^{th} SEPs. The Lyaponov functions $V_i(\Psi^{ij})$ and $V_j(\Psi^{ji})$ can be evaluated from (4.31). The radius of the stability balls r^{ij} and r^{ji} can be evaluated using the equations in (4.36). The value of K_Ψ is chosen as 1.5 for all SEPs. The conditions given by (4.36), are verified for all SEPs by evaluating the corresponding Lyaponov function values and the radius of the stability balls. After establishing the condition given by (4.36), we can find the lower bound on the required dwell time by using equations (4.27) and (4.29) for switching between consecutive SEPs. Dwell times computed for different switching combinations are given in Table 4.2.

4.5.3 Simulation cases

Simulations are carried out using the nonlinear multimachine power system model given by equations (2.25) to (2.32). Prime mover dynamics is not included in the simulation model and it is assumed that prime mover power changes instantaneously.

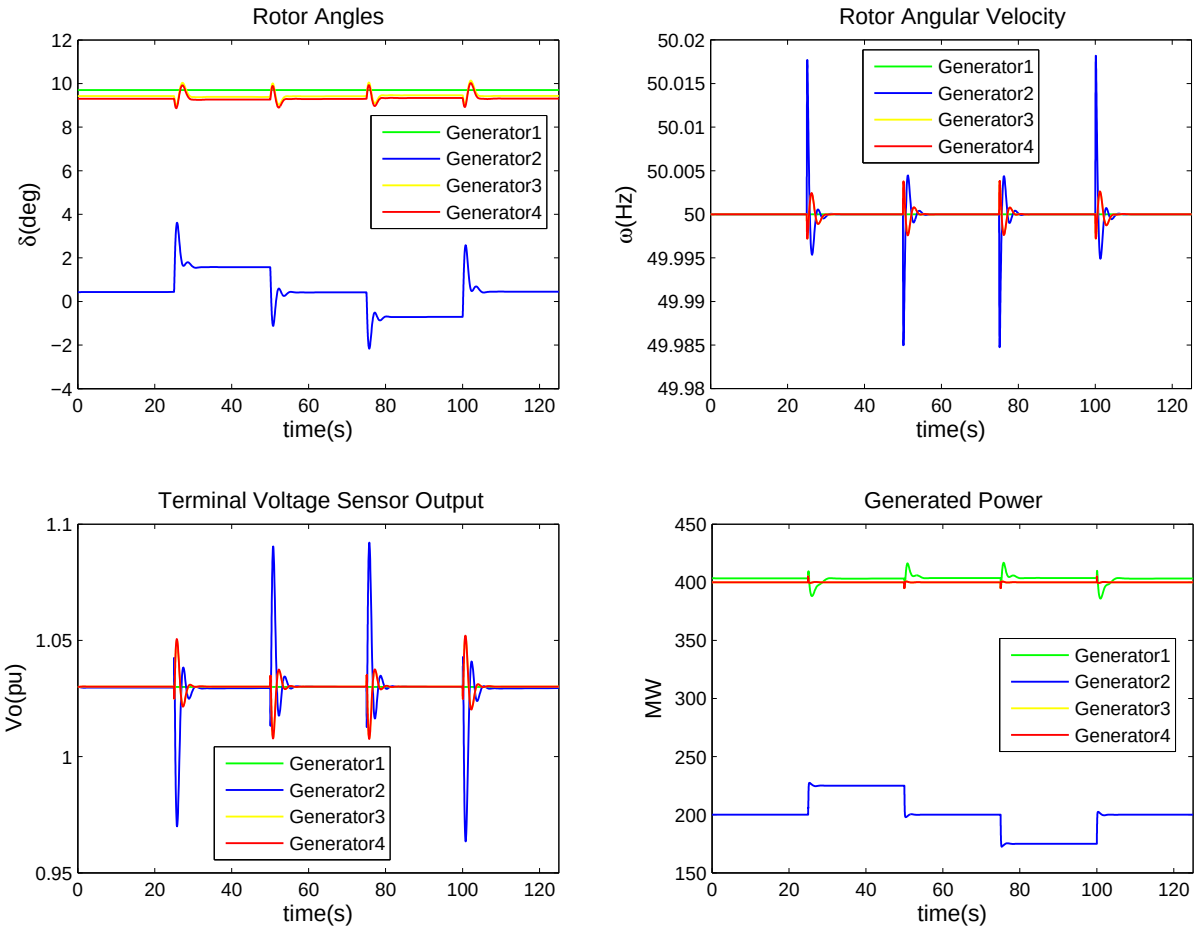

Figure 4.4. Case 1: Simulation responses of generator G_1 to G_4 for switching up and down around 200 MW.

Power Change	Controller	τ_d^{12} (s)	Power Change	Controller	τ_d^{21}(s)
SEP 1 to 2	C_1 to C_2	23.9890	SEP 2 to 1	C_2 to C_1	24.7884
SEP 2 to 3	C_2 to C_3	22.8243	SEP 3 to 2	C_3 to C_2	21.5976
SEP 3 to 4	C_3 to C_4	23.4500	SEP 4 to 3	C_4 to C_3	21.2590
SEP 4 to 5	C_4 to C_5	22.9490	SEP 5 to 4	C_5 to C_4	23.4500
SEP 5 to 6	C_5 to C_6	21.0466	SEP 6 to 5	C_6 to C_5	22.9490
SEP 6 to 7	C_6 to C_7	21.4581	SEP 7 to 6	C_7 to C_6	20.1177
SEP 7 to 8	C_7 to C_8	24.1736	SEP 8 to 7	C_8 to C_7	22.7254
SEP 8 to 9	C_8 to C_9	22.8836	SEP 9 to 8	C_9 to C_8	24.1736
SEP 9 to 10	C_9 to C_{10}	24.0231	SEP 10 to 9	C_{10} to C_9	21.0308
SEP 10 to 11	C_{10} to C_{11}	23.6559	SEP 11 to 10	C_{11} to C_{10}	24.1475
SEP 11 to 12	C_{11} to C_{12}	22.4421	SEP 12 to 11	C_{12} to C_{11}	23.9659
SEP 12 to 13	C_{12} to C_{13}	23.3025	SEP 13 to 12	C_{13} to C_{12}	22.7156
SEP 13 to 14	C_{13} to C_{14}	24.3393	SEP 14 to 13	C_{14} to C_{13}	23.3025
SEP 14 to 15	C_{14} to C_{15}	21.4414	SEP 15 to 14	C_{15} to C_{14}	24.2053
SEP 15 to 16	C_{15} to C_{16}	24.8533	SEP 16 to 15	C_{16} to C_{15}	21.5085

Table 4.2. Values of required dwell time for different controller switchings.

Further details of simulations are included in the Chapter 6. To evaluate the performance of the proposed switching scheme, we have done three cases of simulations. In all the simulations, the necessary controller switchings are carried out after the elapse of the required dwell time.

Case 1: Continuous up and Down

Simulation is carried out for 125 s with generator G_2 initially at 200 MW and operating with controller C_8. At t = 25 s, output of G_2 is increased to 225 MW and corresponding controller C_9 is switched in. At t = 50 s, after the lapse of the corresponding dwell time, output of G_2 is reduced to 200 MW and corresponding controller C_8 is switched in. Again at t = 75 s, output of G_2 is reduced to 175 MW with the corresponding controller C_7 is switched in. At t = 100 s, output of G_2 is increased to 200 MW and corresponding controller C_8 is switched in and the simulation is continued up to t = 125 s. With this continuous up and down switching, with corresponding controllers and after satisfying the required dwell time constraints, the overall system was found to be performing normally. The responses of the generators G_1 to G_4 with respect to rotor angle, angular velocity, terminal voltage sensor output and generated power are given in Figure 4.4.

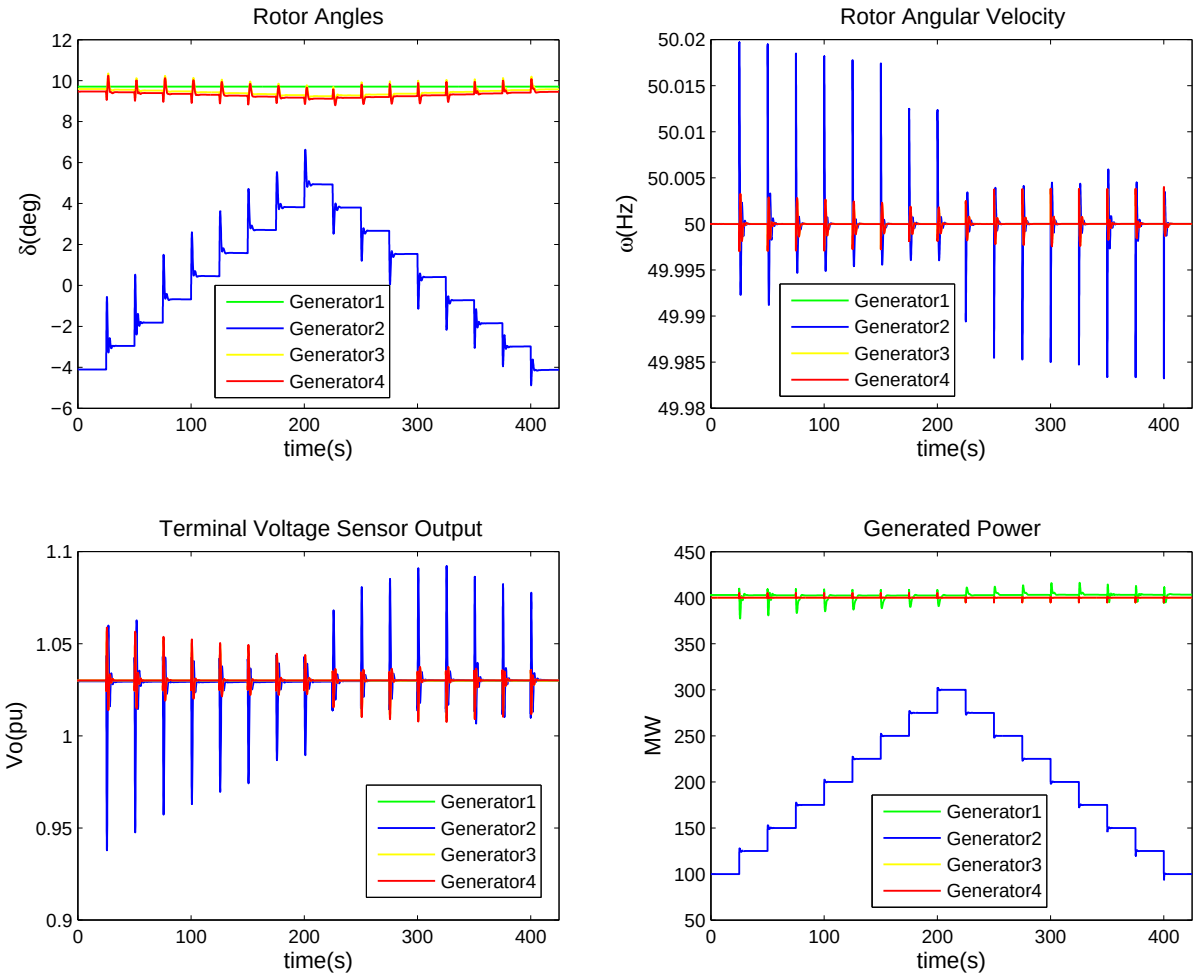

Figure 4.5. Case 2: Simulation responses of generator G_1 to G_4 for generation variation from 25 MW to 400 MW.

Case 2: Generation variation continuous up and down

In this case, power output of generator G_2 is gradually increased from 100 MW to 300 MW in steps of 25 MW. At each step of power change corresponding SEP controller is switched in after meeting the dwell time constraints. Again from 300 MW the power output of generator G_2 is gradually decreased from 300 MW to 100 MW in steps of 25 MW with respective controllers switched in at each power changing instances.

At t = 0 s, output of generator G_2 is at 100 MW with controller C_4, and the t

= 25 s, output of generator G_2 is increased to 125 MW with controller C_5 switched in. At every 25 sec interval the output of generator G_2 is increased by 25 MW with respective controller switched. At t = 200 s, the output of generator G_2 is at 300 MW with controller C_{12}. In similar steps the output of generator G_2 is reduced back to 100 MW with 25 MW power changes at 25 s intervals. Again at each power change respective controllers are switched. The responses of the generators G_1 to G_4 with respect to rotor angle, angular velocity, terminal voltage sensor output and generated power are given in Figure 4.5.

4.5.4 Inferences

From the simulation results in Figures 4.4 and 4.5, it is shown that when controllers are switched during power changes satisfying the dwell time constraints, we can ensure the stability of the switched system. Simulation also validates different switching combinations either progressively load up or down conditions (Figure 4.5) and also for switching up and down conditions around a particular SEP(Figure 4.4).

4.6 Chapter summary

The concept of preserving switching stability through dwell time approach is presented. The conditions for switching stability are stated and the expression for the required dwell time for stable switching while switching between different operating points with jumps in the states are included. Simulations are carried out to validate dwell time switching by selecting a test case power system with multiple controllers. Required dwell times for the possible controller switching combinations are computed. The results of different cases of simulations involving controller switchings are presented.

Chapter 5

Bumpless Switching Scheme

5.1 Introduction

To cover the entire operating regime of the power system, we design one controller each around different SEPs. These controllers are needed to be selected and switched with respect to the power output of the generator. At the instant of controller switching, if there is a difference between the output of the new controller to be switched in and the output of the currently active controller, there will be a jump in the control input to the plant. This jump in the input to the plant will cause switching transients in the plant response. A smooth controller transition could be achieved, if we can minimise the difference between the controller outputs at the time of switching. Also the controllers considered in this work are dynamical systems, their states must have correct values when switching occurs and if this is not the case, the corresponding control loops may experience undesirable and harmful switching transients [66].

To minimise the difference between the outputs of the controller at switching instant, the output difference can be translated into conditions on the states of the new controller to be switched in. A direct approach to bumpless switching between two controller configuration is considered in [74]. Here, the controller switching problem is formulated as an optimal linear quadratic control problem. Solution to this problem yields a feedback gain which acts as bumpless compensator. The bumpless compensator makes the new controller to track the output of the active controller and initialises the states of the new controller to a proper value to minimise the transients at switching. The bumpless scheme in [74], has been applied successfully to aerospace applications [48]. We apply the scheme proposed in [74], for the power system controller switching to avoid the switching transients. It may be noted, here the bumpless switching scheme does not affect the dynamics of the plant as well as the active controller before switching. Also after switching, the new controller is not influenced by the bumpless compensator. The scheme only helps to properly initialise the new controller states to avoid transients.

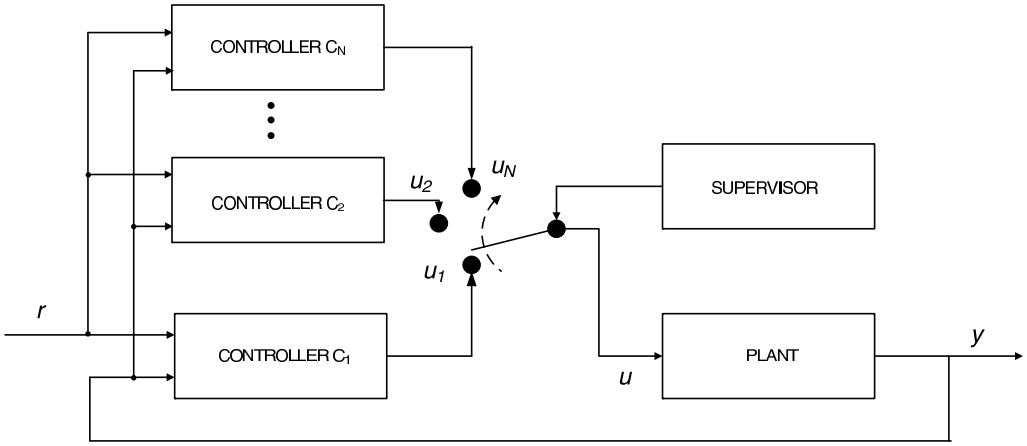

Figure 5.1. Basic controller switching configuration

In the first section of the chapter, we introduce the general bumpless switching scheme and the synthesis of the bumpless compensator. In the next section, we detail the application of the scheme to power system controller switching. In the final section, we demonstrate the efficacy of the scheme through simulations. For this, we select a test case grid system and construct the bumpless compensators and carry out the simulations. In the simulation results, we compare the responses of the generator for controller switching with and without bumpless scheme. Simulation cases which are used to demonstrate bumpless switching are included in this chapter and detailed simulations are given in Chapter 6.

5.2 Principle of Bumpless Transfer

Let us consider a plant as shown in Figure 5.1, which is controlled by by N linear parameter varying controllers and has to be switched according to the scheduling parameter. The switching sequence of the controller is done through a supervisor. Let us describe the plant as follows:

$$\begin{aligned} \dot{x}_i &= f(x,u) \qquad & x, f(\cdot) \in \mathbf{R^n}, u \in \mathbf{R^m} \\ y &= h(x,u) \qquad & y, h(\cdot) \in \mathbf{R^p} \end{aligned} \tag{5.1}$$

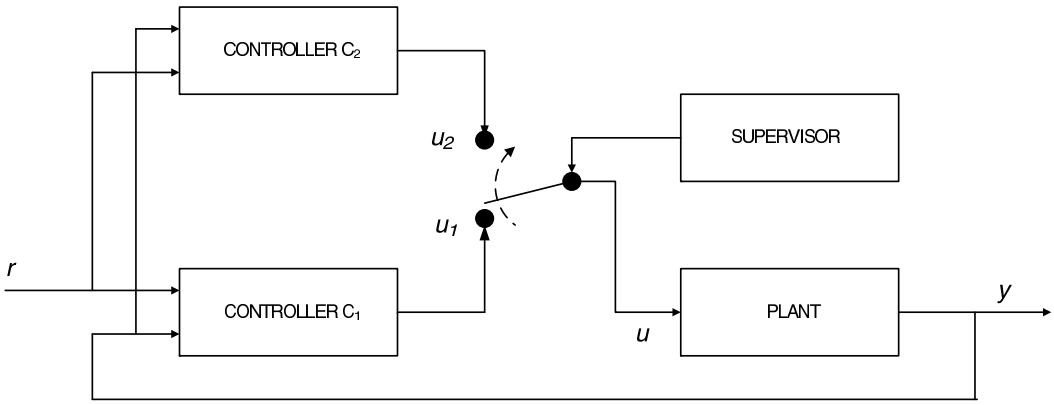

Figure 5.2. Switching involving two controllers.

where x, y and u are the state, measured output and control variables respectively.

First we shall consider the problem of bumpless switching between two controllers as in Figure 5.2 and later we generalise it over N controllers. At any instant of time t, let controller C_1 be the controller driving the plant and the supervisor responsible for the controller switching initiates action to switch over to controller C_2. We have to achieve this with minimum transients. Let the output of C_1 be u_1 and of C_2 be u_2. To minimise the transients the magnitude difference between u_1 and u_2 has to minimised at the switching instance. To get this condition, we drive the output u_2 of C_2 through a bumpless compensator in offline mode so that $u_2 = u_1$.

5.3 Linear Quadratic Bumpless Transfer

We outline the bumpless scheme proposed in [74]. The configuration of a linear quadratic bumpless transfer controller is shown in Figure 5.3. In order to achieve bumpless transfer during switching from online controller to offline controller, the signals u_1 should be equal to u_2. We design a static constant gain controller $\mathbf{F}$, such that $\mathbf{F}$ drives the offline controller to produce the same signal as the online controller. It is also important to drive the input signal of the offline controller also to be equal to the input signal of the online controller to avoid bump during transfer.

A low pass filter included in the input side of the offline controller helps to reduce further the transients during transfer.

It is assumed that the feedback controller **F** has access to controller states as well as the output of the plants as shown in the Figure 5.3. The plant is driven by the online controller and the offline controller is driven by the bumpless compensator **F** and a low pass filter. Low pass filter helps to reduce the switching transients further [48]. It is assumed that the low pass filter is detectable and stabilisable. Using state equations we describe the offline controller in Figure 5.3 as:

$$\begin{aligned} \dot{x(t)} &= Ax(t) + B_1\left[r(t) + \tilde{\alpha}(t)\right] + B_2 y(t) \\ u_2(t) &= Cx(t) + D_1\left[r(t) + \tilde{\alpha}(t)\right] + D_2 y(t) \end{aligned} \tag{5.2}$$

where $x(t)$ is the state of offline controller, $r(t)$ is the input to the online controller, $\tilde{\alpha}(t)$ is the output of the low pass filter, $y(t)$ is the plant output, $u_2(t)$ is the output of the offline controller and $\alpha(t)$ is the output of the bumpless compensator. A, B_1, B_2, C, D_1 and D_2 are the system matrices of the offline controller of appropriate sizes. The low pass filter is represented as:

$$\begin{aligned} \dot{x_l} &= A_l x_l + B_l(\alpha) \\ \tilde{\alpha} &= C_l x_l \end{aligned} \tag{5.3}$$

where $x_l(t)$ is the state of filter and A_l, B_l and C_l are filter matrices.
Let us define:

$$z_u(t) = u_2(t) - u(t) \tag{5.4}$$

$$z_e(t) = \alpha(t) \tag{5.5}$$

where $u(t)$ is the input to the plant from online controller. To avoid transients we have to minimise the signals $z_u(t)$ and $z_e(t)$. We attempt to minimise $\tilde{\alpha}(t)$ not directly, but by minimising $\alpha(t)$ instead. As the input to the offline controller is $r(t) + \tilde{\alpha}(t)$ and $\tilde{\alpha}(t)$ is the output of the low pass filter, this enables the input to the controller gradually to deform into purely $r(t)$ when the offline controller is switched online, which helps to avoid bumps at the controller input. With this background,

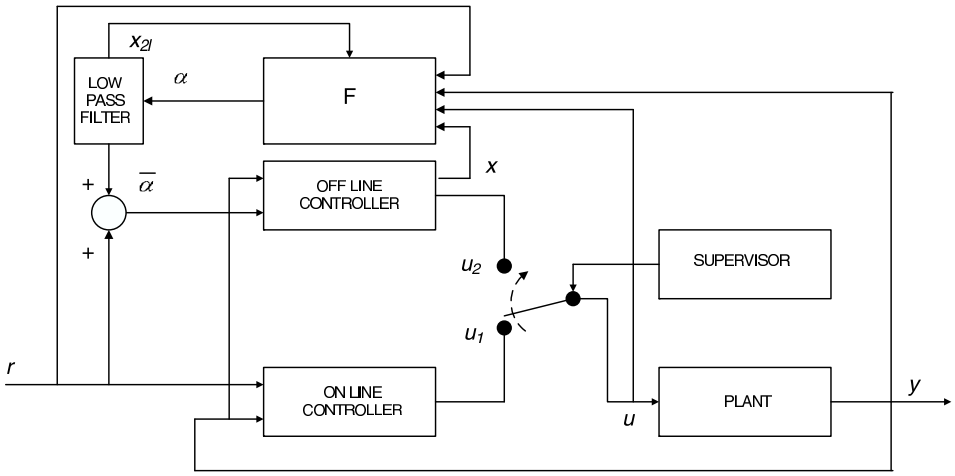

Figure 5.3. Bumpless controller configuration

we shall minimise the following cost functional:

$$J(u,\alpha,t) = \frac{1}{2}\int_0^T \left[z_u(t)'W_u z_u(t) + z_e(t)'W_e z_e(t)\right] dt + \frac{1}{2} z_u(T)'P z_u(T) \tag{5.6}$$

where W_u and W_e are positive semi definite matrices which are used to weigh the relative importance of ensuring $u_2 \approx u$ and minimising α.

Combining the dynamics of the offline controller and the low pass filter gives,

$$\begin{aligned} \dot{\tilde{x}} &= \tilde{A}\tilde{x} + \tilde{B}_1 w + \tilde{B}_2 \alpha \\ u_2 &= \tilde{C}\tilde{x} + \tilde{D}_1 w \end{aligned} \tag{5.7}$$

where

$$\tilde{A} := \begin{bmatrix} A & B_1 C_l \\ 0 & A_l \end{bmatrix}, \quad \tilde{B}_1 := \begin{bmatrix} B_1 & B_2 \\ 0 & 0 \end{bmatrix}, \quad \tilde{B}_2 := \begin{bmatrix} 0 \\ B_l \end{bmatrix}, \quad \tilde{C} := \begin{bmatrix} C & 0 \end{bmatrix},$$

$$\tilde{D}_1 := \begin{bmatrix} D_1 & D_2 \end{bmatrix}, \quad \tilde{x} := \begin{bmatrix} x \\ x_l \end{bmatrix}, \quad w := \begin{bmatrix} r \\ y \end{bmatrix}$$

Substituting (5.7) into performance index equation (5.6) and forming associated Hamiltonian yields,

$$H = \frac{1}{2}\left\{\left(\tilde{C}\tilde{x} + \tilde{D}_1 w - u\right)' W_u \left(\tilde{C}\tilde{x} + \tilde{D}_1 w - u\right) + \alpha' W_e \alpha\right\} + \lambda'\left(\tilde{A}\tilde{x} + \tilde{B}_1 w + \tilde{B}_2\alpha\right) \tag{5.8}$$

The first order necessary conditions for minimum are:

$$\frac{\partial H}{\partial \lambda} = \tilde{A}\tilde{x} + \tilde{B}_1 w + \tilde{B}_2\alpha = \dot{\tilde{x}} \tag{5.9}$$

$$\frac{\partial H}{\partial \tilde{x}} = \tilde{C}' W_u \tilde{C}\tilde{x} + \tilde{A}\lambda' + \tilde{C}' W_u \tilde{D}_1 w - \tilde{C}' W_u u = -\dot{\lambda} \tag{5.10}$$

$$\frac{\partial H}{\partial \alpha} = W_e\alpha + \tilde{B}_2'\lambda = 0 \tag{5.11}$$

Conditions (5.9), (5.10) and (5.11) can be combined to get,

$$\begin{bmatrix} \dot{\tilde{x}} \\ \dot{\lambda} \end{bmatrix} = \begin{bmatrix} \tilde{A} & -\tilde{R} \\ -\tilde{Q} & -\tilde{A}' \end{bmatrix} \begin{bmatrix} \tilde{x} \\ \lambda \end{bmatrix} + \begin{bmatrix} \tilde{B}_1 & 0 \\ -\tilde{C}' W_u \tilde{D}_1 & \tilde{C}' W_u \end{bmatrix} \begin{bmatrix} w \\ u \end{bmatrix} \tag{5.12}$$

where $\tilde{R} = \tilde{B}_2 W_e^{-1} \tilde{B}_2'$ and $\tilde{Q} = \tilde{C}' W_u \tilde{C}$.
Using the method of sweep [48], let us assume:

$$\lambda(t) = \Pi(t)\tilde{x}(t) - g(t) \tag{5.13}$$

from (5.13)

$$-g(t) = \lambda(t) - \Pi(t)\tilde{x}(t) \tag{5.14}$$

To solve for $\Pi(t)$, let us consider the following differential equation [81], [48]:

$$\dot{\Pi}(t) + \Pi(t)\tilde{A} + \tilde{A}'\Pi(t) - \Pi(t)\tilde{R}\Pi(t) + \tilde{Q} = 0 \tag{5.15}$$

Differentiating (5.13),

$$-\dot{g}(t) = \dot{\lambda}(t) - \dot{\Pi}(t)\tilde{x}(t) - \Pi(t)\dot{\tilde{x}}(t) \tag{5.16}$$

Substituting from Equations, (5.9), (5.10) and (5.15) in (5.16) we get,

$$\begin{aligned}
-\dot{g}(t) &= \left(\tilde{C}'W_u\tilde{C}\tilde{x} + \tilde{A}\lambda' + \tilde{C}'W_u\tilde{D}_1 w - \tilde{C}'W_u\right) \\
&+ \left[\Pi(t)\tilde{A} + \tilde{A}'\Pi(t) - \Pi(t)\tilde{R}\Pi(t) + \tilde{Q}\right]\tilde{x}(t) - \Pi(t)\left[\tilde{A}\tilde{x} + \tilde{B}_1 w - \tilde{B}_2 W_e^{-1}\tilde{B}_2\lambda\right] \\
&= \tilde{A}\left[\Pi(t)\tilde{x}(t) - \lambda\right] - \Pi(t)\tilde{R}\left[\Pi(t)\tilde{x}(t) - \lambda\right] - \left[\tilde{C}'W_u\tilde{D}_1 + \Pi\tilde{B}_1\right]w + \tilde{C}'W_u\tilde{u} \\
&= \left[\tilde{A} - \tilde{R}\Pi(t)\right]' g - \left[\tilde{C}'W_u\tilde{D}_1 + \Pi\tilde{B}_1\right]w + \tilde{C}'W_u\tilde{u} \qquad (5.17)
\end{aligned}$$

We solve equations (5.15) and (5.17), to synthesise the bumpless compensator F. To solve these equations we evaluate the end conditions from (5.6) as follows:

$$\begin{aligned}
\lambda(T) &= \frac{\mathrm{d}}{\mathrm{d}\tilde{x}}\left\{\frac{1}{2}\left[z_u(T)'Pz_u(T)\right]\right\} \\
&= \frac{\mathrm{d}}{\mathrm{d}\tilde{x}}\left\{\frac{1}{2}\left[\tilde{C}\tilde{x}(T) + \tilde{D}_1 w(T) - u(T)\right]' P\left[\tilde{C}\tilde{x}(T) + \tilde{D}_1 w(T) - u(T)\right]\right\} \\
&= \tilde{C}'P\tilde{C}\tilde{x}(T) + \tilde{C}'P\tilde{D}_1 w(T) - \tilde{C}'P\tilde{u}(T) \qquad (5.18)
\end{aligned}$$

Now comparing equations (5.13) and (5.18) and equating the coefficients we can get the required end conditions as,

$$\begin{aligned}
\Pi(T) &= \tilde{C}'P\tilde{C} \\
-g(T) &= \tilde{C}'P\tilde{D}_1 w(T) - \tilde{C}'P\tilde{u}(T) \qquad (5.19)
\end{aligned}$$

The above infinite horizon results assume that the switch between the controllers occurs infinitely far in the future ($T \to \infty$). However, if the dynamics are such that a steady state is reached relatively quickly, and the control signal is relatively constant over a period of time, then these infinite horizon results could be confidently applied [48].

In order for the solution of the differential Riccati equation, (5.15), to converge to the positive semi-definite stabilizing solution of

$$\tilde{A}'\Pi + \Pi\tilde{A} - \Pi\tilde{R}\Pi + \tilde{Q} = 0 \qquad (5.20)$$

as $T \to \infty$, $\left(\tilde{A}, \tilde{R}, \tilde{Q}^{\frac{1}{2}}\right)$ is required to be stabilisable and detectable [48]. From the

definitions of $\tilde{R}$ and $\tilde{Q}$, the strict positive definiteness of W_u and W_e and the assumption that the controller is stabilisable and detectable, it follows that $\left(\tilde{A}, \tilde{R}, \tilde{Q}^{\frac{1}{2}}\right)$ is indeed stabilisable and detectable. Hence, a positive semi-definite stabilising solution to equation (5.20) always exists and further more it satisfies [48],

$$\lim_{T\to\infty} \Pi(t) = \Pi(\infty) = \Pi \geq 0 \tag{5.21}$$

As equation (5.17), develops backward in time, and is $\left(\tilde{A} - \tilde{R}\Pi\right)$ is Hurwitz, this implies $-\left(\tilde{A} - \tilde{R}\Pi\right)$ is anti Hurwitz, and hence LQ tracking [102], can be applied [48]. With the assumption that w and $\tilde{u}$ are constant, it then follows that

$$\lim_{T\to\infty} g(t) = \left(\tilde{A} - \tilde{R}\Pi\right)^{-\mathscr{F}} \left[\left(\Pi\tilde{B}_1 + \tilde{C}'W_u\tilde{D}_1\right)w - \tilde{C}'W_u\tilde{u}\right] \tag{5.22}$$

where $(\cdot)^{-\mathscr{F}}$ denotes the inverse of a transposed matrix. From (5.11), we can write,

$$\alpha = -W_e^{-1}\tilde{B}_2'\lambda \tag{5.23}$$

Substituting for λ in (5.23) using (5.13) and (5.22), we can express α as, $\alpha = \mathbf{F}\left[\tilde{x}' \;\; w' \;\; \tilde{u}'\right]$, where $\mathbf{F}$ is given by

$$\mathbf{F} = -W_e^{-1}\tilde{B}_2' \left\{ \begin{array}{c} \Pi \\ -\left[\left(\tilde{A} - \tilde{R}\Pi\right)^{-\mathscr{F}} \left(\Pi\tilde{B}_1 + \tilde{C}'W_u\tilde{D}_1\right)\right]' \\ \left[\left(\tilde{A} - \tilde{R}\Pi\right)^{-\mathscr{F}} \tilde{C}'W_u\right]' \end{array} \right\} \tag{5.24}$$

The offline control loop will be stable as $\Pi \geq 0$ is the stabilising solution to the ARE, equation (5.20). Therefore it follows that the offline A matrix, $\left(\tilde{A} - \tilde{R}\Pi\right)$, is Hurwitz.

To design bumpless compensator for the system considered in (5.1) with N controllers, we assess the number of possible switching controller combinations we propose to have. Suppose if we have K such combinations involving $2K$ controllers then of those switching combinations will be having an online and offline controller and we work with these controllers to get the corresponding bumpless compensator. This will lead to K bumpless compensators to cover the complete set of switching combinations.

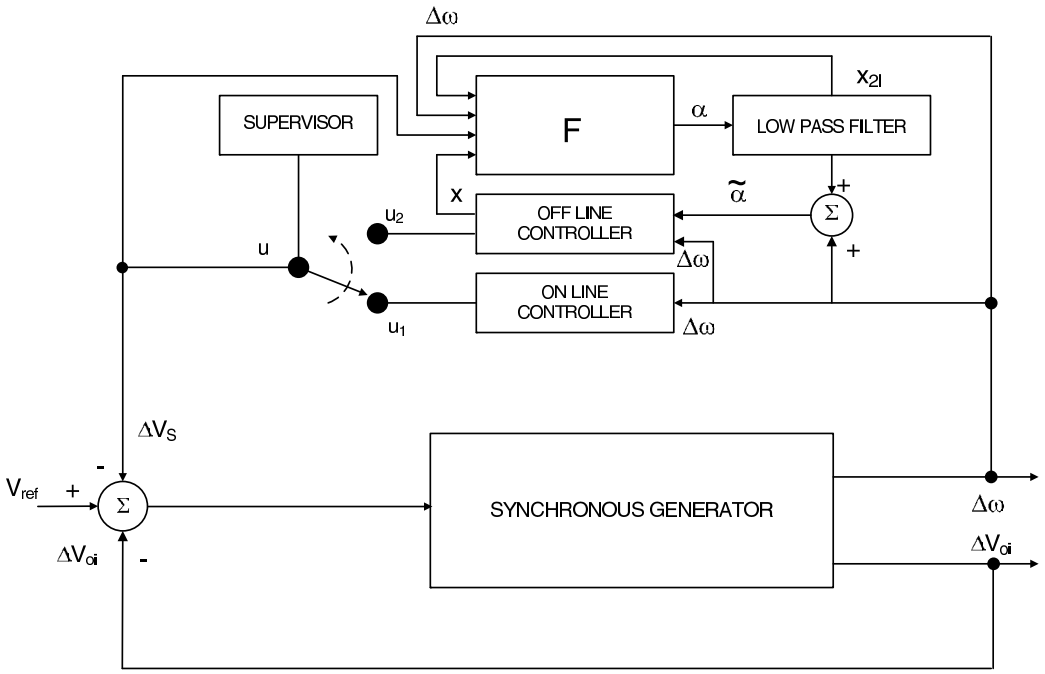

Figure 5.4. Bumpless switching scheme for generator

5.4 Application of bumpless transfer for power system

We apply the bumpless controller switching scheme described in Section 5.3 for switching between power system stabilising controllers when the power delivered by the generator changes. The block diagram in Figure 5.4 shows the implementation of the scheme for a generator. The output signal $\Delta\omega$ is the feedback variable which drives the power system controller to produce the stabilising signal ΔV_S. Let the output of online and offline controllers be u_1 and u_2 respectively. Now the compensator **F** has to be designed such that, it drives output of offline controller u_2 to be equal to u_1 and the signal $\tilde{\alpha}$ approaches zero at the switching instant. Now we shall rewrite the equations described in Section 5.3, to suit the power system model considered. The offline controller is described by the following equations:

$$\begin{aligned} \dot{x}_c &= A_c x_c + B_{1c}\tilde{\alpha} + B_{2c}\Delta\omega \\ u_2 &= K_c x_c \end{aligned} \tag{5.25}$$

and that the low pass filter is detectable and stabilisable and is represented as,

$$\begin{aligned} \dot{x}_l &= A_l x_l + B_l \alpha \\ \tilde{\alpha} &= C_l x_l \end{aligned} \tag{5.26}$$

Combining the dynamics of of the offline controller and the lowpass filter gives,

$$\begin{aligned} \dot{\tilde{x}} &= \tilde{A}\tilde{x} + \tilde{B}_1 w + \tilde{B}_2 \alpha \\ u &= \tilde{C}\tilde{x} \end{aligned} \tag{5.27}$$

where

$$\tilde{A} := \begin{bmatrix} A & B_1 C_l \\ 0 & A_l \end{bmatrix}, \quad \tilde{B}_1 := [B_{2c}], \quad \tilde{B}_2 := \begin{bmatrix} 0 \\ B_l \end{bmatrix}, \quad \tilde{C} := [K_c],$$
$$\tilde{x} := \begin{bmatrix} x_c \\ x_l \end{bmatrix}, \quad w := [\Delta\omega]$$

with new online controller and filter defined, Algebraic Riccati equation (5.20) can be solved to get the compensator **F** defined by (5.24).

5.5 Validation of bumpless switching scheme

5.5.1 Simulation details

To validate the bumpless switching scheme, the grid system shown in Figure 5.5 is used. The system consists of two power system areas Area 1 and Area 2 connected through a twin circuit tie line of 220 km in length. The transmission system nominal voltage is 400 kV. Generation voltages are stepped up by the transformers connected to the generators. Load centers are located at buses 7 and 9. The buses 7 and 9 have shunt capacitors. Generators 1 to 4 and transformers 1 to 4 are identical and their parameters are given in Appendix A, Table A.1 and A.3. The generator AVR parameter are given in Table A.2. Transmission line parameters are given in 400 kV, 100 MVA base in Table A.4. For the analysis of the system, 400 kV and 100 MVA are chosen as base quantities.

Controllers for the considered system are designed as explained in Section 3.4.8. The generators G_1, G_3 and G_4 operate as base generators and deliver 400 MW each. A single controller is designed for each generator G_1, G_3 and G_4 corresponding to

SEP 1	SEP 2	SEP 3	SEP 4	SEP 5	SEP 6	SEP 7	SEP 8
25 MW	50 MW	75 MW	100 MW	125 MW	150 MW	175 MW	200 MW
SEP 9	SEP 10	SEP 11	SEP 12	SEP 13	SEP 14	SEP 15	SEP 16
225 MW	250 MW	275 MW	300 MW	325 MW	350 MW	375 MW	400 MW

Table 5.1. Identification of different the SEPs of generator G_2.

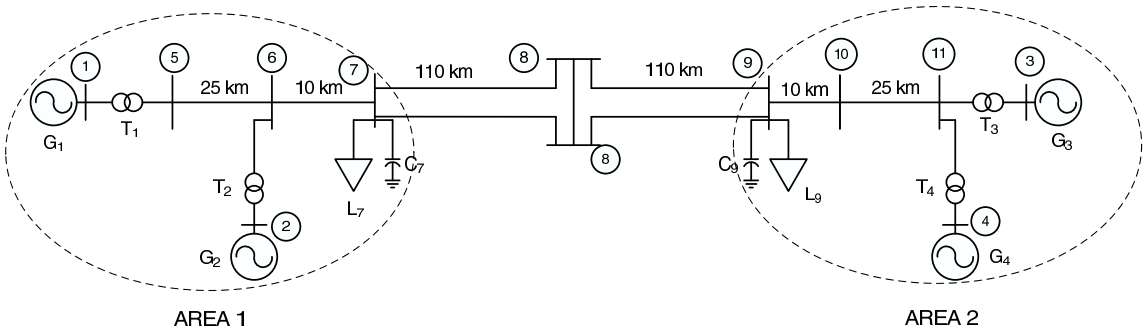

Figure 5.5. Two area four machine system.

this SEP. Generator G_2 takes up the variations in the power demand by the load. The operating range of G_2 is from 0 to 400 MW. We divide the operating range of G_2 into 16 equal power zones of 25 MW each. We have one SEP corresponding to each power zone. We design 16 controllers for G_2 corresponding to each SEP and each controller provides robust stabilisation for a power variation of $\pm$ 25 MW within the zone. Generators G_1, G_3 and G_4 have single controller corresponding to 400 MW SEP. Different SEP identification numbers are given in Table 5.1. For demonstrating the bumpless switching scheme, we carry out two cases of simulations.

Case 1 Switching during normal load variation:

Simulation is carried out for 50 s. Initially the generator G_2 output is set to 200 MW and it operates with controller C_8 corresponding to the output power of 200 MW. We propose 225 MW as the next power change, so we use the corresponding controller C_9 as offline controller with the respective bumpless compensator F. At t = 25 s, generated power of G_2 is increased from 200 MW to 225 MW with corresponding changes in load at t = 25 s. At t = 25 s, we switch in the offline controller C_9 and switching off the controller C_8. The simulation is continued up to t = 50 s. The responses of the generator with respect to rotor angles, angular velocity, terminal

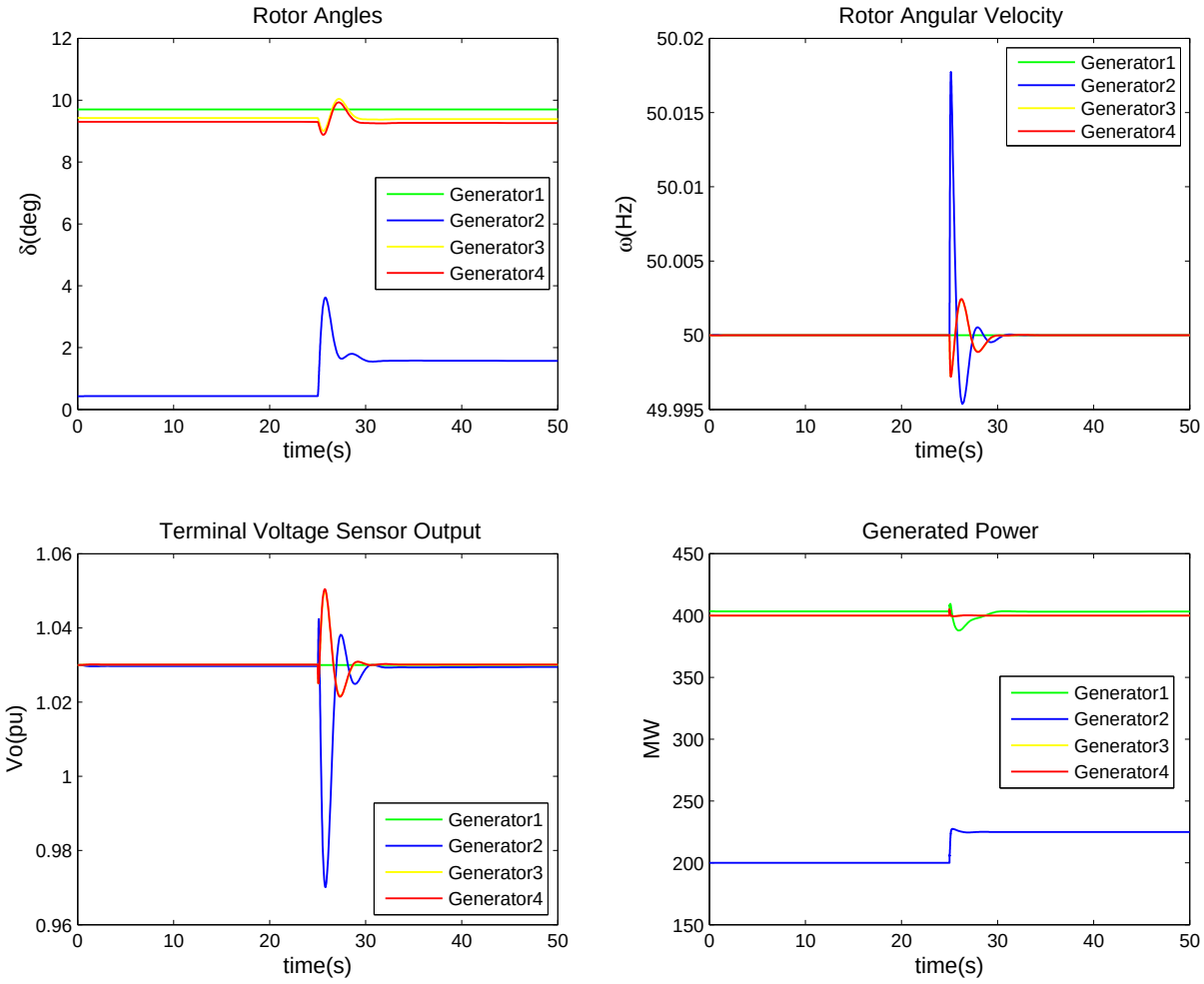

Figure 5.6. Case 1: Simulation responses of generator G_1 to G_4 with bumpless switching.

voltage and generated power are given in Figure 5.6. Comparison of the outputs of on and offline controllers, offline controller input from the bumpless compensator and the states of the offline controller and the filter are given in 5.7.

Case 2 Switching during transient regime:

In the simulation Case 1 above, the switching of controller was carried out in steady state conditions. Since we use the change in speed $\Delta\omega$ as the feedback variable for the controller, $\Delta\omega$ will be almost zero under steady state conditions. To show the effect of bumpless switching, in this case we switch the controllers under transient

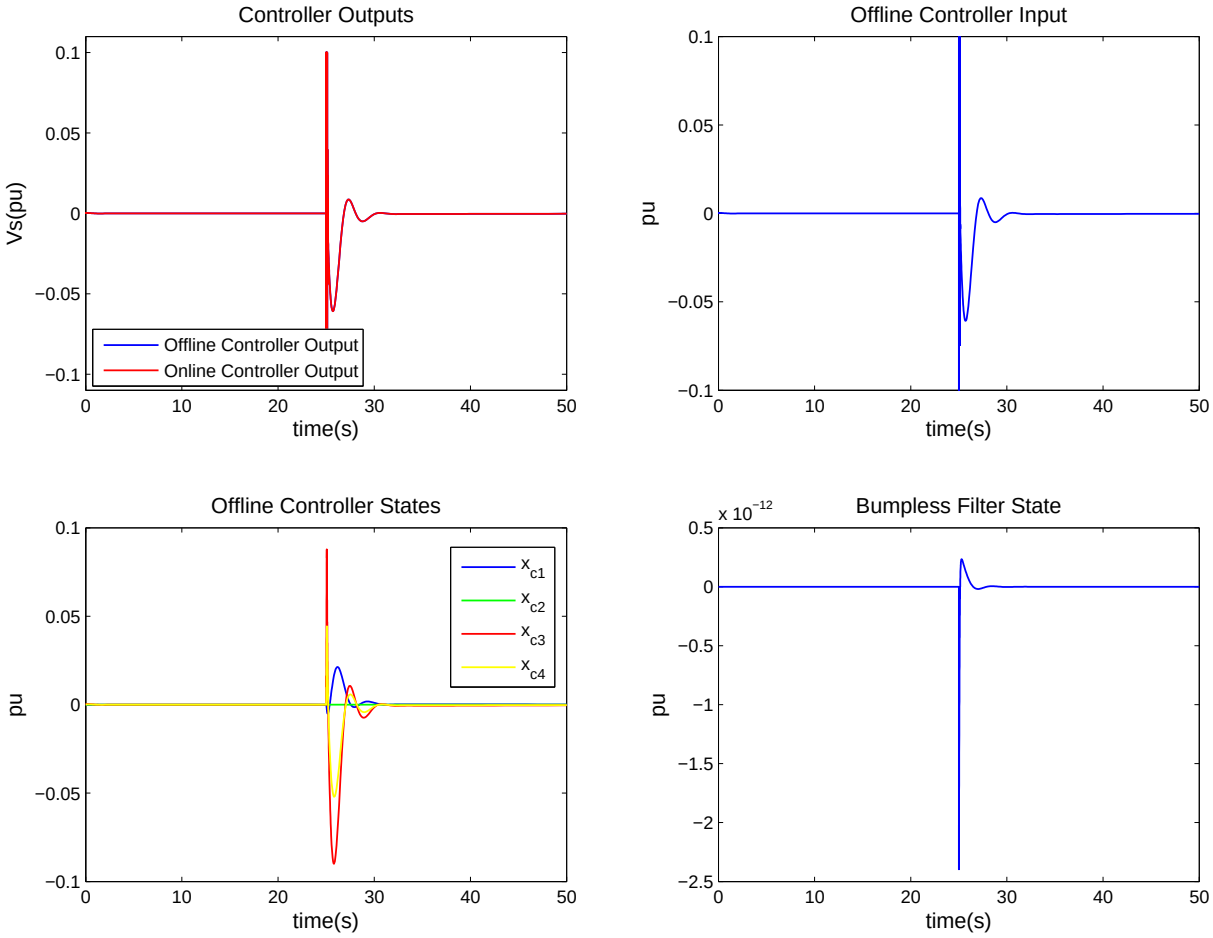

Figure 5.7. Case 1: Offline and Online controller responses

conditions. To start with at t = 0 s, the generator G_2 output is set to 25 MW with controller C_1 as online and controller C_2 as offline. At t = 10 s, output of G_2 is increased to 50 MW with controller C_2 as online and controller C_3 as offline. Before the transients settle, at t = 12 s, output of G_2 is increased to 75 MW with controller C_3 as online and controller C_4 as offline and simulation is continued up to t = 40 s. To compare the situation without bumpless switching, similar simulations are carried out without bumpless scheme. The comparison of responses of generator G_2 with respect to rotor angles, angular velocity, terminal voltage and generated power is given in Figure 5.8.

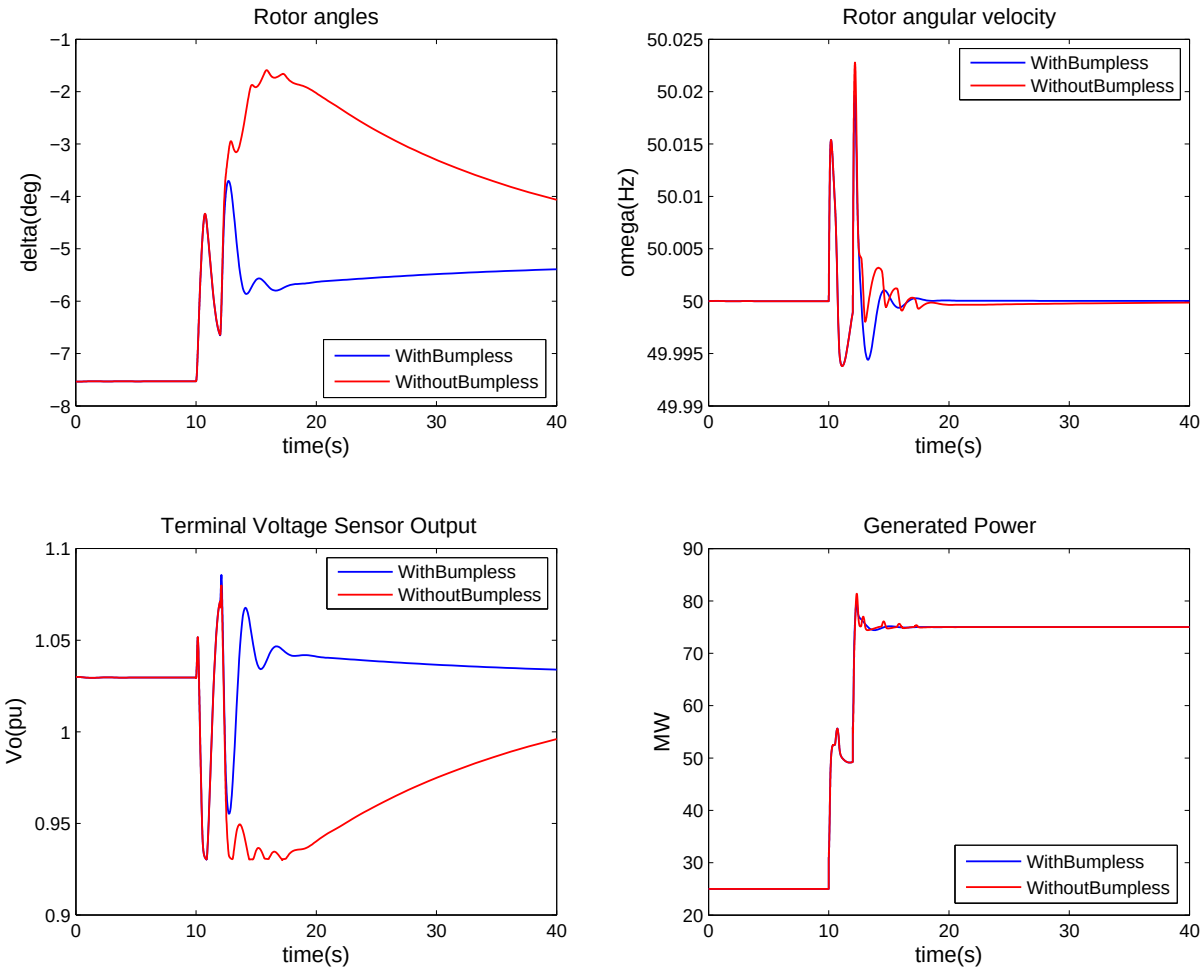

Figure 5.8. Case 2: Comparison of G_2 response with and without bumpless switching.

5.5.2 Inferences from simulation results

Case 1 Switching during normal load variation:

From Figure 5.7, it can be seen that the output of the offline controller driven by the respective bumpless compensator was able to track the online controller output. It can also be seen from Figure 5.6, that the response of the generator parameters with bumpless scheme is found to be normal.

Case 2 Switching during transient regime:

From Figure 5.8, comparison of the case of switching without bumpless, with bumpless switching scheme, the one with bumpless switching produces less overshoot magnitudes and quick settling with respect to rotor angle, angular velocity, terminal voltage and generated power. We can conclude that the bumpless scheme is effective in containing switching transients, if switching is done in unsteady conditions.

5.6 Chapter summary

The principle behind bumpless switching scheme in minimising the switching transients is explained. The linear quadratic bumpless switching scheme and the synthesis of bumpless compensator synthesis are included in detail. Application of the bumpless switching scheme for power system controller switching is outlined. The bumpless switching scheme is evaluated by applying the scheme to a test case power system and simulating the system under different cases. To show the effectiveness of the scheme in containing the switching transients, switching is deliberately done in transient regime and the results of the simulations are presented.

Chapter 6

Simulation Results

6.1 Introduction

Modeling and simulation form an important and integral part in the power system design, planning, investigation and operation. With ever increasing complexity of the power system grid, simulation and analysis become more important than ever before. Simulation has proved to be a necessary and effective tool for the study and analysis of modern power systems [103].

Power system control has been evolving continuously as the power systems grow in size and complexities. To tackle the challenges posed by this, new control methodologies are continuously being developed. Controllers developed using advanced controller design methodologies, use simulations to demonstrate the controller performance [10,31,33–35,37,104,105]. In these works, controllers are designed for a test case power system and the performance is evaluated through simulations done under different scenarios. New control methodologies are validated for their performance by using different simulation methodologies such as computer simulations, digital electromagnetic transient simulations in real time, hybrid simulations, etc., [103].

In this chapter, we demonstrate the performance of the proposed controller design methodology through nonlinear computer simulations. Validation of the controller using Real Time Digital Simulation (RTDS) facility is included in Chapter 7. Two area 11 bus, 4 machine power system is chosen as the test case power system and controllers are designed for the system. Simulations are carried out to cover different situations such as load generation variations, fault conditions and generator reference voltage variations. The performance of the proposed controller is also compared with conventional Power System Stabiliser (PSS).

This chapter is organised as follows: First part consists of the test case system description and controller design. The next part includes the simulation methodology and simulation cases considered and the last part consists of simulation results and inference.

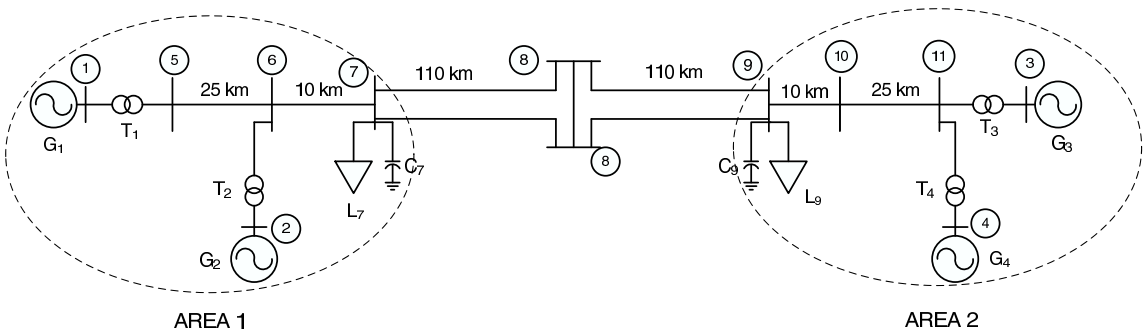

Figure 6.1. Two area four machine system.

6.2 Test Case System

The two area, four machine, 11 bus power grid system shown in Figure 6.1 is considered as a test case system. The system consists of two power system areas Area 1 and Area 2 connected through a twin circuit tie line of 220 km in length. The transmission system nominal voltage is 400 kV. Generation voltages are stepped up by the transformers connected to the generators. Load centers are located at buses 7 and 9. Buses 7 and 9 have shunt capacitors.

Generators 1 to 4 and transformers 1 to 4 are identical and their parameters are given in Appendix A, Table A.1 and A.3. The generator AVR parameters are given in Table A.2. Transmission line parameters are given in 400 kV, 100 MVA base in Table A.4. For the analysis of the system, 400 kV and 100 MVA are chosen as base quantities. For simulation purpose, Generators G_1, G_3 and G_4 are assumed to function as base generators with constant power output. Load variations from base load is catered for by generator G_2.

For the assumed conditions, the power system considered is open loop unstable. The pole locations of the model linearised about the SEP corresponding to G_1, G_3 and G_4 at 400 MW and G_2 at 200 MW (this SEP is designated as SEP 8, refer Table 6.2) are given in Figure 6.2 and Table 6.1. The open loop pole locations indicate that the system is marginally unstable and a power stabiliser is required to stabilise and to increase the damping of the system.

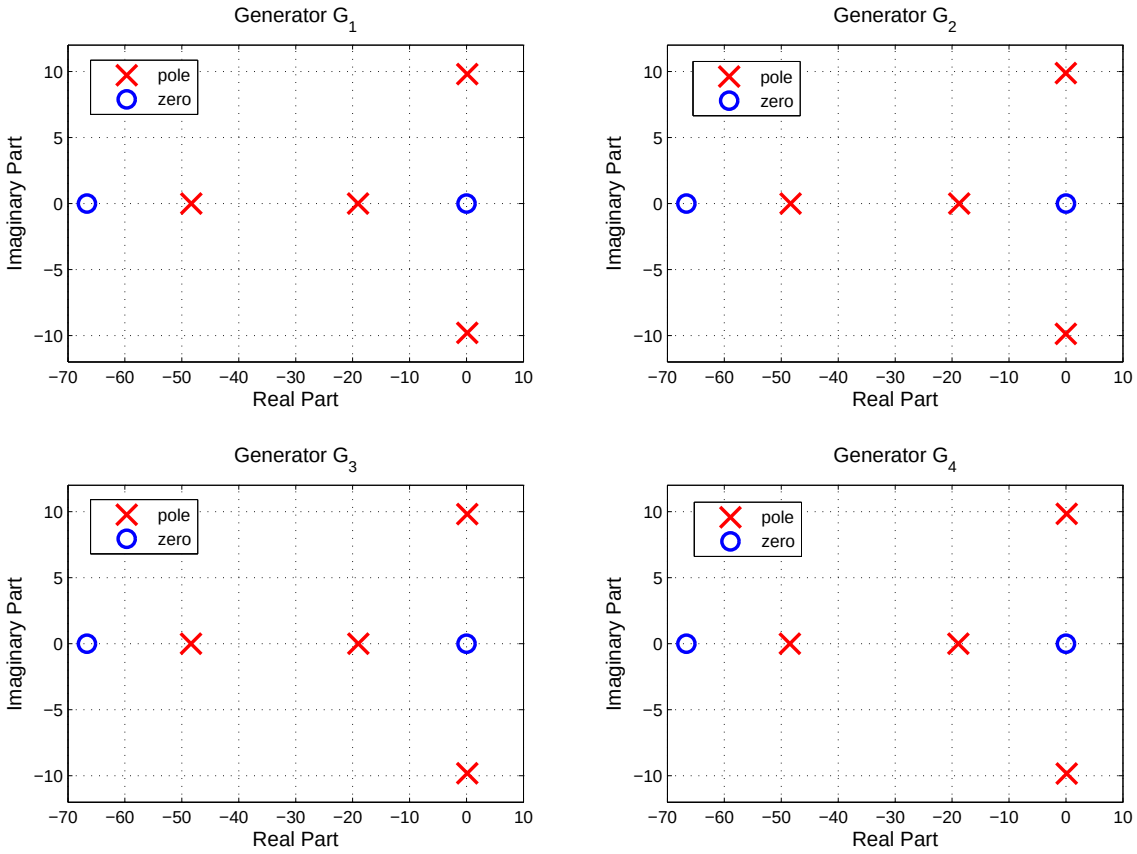

Figure 6.2. Locations of open loop poles and zeros for Generator G_1 to G_4 corresponding to the SEP 8.

Generator G_1	Poles	-48.3470 + $\jmath$ 0.0000	-19.0430 − $\jmath$ 0.0000
		0.1355 + $\jmath$ 9.7952	0.1355 − $\jmath$ 9.7952
	Zeros	-66.6670 + $\jmath$ 0.0000	0.0000 + $\jmath$ 0.0000
Generator G_2	Poles	-48.3630 + $\jmath$ 0.0000	-0.0068 − $\jmath$ 9.8727
		-0.0068 − $\jmath$ 9.8727	-18.7450 + $\jmath$ 0.0000
	Zeros	-66.6670 + $\jmath$ 0.0000	0.0000 + $\jmath$ 0.0000
Generator G_3	Poles	-48.3780 + $\jmath$ 0.0000	-19.0060 − $\jmath$ 0.0000
		0.1315 + $\jmath$ 9.8057	0.1315 − $\jmath$ 9.8057
	Zeros	-66.6670 + $\jmath$ 0.0000	0.0000 + $\jmath$ 0.0000
Generator G_4	Poles	-48.4890 + $\jmath$ 0.0000	-18.8990 − $\jmath$ 0.0000
		0.1325 + $\jmath$ 9.8290	0.1325 − $\jmath$ -9.8290
	Zeros	-66.6670 + $\jmath$ 0.0000	0.0000 + $\jmath$ 0.0000

Table 6.1. Locations of open loop poles and zeros for Generator G_1 to G_4 corresponding to the SEP 8.

SEP 1	SEP 2	SEP 3	SEP 4	SEP 5	SEP 6	SEP 7	SEP 8
25 MW	50 MW	75 MW	100 MW	125 MW	150 MW	175 MW	200 MW
SEP 9	SEP 10	SEP 11	SEP 12	SEP 13	SEP 14	SEP 15	SEP 16
225 MW	250 MW	275 MW	300 MW	325 MW	350 MW	375 MW	400 MW

Table 6.2. Identification of different the SEPs of generator G_2.

6.3 Controller Design

Controllers are designed for the generators connected to the grid using the methodology described in Chapter 3. For this test system, we assume that all the change in the load is supplied by Generator G_2. The variations in the output power for the Generators G_1, G_3 and G_4 are minimal hence it is proposed to have a single controller with a parameter variation uncertainty corresponding to 400 $\pm$ 25 MW and SEP 16 conditions.

The power output of Generator G_2 is assumed to vary from 0 to 400 MW. In order to design parameter varying switching controllers for G_2, the operating regime of G_2 is divided into 16 equal power output regions of 25 MW each. Each region is considered to have a SEP and 16 controllers are designed for G_2 with a robust stabilisation region of $\pm$ 25 MW. Therefore we have 16 SEPs corresponding to each regime. Different SEP identification numbers are given in Table 6.2.

For the controller design, we get the system matrices corresponding to the SEPs and SEP $\pm$ 25 MW conditions. To get these system matrices, NR load flow analysis is carried out for these operating points and reduced network models are arrived at, as described in Chapter 2. The results of the Matlab code developed for this purpose are verified by comparing them with PSS/E Siemens software results. System matrices are computed for the SEPs using the linearised multimachine power system model given by (2.33), (2.38), (2.39), (2.44) and (2.49). The load flow results and system matrices corresponding to the SEP 8 are given in Figure 6.3 and equations 6.1 and 6.2. The subsystem matrices A_i, B_i and L_i can be obtained for the SEPs using equations (3.36) to (3.38) from the corresponding system matrices A_{SYS} and B_{SYS}. The parametric uncertainty around the SEP is included by computing the system matrices corresponding to SEP $\pm$ 25 MW points. Now by using these matrices, the values α_i and β_i can be selected so that the condition laid by inequality 3.40 is satisfied. The selected values of α_i and β_i for different SEPs are given in Table 6.3.

Now having the subsystem matrices and uncertainties defined, we can synthesise the controller by solving the optimisation control problem through rank constrained LMIs as outlined in Chapter 3. The controller design steps corresponding to a SEP can be summarised as follows:

(i) Using the load flow results corresponding to the SEP, the system matrices A_{SYS} and B_{SYS} can be found using (2.33), (2.38), (2.39), (2.44) and (2.49).

(ii) From the system matrices A_{SYS} and B_{SYS}, the subsystem matrices and uncertainty definitions can be found using (3.36), (3.37), (3.38) and (3.40).

(iii) With the subsystem matrices and uncertainties defined, the rank constrained LMI problem (3.117) is solved, to a desired accuracy, obtaining a collection of $\theta_i, \tau_i, \eta_i, \tilde{X}_i, Y_i$.

(iv) Substituting the found θ_i, τ_i, η_i into GAREs (3.48) and solving (3.48) to obtain X_i. Note that Y_i can be selected from the found feasible solution the problem (3.117) (refer the proof of Theorem 3 of [97]).

(v) The robust stabilising controller can be constructed (3.51) using the computed θ_i, τ_i, η_i, X_i and Y_i.

The designed controller matrices corresponding to SEP 8 are given in Table 6.4. The closed loop pole locations are investigated with the designed controllers. The closed loop pole locations with the designed controllers corresponding to SEP 8 conditions are given in Figure 6.4 and in Table 6.5.

For comparison purpose, conventional IEE 2ST PSS is used in the simulations and the PSS controller parameters are given in Appendix A, Table A.5. Having the controllers designed for the SEPs, the dwell time required for stable switching are computed and the bumpless compensators for reducing switching transients are designed next.

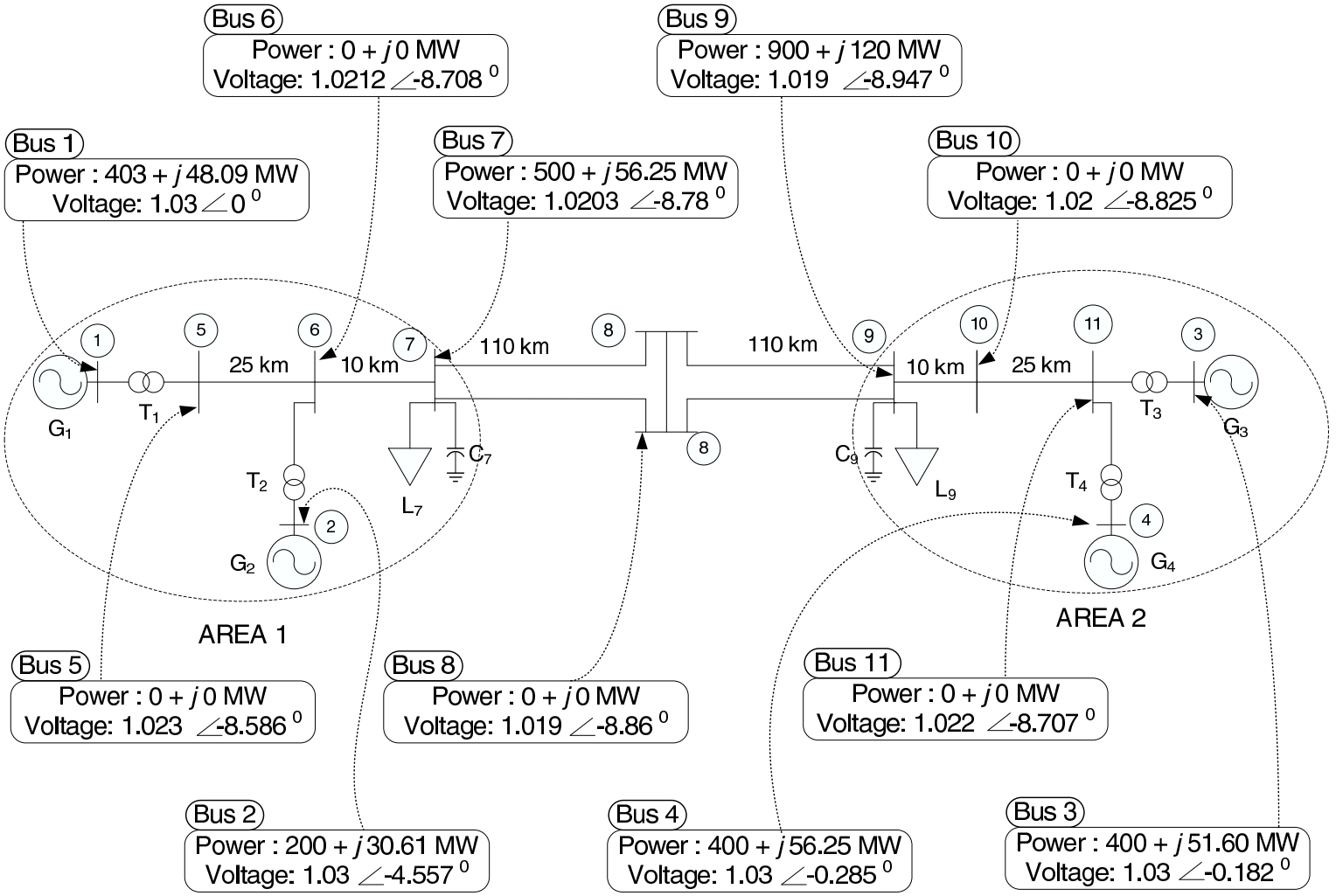

Figure 6.3. Load flow results corresponding to the SEP 8.

$$A_{SYS1} = \begin{bmatrix} 0.0000 & 376.0000 & 0.0000 & 0.0000 & 0.0000 & 0.0000 & 0.0000 & 0.0000 \\ -0.2473 & 0.0000 & -0.1308 & 0.0000 & 0.0821 & 0.0000 & -0.0379 & 0.0000 \\ -0.1096 & 0.0000 & -0.4541 & -22.2220 & 0.0517 & 0.0000 & 0.1022 & 0.0000 \\ -4.2570 & 0.0000 & 39.3320 & -66.6670 & 2.6168 & 0.0000 & 8.6555 & 0.0000 \\ 0.0000 & 0.0000 & 0.0000 & 0.0000 & 0.0000 & 376.0000 & 0.0000 & 0.0000 \\ 0.0904 & 0.0000 & -0.0108 & 0.0000 & -0.2584 & 0.0000 & -0.0778 & 0.0000 \\ 0.0153 & 0.0000 & 0.1126 & 0.0000 & -0.0390 & 0.0000 & -0.4559 & -22.2220 \\ 0.3974 & 0.0000 & 9.0011 & 0.0000 & -0.7622 & 0.0000 & 39.3810 & -66.6670 \\ 0.0000 & 0.0000 & 0.0000 & 0.0000 & 0.0000 & 0.0000 & 0.0000 & 0.0000 \\ 0.0826 & 0.0000 & -0.0196 & 0.0000 & 0.0769 & 0.0000 & -0.0325 & 0.0000 \\ 0.0273 & 0.0000 & 0.1008 & 0.0000 & 0.0443 & 0.0000 & 0.0957 & 0.0000 \\ 0.7125 & 0.0000 & 8.2299 & 0.0000 & 2.1387 & 0.0000 & 8.0530 & 0.0000 \\ 0.0000 & 0.0000 & 0.0000 & 0.0000 & 0.0000 & 0.0000 & 0.0000 & 0.0000 \\ 0.0831 & 0.0000 & -0.0201 & 0.0000 & 0.0775 & 0.0000 & -0.0330 & 0.0000 \\ 0.0279 & 0.0000 & 0.1014 & 0.0000 & 0.0449 & 0.0000 & 0.0962 & 0.0000 \\ 0.7494 & 0.0000 & 8.2780 & 0.0000 & 2.1831 & 0.0000 & 8.0950 & 0.0000 \end{bmatrix}$$

$$A_{SYS2} = \begin{bmatrix} 0.0000 & 0.0000 & 0.0000 & 0.0000 & 0.0000 & 0.0000 & 0.0000 & 0.0000 \\ 0.0823 & 0.0000 & -0.0204 & 0.0000 & 0.0828 & 0.0000 & -0.0211 & 0.0000 \\ 0.0284 & 0.0000 & 0.1006 & 0.0000 & 0.0294 & 0.0000 & 0.1010 & 0.0000 \\ 0.7833 & 0.0000 & 8.2243 & 0.0000 & 0.8570 & 0.0000 & 8.2691 & 0.0000 \\ 0.0000 & 0.0000 & 0.0000 & 0.0000 & 0.0000 & 0.0000 & 0.0000 & 0.0000 \\ 0.0837 & 0.0000 & -0.0080 & 0.0000 & 0.0843 & 0.0000 & -0.0087 & 0.0000 \\ 0.0114 & 0.0000 & 0.1041 & 0.0000 & 0.0123 & 0.0000 & 0.1047 & 0.0000 \\ 0.1478 & 0.0000 & 8.3066 & 0.0000 & 0.2170 & 0.0000 & 8.3565 & 0.0000 \\ 0.0000 & 376.0000 & 0.0000 & 0.0000 & 0.0000 & 0.0000 & 0.0000 & 0.0000 \\ -0.2480 & 0.0000 & -0.1304 & 0.0000 & 0.0885 & 0.0000 & -0.0256 & 0.0000 \\ -0.1073 & 0.0000 & -0.4550 & -22.2220 & 0.0357 & 0.0000 & 0.1078 & 0.0000 \\ -4.1128 & 0.0000 & 39.2780 & -66.6670 & 1.2616 & 0.0000 & 8.8799 & 0.0000 \\ 0.0000 & 0.0000 & 0.0000 & 0.0000 & 0.0000 & 376.0000 & 0.0000 & 0.0000 \\ 0.0886 & 0.0000 & -0.0253 & 0.0000 & -0.2493 & 0.0000 & -0.1296 & 0.0000 \\ 0.0351 & 0.0000 & 0.1080 & 0.0000 & -0.1079 & 0.0000 & -0.4569 & -22.2220 \\ 1.2219 & 0.0000 & 8.8845 & 0.0000 & -4.1543 & 0.0000 & 39.1270 & -66.6670 \end{bmatrix}$$

$$A_{SYS} = [A_{SYS1} \quad A_{SYS2}] \tag{6.1}$$

$$B_{SYS} = \Big[0.0,\ 0.0,\ 22.22,\ 0.0,\ 0.0,\ 0.0,\ 22.22,\ 0.0,\ 0.0,\ 0.0,\ 22.22,\ 0.0,\ 0.0,\ 0.0,\ 22.22,\ 0.0\Big] \tag{6.2}$$

SEP	1	2	3	4	5	6	7	8
$\alpha_i = \beta_i$	0.6341	0.8964	0.8957	0.8950	0.8944	0.8937	0.8931	0.8925
SEP	9	10	11	12	13	14	15	16
$\alpha_i = \beta_i$	0.8918	0.8912	0.8906	0.8900	0.8894	0.8887	0.8881	0.6277

Table 6.3. Value of parameter variation constants α_i and β_i.

	A_c				B_c	K'_c
Generator G_1	0.00	485.96	0.00	0.00	−219.92	−52.91
	−0.25	−15.32	−0.13	0.00	30.64	7.143e4
	−1175.90	1.5875e6	−650.12	−0.57	−356.09	−29.24
	−3.96	111.09	39.14	−66.67	−222.35	0.97
Generator G_2	0.00	482.85	0.00	0.00	−106.85	−109.54
	−0.26	−14.24	−0.06	0.00	14.25	1.3515e4
	−2434.30	3.0034e6	−585.37	0.27	−185.49	−26.32
	0.43	131.96	39.46	−66.67	−132.00	1.01
Generator G_3	0.00	484.70	0.00	0.00	−217.39	−53.29
	−0.25	−15.21	−0.13	0.00	30.44	7.143e4
	−1184.30	1.5875e6	−647.50	−0.52	−350.44	−29.12
	−3.74	109.63	39.05	−66.67	−219.44	0.98
Generator G_4	0.00	483.90	0.00	0.00	−215.81	−53.72
	−0.25	−15.18	−0.13	0.00	30.38	7.1429e4
	−1193.90	1.5875e6	−645.48	−0.52	−349.95	−29.03
	−3.78	108.84	38.89	−66.67	−217.86	0.98

Table 6.4. Designed controllers for generators G_1 to G_4 corresponding to the SEP 8 conditions.

6.4 Controller Switching

6.4.1 Dwell time

Generators G_1, G_3 and G_4 have controllers corresponding to the power output of 400 MW. The controller for generator G_2 is selected with respect to the power output of G_2. To preserve switching stability we use dwell time constrained switching as described in Chapter 4. We compute dwell time required for different switching combinations. The computed dwell time for different switching sequence are given in Table 6.7.

Generator G_1	Poles	-317.0900 + $\jmath$ 318.6300	-317.0900 − $\jmath$ 318.6300
		-66.6540 + $\jmath$ 0.0000	-48.2000 + $\jmath$ 0.0000
		-0.0075 + $\jmath$ 0.0000	-0.0075 + $\jmath$ 0.0000
		-5.4269 + $\jmath$ 6.3017	-22.3710 − $\jmath$ 6.3017
	Zeros	-332.7100 + $\jmath$ 333.6000	-332.7100 − $\jmath$ 333.6000
		-0.0109 + $\jmath$ 0.0000	0.0000 + $\jmath$ 0.0000
		-66.6670 − $\jmath$ 0.0000	66.6600 + $\jmath$ 0.0000
Generator G_2	Poles	-292.6600 + $\jmath$ 292.7500	-292.6600 + $\jmath$ -292.7500
		-292.6600 + $\jmath$ 292.7500	-292.6600 − $\jmath$ 292.7500
		-66.6720 + $\jmath$ 0.0000	-0.0288 + $\jmath$ 0.0000
		-7.6812 + $\jmath$ 8.6070	-7.6812 − $\jmath$ 8.6070
		-17.6210 + $\jmath$ 0.0000	-48.3900 + $\jmath$ 0.0000
	Zeros	-299.7800 + $\jmath$ 299.7700	-299.7800 − $\jmath$ 299.7700
		-0.0352 + $\jmath$ 0.0000	0.0000 + $\jmath$ 0.0000
		-66.6670 + $\jmath$ 0.0000	-66.6710 + $\jmath$ 0.0000
Generator G_3	Poles	-315.7300 + $\jmath$ 317.2600	-315.7300 − $\jmath$ 317.2600
		-66.6550 + $\jmath$ 0.0000	-48.1590 + $\jmath$ 0.0000
		-0.0076 + $\jmath$ 0.0000	-5.4395 + $\jmath$ 0.0000
		-22.3910 + $\jmath$ 6.0905	-22.3910 − $\jmath$ 6.0905
	Zeros	-331.3500 + $\jmath$ 332.2400	-331.3500 − $\jmath$ 332.2400
		0.0000 + $\jmath$ 0.0000	-0.0110 + $\jmath$ 0.0000
		-66.6670 + $\jmath$ 0.0000	-66.6610 + $\jmath$ 0.0000
Generator G_4	Poles	-314.7300 + $\jmath$ 316.2700	-314.7300 − $\jmath$ 316.2700
		-66.6550 + $\jmath$ 0.0000	-48.2580 + $\jmath$ 0.0000
		-0.0077 + $\jmath$ 0.0000	-5.4713 + $\jmath$ 0.0000
		-22.2990 + $\jmath$ 6.0267	-22.2990 − $\jmath$ 6.0267
	Zeros	-330.3300 + $\jmath$ 331.2200	-330.3300 − $\jmath$ 331.2200
		0.0000 + $\jmath$ 0.0000	-0.0111 + $\jmath$ 0.0000
		-66.6670 + $\jmath$ 0.0000	-66.6610 + $\jmath$ 0.0000

Table 6.5. Locations of closed loop poles and zeros for Generator G_1 to G_4.

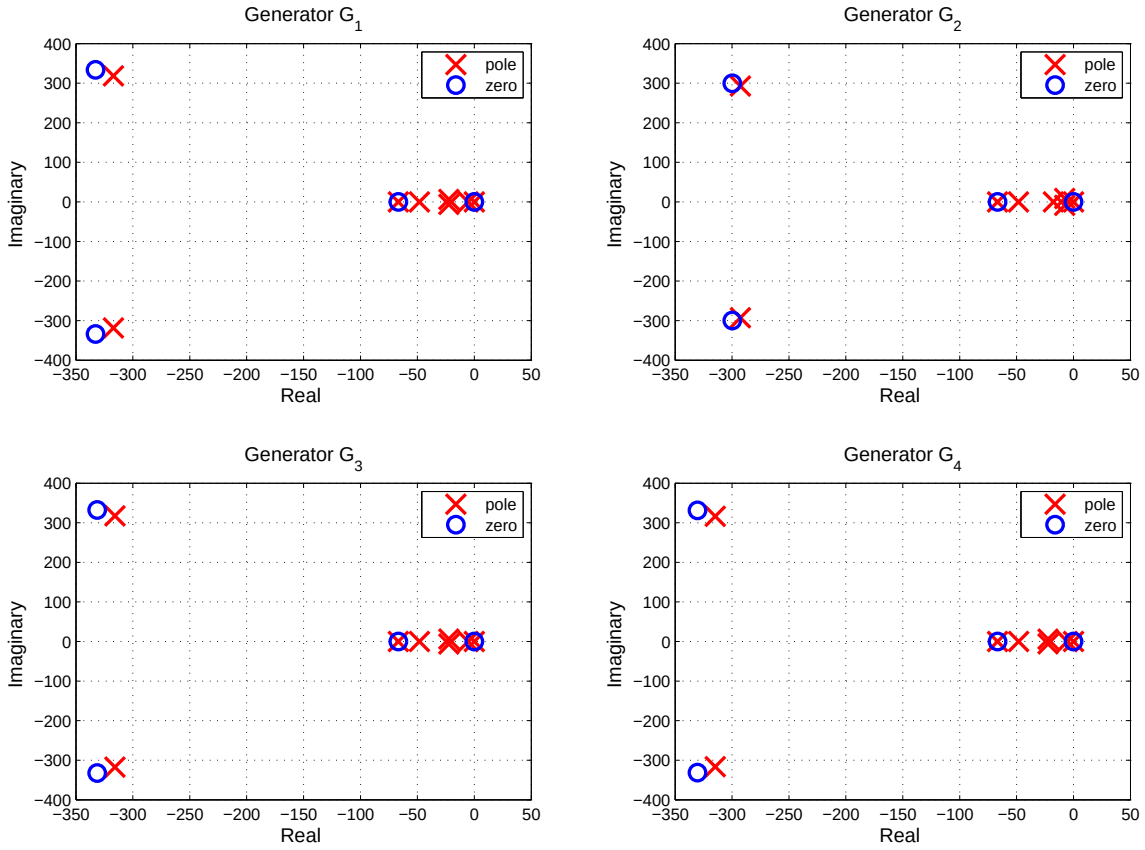

Figure 6.4. Locations of closed loop poles and zeros for Generator G_1 to G_4.

Parameter	Value
Gain K_1	10
Time constant T_1	0.0 s
Wash out time constant T_3	10.0 s
Wash out time constant T_4	10.0 s
First lead-lag time constant T_5	0.55 s
First lead-lag time constant T_6	0.2 s
Second lead-lag time constant T_7	0.55 s
second lead-lag time constant T_8	0.2 s
Third lead-lag time constant T_9	0.55 s
Third lead-lag time constant T_{10}	0.2 s
PSS voltage upper limit	0.1 pu
PSS voltage lower limit	-0.1 pu

Table 6.6. Conventional PSS Parameters

Power Change	Controller	τ_d^{12} (s)	Power Change	Controller	τ_d^{21}(s)
SEP 1 to 2	C_1 to C_2	23.9890	SEP 2 to 1	C_2 to C_1	24.7884
SEP 2 to 3	C_2 to C_3	22.8243	SEP 3 to 2	C_3 to C_2	21.5976
SEP 3 to 4	C_3 to C_4	23.4500	SEP 4 to 3	C_4 to C_3	21.2590
SEP 4 to 5	C_4 to C_5	22.9490	SEP 5 to 4	C_5 to C_4	23.4500
SEP 5 to 6	C_5 to C_6	21.0466	SEP 6 to 5	C_6 to C_5	22.9490
SEP 6 to 7	C_6 to C_7	21.4581	SEP 7 to 6	C_7 to C_6	20.1177
SEP 7 to 8	C_7 to C_8	24.1736	SEP 8 to 7	C_8 to C_7	22.7254
SEP 8 to 9	C_8 to C_9	22.8836	SEP 9 to 8	C_9 to C_8	24.1736
SEP 9 to 10	C_9 to C_{10}	24.0231	SEP 10 to 9	C_{10} to C_9	21.0308
SEP 10 to 11	C_{10} to C_{11}	23.6559	SEP 11 to 10	C_{11} to C_{10}	24.1475
SEP 11 to 12	C_{11} to C_{12}	22.4421	SEP 12 to 11	C_{12} to C_{11}	23.9659
SEP 12 to 13	C_{12} to C_{13}	23.3025	SEP 13 to 12	C_{13} to C_{12}	22.7156
SEP 13 to 14	C_{13} to C_{14}	24.3393	SEP 14 to 13	C_{14} to C_{13}	23.3025
SEP 14 to 15	C_{14} to C_{15}	21.4414	SEP 15 to 14	C_{15} to C_{14}	24.2053
SEP 15 to 16	C_{15} to C_{16}	24.8533	SEP 16 to 15	C_{16} to C_{15}	21.5085

Table 6.7. Values of required dwell time for different controller switchings.

6.4.2 Bumpless switching

The transients during switching are avoided by using bumpless switching scheme. Bumpless compensators are to be designed as per the procedure outlined in Chapter 5. To allow switchings above and below the current operating points, corresponding adjacent bumpless compensators are kept ON.

6.5 Simulation

6.5.1 Simulation model

The nonlinear model of the i^{th} generator in a multimachine power system consisting of n generators given by equations (2.25) to (2.32) are used for simulation. It is assumed that the prime mover mechanical power changes are achieved instantaneously. The rotor angle δ_i, rotor angular velocity ω_i, equivalent q-axis voltage E_{qi} and the sensor output voltage V_{oi} are used as variables for integration along with the states of controllers.

6.5.2 Simulation software

Matlab simulation software is developed for simulating the multimachine system. The Matlab integration routine "ode15s" is used for integration.

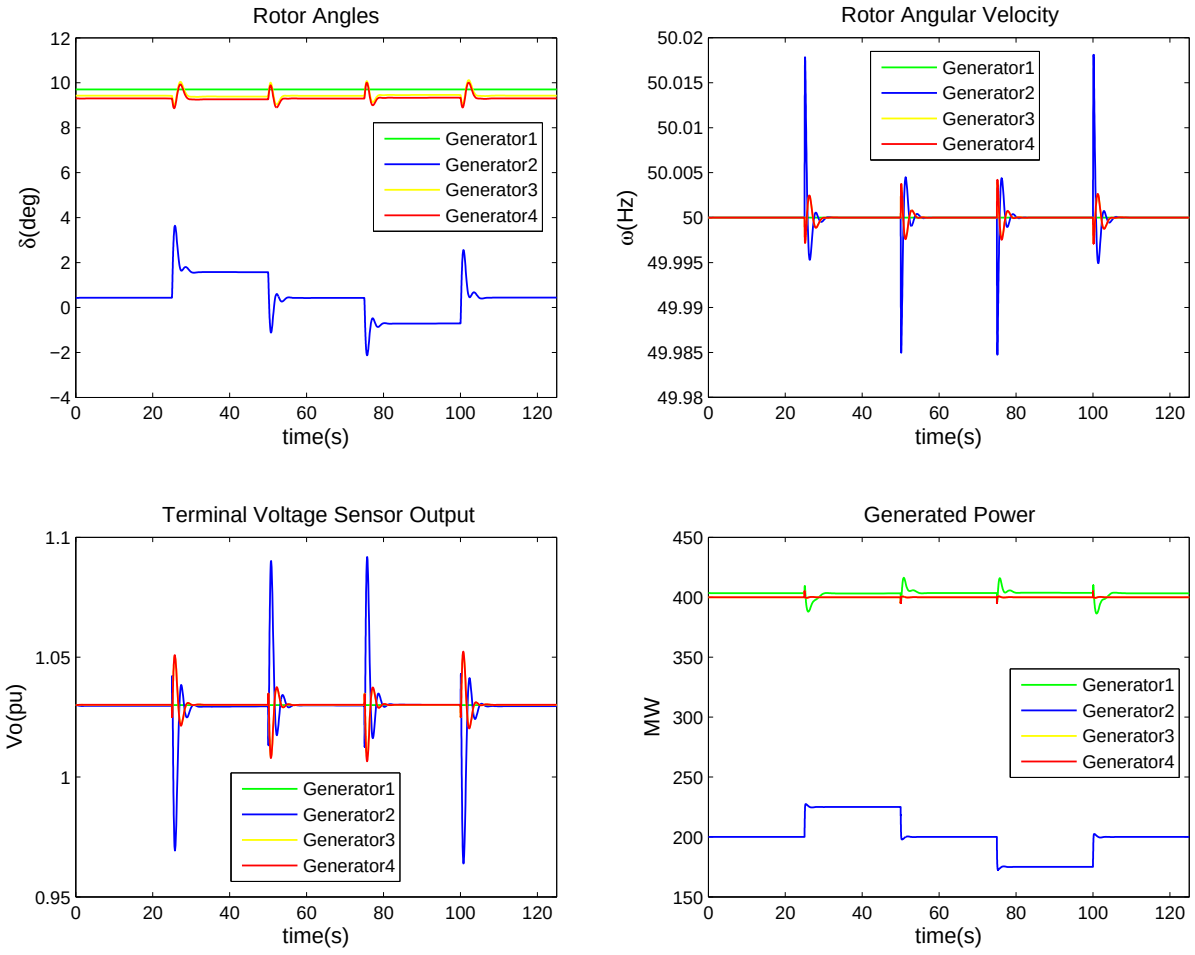

Figure 6.5. Case 1: G_2 generation varied within the SEP 8 zone - responses of generators G_1 to G_4.

6.5.3 Simulation Cases

The performance of the proposed controller is evaluated against parameter variations, fault conditions and Automatic Voltage Regulator (AVR) reference voltage variations, through the following cases of simulation studies. The performance of the controller under each case is also compared with conventional IEE 2ST PSS operating under similar conditions. Simulated responses of the generators G_1 to G_4 with respect to rotor angle, angular velocity, terminal voltage sensor output, generated power, equivalent q-axis voltage, field voltage, controller output and generator

G_2 controller states are plotted for each simulation case. Simulation results under each case are analysed.

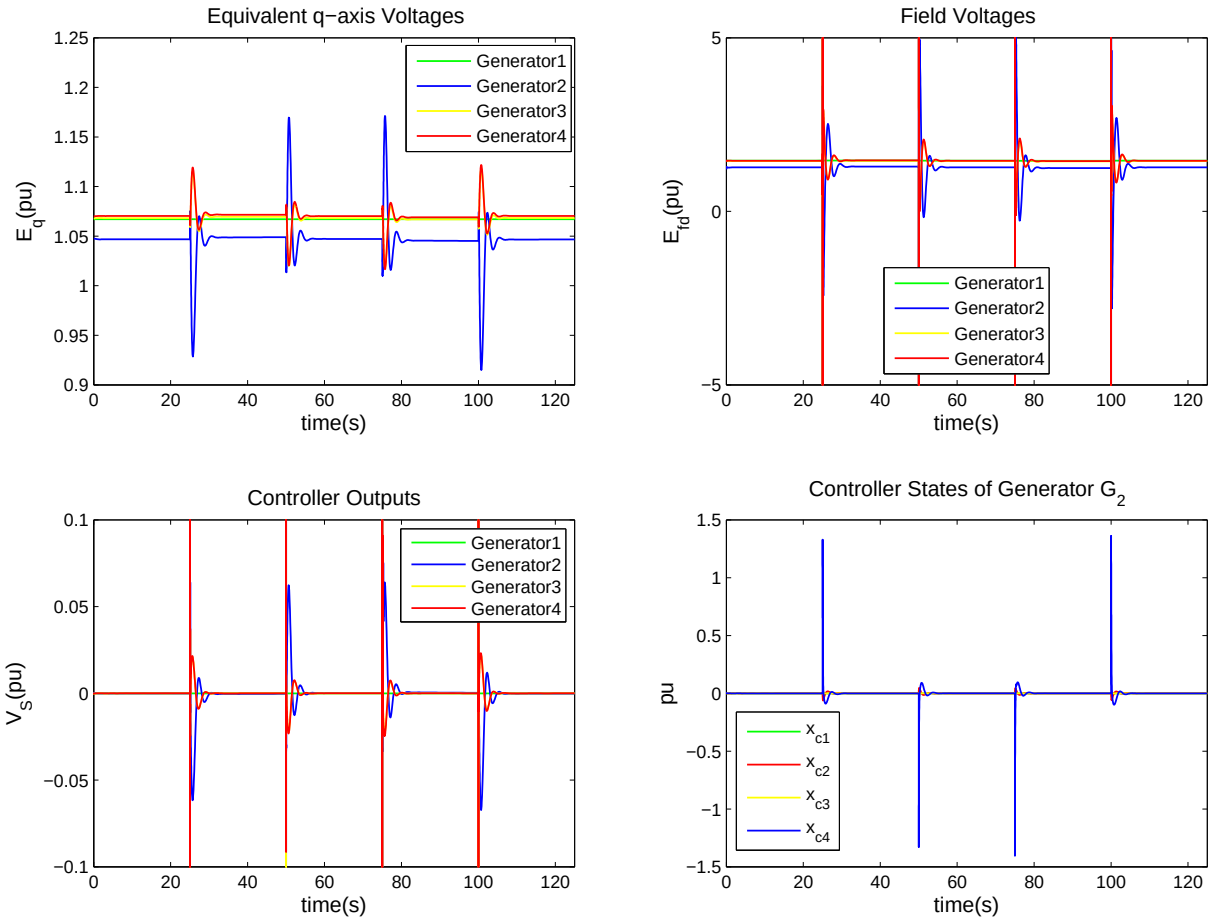

Figure 6.6. Case 1: G_2 generation varied within the SEP 8 zone - responses of generators G_1 to G_4.

Case 1: Load variation within a zone

To evaluate the performance of the controller for load variations within a zone SEP 8 is considered. Generated power of G_2 is varied through a range of 200 ± 25 MW. Controller C_8 corresponding to SEP 8 is used for G_2. The power variation schedule for G_2 is given in Table 6.8.

Time	0 - 25 s	25 - 50 s	50 - 75 s	75 - 100 s	100 - 125 s
G_2 Power	200 MW	225 MW	200 MW	175 MW	200 MW

Table 6.8. Case 1: Generation schedule for generator G_2

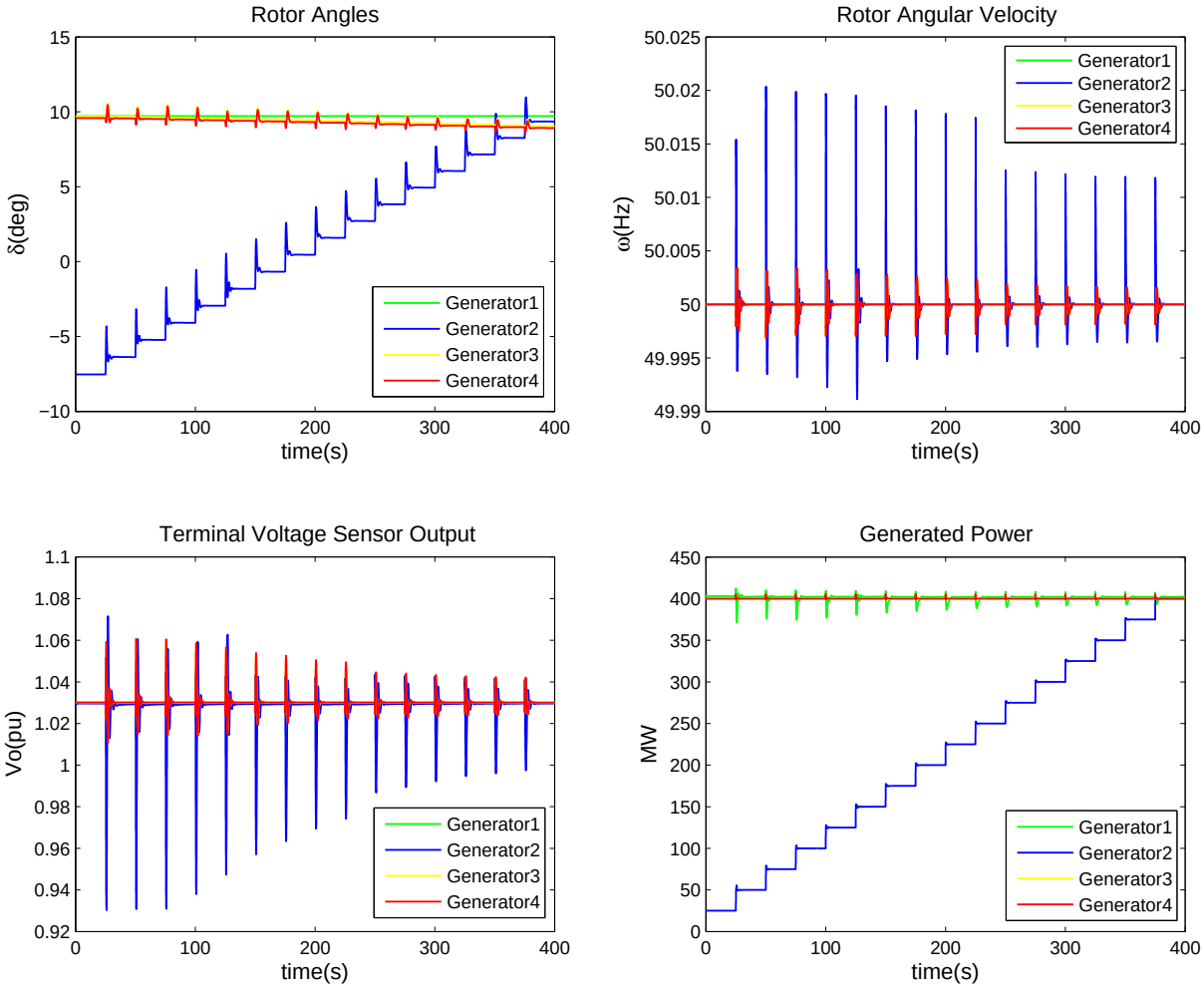

Figure 6.7. Case 2: G_2 generation increased from 25 to 400 MW - responses of generators G_1 to G_4.

Results

The responses of the generators are given in Figures 6.5 and 6.6. For the prescribed up and down load variations around the SEP, the proposed controller produces a satisfactory response with the transient responses settling down quickly, with less

oscillations.

Case 2: G_2 power output increase from minimum to maximum

To validate the controller performance over the entire operating range of the generator, generated power of G_2 is increased from 25 MW to 400 MW in steps of 25 MW with corresponding changes in load. At each step of power change, controller corresponding to the respective SEP is switched in. The generator G_2 power is changed at 25 s interval meeting the dwell time constraint for the controller switching.

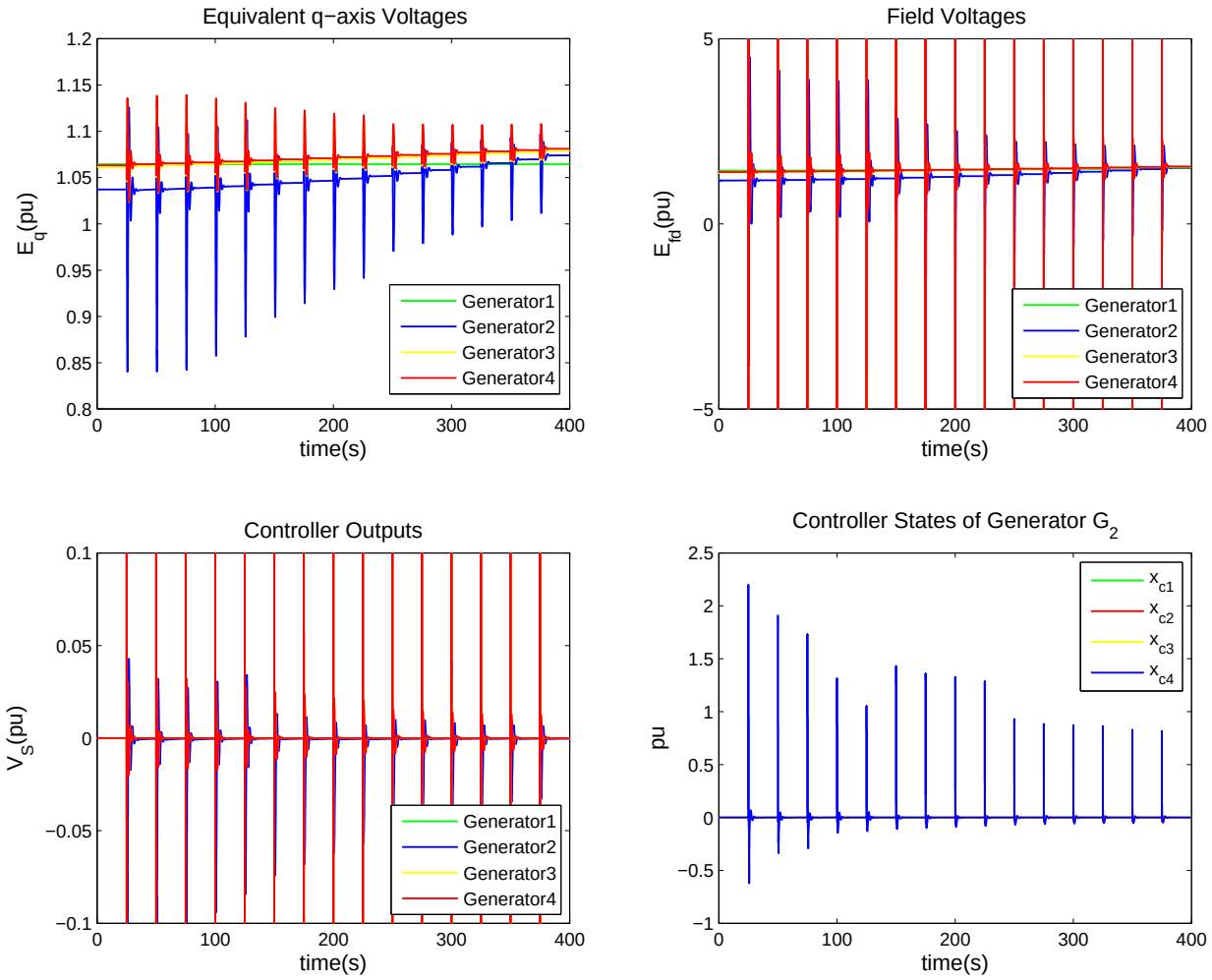

Figure 6.8. Case 2: G_2 generation increased from 25 to 400 MW - responses of generators G_1 to G_4.

Results

The responses of the generators for the G_2 power output increase from minimum to maximum are given in Figures 6.7 to 6.9. The system responses with conventional PSS are given in Figure 6.9. Comparing the responses produced by the proposed controller and conventional PSS, from the settling time values, it can be seen that the proposed controller contains the oscillations faster than the conventional controller.

Apart from this, from the rotor angular velocity responses in Figures 6.7 and 6.9, it can be seen that with respect to the settling time taken for power change disturbances by conventional PSS are not uniform over the entire operating range of G_2. This is because, same PSS is used under different system parameter conditions arising due to generation and load changes. Whereas the proposed controller provides a better and uniform response over the entire operating range. The overshoot above the steady state settling value and settling time taken to settle with in $\pm$ 5 % of the steady state value, with respect to the rotor angle response of G_2 is given in Table 6.9. With the proposed controller, for the simulated power changes, the overshoot varies between 1.6049 deg and 2.3948 deg and settling time between 4.5302 and 5.9922 s. With conventional PSS overshoot varies between 0.7521 deg and 2.9714 deg and settling time between 10.7858 s and 13.4199 s producing a wide difference in performance as the operating point changes.

Case 3: G_2 power output decrease from maximum to minimum

The situation is similar to Case 2 above, but the generated power of G_2 is decreased from 400 MW to 25 MW in steps of 25 MW. At each step of power change, controller corresponding to the respective SEP is switched in.

Results

The responses of the generators for the G_2 power output decrease from maximum to minimum are given in Figures 6.10 to 6.12. The system responses with conventional PSS are given in Figure 6.12. As in the generation increase case, for the load decrease case also, the proposed controller produces a better response for the load decrease case when compared with conventional PSS.

Again from the rotor angular velocity responses in Figures 6.10 and 6.12, it can be seen that the responses produced by conventional PSS are not uniform for the power variation over the entire operating range of G_2. Whereas the proposed controller provides a better and uniform response over the entire operating range.

Power Change	With proposed controller		With conventional PSS	
	Over shoot (deg)	Set. time (s)	Over shoot (deg)	Set. time (s)
SEP 1 to SEP 2	2.0479	5.4386	0.7521	10.7858
SEP 2 to SEP 3	2.0630	4.6268	0.9846	11.4481
SEP 3 to SEP 4	2.3866	4.9204	1.2665	12.0542
SEP 4 to SEP 5	2.3948	5.0810	1.5481	12.5884
SEP 5 to SEP 6	2.3522	4.8932	1.7789	13.0229
SEP 6 to SEP 7	2.1895	4.5302	2.0056	13.4199
SEP 7 to SEP 8	2.1455	4.6054	2.1500	12.6432
SEP 8 to SEP 9	2.0512	4.7568	2.3160	12.9374
SEP 9 to SEP 10	2.0199	4.8465	2.4465	11.9951
SEP 10 to SEP 11	1.7053	5.8360	2.5511	12.0810
SEP 11 to SEP 12	1.6910	5.9922	2.6410	11.4172
SEP 12 to SEP 13	1.7018	4.8778	2.7410	11.6502
SEP 13 to SEP 14	1.6049	4.9519	2.7938	11.8375
SEP 14 to SEP 15	1.6206	4.9884	2.8837	12.0367
SEP 15 to SEP 16	1.6305	5.0497	2.9714	12.1813

Table 6.9. Case 2: G_2 power output increase - Comparison of Overshoot and Settling time

The overshoot above the settling value and settling time with respect to the rotor angle response of G_2 are given in Table 6.10. With the proposed controller for the simulated power changes, the overshoot varies between 0.6578 deg and 2.3866 deg and settling time between 4.4698 and 6.1738 s. With conventional PSS, overshoot varies between 0.1600 deg and 0.8031 deg and settling time between 5.8045 and 16.0265 s producing a wide difference in performance as the operating point changes.

Case 4: Tie line tripping due to fault

To evaluate the performance of the controller under fault conditions, a fault scenario is simulated by tripping one of the circuits between buses 7 and 9. The output of generators G_1, G_3 and G_4 are at 400 MW and G_2 at 200 MW. Tie line is tripped at t = 3 s and at, t = 9 s, the tie line circuit is energised back and the simulation is continued with pre-fault system. Controller is not changed in this case.

Results

The responses of the generators for the fault scenario simulated are given in Figures 6.13 to 6.15. The system responses with conventional PSS are given in Figure 6.15. With reference to the responses in Figures 6.13 to 6.15, the proposed controller

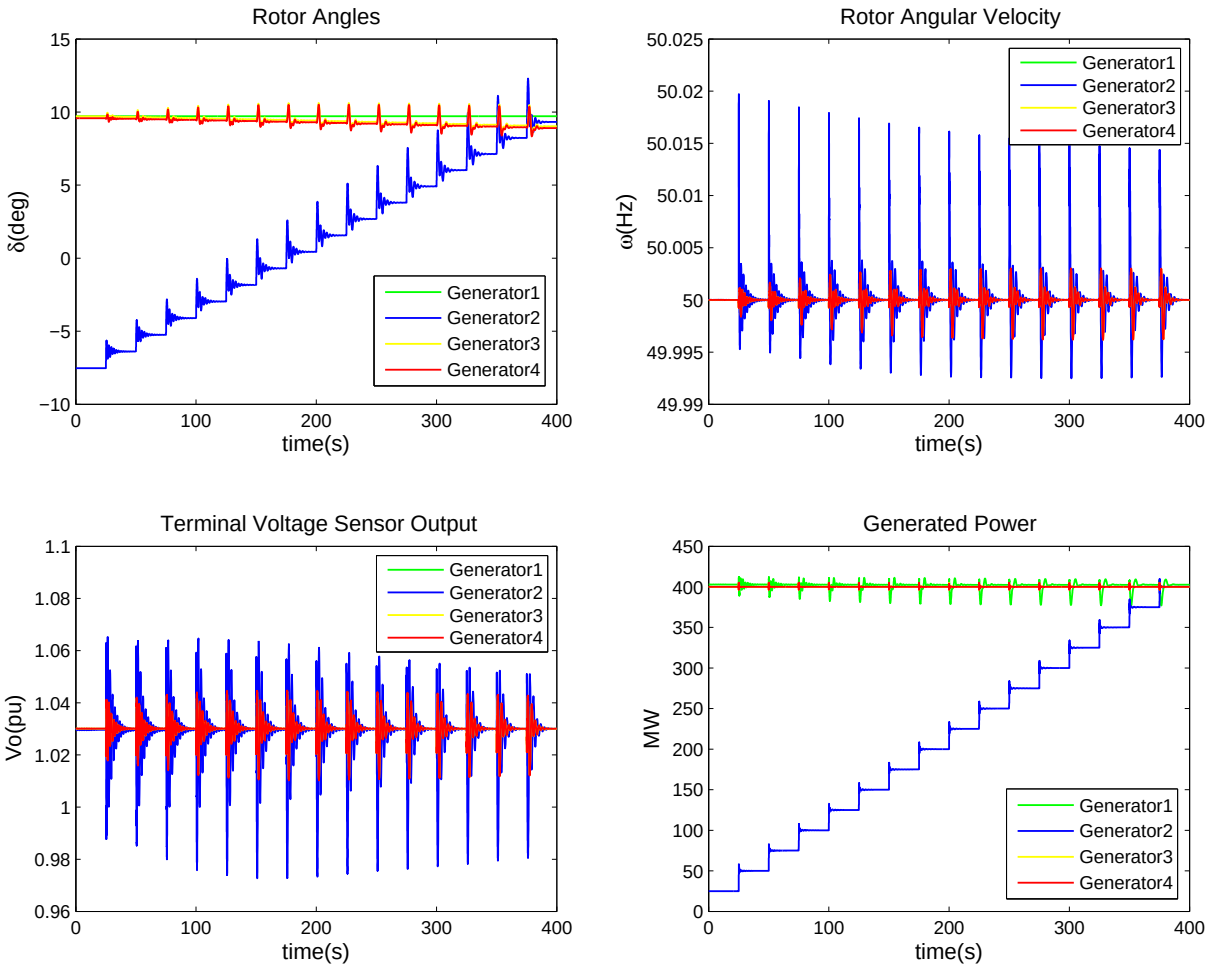

Figure 6.9. Case 2: G_2 generation increased from 25 to 400 MW with conventional PSS - responses of generators G_1 to G_4.

contains the disturbance produced during fault more effectively than conventional PSS and quickly settles back when the system is restored, in comparison with conventional PSS. When the system is restored after fault clearance, with respect to the rotor angle response of generator G_2, proposed controller gives an overshoot of 5.1510 deg and a settling time of 8.4809 s in comparison to an overshoot of 13.8485 deg and a settling time of 13.3637 s with conventional PSS.

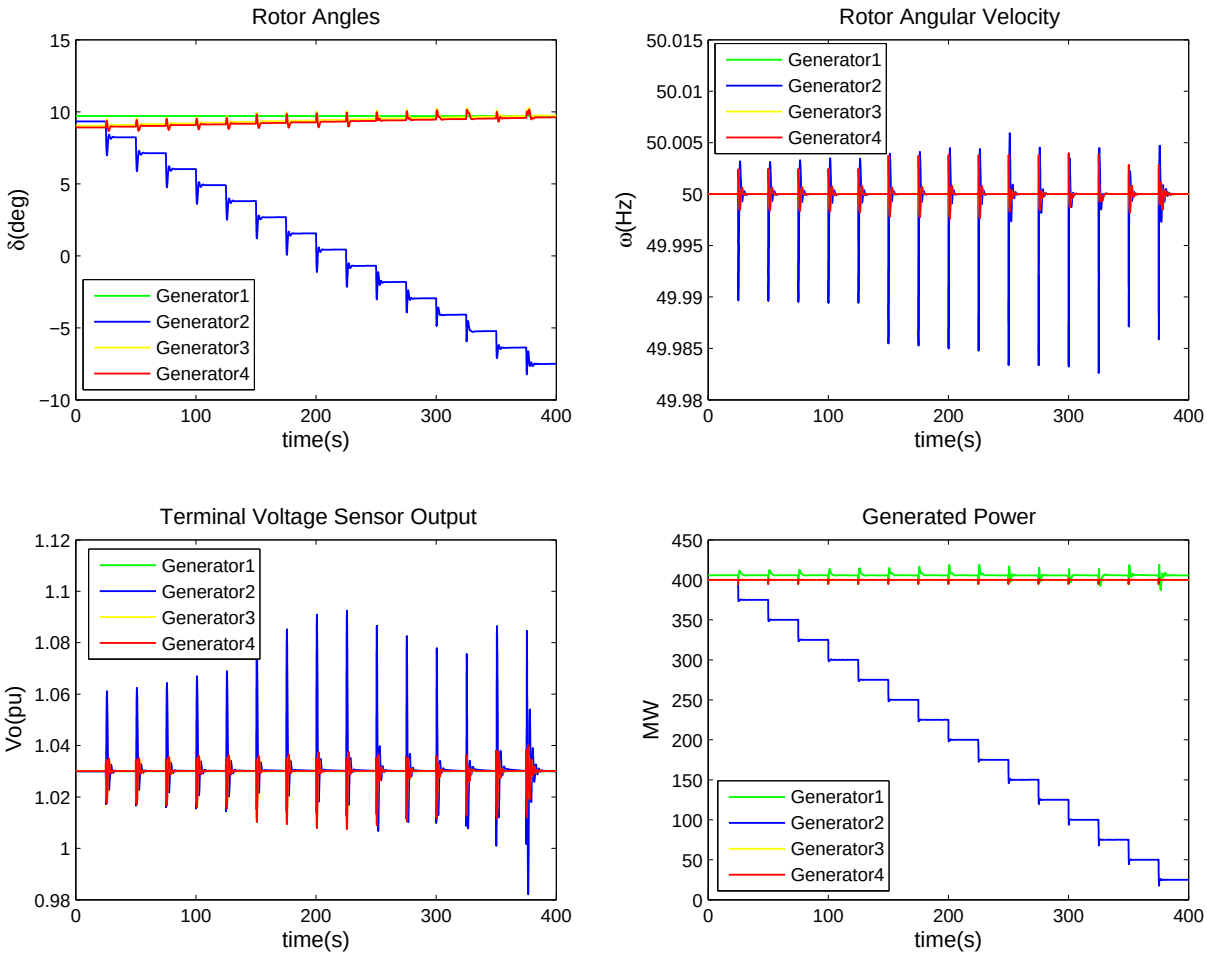

Figure 6.10. Case 3: G_2 generation decreased from 400 to 25 MW - responses of generators G_1 to G_4.

Case 5: Reference voltage variation

To assess the controller performance for voltage and reactive power changes, AVR reference voltage of generators G_2, G_3 and G_4 are varied through a range of $\pm$ 10 % of normal setting as given in Table 6.11. The output of all generators is set at 400 MW. Controller is not changed in this case.

Results

The responses of the generators for the reference voltage variation case are given in Figures 6.16 to 6.18. The system responses with conventional PSS are given in Figure

Power Change	With proposed controller		With conventional PSS	
	Over shoot (deg)	Set. time (s)	Over shoot (deg)	Set. time (s)
SEP 16 to SEP 15	2.0321	5.5524	0.2606	7.9690
SEP 15 to SEP 14	2.0504	4.8753	0.2546	7.7334
SEP 14 to SEP 13	2.3741	5.1295	0.2592	7.6339
SEP 13 to SEP 12	2.3866	5.1297	0.2577	7.4596
SEP 12 to SEP 11	1.7322	4.9140	0.2548	7.3059
SEP 11 to SEP 10	0.6578	4.4698	0.2557	7.1305
SEP 10 to SEP 9	2.1327	4.5399	0.2429	6.9237
SEP 9 to SEP 8	2.0374	4.6686	0.2284	6.7604
SEP 8 to SEP 7	2.0061	4.7502	0.1803	6.4155
SEP 7 to SEP 6	1.6966	6.1382	0.1600	6.1717
SEP 6 to SEP 5	1.6840	6.1738	0.2327	5.8045
SEP 5 to SEP 4	1.6947	6.1319	0.3576	9.6256
SEP 4 to SEP 3	1.5976	4.9002	0.5159	11.4202
SEP 3 to SEP 2	1.6131	4.9366	0.6854	14.8545
SEP 2 to SEP 1	1.6227	4.9918	0.8031	16.0265

Table 6.10. Case 3: G_2 power output decrease - Comparison of Overshoot and Settling time

Simulation time	0 - 20s	20 - 40 s	40 - 60 s	60 - 80 s	80 - 100 s
AVR setting	normal	+ 10%	normal	- 10%	normal

Table 6.11. Case 3 Reference voltage variation AVR settings

6.18. In this case also, from the responses in Figures 6.16 to 6.18, it can be seen that, proposed controller produces less oscillations and overshoot when compared with conventional PSS. With respect to the rotor angle response of generator G_2, proposed controller gave an overshoot of 0.6881 deg and a settling time of 3.1986 s in comparison to an overshoot of 7.6646 deg and a settling time of 7.2809 s with conventional PSS.

6.6 Chapter Summary

The performance of the proposed controller is validated through different cases of nonlinear computer simulations. For this, a two area, four machine, 11 bus power grid system is considered as test case power system. Multimachine nonlinear power system model is used for the simulations. Controllers are designed using the proposed methodology for the generators in the grid system. Different practical power

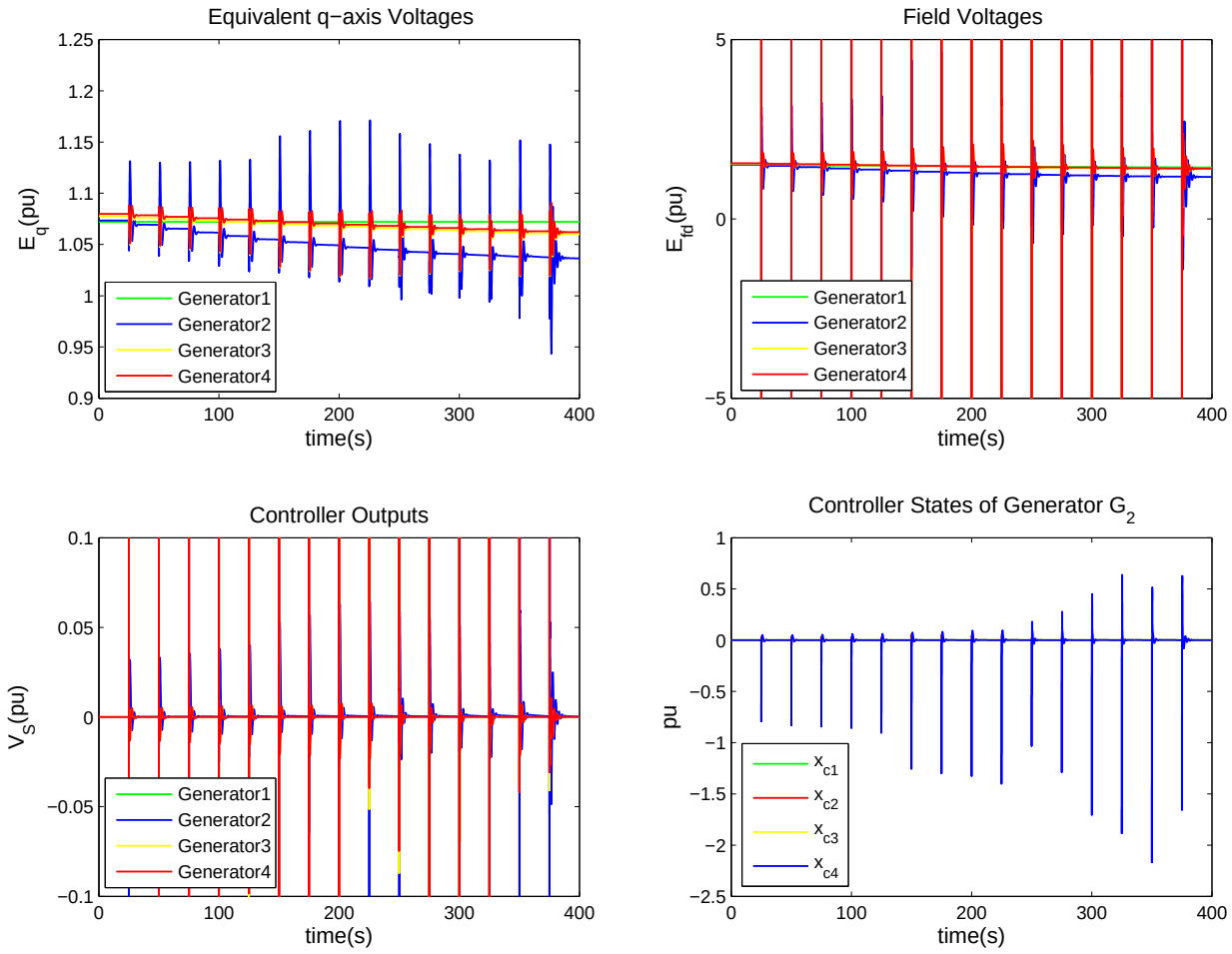

Figure 6.11. Case 3: G_2 generation decreased from 400 to 25 MW - responses of generators G_1 to G_4.

system scenarios such as load generation variations, fault conditions and generator AVR reference voltage variations are simulated. Identified simulation cases are simulated with both proposed controllers and conventional PSS and the simulation results are compared. The generator responses with respect to rotor angle, angular velocity, terminal voltage sensor output, generated power, equivalent q-axis voltage, field voltage, controller output and controller states are analysed further. For the simulation cases considered, the proposed controller gave a satisfactory performance. When compared with the conventional PSS, proposed controllers provided effective damping, less overshoot and settling time with uniform performance over a wide

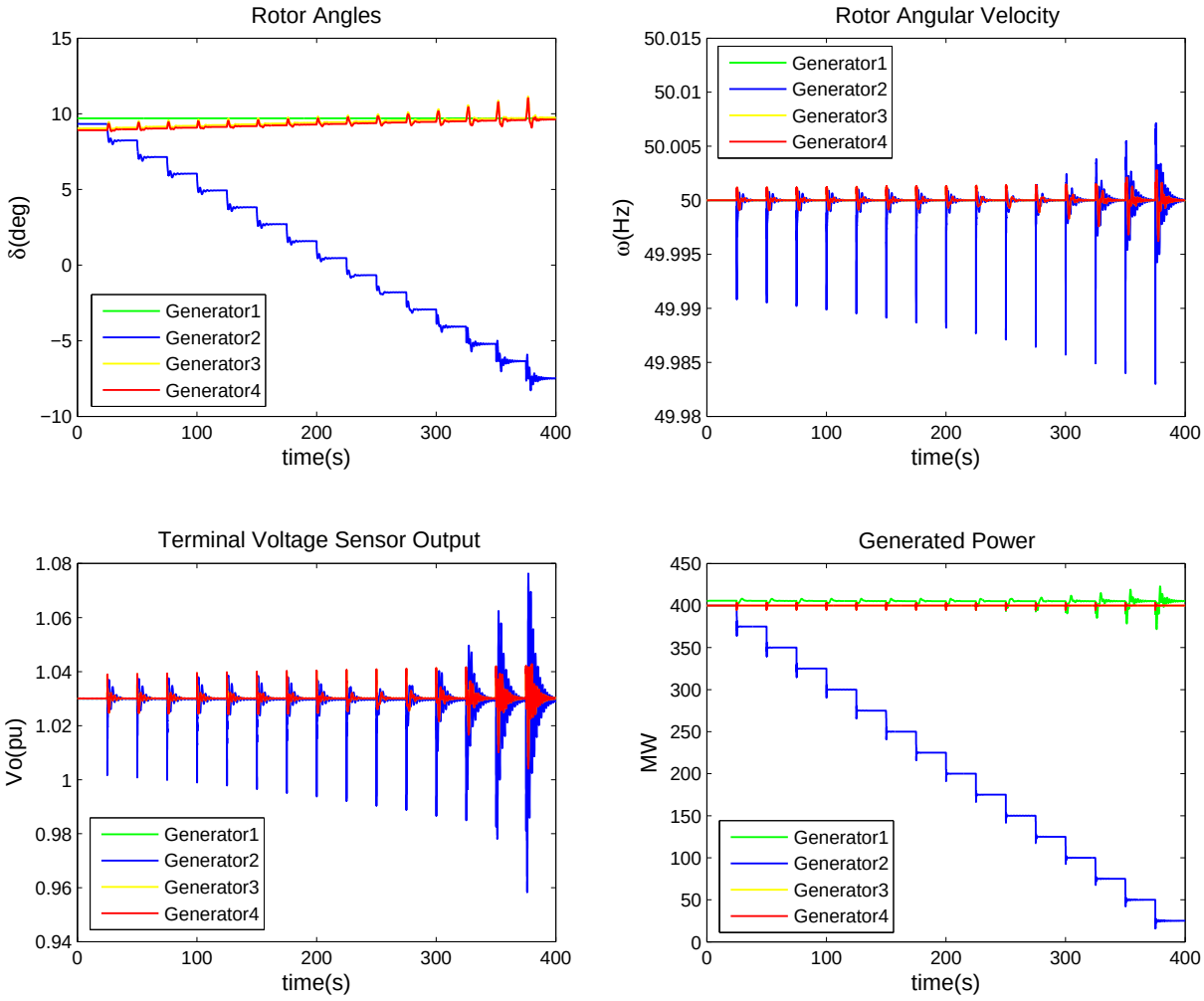

Figure 6.12. Case 3: G_2 generation decreased from 400 to 25 MW with conventional PSS - responses of generators G_1 to G_4.

range of parameter variations.

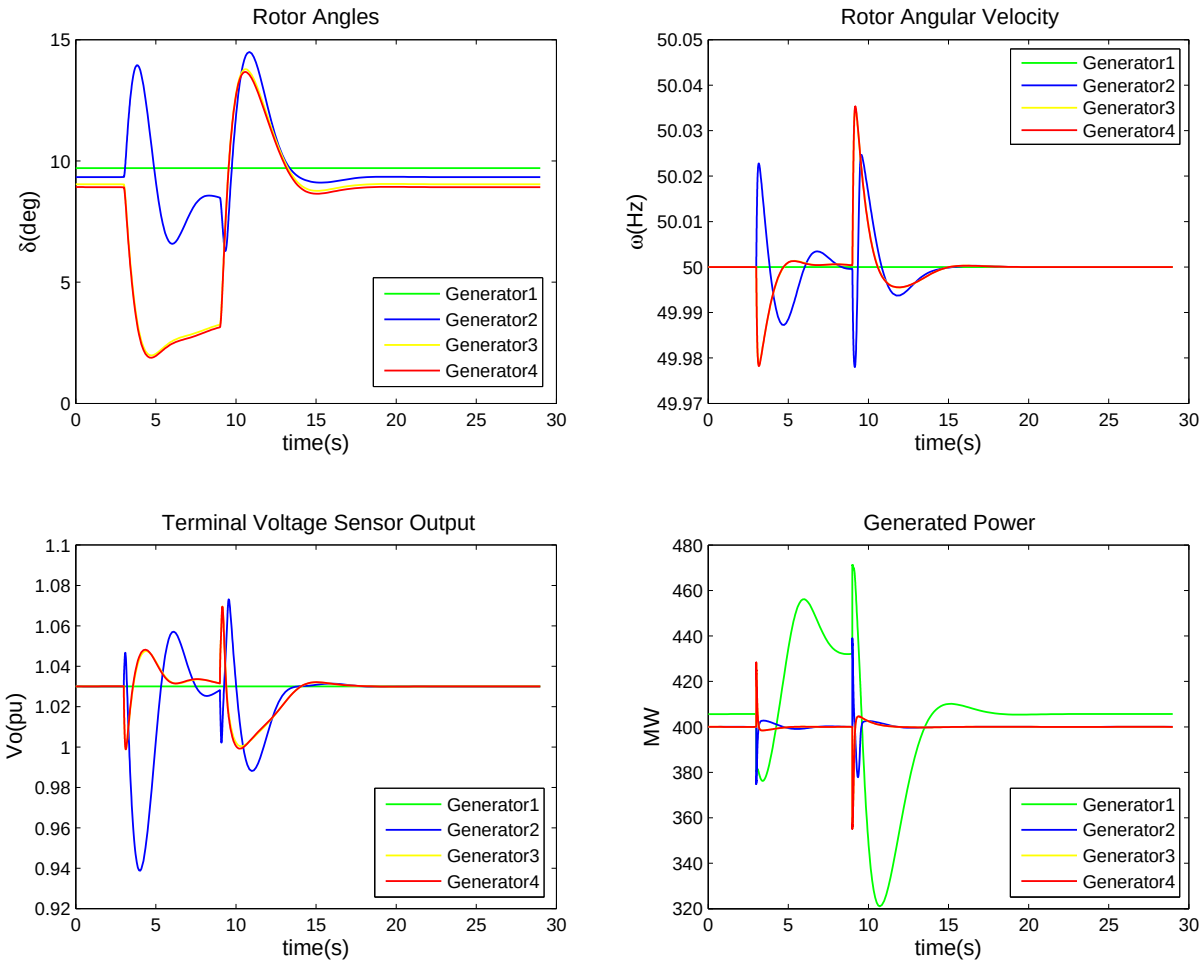

Figure 6.13. Case 4: Fault at tie line 7 - 9 - responses of generators G_1 to G_4.

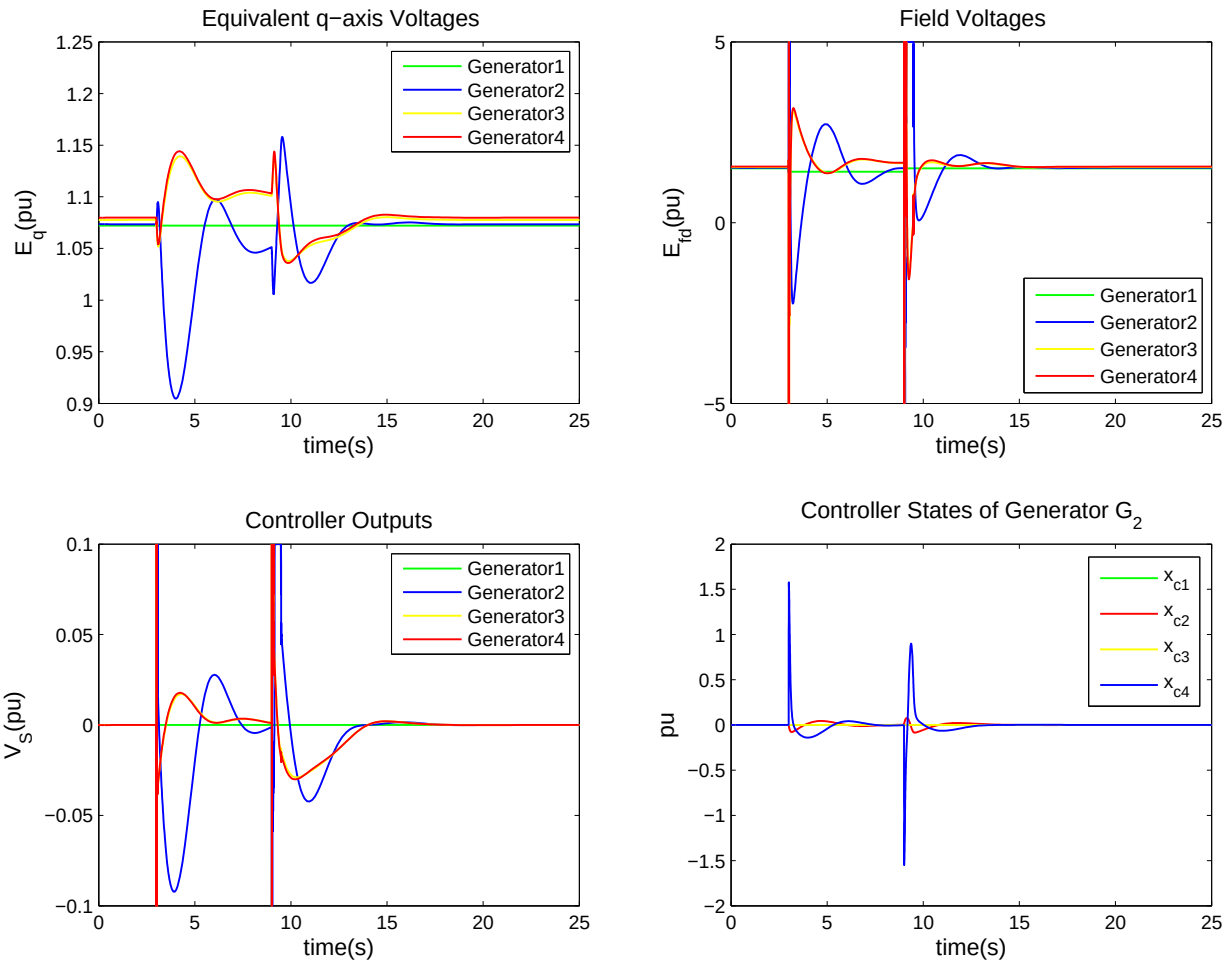

Figure 6.14. Case 4: Fault at tie line 7 - 9 - responses of generators G_1 to G_4.

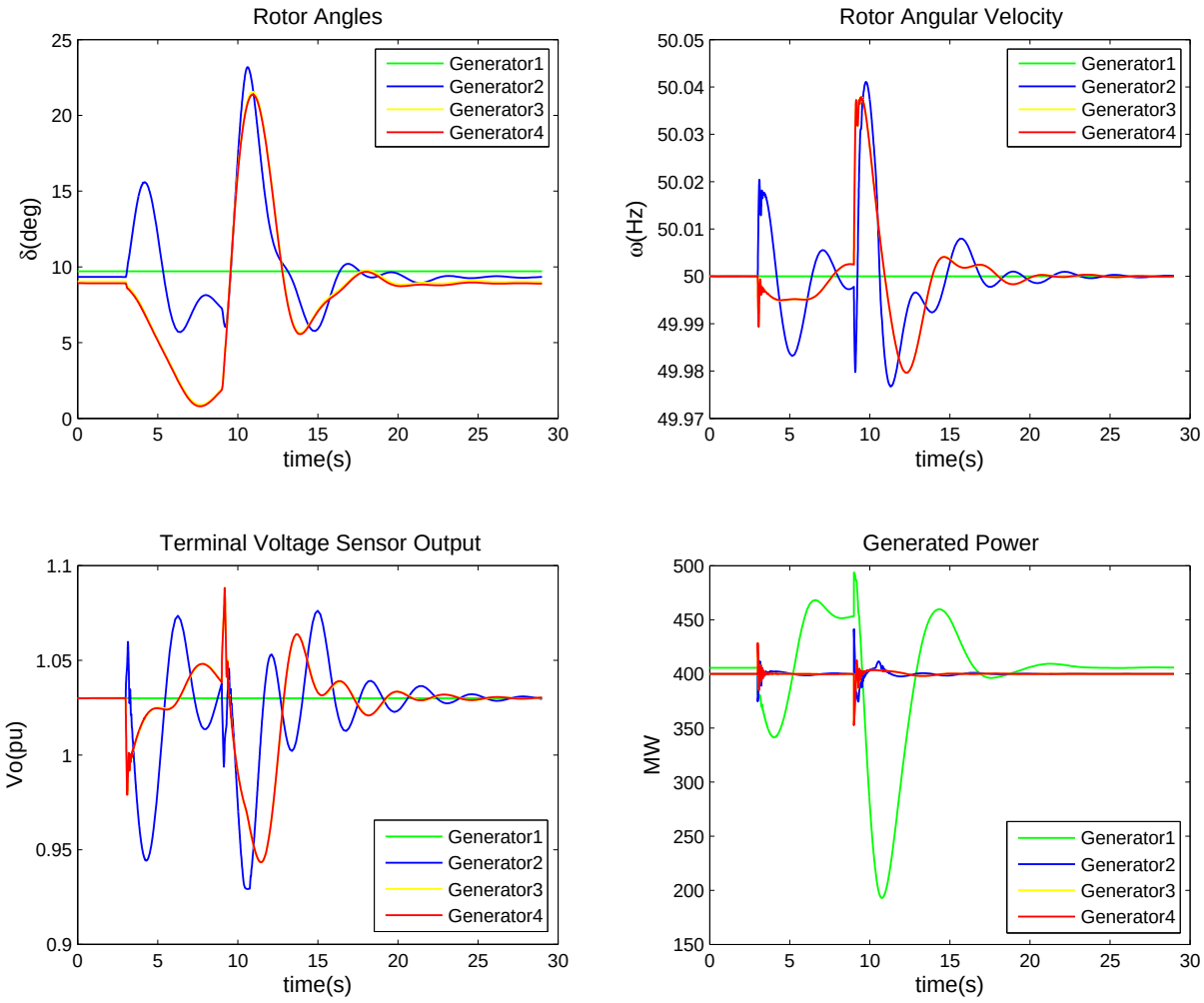

Figure 6.15. Case 4: Fault at tie line 7 - 9 - responses of generators G_1 to G_4 with conventional PSS.

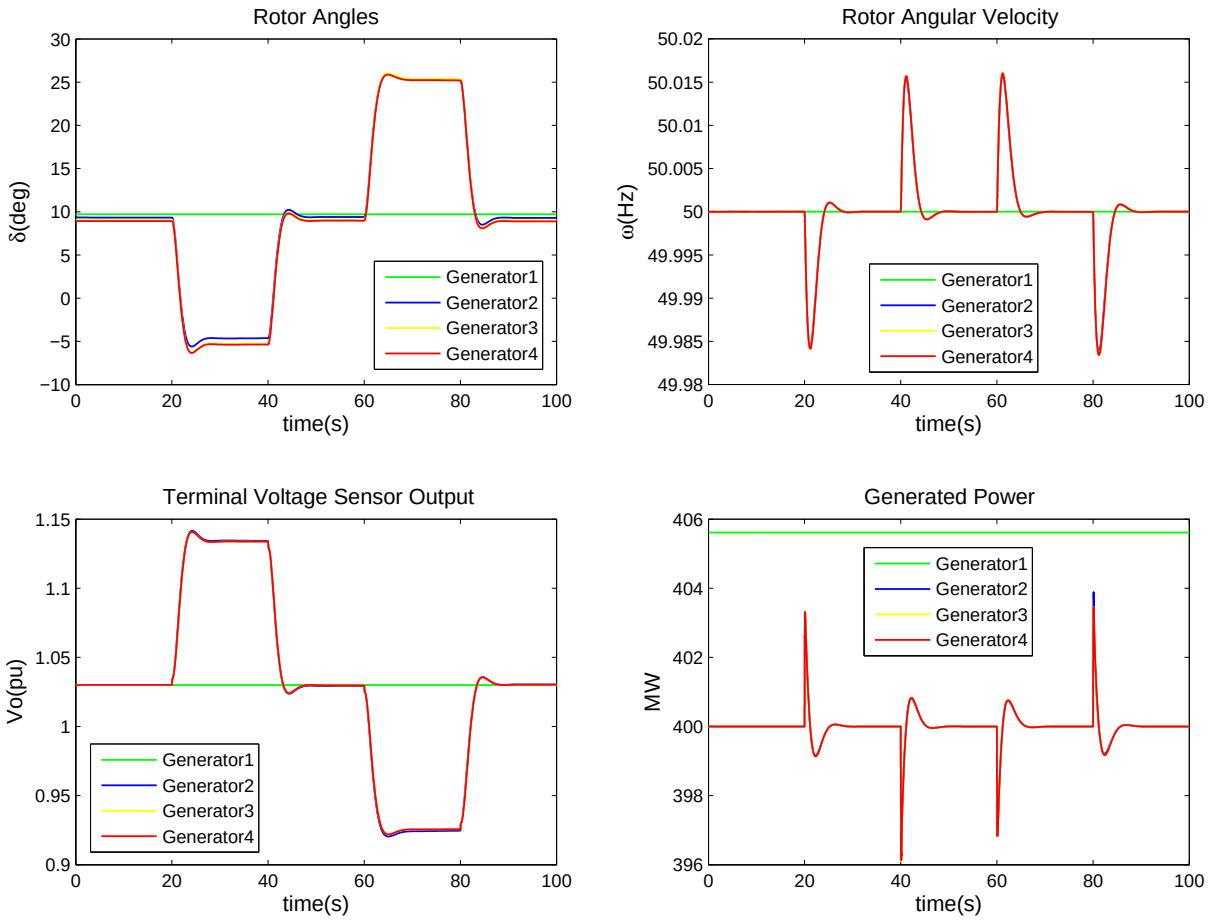

Figure 6.16. Case 5: ± 10 % reference voltage variation - responses of generators G_1 to G_4.

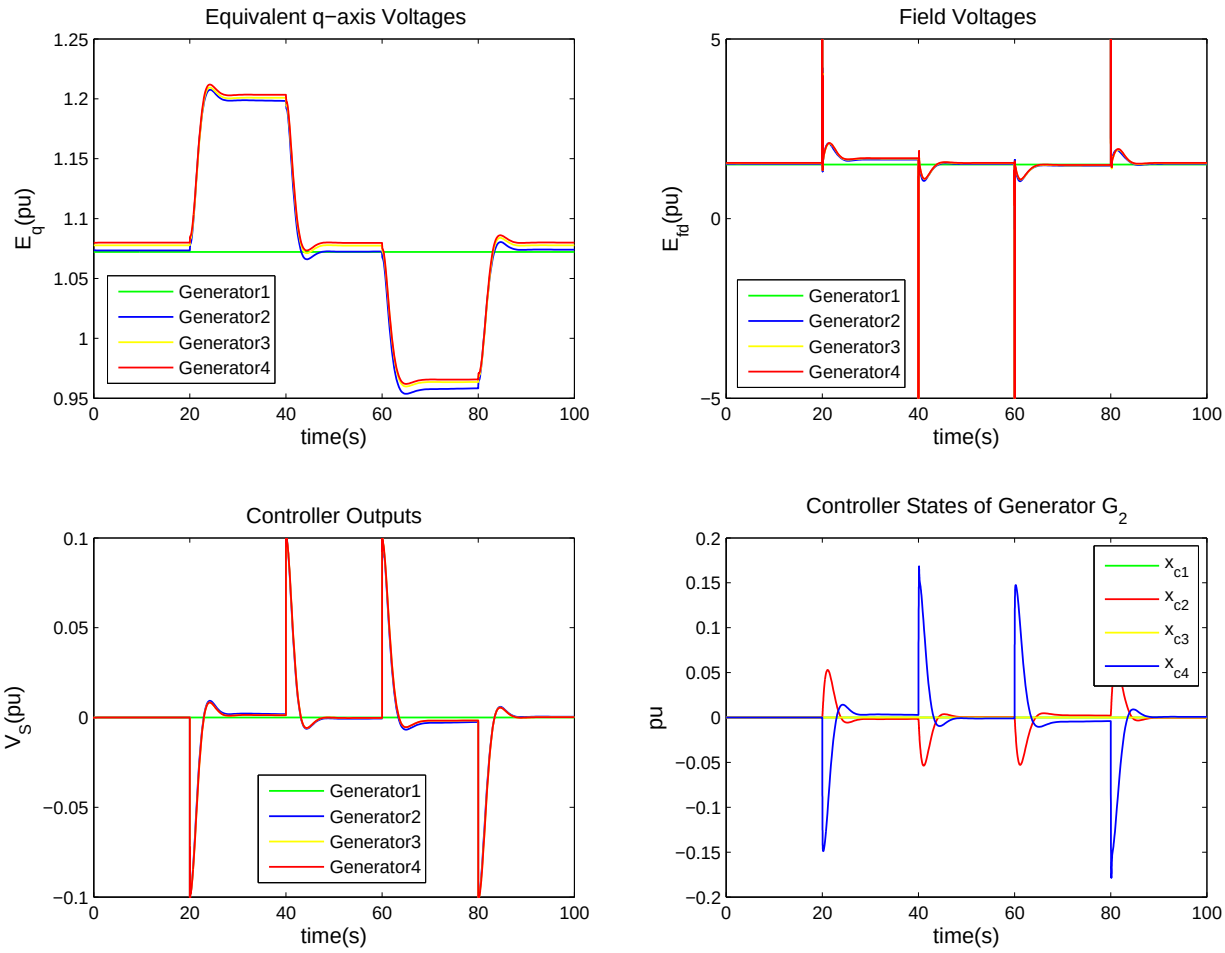

Figure 6.17. Case 5: ± 10 % reference voltage variation - responses of generators G_1 to G_4.

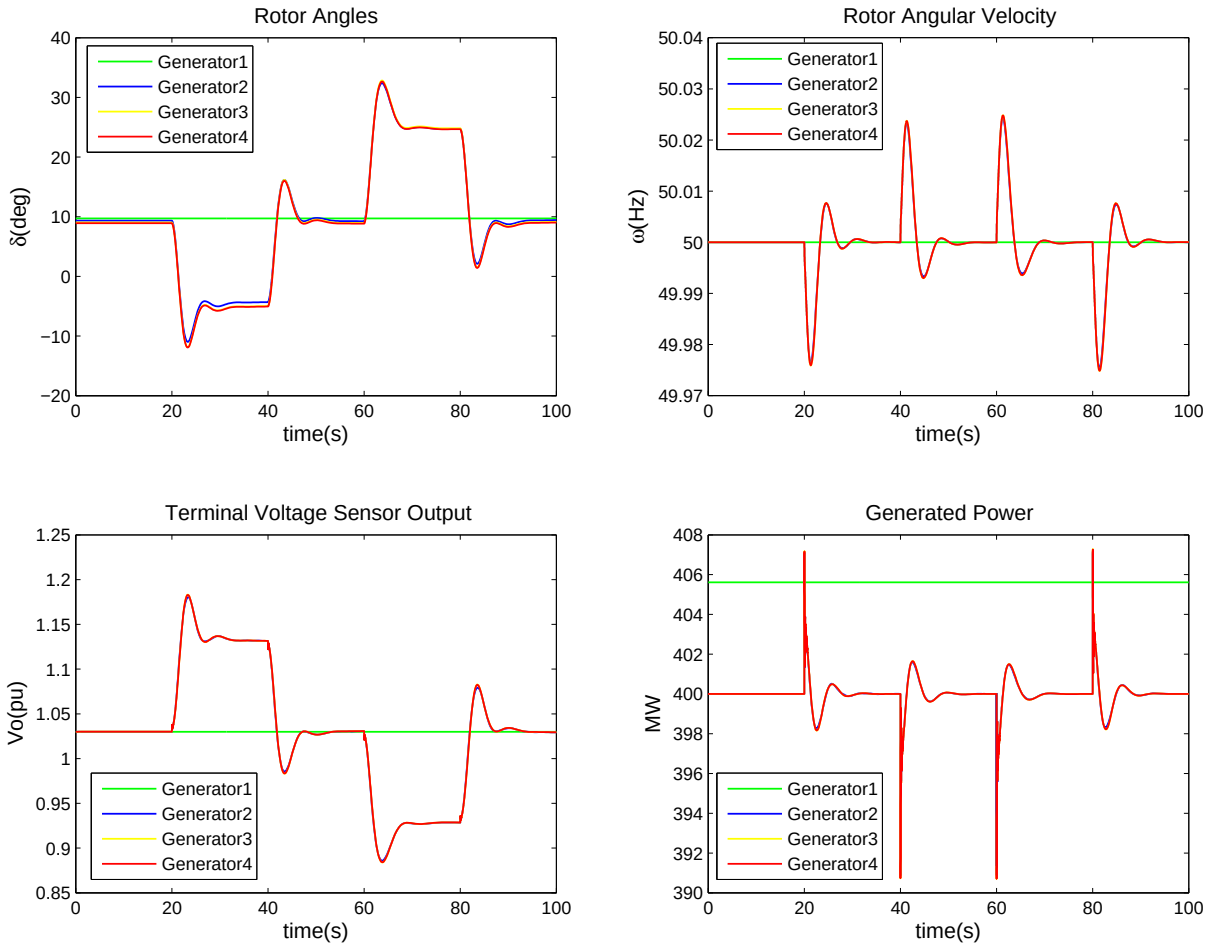

Figure 6.18. Case 5: ± 10 % reference voltage variation - responses of generators G_1 to G_4 with conventional PSS.

Chapter 7

Real Time Digital Simulation

Testing of new controllers by integrating them into actual power system is not possible always. In the absence of facilities to test the controllers in real power system, RTDS simulation facility provides next possible test bed closest to real system to test the controllers. RTDS facility employs an elaborate power system simulation modules which solves the power system equations and simulates various scenarios in real time. Central Power Research Institute (CPRI), at Bangalore, India has Real Time Digital Simulation (RTDS) facility to carry out detailed real time simulation of interconnected grid systems. This facility is used to test the proposed controller design. We have a setup a test case power system and carried out simulations with proposed controllers and conventional PSS under different load variations, reference voltage variations and fault conditions. The chapter discusses the simulations carried out in the RTDS facility [106] at CPRI.

7.1 RTDS Facility

Power systems are studied either to analyse their steady state behavior or transient (time domain) behavior. Transient analysis is conducted in order to analyse system stability at the power frequency or to analyse instantaneous system response over time. The instantaneous response, which is often referred to as the electromagnetic transient response can provide detailed information about the system under study, such as the maximum over-voltage, harmonic distortions, voltage sags etc. It can also accurately show the control system behavior.

A better understanding of systems prior to their manufacture leads to optimally designed devices and an analysis of the impact of the introduction of new devices prior to their installation in the network results in optimised power systems and fewer operational problems.

In the past, analog simulators (Transient Network Analysers and HVDC simulators) were used to perform real time simulation studies. Using scaled down passive components such as resistors, inductors and capacitors, analog simulators represent the electrical characteristics of the actual power system components. The individual

component models can be configured and interconnected to form the system model for the study at hand. Since the source models and the generator models operate at real system frequency the analog simulators operates inherently in real time.

In addition to analog simulator, computer based electromagnetic transient simulation software (non-real time) has been available for many years and has been used to study power system phenomenon. The modeling capabilities of modern electromagnetic transients software such as Electro-Magnetic Transients Program EMTP, Alternative Transients Program (ATP-EMTP), etc., are able to represent individual power system components in great detail. The digital simulation software relies on mathematical models for representing the individual power system components, whereby the user can connect these models to form overall power system model for study.

The most common solution employed by electromagnetic transient power system simulation software is the Dommel's Algorithm [106]. In this algorithm, the trapezoidal rule of integration is used to convert integral equations, which result from nodal analysis of the power system, into algebraic equations. Application of trapezoidal rule requires that the solution be computed only at discrete instants in time (time between computed instants - time step Δt), rather than a continuous solution. All of the equations representing the power system model must be computed at each time step. As the size of the power system increases the number of calculations which must be performed increases and a single CPU needs excessive time to compute the results even for a single time step. In this case, the simulation is said to be in 'non-real time'.

The recent advances in digital signal processing using fast computers have had a significant effect on digital simulation technology. The burden of calculation is divided into several modules which can be solved in parallel, so as to perform the necessary calculations for a single time step, in a time less than or equal to the time step thereby achieving 'real time'.

The RTDS is one such tool which comprises of specialized hardware and software to achieve continuous real time simulation. A state-of-the-art real time digital simulator facility procured from RTDS Technologies, Canada was established at the Power Systems Division of CPRI in June-2003, to meet the needs of the utilities, electrical industries, manufacturers, etc., Figure 7.1, shows the setup of the Real

Figure 7.1. RTDS facility at CPRI, Bangalore, India.

Time Digital Simulator Facility. An extensive power system component library together with a friendly graphical user interface, facilitate the assembly and study of wide variety of AC, DC and integrated AC/DC power systems. Because of the continuous real time operation achievable on RTDS, it can be applied in areas traditionally reserved for analog simulators eg. testing of protective relays, testing of system controllers etc.

7.2 Test Case Power System

To validate the proposed controller design methodology in RTDS, a two area power system consisting of 4 generators and 11 buses is considered. The layout of the power system is given in Figure 7.2. Area 1 and 2 are interconnected by a tie-line. Generator 1 bus is considered as the reference slack bus.

Area 1 is connected to Area 2 through a two circuit tie line of length 220 km. The transmission system nominal voltage is 400 kV. Generation voltage are stepped up by the transformers connected to the generators. Load centers are at buses 7 and 9 also buses 7 and 9 have shunt capacitors.

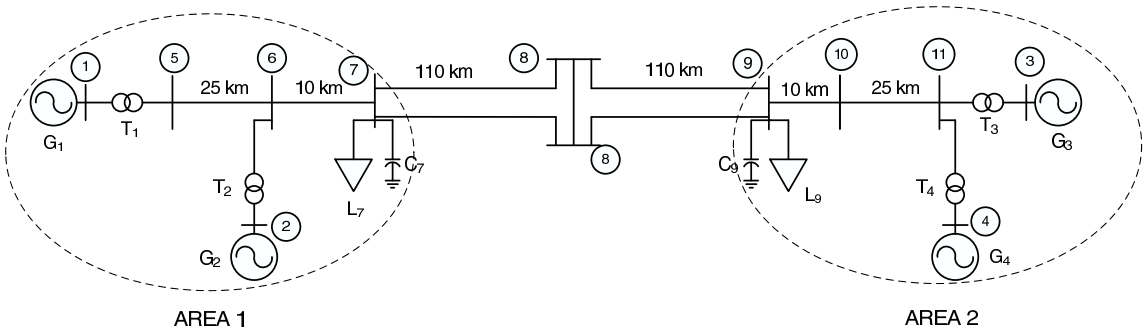

Figure 7.2. Two area four machine system.

Generators 1 to 4 and transformers 1 to 4 are identical and their parameters are given in Appendix A, Table A.1 and A.3. The generator AVR parameter are given in Table A.2. Transmission line parameters are given in 400 kV, 100 MVA base in Table A.4. For the analysis of the system, 400 kV and 100 MVA are chosen as base quantities.

7.3 Controller Design

Decentralised robust output feedback controllers of the form given by (3.44) are designed for the system in Figure 7.2. For the RTDS validation purpose, one SEP corresponding to generator output condition with the all generators G_1, G_2, G_3 and G_4 operating at 400 MW is considered. The controllers are designed for robust performance for a load variation of $\pm$ 30 MW around the SEP. For the considered SEP, the open-loop system is unstable and a stabiliser is necessary to stabilise the system.

Load flow studies corresponding to the SEP are carried out to evaluate the system matrices A_{SYS} and B_{SYS}. The subsystem matrices A_i, B_i and L_i are obtained from the system matrices A_{SYS} and B_{SYS} using equations (3.36) to (3.38). Parametric uncertainty around the SEP is defined using α_i and β_i. The values of α_i and β_i are selected to satisfy (3.40).

With the subsystem matrices and uncertainties defined, the controllers are synthesised by solving the optimisation control problem through rank constrained LMIs as outlined in Chapter 3. The designed controller matrices corresponding to the SEP are given in Table 7.1. To compare the performance of the designed controller with

	A_c				B_c	K_c'
Generator G_1	0.00	898.81	0.00	0.00	−522.81	−82.37
	−0.25	−47.83	−0.13	0.00	47.84	$1.69e^5$
	−1830.40	$3.7726e^6$	−999.65	1.37	−2709.20	−44.96
	−4.11	1641.10	39.27	−66.67	−1641.2	1.06
Generator G_2	0.00	938.09	0.00	0.00	−562.09	−68.23
	−0.24	−52.63	−0.02	0.00	52.64	$1.42e^5$
	−1516.40	$3.1788e^6$	−999.01	1.02	−3085.80	−44.94
	−5.46	1800.80	38.78	−66.67	−1800.90	1.05
Generator G_3	0.00	897.73	0.00	0.00	−521.73	−82.82
	−0.25	−47.73	−0.13	0.00	47.74	$1.69e^5$
	−1840.60	$3.7726e^6$	−997.35	1.35	−2699.40	−44.86
	−3.93	1633.90	39.00	−66.67	−1634.00	1.06
Generator G_4	0.00	897.01	0.00	0.00	−521.01	−83.50
	−0.25	−47.71	−0.13	0.00	47.73	$1.69e^5$
	−1855.60	$3.7726e^6$	−994.29	1.40	−2695.30	−44.72
	−3.97	1624.60	39.05	−66.67	−1624.70	1.06

Table 7.1. Designed controllers for generators G_1 to G_4 corresponding to the SEP.

the conventional PSS, IEE 2ST PSS model available at RTDS is used. Conventional PSS parameters are given in Table 6.6.

7.4 RTDS simulations

7.4.1 Simulation setup

The power system shown in Figure 7.2 is configured in RSCAD (RSCAD is the software associated with RTDS where the power system to be simulated is configured.). The power system configured in RSCAD is shown in Figures 7.3 and 7.4. This configured system is linked to RTDS racks for simulation.

The system is initialised to the load flow results. Simulation is carried out with designed controller as well as with conventional IEE 2ST PSS and with IEEE Type ST1 excitation system.

7.5 Simulation cases and analysis

Following case studies are identified for the simulation. The response of Generators G_1 to G_4 are similar for all cases of simulation. Graphical response of Generator G_2 with the proposed controller and conventional PSS with respect to load angle, speed,

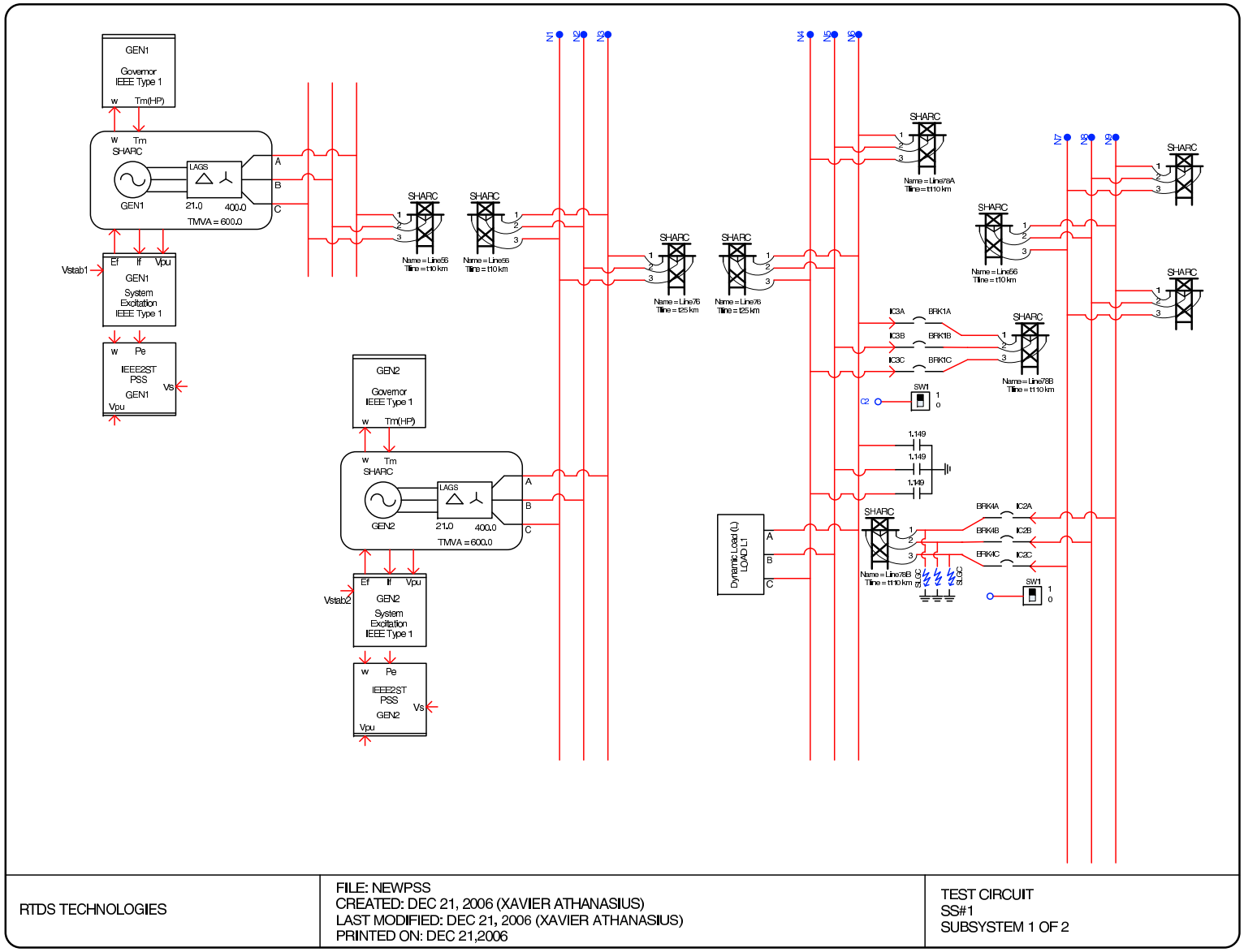

Figure 7.3. RTDS power system grid set up Section 1.

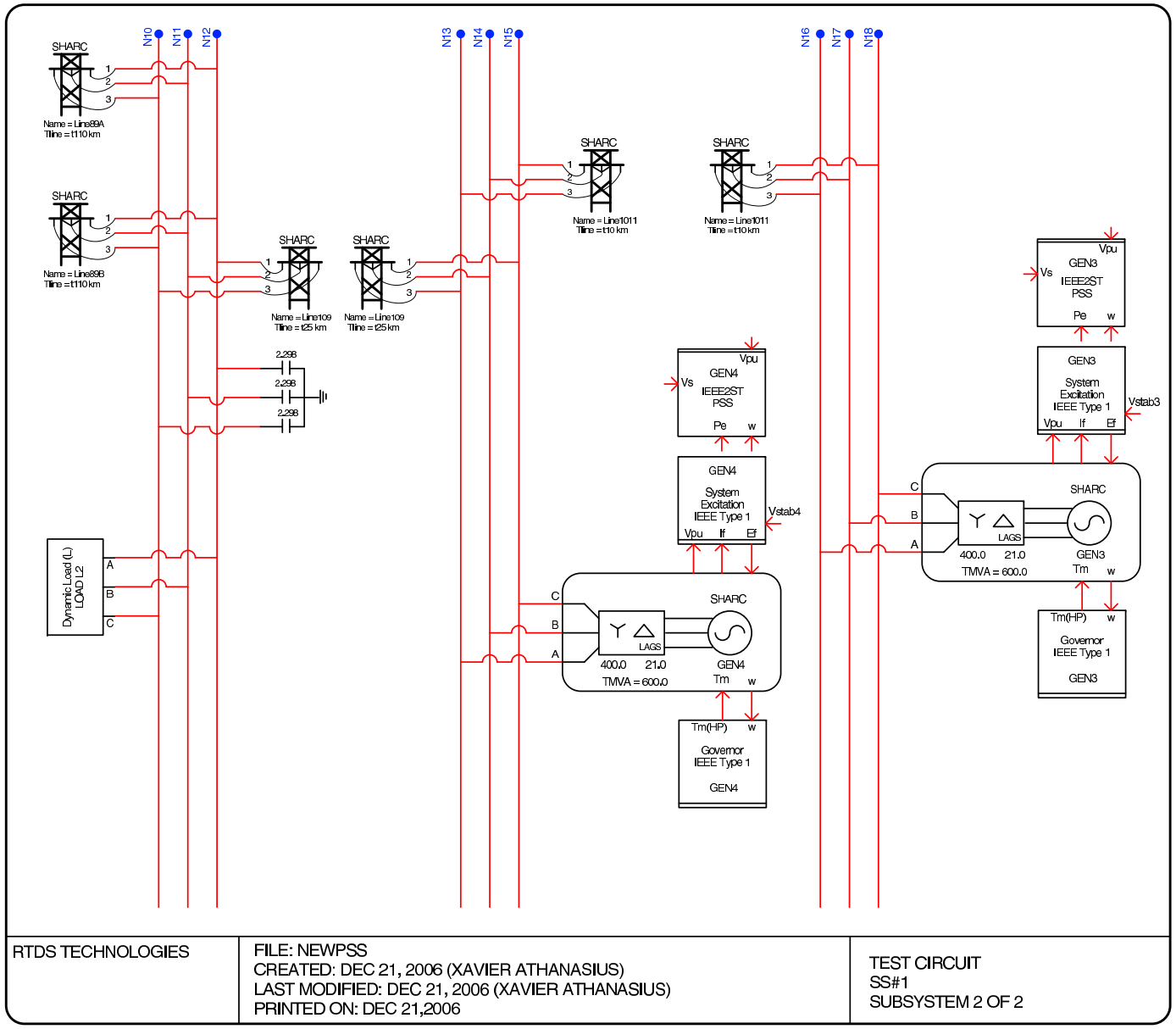

Figure 7.4. RTDS power system grid set up Section 2.

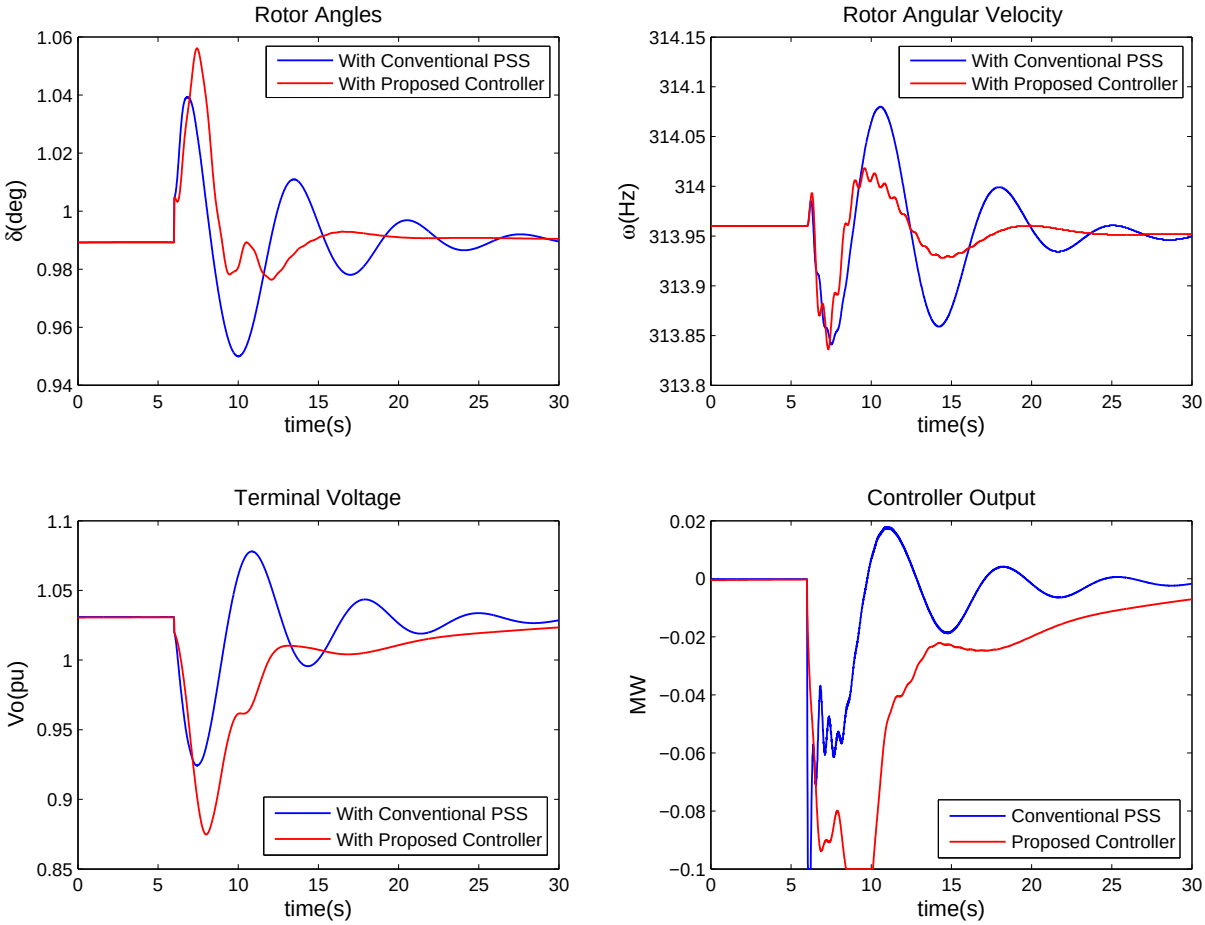

Figure 7.5. Case1. Generator 2 response for load increase.

terminal voltage and controller output are plotted and analysed for each simulation case.

7.5.1 Case 1 - Load increase

To study the performance of the controller for parameter variation due to load changes, load on bus 9 is increased by 100 MW + j 10 MVAR from the SEP conditions. The increased load is allowed to be shared by all the generators.

Results

From the generator responses in Figure 7.5, it can be inferred that the damping of the system improves with the proposed controller in comparison with conventional

PSS. The transient overshoot magnitude and the transient settling time are better with the proposed controller.

7.5.2 Case 2 - Load decrease

Similar to the case 1 above, but the load on bus 9 is decreased by 100 MW - j 10 MVAR from the SEP conditions. The decreased load is allowed to be shared by all the generators.

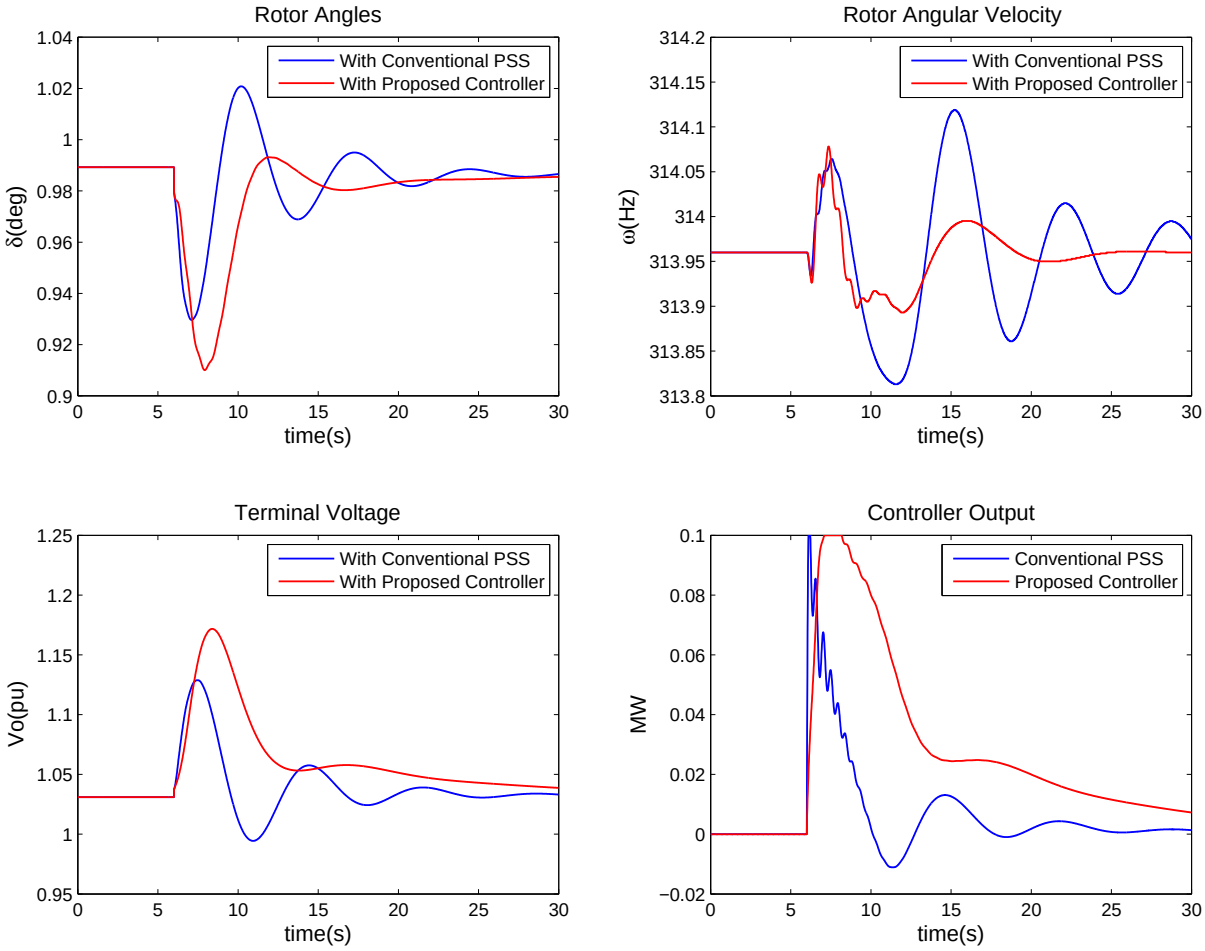

Figure 7.6. Case2. Generator 2 response for load increase.

Results

From the generator responses in Figures 7.6 it can be inferred that the damping of the system improves with the proposed controller in comparison with conventional PSS in the load decrease case also.

7.5.3 Case 3 - Generator reference voltage increase

To evaluate the performance of the controller for the change in reference voltage, the reference voltage of Generator 2 is suddenly increased by 10 %.

Results

From the simulation responses in Figure 7.7, the transient response produced by the proposed controller is found to be better than the conventional PSS in terms of settling time.

7.5.4 Case 4 - Generator reference voltage decrease

Similar to Case 3 above, but the reference voltage of Generator 2 is suddenly decreased by 10 %.

Results

In the reference voltage decrease case also, from the simulation responses in Figure 7.8, the transient response produced with the proposed controller is found to be better than the conventional PSS in terms of settling time.

7.5.5 Case 5 - Fault

To study the performance of the controller under fault conditions, three phase to earth fault is initiated in the tie line between bus 7 and 8. Circuit breaker BRK4 trips the section of the line78B (as shown in Figure 7.3) at t = 6 s and re-closes at t = 16 s, after the clearance of the fault.

Results

The responses of the fault case are given in Figure 7.9. For the fault case also, the initial overshoot produced with the proposed controller is less compared with conventional. Also the settling time taken with the proposed controller is less.

7.6 Chapter summary

The performance of the proposed controllers is validated using the RTDS facility available at CPRI, Bangalore, India. To validate the controller, two area, four machine, 11 bus power grid system is considered as test case system. Power system

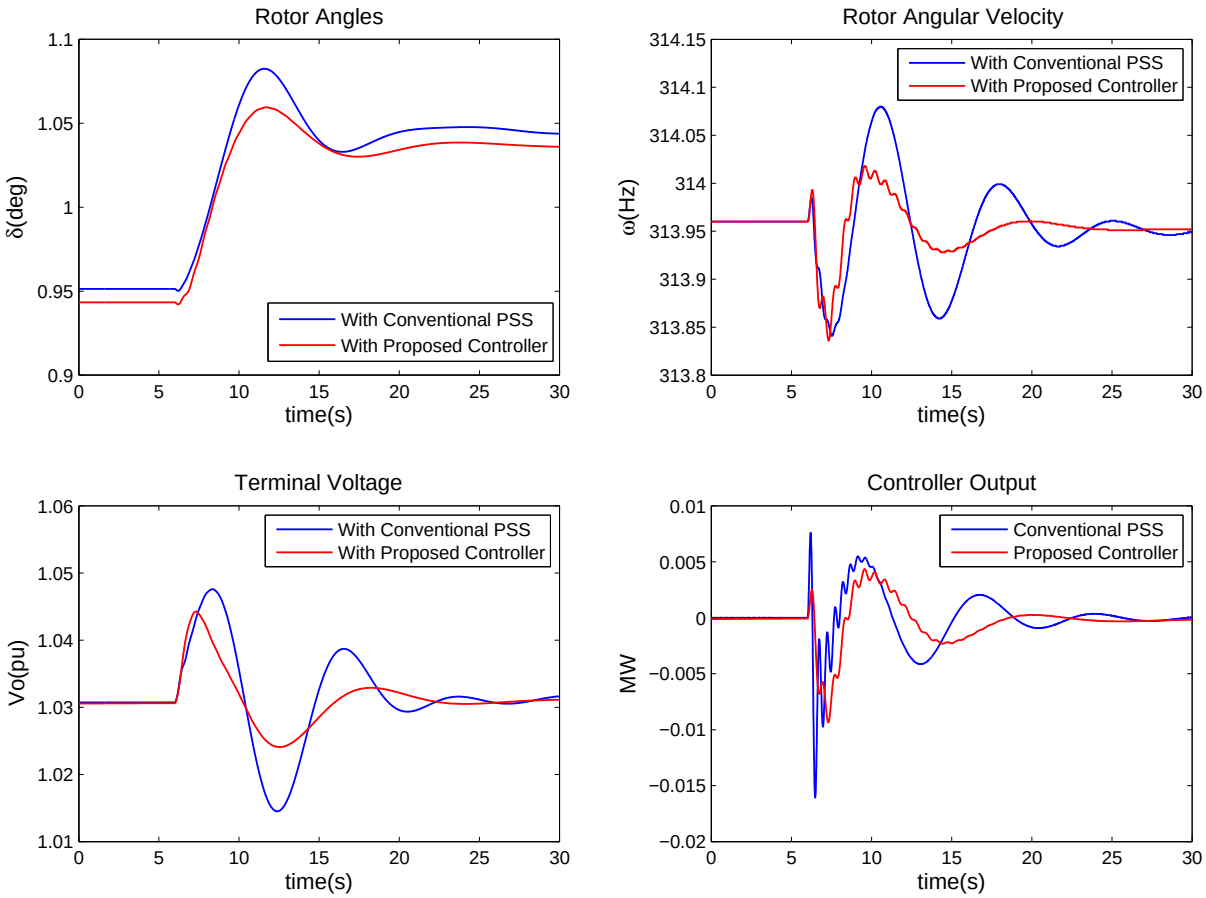

Figure 7.7. Case3. Generator 2 response for reference voltage increase.

controllers are designed for the selected system using the proposed design methodology. The designed controllers are configured in RTDS and simulations are carried out. Load variations, AVR reference voltage variations and fault conditions are the perturbations considered for the simulations. From the simulation results, it is found that the proposed controller improved the damping of the system with reduced overshoot and settling times.

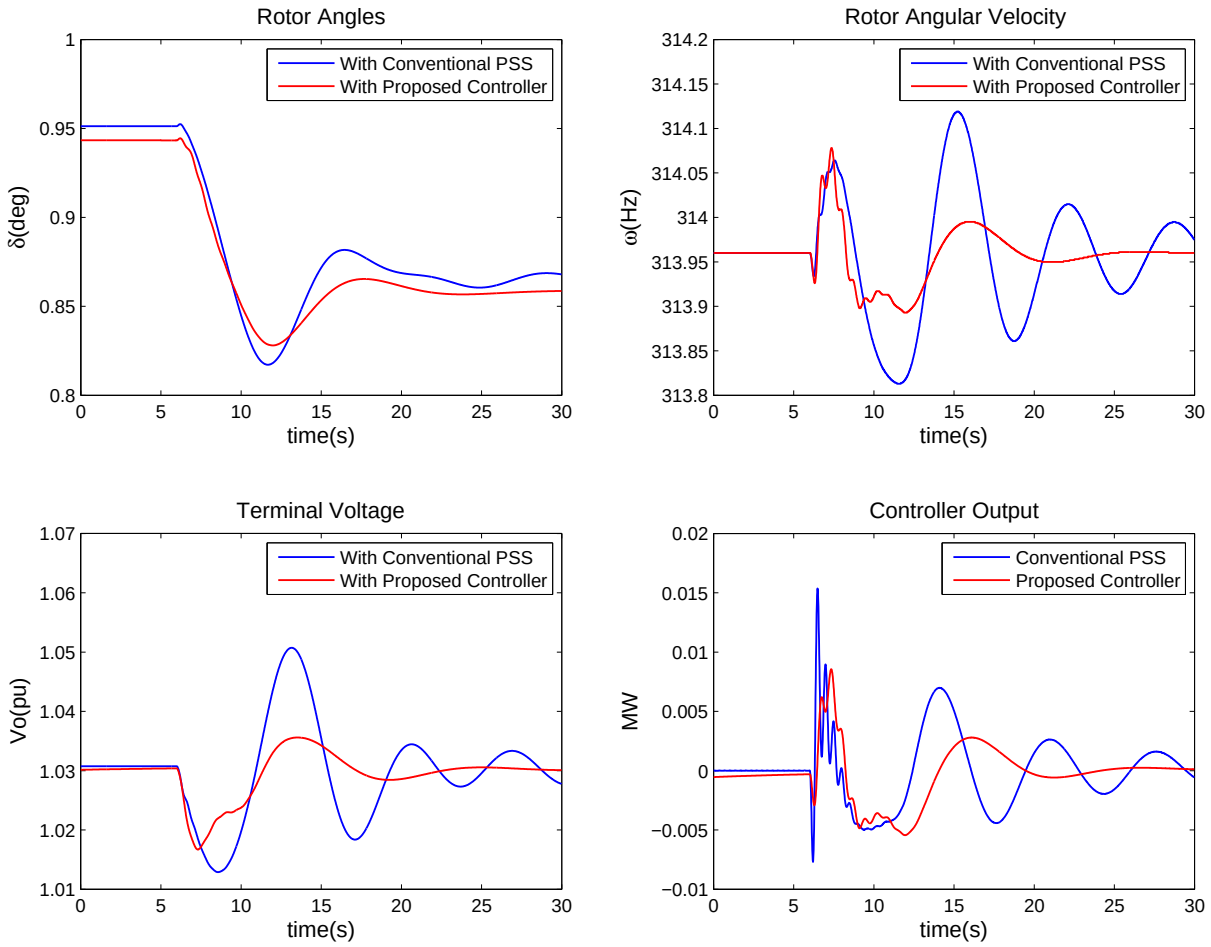

Figure 7.8. Case1. Generator 2 response for reference voltage decrease.

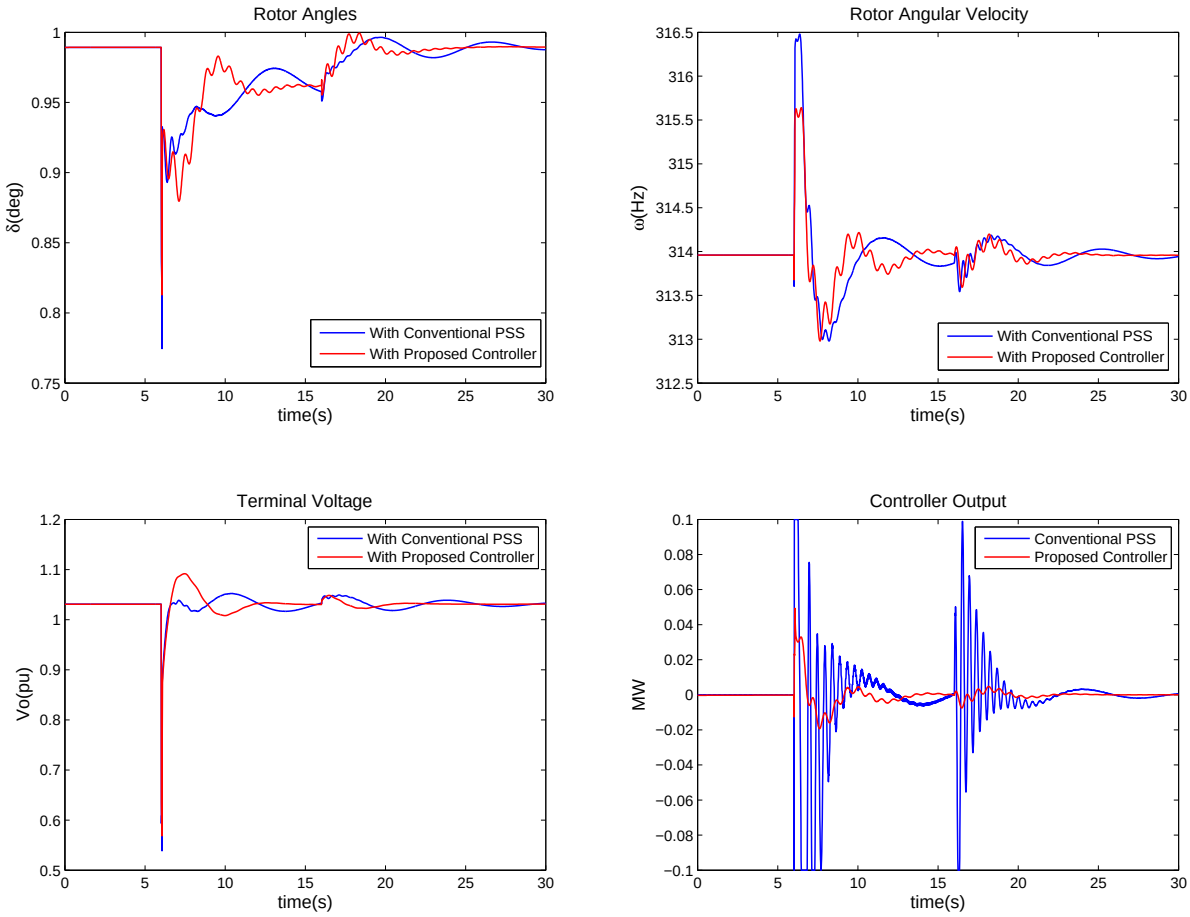

Figure 7.9. Case1. Generator 2 response for Fault.

Chapter 8

Power System Controller Design with OLTC Dynamics

8.1 Introduction

The main purpose of Automatic Voltage Regulators (AVR) for power transformers with OLTC is to keep the voltage on the low voltage side within the predefined band. The AVR controls the tap position of the OLTC in accordance with the voltage variations of the transformer [107]. This voltage correction effect of OLTCs have a negative impact on the voltage stability of the system during fault conditions. Following the disturbance due to fault, the OLTCs will act in a way to restore the load power to the pre-fault levels. This will increase the burden on the already weak generating units to meet the increased real and reactive power requirement, often leading to voltage collapse [67–69].

As far as the voltage stability of the system is concerned, the generator excitation and OLTCs play an important role. The voltage stability of the system is determined by the excitation limit of the generator, dynamic characteristics of OLTCs and the load [68]. Operation of OLTCs, in relation to voltage instability is well researched [67, 108–110]. Many suggestions are proposed to improve the voltage instability due to OLTCs, including the improvements in the OLTC operating logic [107] and even blocking OLTC during contingency periods [67]. In this research, we consider the dynamic effect of OLTCs on the generator dynamics and vice versa and include these effects in the controller design.

The small signal stability of the interconnected system is affected by the dynamics of the generators as well as by the dynamics of OLTCs. So it is important to include the interconnection effects due to OLTCs while designing PSS and also the interconnection effects of generators on OLTCs in the design of controllers for OLTC. The effects of the dynamics of OLTC with respect to voltage collapse, stability and power transfer ability are considered in [67, 70, 72]. In the works mentioned in [67, 72], the generators feeding the OLTC are assumed as constant voltage sources

but the secondary voltage of the OLTC is affected by the changes in the primary voltage as well as the load connected to the OLTC. In this work, we include the interconnection effects of OLTCs as additional uncertainty and include in the PSS design and also in OLTC controller design, the interconnection effects of generators are included. For this purpose a simplified power system model is developed which links the dynamics of the generators and OLTCs in the grid system. Even though the model does not cater to full fledged power system controller design, the model will certainly help to understand the extend to which dynamics of OLTCs will affect the controller design.

The controller design methodology is the same as described in Chapter 3. Interconnection effects from OLTCs are also included along with the effects from other generators in the grid. Similarly the interconnection effects from the generators are included in the controller design for the OLTC. Along with this, the effects of parameter variation in the system due to load/generation changes are also considered in the design. These effects are considered as uncertainties in the controller design and are bounded by using IQCs. As discussed in the previous chapters, the operating regime of the generators are divided into smaller zones and have separate controllers for each zone, to make the design less conservative. The controllers are switched as the generator's operating regime changes. The stability of the switched system is preserved through dwell time as described in Chapter 4 and the switching transients are reduced by using bumpless switching scheme as given in Chapter 5.

The proposed controller design method is validated by designing stabilisers for a test case power system. For this purpose a 9 bus system, with 3 generators and one OLTC is selected. The performance of the designed controller is validated through nonlinear simulations. This chapter is organised into three parts. First part gives the power system model, the next part covers the controller design and in the last part simulation and results are presented.

8.2 Power system model

The main assumptions made in obtaining a linear model for interconnected power system are:

1. All loads are modeled as constant admittances [111].
2. The change in reactive power due to small changes in generator angles is negligible [112].

3. Real power (P_m) and reactive power (Q_m) inputs to the generators and the reference voltage (E_u) to the OLTC are the controlled parameters [113].

8.2.1 Network Model

Let us consider a network consisting of n generators and m load buses; generator buses are numbered from $1, \cdots, n$ and load buses are numbered from $n+1, \cdots, n+m$. Loads are modeled as constant admittance and the admittance of the i^{th} node is written as,

$$y_{l_i} = \frac{P_{l_i} - \jmath Q_{l_i}}{|V_i|^2}, \quad i = n+1, \cdots, n+m, \tag{8.1}$$

where P_{l_i} and Q_{l_i} are real and reactive load values respectively. We can reduce the admittance matrix by eliminating the load nodes using the following procedure.
Now each generator is modeled as a current source. Let $I_G = [I_{g_1}, \cdots, I_{g_n}]'$, $E_G = [E_1, \cdots, E_n]'$, and $V_D = [V_{n+1}, \cdots, V_{n+m}]'$ be the vectors of generator currents, generator voltages, and load bus voltages, respectively. With this notation, the node equations for the entire power system are written as [77]:

$$\begin{bmatrix} I_G \\ 0 \end{bmatrix} = \begin{bmatrix} Y_A & Y_B \\ Y_C & Y_D \end{bmatrix} \begin{bmatrix} E_G \\ V_D \end{bmatrix}. \tag{8.2}$$

The above equation (8.2) can be solved to obtain $V_D = -Y_D^{-1} Y_C E_G$, giving $I_G = \left[Y_A - Y_B Y_D^{-1} Y_C\right] V_G$. The matrix $[Y_A - Y_B Y_D^{-1} Y_C]$ is the reduced admittance matrix Y_{RED} of the given network. Let the ij^{th} element of the matrix Y_{RED} be denoted as $Y_{ij} = G_{ij} + \jmath B_{ij}$. Now we have an equivalent network with only generator nodes included. The complex power at i^{th} node is give by $S_i = P_{g_i} + \jmath Q_{g_i} = E_i I_{gi}^*$, $i = 1, 2, \cdots, n$. The expression for the real and reactive power at the i^{th} node are written using the equation (2.12) as,

$$P_{g_i} = |E_i|^2 G_{ii} + \sum_{\substack{j=1 \\ j \neq i}}^{n} |E_i||E_j| \left(B_{ij} \sin \delta_{ij} + G_{ij} \cos \delta_{ij}\right) \tag{8.3}$$

$$Q_{g_i} = -|E_i|^2 B_{ii} + \sum_{\substack{j=1 \\ j \neq i}}^{n} |E_i||E_j| \left(G_{ij} \sin \delta_{ij} - B_{ij} \cos \delta_{ij}\right) \tag{8.4}$$

We can linearise the equations (8.3) and (8.4) about the operating point. Let $\Delta P_g = [\Delta P_{g_1}, \cdots, \Delta P_{g_n}]'$, $\Delta Q_g = [\Delta Q_{g_1}, \cdots, \Delta Q_{g_n}]'$, $\Delta|E| = [\Delta|E_1|, \cdots, \Delta|E_n|]'$

and $\Delta\delta = [\Delta\delta_1, \cdots, \Delta\delta_n]'$ denote the change from the equilibrium point and V_i^0 and δ_{ij}^0 denote the equilibrium values of voltages and voltage angles, then

$$\begin{aligned}\Delta Q_{g_i} = &\sum_{\substack{j=1\\ j\neq i}}^{n} |E_i^0| \left(G_{ij}\sin\delta_{ij}^0 - B_{ij}\cos\delta_{ij}^0\right)\Delta|E_j| - 2|E_i^0|B_{ii}\Delta|E_i| \\ &+ \left[\sum_{\substack{l=1\\ l\neq i}}^{n} |E_l^0| \left(G_{il}\sin\delta_{il}^0 - B_{il}\cos\delta_{il}^0\right)\right]\Delta|E_i| \end{aligned} \tag{8.5}$$

$$\Delta Q_g = N\Delta|E| \tag{8.6}$$

where

$$N_{ij} = \begin{cases} |E_i^0| \left(G_{ij}\sin\delta_{ij}^0 - B_{ij}\cos\delta_{ij}^0\right) & i \neq j \\ \left[\sum_{\substack{l=1\\ l\neq i}}^{n} |E_l^0| \left(G_{il}\sin\delta_{il}^0 - B_{il}\cos\delta_{il}^0\right)\right] - 2|E_i^0|B_{ii} & i = j, \end{cases} \tag{8.7}$$

$$\begin{aligned}\Delta P_{g_i} = &\sum_{\substack{j=1\\ j\neq i}}^{n} |E_i^0| \left(B_{ij}\sin\delta_{ij}^0 + G_{ij}\cos\delta_{ij}^0\right)\Delta|E_j| + 2|E_i^0|G_{ii}\Delta|E_i| \\ &+ \left[\sum_{\substack{l=1\\ l\neq i}}^{n} |E_l^0| \left(B_{il}\sin\delta_{il}^0 + G_{il}\cos\delta_{il}^0\right)\right]\Delta|E_i| \\ &+ \sum_{\substack{j=1\\ j\neq i}}^{n} |E_i^0||E_j^0| \left(-B_{ij}\cos\delta_{ij}^0 + G_{ij}\sin\delta_{ij}^0\right)\Delta\delta_j \\ &+ \left[\sum_{\substack{l=1\\ l\neq i}}^{n} |E_i^0||E_l^0| \left(B_{il}\cos\delta_{il}^0 - G_{il}\sin\delta_{il}^0\right)\right]\Delta\delta_i. \end{aligned} \tag{8.8}$$

We can write,

$$\Delta P_g = R\Delta\delta + S\Delta|E|, \tag{8.9}$$

where

$$R_{ij} = \begin{cases} |E_i^0||E_j^0| \left(-B_{ij}\cos\delta_{ij}^0 + G_{ij}\sin\delta_{ij}^0\right), & i \neq j \\ \left[\sum_{\substack{l=1\\ l\neq i}}^{n} |E_i^0||E_l^0| \left(B_{il}\cos\delta_{il}^0 - G_{il}\sin\delta_{il}^0\right)\right], & i = j \end{cases} \tag{8.10}$$

$$S_{ij} = \begin{cases} |E_i^0| \left(B_{ij} \sin \delta_{ij}^0 + G_{ij} \cos \delta_{ij}^0\right) & i \neq j, \\ \left[\sum_{\substack{l=1 \\ l \neq i}}^{n} |E_l^0| \left(B_{il} \sin \delta_{il}^0 + G_{il} \cos \delta_{il}^0\right)\right] + 2|E_i^0| G_{ii}, & i = j \end{cases} \tag{8.11}$$

8.2.2 Algebraic Constraints on OLTCs

Using the network equations developed in the above Section 8.2.1, we shall relate it with OLTCs. Let us consider a power system consisting of n generators and t OLTCs. For the i^{th} OLTC let the primary voltage $|E_{T_i}|$ and secondary voltage $|E_{S_i}|$ are related as

$$|E_{S_i}| = Tn_i |E_{T_i}| \tag{8.12}$$

where Tn_i is the turns ratio of i^{th} OLTC. Let the reactive power at OLTC node be $Q_T = [Q_{T_1}, \cdots, Q_{T_t}]^T$. The reactive power due to the reactor L_i connected on the secondary side of the OLTC is

$$Q_{T_i} = \frac{|E_{S_i}|^2}{2\pi f L_i} \tag{8.13}$$

where f is the system frequency in Hz.

In this work we consider the effect of tap-change only on reactive part of the load. It is assumed that the real load doesn't change much with the changing tap position. This is a common assumption in the literature [72]. In practice the OLTC tap changes are done in discrete steps, however here we assume the changes in tap position as continuous and smooth.

For small variations in $|E_{S_i}|$ expressions (8.12) and (8.13) are written as:

$$\Delta Q_{T_i} = 2 \frac{Q_{T_i}^0}{|E_{S_i}^0|} \Delta |E_{S_i}| \tag{8.14}$$

$$\Delta |E_{S_i}| = \Delta Tn_i |E_{T_i}^0| + Tn_i^0 \Delta |E_{T_i}|. \tag{8.15}$$

where the superscript '0' is used with the variables to denote their equilibrium or steady-state value.

Reactive power equality constraint is used to obtain an expression for $\Delta|E_T|$ in terms of input reactive power $\Delta|Q_g|$ and ΔTn, where $\Delta Tn = [\Delta Tn_1, \cdots, \Delta Tn_t]'$ and $\Delta|E_T| = [\Delta E_{T_1}, \cdots, \Delta E_{T_t}]'$.

Let $K_{T_i} = 2\frac{Q_{T_i}^0}{|E_{S_i}^0|}$, substituting (8.15) in (8.14) we get

$$\Delta Q_{T_i} = K_{T_i} (\Delta Tn_i |E_{T_i}^0| + Tn_i^0 \Delta |E_{T_i}|) \tag{8.16}$$

Let $[\Delta Q_{g_1}, \cdots, \Delta Q_{g_{n+t}}]^T = [\Delta Q_g \;\; \Delta Q_T]^T$ and using (8.6) we can write

$$\begin{bmatrix} \Delta Q_g \\ \Delta Q_T \end{bmatrix} = \begin{bmatrix} N_{11} & N_{12} \\ N_{21} & N_{22} \end{bmatrix} \begin{bmatrix} \Delta|E_g| \\ \Delta|E_T| \end{bmatrix} \tag{8.17}$$

where subscript g indicates generator and T indicates OLTC. Let $K_T = \text{diag}(K_{T_i})$, $\Lambda_{Tn_i^0} = \text{diag}(Tn_i^0)$, $\Lambda_{|E_{T_i}^0|} = \text{diag}(|E_{T_i}^0|)$, and $\Lambda_{T_i} = \text{diag}(1/T_i)$ then from (8.16) and (8.17) we can write

$$\begin{aligned} K_T(\Lambda_{|E_{T_i}^0|}\Delta Tn + \Lambda_{Tn_i^0}\Delta|E_T|) &= N_{21}N_{11}^{-1}\Delta Q_m - N_{21}N_{11}^{-1}N_{12}\Delta|E_T| + N_{22}\Delta|E_T| \\ \Rightarrow \Delta|E_T| &= \left(K_T\Lambda_{Tn_i^0} + N_{21}N_{11}^{-1}N_{12} - N_{22}\right)^{-1} \\ &\quad \left(N_{21}N_{11}^{-1}\Delta Q_m - K_T\Lambda_{|E_{T_i}^0|}\Delta n\right) \end{aligned} \tag{8.18}$$

Defining

$$M_{21} = \left(K_T\Lambda_{Tn_i^0} + N_{21}N_{11}^{-1}N_{12} - N_{22}\right)^{-1}\left(N_{21}N_{11}^{-1}\right)$$

and

$$M_{22} = -\left(K_T\Lambda_{Tn_i^0} + N_{21}N_{11}^{-1}N_{12} - N_{22}\right)^{-1}\left(K_T\Lambda_{|E_{T_i}^0|}\right)$$

we can write

$$\Delta|E_T| = M_{21}\Delta Q_m + M_{22}\Delta Tn. \tag{8.19}$$

The above equation (8.19) gives the algebraic constraint the system must satisfy at all times. In the next section, we put together the algebraic constraints derived in this section with the dynamic equations for the generators and the OLTCs to arrive at the interconnected system dynamic equations.

8.2.3 The System Dynamic Model

The swing equations which describe the generator dynamics are [111]:

$$m_i\dot{\omega}_i + d_i\omega_i + P_{g_i} = P_{m_i}, \;\; i = 1, \cdots, n \tag{8.20}$$

and the reactive power constraint equations are:

$$Q_{g_i} = Q_{m_i}, \;\; i = 1, \cdots, n \tag{8.21}$$

where δ_i is the angle between the generator rotor and a reference frame rotating at the synchronous frequency; ω_i is the rate of change of angle δ_i; P_{m_i} is the real power input and Q_{m_i} is reactive power input of the i^{th} generator.

The swing equation (8.20) is linearised about the equilibrium point to obtain a linear model for the interconnected system [3, 112].

The dynamic equation for the tap changing of the i^{th} transformer is given as

$$\dot{Tn_i} = \frac{1}{T_i}\left(|E_{u_i}| - |E_{S_i}|\right) \tag{8.22}$$

and its linearised form is

$$\begin{aligned}\Delta\dot{Tn_i} &= \frac{1}{T_i}\left(|E^0_{u_i}| + \Delta|E_{u_i}| - |E^0_{S_i}| - \Delta|E_{S_i}|\right)\\ &= \frac{1}{T_i}\left(\Delta|E_{u_i}| - \Delta|E_{S_i}|\right)\\ &= \frac{1}{T_i}\left(\Delta|E_{u_i}| - \Delta Tn_i|E^0_{T_i}| - Tn^0_i\Delta|E_{T_i}|\right)\end{aligned} \tag{8.23}$$

under steady state conditions $|E^0_{u_i}| = |E^0_{S_i}|$. The above equation (8.23) is collected for all OLTCs and written as

$$\Delta\dot{Tn} = -(\Lambda_{T_i}\Lambda_{|E^0_{T_i}|} + \Lambda_{T_i}\Lambda_{Tn^0_i}M_{22})\Delta Tn - \Lambda_{T_i}\Lambda_{Tn^0_i}M_{21}\Delta Q_m + \Lambda_{T_i}\Delta|E_u| \tag{8.24}$$

The linearised power-flow relationship for generators and OLTCs (assuming that no real power is supplied at any OLTC bus) is written using (8.9) (with $\Delta P_{g_i} = 0, i = n+1, \cdots, n+t$ and $\Delta P_g = [\Delta P_{g_1}, \cdots, \Delta P_{g_n}]$ as [89],

$$\begin{bmatrix}\Delta P_g\\ 0_{t\times 1}\end{bmatrix} = \begin{bmatrix}R_{11} & R_{12}\\ R_{21} & R_{22}\end{bmatrix}\begin{bmatrix}\Delta\delta_g\\ \Delta\delta_T\end{bmatrix} + \begin{bmatrix}S_{11} & S_{12}\\ S_{21} & S_{22}\end{bmatrix}\begin{bmatrix}\Delta|E_g|\\ \Delta|E_T|\end{bmatrix} \tag{8.25}$$

We can eliminate $\Delta\delta_T$ from the above equation (8.25) as,

$$\begin{aligned}\Delta P_g &= \left[R_{11} - R_{12}R^{-1}_{22}R_{21}\right][\Delta\delta_g] + \left[\left(S_{11} - R_{12}R^{-1}_{22}S_{21}\right)\left(S_{12} - R_{12}R^{-1}_{22}S_{22}\right)\right]\begin{bmatrix}\Delta|E_g|\\ \Delta|E_T|\end{bmatrix}\\ &= \left[\tilde{R}\right][\Delta\delta_g] + \begin{bmatrix}\tilde{S}_1 & \tilde{S}_2\end{bmatrix}\begin{bmatrix}\Delta|E_g|\\ \Delta|E_T|\end{bmatrix}\end{aligned} \tag{8.26}$$

where $\tilde{R} = \Big[R_{11} - R_{12}R_{22}^{-1}R_{21} \Big]$, $\tilde{S}_1 = \Big[S_{11} - R_{12}R_{22}^{-1}S_{21} \Big]$, and $\tilde{S}_2 = \Big[S_{12} - R_{12}R_{22}^{-1}S_{22} \Big]$.

The swing equation for each generator is

$$\Delta\delta_i = \delta_i - \delta_i^0, \quad \Delta\dot{\delta}_i = \omega_i, \quad \Delta\ddot{\delta}_i = \dot{\omega}_i$$

$$\dot{\omega}_i = -\frac{d_i}{m_i}\omega_i - \frac{1}{m_i}\left(\Delta P_{g_i}\right) + \frac{1}{m_i}\left(\Delta P_{m_i}\right) \tag{8.27}$$

The swing equations of all the generators are collected and written as a vector equation in terms of states and inputs as follows:

$$\dot{\omega} = -\Lambda_d\Lambda_m\omega - \Lambda_m\tilde{R}\Delta\delta_g - \Lambda_m\begin{bmatrix}\tilde{S}_1 & \tilde{S}_2\end{bmatrix}\begin{bmatrix}\Delta|E_g| \\ \Delta|E_T|\end{bmatrix} + \Lambda_m\Delta P_m \tag{8.28}$$

$\Lambda_m = \text{diag}\{\frac{1}{m_1}, \cdots, \frac{1}{m_n}\}$ and $\Lambda_d = \text{diag}\{d_1, \cdots, d_n\}$. Using (8.17) and (8.21) we can write,

$$\Delta|E_g| = N_{11}^{-1}\Delta Q_m - N_{11}^{-1}N_{12}\Delta|E_T|$$

and further using the expression for $\Delta|E_T|$ in (8.19) we can write (8.28) as

$$\begin{aligned}\dot{\omega} = &-\Lambda_d\Lambda_m\omega - \Lambda_m\tilde{R}\Delta\delta_g - \Lambda_m\left(\tilde{S}_2 - \tilde{S}_1N_{11}^{-1}N_{12}\right)M_{22}\Delta Tn \\ &-\Lambda_m\left(\tilde{S}_1N_{11}^{-1} - \tilde{S}_1N_{11}^{-1}N_{12}M_{21} + \tilde{S}_2M_{21}\right)\Delta Q_m + \Lambda_m\Delta P_m\end{aligned} \tag{8.29}$$

We can write the linearised dynamic equations for the entire system in a matrix form as,

$$\begin{bmatrix}\Delta\dot{\delta}_g \\ \dot{\omega} \\ \Delta\dot{T}n\end{bmatrix} = \bar{A}\begin{bmatrix}\Delta\delta_g \\ \omega \\ \Delta Tn\end{bmatrix} + \bar{B}_1\Delta P_m + \bar{B}_2\Delta Q_m + \bar{B}_3\Delta|E_u| \tag{8.30}$$

where,

$$\bar{A} = \begin{bmatrix} 0_{n\times n} & I_{n\times n} & 0_{n\times t} \\ -\Lambda_m\tilde{R} & -\Lambda_d\Lambda_m & -\Lambda_m\left(\tilde{S}_2 - \tilde{S}_1 N_{11}^{-1} N_{12}\right) M_{22} \\ 0_{t\times n} & 0_{t\times n} & -(\Lambda_{T_i}\Lambda_{|E^0_{T_i}|} + \Lambda_{T_i}\Lambda_{Tn_i^0} M_{22}) \end{bmatrix}$$

$$\bar{B}_2 = \begin{bmatrix} 0_{n\times n} \\ -\Lambda_m\left(\tilde{S}_1 N_{11}^{-1} - \tilde{S}_1 N_{11}^{-1} N_{12} M_{21} + \tilde{S}_2 M_{21}\right) \\ -\Lambda_{T_i}\Lambda_{Tn_i^0} M_{21} \end{bmatrix}$$

$$\bar{B}_1 = \begin{bmatrix} 0_{n\times n} \\ \Lambda_m \\ 0_{t\times n} \end{bmatrix}, \bar{B}_3 = \begin{bmatrix} 0_{n\times t} \\ 0_{n\times t} \\ \Lambda_{T_i} \end{bmatrix}$$

Equation (8.30) gives the linearised power system model to be used in the controller design.

8.3 Controller Design

For the purpose of controller design, we can consider each generator and OLTC connected to the grid as a subsystem and formulate the control problem for a system affected by parameter variations and by the interconnection effects from other machines connected in the grid. Here we consider parameterising, the system consisting of the generators and OLTCs with respect to the power output of the generators. Corresponding to each such parameterised operating points we have a SEP. Now we consider designing a controller corresponding to a particular SEP. Repeating the design procedure we can obtain controllers for all SEPs considered. These controllers are selected and switched as the generators operating point changes.

Now we design controllers which guarantee robust performance in the presence of interconnection and parameter variation effects for a SEP. We use the controller design methodology described in Chapter 3 for the design. We setup the control problem for the power system including OLTC's. We briefly present the steps involved in the controller design. Effects due to parameter variation around the operating point and interconnection effects are treated as uncertainties on the sub system. Integral Quadratic Constraints (IQCs) are used to describe the uncertainties and Linear Matrix Inequality (LMI) optimisation technique is used to solve the optimisation problem.

We consider a large scale system $\mathbb{S}$ comprising of N subsystems $\mathbb{S}_i$, including both generators and OLTCs. The variable power output of the generators are described $\rho(\cdot)$. Then the subsystem $\mathbb{S}_i$ is described as:

$$\begin{aligned}
\mathbb{S}_i : \dot{x}_i(t) &= A_i(\gamma)x_i(t) + B_i u_i(t) + E_i\xi_i(t) + \beta_i\phi_i(t) + L_i r_i(t),\\
z_i(t) &= C_i x_i(t) + D_i u_i(t),\\
\zeta_i(t) &= H_i x_i(t) + G_i u_i(t),\\
\hat{\zeta}_i(t) &= \alpha_i I x_i(t),\\
y_i &= C_{y,i}x_i(t) + D_{y,i}\xi_i(t),
\end{aligned} \tag{8.31}$$

where $A_i(\gamma)$ is the system matrix corresponding to the SEP with power output $\rho(\cdot) = \gamma$, x_i is state vector, u_i the control inputs, $\xi_i \in \mathbf{R}^{p_i}$ is the perturbation, $\zeta_i \in \mathbf{R}^{h_i}$ is the uncertainty output (made up of both the system states, and the control inputs), $\hat{\zeta}_i$ is the uncertainty output due to parameter variation around operating point, $z_i \in \mathbf{R}^{q_i}$ is the controlled output of the subsystem which consists of both the subsystem states and control inputs, and y_i is output of the system which is feedback to the controller. The input r_i describes the effect of the subsystems S_j, $j \neq i$, on the subsystem S_i. The input ξ_i describes the effect of local uncertain modeling errors in this subsystem.

The variations in $A_i(\cdot)$ due to load and generation changes are treated as an additional disturbance and the system is regarded as a perturbation of a linear fixed parameter system. The variations in the matrix $A_i(\cdot)$ is regarded as modeling uncertainty and driven by $\phi_i(t)$, [91], where

$$\phi_i(t) := \frac{1}{\beta_i}\left[A_i(\gamma + \Delta\gamma) - A_i(\gamma)\right] x_i(t) \tag{8.32}$$

The designed controller will stabilize the nominal plant corresponding to the SEP with the specified parameter variations around the SEP provided, the constraint (8.32) is satisfied. The size of neighborhood is determined by the choice of α_i and β_i where positive real numbers α_i, β_i and $\gamma \in \Gamma$ be so chosen that

$$\sup_{\rho\in\Omega_\gamma} \|A_i(\rho) - A_i(\gamma)\| < \alpha_i\beta_i \tag{8.33}$$

where $\|\cdot\|$ in (3.40) denotes the largest singular value.

The system matrices and signals for subsystems representing generator and OLTC are obtained from (8.30), as follows,

for generators:

$$
\begin{aligned}
A_i &= \begin{bmatrix} \bar{A}(i,i) & \bar{A}(i,n+i) \\ \bar{A}(n+i,i) & \bar{A}(n+i,n+i) \end{bmatrix} \\
B_i &= \begin{bmatrix} \bar{B}_1(i,i) & \bar{B}_2(i,i) \\ \bar{B}_1(n+i,i) & \bar{B}_2(n+i,i) \end{bmatrix} \\
L_i &= \begin{bmatrix} \bar{A}(i,j) & \bar{A}(i,n+j) & \bar{A}(i,2n+k) & \bar{B}_1(i,j) & \bar{B}2(i,j) \\ \bar{A}(n+i,n+j) & \bar{A}(n+i,n+j) & \bar{A}(n+i,2n+k) & \bar{B}_1(n+i,j) & \bar{B}_2(n+i,j) \end{bmatrix}
\end{aligned}
\tag{8.34}
$$

where the elements for example $\bar{A}(i,i)$ refers to $(i,j)^{th}$ element of the matrix $\bar{A}$ and the signals are defined as,

$$x_i(t) = [\Delta\delta_i, \omega_i]^T, u_i(t) = [\Delta P_{mi}, \Delta Q_{mi}]^T,$$

$$r_i(t) = [\Delta\delta_j, \omega_j, \Delta n_k, \Delta P_{mj}, \Delta Q_{mj}, \Delta|E_{uj}|]^T$$

where $j = 1, \cdots, n$, and $j \neq i$; $k = 1, \cdots, t$ and $k \neq i$.

For OLTC

$$
\begin{aligned}
A_i &= \begin{bmatrix} \bar{A}(2n+i, 2n+i) \end{bmatrix} \\
B_i &= \begin{bmatrix} \bar{B}_3(2n+i, i) \end{bmatrix} \\
L_i &= \begin{bmatrix} 0_{1\times n} & \bar{A}(2n+i,k) & \bar{B}_1(2n+i,j) & \bar{B}2(2n+i,j) \end{bmatrix}
\end{aligned}
\tag{8.35}
$$

and the signals are defined as,

$$x_i(t) = [\Delta n_i], u_i(t) = [\Delta|E_{uj}|],$$

$$r_i(t) = [\Delta\delta_j, \omega_j, \Delta n_k, \Delta P_{mj}, \Delta Q_{mj}, \Delta|E_{uj}|]^T$$

where $j = 1, \cdots, n$, and $j \neq i$; $k = 1, \cdots, t$ and $k \neq i$.

To meet the requirements of the controller design methodology proposed in

Chapter 3, the subsystem $\mathbb{S}_i$ described by (8.31) should satisfy the following assumptions [73]:

Assumption 7 *For each $i = 1, \cdots, N$, given locally square integrable signals $[u_i(\cdot), r_i(\cdot), \xi_i(\cdot), \phi_i(\cdot)]$ for any initial condition $x_i(0) = x_{i0}$, the solution to the subsystem (8.31) exists on any finite time interval [0,T] of the interval [0, $+\infty$) and is locally square integrable i.e, $\int_0^T \|x_i(\cdot)\|^2 dt | x_{i0} < \infty$*

Assumption 8 *For all $i = 1, \cdots, N \quad D_i' D_i + G_i' G_i > 0, \quad D_{yi} D_{yi}' > 0.$*

Assumption 9 *The pair $(A_i, C_i' C_i)$, $i = 1, \cdots, N$, is observable.*

Assumption 10 *The pair (A_i, B_i), $i = 1, \cdots, N$, is stabilisable.*

Assumption 11 *For all $i = 1, \cdots, N$, $C_i' D_i = 0$, $H_i' G_i = 0$, $E_i D_{yi}' = 0$.*

Assumption 12 *For all $i = 1, \cdots, N$, $[E_i \; L_i] \neq 0$.*

8.3.1 Uncertainty Description

With subsystem (8.31) meeting the Assumptions 7 to 12, we shall define the admissible uncertainties considered in the controller design. From (8.31), the uncertainties are driven by signals $\xi_i(t)$, $r_i(t)$ and $\phi_i(t)$ and their corresponding outputs are $\zeta_i(t)$, $\zeta_\mu(t)_{\mu \neq i}$ and $\hat{\zeta}_i(t)$. Even though we do not know the magnitude of these signals, we can impose bounds on these signals using IQCs. Let M_{1i}, M_{2i}, M_{3i}, $i = 1, \cdots, N$ be three collections of positive definite symmetric matrices. The following definitions [73] describe the three kinds of feasible uncertainty sets considered in this work.

Definition 10 *A collection of uncertainty inputs $\xi_i(\cdot), i = 1, \cdots, N$, represents an admissible uncertainty for the large scale system $\mathbb{S}$ if the following conditions hold: Given locally square integrable control inputs $u_i(\cdot)$, locally square integrable parameter variation inputs $\phi_i(\cdot)$,and locally square integrable interconnection inputs $r_i(\cdot), i = 1, \cdots, N$ there exists a sequence$\{t_l\}_{l=1}^{+\infty}, t_l \to +\infty$, such that*

$$\int_0^{t_l} \left(\|\zeta_i(t)\|^2 - \xi_i(t)\|^2 \right) dt \geq -x_{i0}' M_{1i} x_{i0}, M_{1i} = M_{1i}' > 0, \quad \forall i = i = 1, \cdots, N \tag{8.36}$$

The set of all such admissible uncertainties is denoted by Ξ.

Definition 11 *A collection of uncertainty inputs $\phi_i(\cdot), i = 1, \cdots, N$ represents an admissible parameter variation for the large scale system $\mathbb{S}$ if the following conditions hold: Given any locally square integrable control inputs $u_i(\cdot)$, locally square integrable local uncertainty inputs $\xi_i(\cdot)$, and locally square integrable interconnection inputs $r_i(\cdot), i = 1, \cdots, N$ there exists a sequence$\{t_l\}_{l=1}^{+\infty}, t_l \to +\infty$, such that*

$$\int_0^{t_l} \left(\|\hat{\zeta}_i(t)\|^2 - \|\phi_i(t)\|^2 \right) dt \geq -x'_{i0} M_{2i} x_{i0}, M_{2i} = M'_{2i} > 0, \quad \forall i = i = 1, \cdots, N \tag{8.37}$$

The set of all such admissible parameter variation uncertainties is denoted by Ψ.

Definition 12 *The subsystem $\mathbb{S}_i$ of the large scale system $\mathbb{S}$ is said to have admissible interconnections to other subsystems of this large-scale system, if the following hold: Given any locally square integrable control inputs $u_i(\cdot)$, locally square integrable local uncertainty inputs $\xi_i(\cdot)$ and locally square integrable parameter variation inputs $\phi_i(\cdot), i = 1, \cdots, N$ there exists a sequence$\{t_l\}_{l=1}^{+\infty}, t_l \to +\infty$, such that*

$$\int_0^{t_l} \left(\sum_{\mu \neq i} \|\zeta_\mu(t)\|^2 - \|r_i(t)\|^2 \right) dt \geq -x'_{i0} M_{3i} x_{i0}, M_{3i} = M'_{3i} > 0, \quad \forall i = 1, \ldots, N; \tag{8.38}$$

The corresponding uncertain interconnection input $r_i(\cdot)$ is referred to as an admissible uncertain interconnection input. The set admissible interconnection inputs is denoted by Π.

Now we consider a problem of decentralized absolute stabilization via output feedback control. The controllers considered are decentralized linear output feedback controllers of the form

$$\begin{aligned} \dot{x}_{c,i}(t) &= A_{c,i}(\gamma) x_{c,i}(t) + B_{c,i}(\gamma) y_i(t); \\ u_i(t) &= K_{c,i}(\gamma) x_{c,i}(t), \end{aligned} \tag{8.39}$$

where $x_{c,i} \in \mathbf{R}^{n_{c,i}}$ is the i^{th} controller state vector.

Having the uncertainties, controller structure and load variation parameter defined, we can find the decentralised controllers using similar procedure outlined in

Chapter 3 as follows:
Let $\tau_i > 0, \eta_i > 0, \theta_i > 0, i = 1, \cdots, N$, be given constants, and $\bar{\theta}_i = \sum_{j=1, j\neq i}^{N} \theta_j$. We consider a collection of the generalized algebraic Riccati equations (GAREs):

$$A_i' X_i + X_i A_i + \hat{C}_i' \hat{C}_i - X_i \left(B_i R_i^{-1} B_i' - \hat{B}_{2,i} \hat{B}_{2,i}' \right) X_i = 0, \tag{8.40}$$

$$A_i' Y_i + Y_i A_i + Y_i \hat{B}_{2,i} \hat{B}_{2,i}' Y_i - \left(C_{y,i}' W_i^{-1} C_{y,i} - \hat{C}_i' \hat{C}_i \right) = 0, \tag{8.41}$$

where $R_i = \hat{D}_i' \hat{D}_i, \quad W_i = \hat{D}_{y,i} \hat{D}_{y,i}'$ and

$$\begin{aligned}
\hat{C}_i &= \begin{bmatrix} C_i \\ (\tau_i + \bar{\theta}_i)^{\frac{1}{2}} H_i \\ \eta^{\frac{1}{2}} \alpha I \end{bmatrix}, \\
\hat{D}_i &= \begin{bmatrix} D_i \\ (\tau_i + \bar{\theta}_i)^{\frac{1}{2}} G_i \\ 0 \end{bmatrix}, \\
\hat{B}_{2,i} &= \begin{bmatrix} \tau_i^{-\frac{1}{2}} E_i & \theta_i^{-\frac{1}{2}} L_i & \eta^{-\frac{1}{2}} \beta I \end{bmatrix}, \\
\hat{D}_{y,i} &= \begin{bmatrix} \tau_i^{-\frac{1}{2}} D_{y,i} & 0 & 0 \end{bmatrix}.
\end{aligned} \tag{8.42}$$

Then associated with (8.40) and (8.41) is a collection of decentralized dynamic output feedback controllers of the form

$$\begin{aligned}
\dot{x}_{c,i} &= \left[A_i - \left(B_i R_i^{-1} B_i' - \hat{B}_{2,i} \hat{B}_{2,i}' \right) X_i \right] x_{c,i}(t) + (Y_i - X_i)^{-1} C_{y,i}' W_i^{-1} \left(y_i(t) - C_{y,i} x_{c,i}(t) \right), \\
u_i &= \left(-R_i^{-1} B_i' X_i \right) x_{c,i}(t).
\end{aligned} \tag{8.43}$$

Furthermore, consider a set of vectors, $\mathcal{T} = \{\{\tau_i, \eta_i, \theta_i\}_{i=1}^{N} \in \mathbf{R}^{3N}, \tau_i > 0, \eta_i > 0, \theta_i > 0$: the set of GAREs (8.40) admits a set of solutions $X_i \geq 0$ and the set of GAREs (8.41) admits a set of solutions $Y_i \geq 0$ such that $Y_i > X_i$ $\}$.

Note that the minimal positive definite solutions X_i to the equations (8.40) as well as solutions Y_i to the GAREs (8.41) depending upon the chosen $\{\tau_i, \eta_i, \theta_i\}_{i=1}^{N} \in \mathcal{T}$.

The stabilisation conditions and proofs are established in Chapter 3. Now, as given in Chapter 3, Theorem 4 presents necessary and sufficient condition for the uncertain interconnected system $\mathbb{S}$ to be robustly stabilisable by means of the controller (8.39). Theorem 5 characterises guaranteed robust performance achievable by means of such controller. The optimisation problem on the right hand side of (3.53) is solved by using a rank constrained LMI optimisation technique given in Chapter 3.

Controller design procedure is summarised as follows:

(i) Depending upon the operating range of the generators connected to the grid, SEPs are selected for each generator with respective to its power output. Using the load flow results corresponding to each SEP, system equations (8.30) for respective SEPs are obtained.

(ii) Generator/OLTC at each node of the grid is considered as subsystem and corresponding system matrices are arrived for the SEPs using (8.34) and (8.35) from (8.30).

(iii) Parameter variation around the operating point $A(\gamma + \Delta\gamma)$ is worked out in accordance to (8.33).

(iv) LMI optimisation problem is formulated as given in Chapter 3 and the solutions for the GAREs (8.40) and (8.41), X_i and Y_i are obtained.

(v) Substituting the solutions X_i and Y_i in (8.43) the required decentralised controller of the corresponding subsystem is obtained.

Using the procedure explained above controllers are designed for each generator covering all SEPs. Now we shall consider the switching between these controllers as the power output of the generator changes.

8.4 Switching system and stability

Controllers designed as given in Section 8.3 are capable of providing robust stabilisation over a range of power output variations. When the power output of the generator exceeds the stabilisation range of a particular controller, the next suitable controller needs to be selected and switched in. Even though the controllers and plant are closed loop stable, we ensure the stability of the switched system. We have already established switching stability through dwell time in Chapter 4. We use this dwell time approach to preserve switching stability.

Let us consider the switching between two systems P_1 and P_2 which are defined as:

$$P_1 : \dot{x} = A_1 x, \tag{8.44}$$

$$P_2 : \dot{x} = A_2 x - A_2 \Psi, \tag{8.45}$$

where $x \in R^n$ is the state-vector and $\Psi \in R^n$ is a constant vector; the equilibrium point for P_1 is 0 and that of P_2 is Ψ; matrices A_1 and A_2 are stable matrices and further there exist Lyapunov functions $V_1(x)$ and $V_2(x-\Psi)$ for P_1 and P_2 respectively.

We shall consider the switching sequence $P_1 \rightarrow P_2 \rightarrow P_1$, the dwell time required to have stable switching, the dwell time τ_d^{12} required is given by (4.27),

$$\tau_d^{12} > \frac{1}{2\lambda_2} \log \left[\frac{a_1 a_2 \left(K_\Psi^{12} - 1\right)}{2\left(2b_1 b_2 K_\Psi^{12} + a_1 b_2\right)} \right] \tag{8.46}$$

The variables of equation (8.46) are detailed in Chapter 4. Similarly we can consider the switching sequence $P_2 \rightarrow P_1 \rightarrow P_2$. The required dwell time is given by (4.29)

$$\tau_d^{21} > \frac{1}{2\lambda_1} \log \left[\frac{a_1 a_2 \left(K_\Psi^{21} - 1\right)}{2\left(2b_1 b_2 K_\Psi^{21} + a_2 b_1\right)} \right] \tag{8.47}$$

We employ the dwell time constraint on the allowable switching signals for the stability of switched system.

8.5 Switching Transients

Switching transients will occur when we switch between two controllers. Especially we consider here the switching between dynamic controllers and the plant corresponding to two different SEPs. We can minimise the switching transients by using the bumpless switching scheme. This scheme is explained in detail in Chapter 5. The basic configuration of the scheme is given in Figure 8.1.

The bumpless compensator F drives the output u_2 of the offline controller to be equal to output of the online controller u_1, at the time of switching. By this, the switching transients are minimised. The expression to synthesise the bumpless

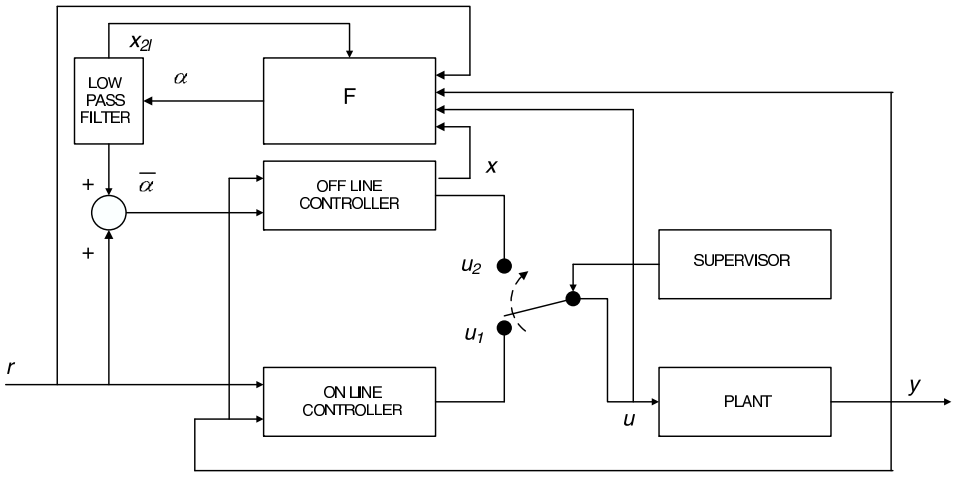

Figure 8.1. Bumpless controller configuration

compensator is given by,

$$\mathbf{F} = -W_e^{-1}\tilde{B}_2' \begin{Bmatrix} \Pi \\ -\left[\left(\tilde{A} - \tilde{R}\Pi\right)^{-T}\left(\Pi\tilde{B}_1 + \tilde{C}'W_u\tilde{D}_1\right)\right]' \\ \left[\left(\tilde{A} - \tilde{R}\Pi\right)^{-T}\tilde{C}'W_u\right]' \end{Bmatrix} \tag{8.48}$$

The variables in (8.48) are explained in Chapter 5.

8.6 Simulations

8.6.1 Test Case Power System

To demonstrate the design, a nine bus power grid system consisting of 3 generator buses, 3 load buses, 2 Static Var Systems (SVSs) and one OLTC is considered here. One-line diagram of the test system is shown in Figure 8.2. The OLTC node has a purely inductive load connected to it. Each machine is considered as a subsystem interconnected by two weak tie-lines to the other two machines.

Generators 1 to 3 have a capacity of 300 MW each and buses 5, 7 and 9 are load buses. Buses 7 and 9 have shunt capacitors and an OLTC is included at bus 4.

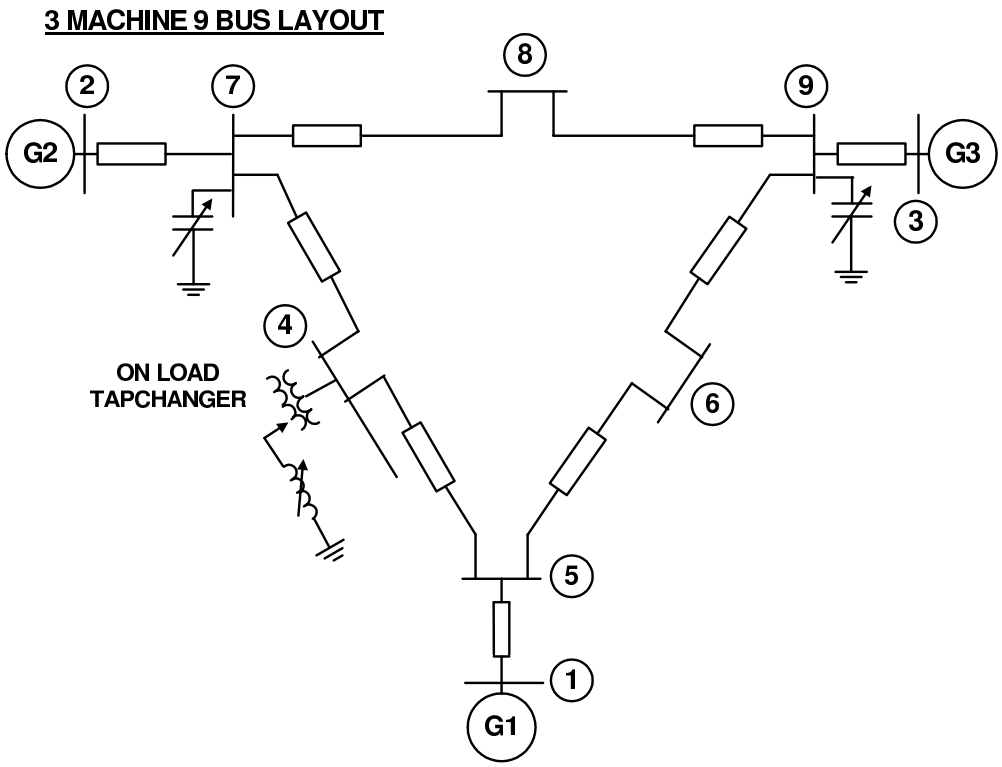

Figure 8.2. One-Line Diagram on Nine-Bus Three-Generator System

From Bus No.	To Bus No.	Impedance in pu
1	5	$\jmath$ 0.0576
2	7	$\jmath$ 0.0625
3	9	$\jmath$ 0.0586
4	5	$(0.5+ \jmath\ 4.3) \times 10^{-3}$
5	6	$(0.9+ \jmath\ 4.6) \times 10^{-3}$
4	7	$(1.6+ \jmath\ 8) \times 10^{-3}$
7	8	$(0.4+ \jmath\ 3.6) \times 10^{-3}$
8	9	$(0.6+ \jmath\ 5) \times 10^{-3}$
6	9	$(0.2+ \jmath\ 8.5) \times 10^{-3}$

Table 8.1. Line parameters

For the analysis of the system 100 MVA is chosen as base and generator G_1 bus is considered as reference slack bus.

The numerical value of system parameters are given in Table 8.1 and the generator parameters in Table 8.2 on a 100 MVA base.

Generators G_1 and G_3 are base generators and supply a power output of 300 MW each. Single controller is designed for G_1 and G_3 corresponding to the operating

Parameter	Generator G_1	Generator G_2	Generator G_3
Inertia Constant	8.1 s^2/rad	10.39 s^2/rad	8.59 s^2/rad
Synchronous Impedance x_d	0.146 pu	0.155 pu	0.130 pu
Damping	1	1	1

Table 8.2. Generator parameters

Bus Number	Bus type	Power (MW / MVAR)	Voltage (pu)	Angle (deg)
1	Generator	300.19 $-\jmath$ 149.47	1.0300	0.0000
2	Generator	150.00 $-\jmath$ 58.49	1.0300	-21.9210
3	Generator	300.00 $-\jmath$ 166.24	1.0300	1.7841
4	Load	0.00 $-\jmath$ 25.00	0.9641	-41.6770
5	Load	-300.00 $-\jmath$ 80.00	0.9552	-41.6030
6	Load	0.00 $-\jmath$ 0.00	0.9462	-41.4900
7	Load	-150.00 $-\jmath$ 25.00	0.9600	-41.6480
8	Load	0.00 $-\jmath$ 0.00	0.9472	-41.5710
9	Load	-300.00 $-\jmath$ 25.00	0.9295	-41.4510

Table 8.3. Load flow results corresponding to SEP with G_1 and G_3 at 300 MW and G_2 at 150 MW.

point of 300 MW. Generator G_2 takes up the variation in system load and its power output is varied from 0 to 300 MW. The operating region of G_2 is divided into 10 equal zones of 30 MW each and each zone consists of a SEP. A separate controller is designed for the system around the SEP in each zone and is capable of providing robust stabilisation for $\pm$ 30 MW generation change about the SEP.

8.6.2 Power system model and controller design

Load flow and network reduction

We have divided the operating regime of generator G_2 into 10 zones, therefore we get the network model corresponding to these 10 SEPs. As the first step we do the load flow computations corresponding to these SEPs. The load flow results corresponding to G_1 and G_3 at 300 MW and G_2 at 150 MW are given in Table 8.3. Using the load flow results, the network is reduced by eliminating the bus nodes other than generator and OLTC buses with the procedure given in Section 8.2.

Controller design

With the complex voltages and reduced network admittance data, we can get the state equation matrices described by (8.30) for the SEP. Using the similar procedure we can find the state equations corresponding to all the SEPs. We include the

SEP for Generator G_2	$\|A_i(\rho) - A_i(\gamma)\|$	$\alpha_i = \beta_i$
30 MW	0.0048	0.0693
60 MW	0.0057	0.0752
90 MW	0.0019	0.0438
120 MW	0.0091	0.0955
150 MW	0.0165	0.1284
180 MW	0.0246	0.1567
210 MW	0.0341	0.1845
240 MW	0.0464	0.2154
270 MW	0.0657	0.2563
300 MW	0.0389	0.1972

Table 8.4. Parameter variation norm and selected α_i, β_i values for controller design for different SEPs of Generator G_2.

System	A_c	B_c	K_c
Generator G_1	$\begin{bmatrix} -1.4833 & -0.52413 \\ -194.9 & -191.96 \end{bmatrix}$	$\begin{bmatrix} 1.5246 \\ 1.2889 \end{bmatrix}$	$\begin{bmatrix} -819.21 & -807.43 \\ 782.14 & 770.9 \end{bmatrix}$
Generator G_2	$\begin{bmatrix} -1.3531 & -0.39841 \\ -232.6 & -228.38 \end{bmatrix}$	$\begin{bmatrix} 1.3988 \\ 0.9723 \end{bmatrix}$	$\begin{bmatrix} -1385.4 & -1361.2 \\ 1187.8 & 1167.1 \end{bmatrix}$
Generator G_3	$\begin{bmatrix} -1.5912 & -0.63205 \\ -183.98 & -181.26 \end{bmatrix}$	$\begin{bmatrix} 1.6325 \\ 1.2321 \end{bmatrix}$	$\begin{bmatrix} -818.79 & -806.89 \\ 783.37 & 771.98 \end{bmatrix}$
$OLTC_1$	$\begin{bmatrix} -1.1128e+05 \end{bmatrix}$	$\begin{bmatrix} 172.11 \end{bmatrix}$	$\begin{bmatrix} -11111 \end{bmatrix}$

Table 8.5. Controller matrices for the SEP corresponding to G_1 and G_3 at 300 MW and G_2 at 150 MW conditions.

parametric variations corresponding to ± 30 MW generation change about the SEP in the controller design. For this, the system matrices corresponding to SEP - 30 MW and SEP + 30 MW are be obtained as per the procedures explained above. From these system matrices we can work out the norm of parametric variations $\|A_i(\rho) - A_i(\gamma)\|$ defined in (8.33) for each SEPs and these values are given in Table 8.4. Using these norm values, α_i and β_i values are so selected that it meets the requirements given in equation (8.33) and included in the controller design. With these values the designed controller will be robust for ± 30 MW generation change about the SEP. The interconnection uncertainty matrix L_i for generators and OLTCs are obtained from the system matrices using (8.34) and (8.35). With the system matrices and uncertainties defined we use the methodology briefed in Section 8.3 to synthesise the controller. The controller values for the SEP corresponding to G_1 and G_3 at 300 MW and G_2 at 150 MW conditions are given in Table 8.5.

The dwell time required for stable controller switching can obtained from (8.46) and (8.47). For $K_\psi = 1.5$, the corresponding values of dwell time are found to be less than 2 s. For the power system selected the dwell time is found to be not critical. The bumpless compensator required to reduce the switching transients is obtained by using (8.48).

8.6.3 Simulation

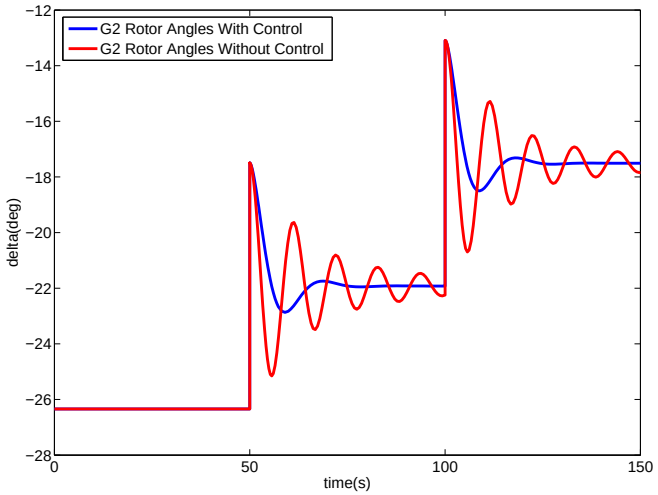

Figure 8.3. Generator G_2 rotor angles δ with and without control.

To validate the designed controllers, different simulation cases are considered. Simulations are done using the nonlinear model of the power system described in Section 8.2. It is assumed that prime mover power P_m, changes instantaneously and the prime mover dynamics are neglected in the simulations.

To start with the simulations, the system response with controller is compared with the open loop response. For this, power output of Generator G_2 is varied from 120 MW to 180 MW in steps of 30 MW. The rotor angle responses are compared in Figure 8.3. The simulation results show that the system under consideration is lightly damped and the effectiveness of the damping provided by the controller. To further evaluate the performance of the controller following cases of simulations are carried out.

Case 1: Parameter Variation within a zone The controller is evaluated for

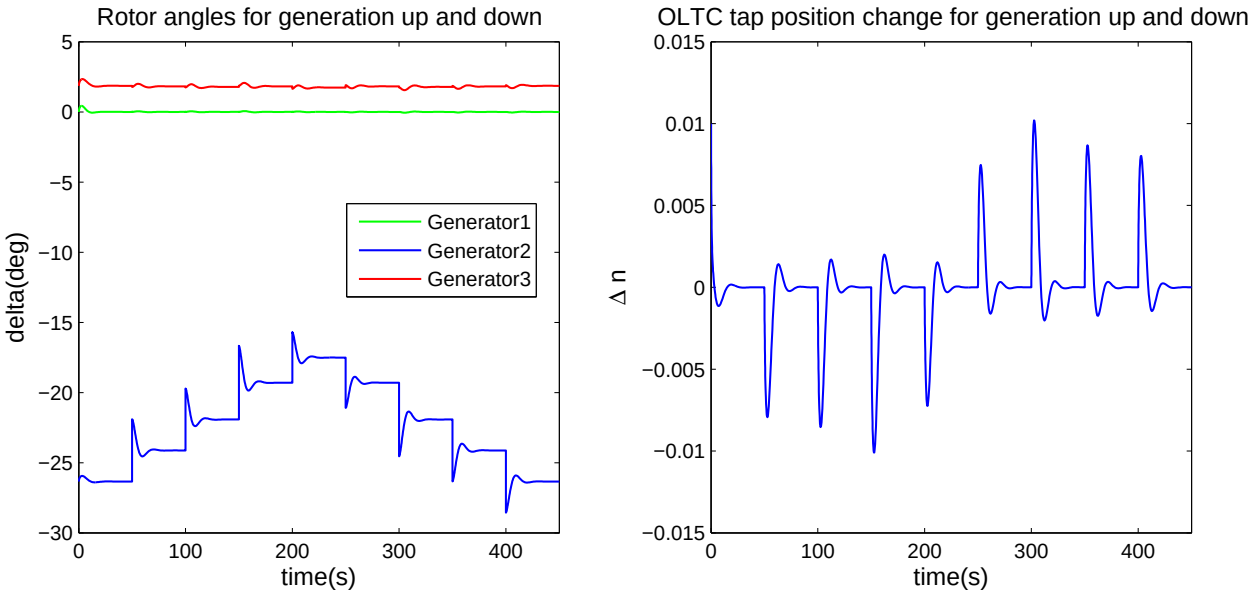

Figure 8.4. Case 1: Simulation responses of generator G_1 to G_3 and OLTC for load variation within a zone.

its robustness against parameter variation within a zone. For simulation, the zone 150 ± 30 MW is selected and corresponding controller is included for G_2. The G_2 controller remains same through out simulation. The load on G_2 is varied from 120 MW to 180 MW in steps of 15 MW and brought back to 120 MW by the same steps with 50 sec interval at each step. Generator rotor angles and OLTC tap responses Δn are given in Figure 8.4 respectively.

Case 2: Continuous generation increase In this case of simulation, the controllers are tested for a power variation to cover the entire operating regime of Generator G_2. The power output of G_2 is varied from 0 MW to 300 MW in steps of 30 MW. At each power change, controllers corresponding to the respective SEP are switched in. Rotor angle responses of the generators and change in OLTC tap position Δn are given in Figure 8.5.

Case 3: Continuous generation decrease Similar to Case 1 above but the output of G_2 is reduced from 300 MW to 0 MW. Rotor angle responses of the generators and change in OLTC tap position Δn are given in Figure 8.5.

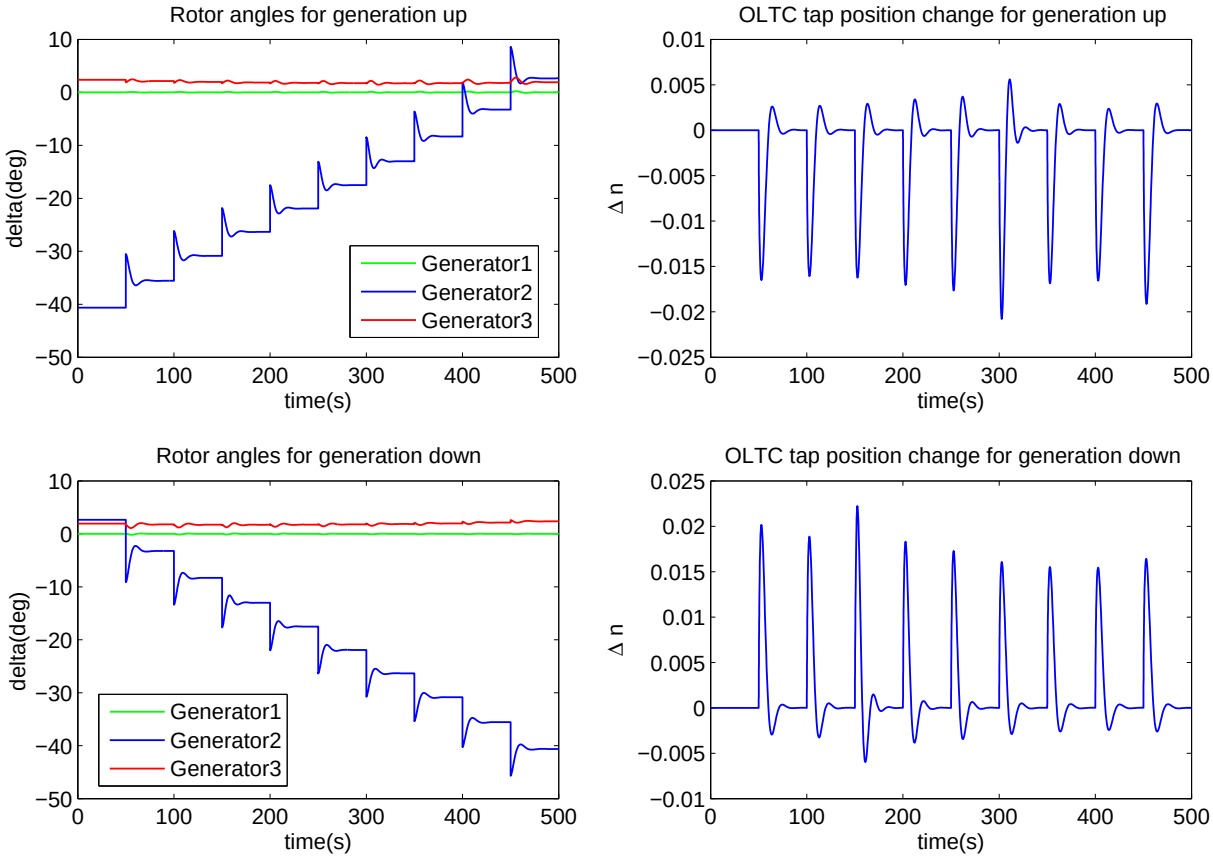

Figure 8.5. Case 2 & Case 3: Simulation responses of generator G_1 to G_3 and OLTC for load up and down cases.

Case 4: Simulation with PSS To compare the performance of the controller with conventional PSS, simulations similar to Case 2 and Case 3 are done with IEE 2ST PSS. For this simulation, nonlinear power system model described in [88] used and the dynamics of OLTCs are neglected. For the entire power variation the same PSS is used. Rotor angle responses of the Generator are given in Figure 8.6.

8.6.4 Inferences

From the rotor angle responses in the Figure 8.3, it can be seen that the damping of the open loop system is relatively low and the proposed controller improves the damping of the system considerably. In Case 2 simulations for parameter variations within the zone, from rotor angle responses in Figure 8.4, the responses of the generator with the proposed controller are satisfactory and the disturbances created

in the response of G_1 and G_3 are minimal. Also the OLTC response Δn is also found to be satisfactory. The rotor angle responses for the Cases 3 and 4 in Figure 8.5 show that proposed controller produces a satisfactory responses for continuous generation increase and decrease. When the responses of the proposed controller are compared with the response produced by conventional PSS in Figure 8.6, it can be seen that the proposed controller dampens the oscillations more quickly and produces uniform response for different operating conditions. Also the disturbance created in other machines due to power change in generator G_2 is minimal in the case of proposed controller against the conventional PSS.

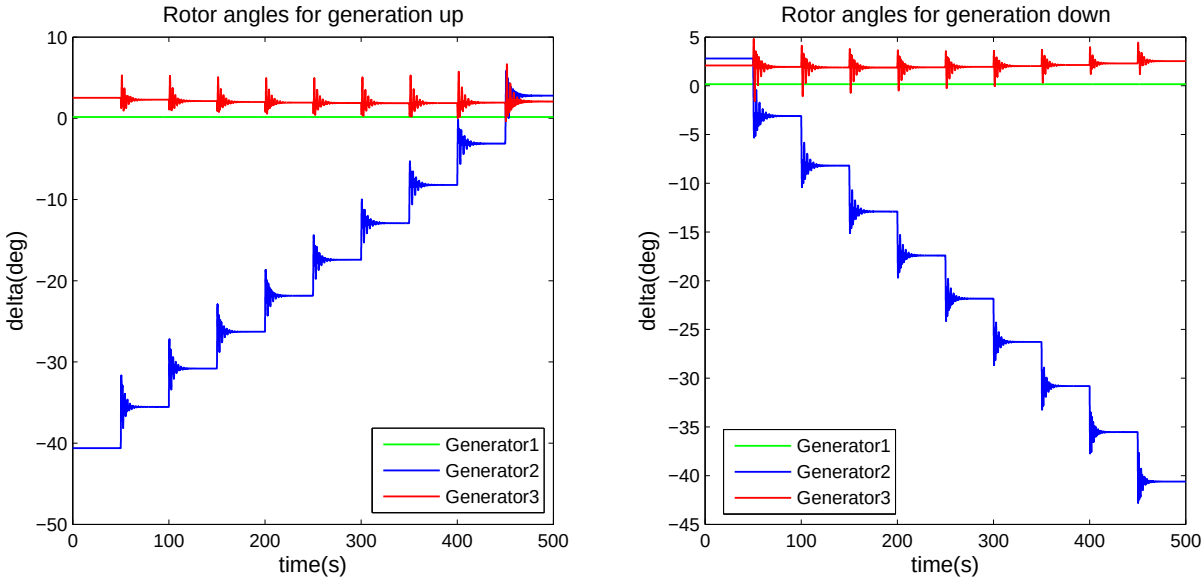

Figure 8.6. Case 4: Simulation responses of generator G_1 to G_3 for generation up and down with conventional PSS.

8.7 Chapter summary

The chapter demonstrates a methodology to include the dynamics of OLTC along with the dynamics of generators in the grid while designing PSS. Using IQCs, the interconnection effects from other machines in the grid and parameter variation around the operating point are included in the controller design, making the stabiliser robust in the presence of these effects. To validate the controller design methodology, 3 machine 9 bus power system is considered as a numerical example and nonlinear simulations are carried out with wide generation-load variations. To

demonstrate the damping provided by the controller, the performance is compared with and without control in Figure 8.3. In simulation Case 1, robustness of the controller is validated for parameter variations within the zone. In simulation Cases 2 and 3, the performance is evaluated for continuous generation up and down conditions. The results of simulation are included in Figures 8.4 and 8.5. These results show the effectiveness of the scheme under different generation conditions and the improvement of the overall damping of the system. Again, through Case 4, the performance of the controller is compared with conventional PSS and the results are given in Figure 8.6. The results show that the proposed controller is capable of providing an effective and uniform response over the entire operating regime when compared with conventional PSS.

Chapter 9

Conclusion

The work presented in this thesis demonstrates that switched controllers are feasible for interconnected power systems. As against single PSS, several power system controllers are designed around different linearised SEPs to cover the entire operating regime of the power system and appropriately switching the controllers as the operating point changes. Simulation results show that this approach provides uniform controller performance and better damping over the complete operating range when compared with single PSS. Use of switched controllers helps to reduce the conservatism and improve the uncertainty handling capacity of the controller design.

Use of multiple IQCs to represent the interconnection effects from other generators and parameter variation effects due to load and generation changes helps to include these effects as uncertainties in the controller design. By this approach, the possible uncertainties in the power system control are addressed which will help to increase the confidence in the control design. Minimax-LQG technique is used for the controller design and this method provides controller solution which guarantee robust performance in the presence of the uncertainties considered.

When we switch between two controllers, switching stability and switching transients are matters of concern. Switching stability of the system is preserved through the dwell time method by constraining the minimum time required between two consecutive switchings. An expression to compute the required dwell time between consecutive switchings is developed including the effect of jumps in the states while switching between two different operating conditions. Switching transients are minimised by using bumpless switching scheme. Through this the states of the new controller to be switched in are initialised in a way to minimise the transients.

The performance of the proposed controllers are validated through nonlinear computer simulations and by using RTDS facility at CPRI, Bangalore, India. A test case power system is selected and controllers are designed for the system. Different cases of simulations are carried out including load and generation changes, fault conditions and generator AVR reference voltage changes. The performance of the

proposed controllers is also compared with conventional PSS simulated under similar conditions. The simulation results show that the proposed controllers are capable of providing better damping with less settling time during normal and abnormal power system operating conditions.

Another contribution of the thesis is the incorporation of dynamics of OLTCs in the power system controller design. OLTCs are important dynamical elements of a power system and play an important role in the voltage stability and reactive power flow of the system. Generally the OLTC dynamics is not considered in the PSS design. In this research, a simple power system model has been developed and the OLTC dynamics are included. Using this model, the effects of OLTCs on the synchronous machines along with parameter variations and interconnection effects are included in the generator controller design. Also, the effect of generators on OLTCs is included in the OLTC controller design. Simulations are carried out to validate the proposed control method using a test case power system under different conditions. Using this method the effect of OLTCs in the power system control can be studied.

9.1 Directions for future research

The proposed power system design method can be improved and consolidated further through the following suggestions:

i) Proposed controllers are validated using computer simulations for a selected test case system. It will give more confidence in the proposed method, if the controllers can be implemented in the real power system.

ii) The synthesis of controllers for large power systems involving many generators are found to be infeasible as the LMI optimisation method proposed does not yield solutions for the large systems. A better numerical solution method can be developed to facilitate controller design for large systems.

iii) Loads connected to the power system are treated as constant loads. Improvement in the model can be achieved by including dynamic loads into the model.

iv) In the power system simulation, loads are varied from one value to another instantaneously, which may not reflect the actual load dynamics happening in the power system. This can be improved upon by computing the power flow solutions corresponding to the gradual load variations to include in the simulation loop.

v) The simplified power system model to study the effects of OLTCs proposed in Chapter 8 does not cater for full fledged power system controller design. The model can be perfected by including the OLTC dynamics in the multimachine power system model described in Chapter 2. Also the tap variation is assumed to be continuous and smooth in the model included in the thesis, in practice the tap changes at discrete positions. This need to be included in the model.

Appendix A

Power System Parameters

A.1 Test Case System

The two area, four machine, 11 bus power grid system shown in Figure A.1 is considered as a test case system for simulation studies. The system consists of two power system areas Area 1 and Area 2 connected through a twin circuit tie line of 220 km in length. The transmission system nominal voltage is 400 kV. Generation voltages are stepped up by the transformers connected to the generators. Load centers are located at buses 7 and 9. The buses 7 and 9 have shunt capacitors.

Generators 1 to 4 and transformers 1 to 4 are identical and their parameters are given in Table A.1 and A.3. The generator AVR parameter are given in Table A.2. Transmission line parameters are given in 400 kV, 100 MVA base in Table A.4. For the analysis of the system, 400 kV and 100 MVA are chosen as base quantities.

A.2 Conventional power system stabiliser

To compare the performance of the proposed controllers with conventional PSS, IEE 2ST PSS is used [114]. The block diagram of the PSS is given in Figure A.2 and the parameters of the PSS are given in Table A.5.

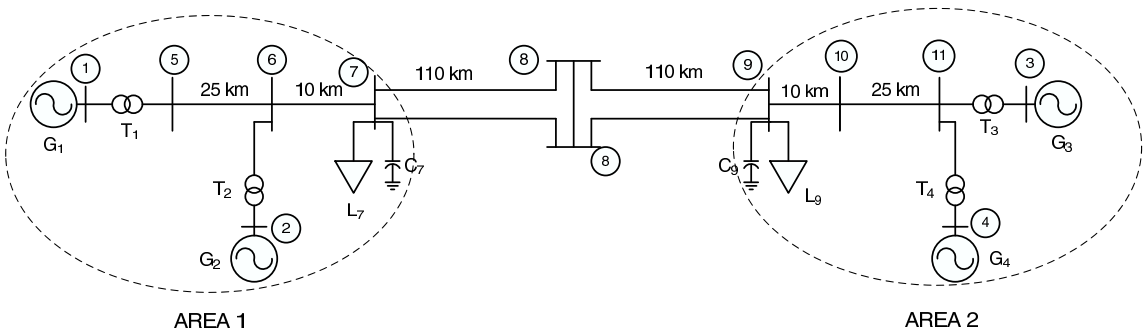

Figure A.1. Two area four machine system.

Parameter	Value
Rated Voltage line to line rms	21.0 kV
Rated Capacity	588 MVA
Base angular frequency	50 Hz
Inertia Constant(H)	3.07
Direct axis reactance (x_d)	2.31 pu
Quadrature axis reactance (x_q)	2.19 pu
Transient reactance direct axis (x'_d)	0.27 pu
Transient reactance quadrature axis (x'_q)	0.70 pu
Transient open circuit time constant (τ'_d)	9.0 s
Transient q-axis open circuit time constant (τ'_q)	2.5 s
Transducer time constant (T_r)	0.015 s

Table A.1. Generator Parameters

Parameter	Value
Amplifier gain Ka	200
Time constant Tc	1.0 s
Time constant Tb	20.0 s
Time constant Ta	0.02 s
Gain constant Kc	0.175
Regulator voltage upper limit	5.7 pu
Regulator voltage lower limit	-4.9 pu

Table A.2. AVR Parameters

Parameter	Value
Rated primary line to line rms voltage	21.0 kV
Rated secondary line to line rms voltage	400.0 kV
Rating	600 MVA
Positive sequence reactance	0.15 pu

Table A.3. Transformer Parameters

voltage	Resistance (r)	Reactance (x_L)	Susceptance (b_C)
400 kV	1.862 e-05	2.075 e-04	5.55 e-03

Table A.4. Line Parameters per km per circuit on 100 MVA base

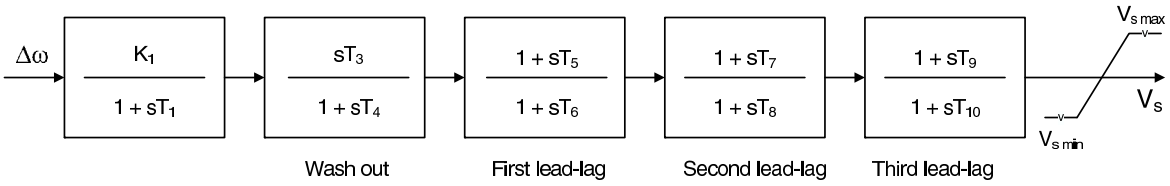

Figure A.2. IEE 2ST conventional PSS

Parameter	Value
Gain K_1	10
Time constant T_1	0.0 s
Wash out time constant T_3	10.0 s
Wash out time constant T_4	10.0 s
First lead-lag time constant T_5	0.55 s
First lead-lag time constant T_6	0.2 s
Second lead-lag time constant T_7	0.55 s
Second lead-lag time constant T_8	0.2 s
Third lead-lag time constant T_9	0.55 s
Third lead-lag time constant T_{10}	0.2 s
PSS voltage upper limit	0.1 pu
PSS voltage lower limit	-0.1 pu

Table A.5. Conventional PSS Parameters

References

[1] Prabha Kundur et al. Definition and classification of power system stability. *IEEE Transactions on Power Systems*, 19(2):1387–1401, May 2004.

[2] P. Kundur. *Power system stability and control*. McGraw-Hill, Inc., New York, 1994.

[3] K. A. Loparo and G. L. Blankenship. A probabilistic mechanism for small disturbance instabilities in electric power systems. *IEEE Transactions on Circuit and Systems*, CAS-32(2):177–184, February 1985.

[4] G. J. Rogers. Control for stability in interconnected power systems. *IEEE Control Systems Magazine*, 9(1):19–22, Jan. 1989.

[5] P. Kundur, D. C. Lee, and H. M. Zein ElDin. Power system stabilisers for thermal units; Analytical techniques and onsite validation. *IEEE Transaction PAS*, 100:81–95.

[6] S. Cheng and L. Guan. An on-line self-learning power system stabilizer using a neural network method. *IEEE Transaction on Power System*, 12(2):926–931, 1997.

[7] H. Jiang, J.F. Dorsey, Z. Qu, J. Bond, and J.M. McCalley. Global robust adaptive control of power systems. *IEE Proc.-Gener. Transm. Distrib.*, 141(5):429–436, 1994.

[8] S. Lee. Optimal decentralised design for output-feedback power system stabilisers. *IEE Proc.-Generation, Transmission and Distribution*, 152(4):449–459, July 2005.

[9] A.M.D. Ferreira, J. A. L. Barreiros, W. Barra Jr., and J. R. Brito de Souza. A robust adaptive LQG/LTR TCSC controller applied to damp power system oscillations. *Electric Power Systems Research*, 77:956 – 964, 2007.

[10] G. Guo, Y. Wang, and D. J. Hill. Nonlinear output stabilization control for multimachine power systems. *IEEE Transactions on Circuits and Systems, Part 1*, 47(1):46–53, January 2000.

[11] K. El-Metwally and O. P. Malik. Application of of fuzzy logic stabilizers in a multi-machine power system environment. *IEE Proc. Generation, Transmission and Distribution*, 143(3):263–268, 1996.

[12] A. El-Shafei and K. El-Metwally. Power system stabilization via adaptive fuzzy logic control. In *Proceedings of the 12th IEEE international symposium on intelligent control*, pages 89–94, Istanbul, Turkey, 1997.

[13] M. Hassan, O. P. Malik, and G. Hope. A fuzzy logic based stabilizer for a synchronous machine. *IEEE Transaction on Energy Conservation*, 6(3):407–413, 1992.

[14] A. L. Elshafei. Modern trends in power system control. In *Proceedings of the 1998 IEEE International Conference on Control Applications*, pages 1383–1387, Trieste, Italy, September 1998.

[15] Y. Hsu and L. Jeng. Damping of sub-synchronous oscillations using adaptive controllers tuned by artificial neural networks. *IEE Proc.Generation, Transmission and Distribution*, 142(4):415–422, 1995.

[16] D. Kennedy and V. Quintana. Neural network regulator for synchronous machines. In *Proceedings of IFAC world congress*, volume 5, pages 131–136, 1993.

[17] G. Chen and O. P. Malik. Tracking constrained adaptive power system stabiliser. *IEE Proceedings on Generation, Transmission and Distribution*, 142(2):149–156, 1995.

[18] G. Chen, O. P. Malik, and G. Hancock. Implementation and experimental studies of an adaptive self optimizing power system stabilizer. *IFAC J. of Engineering Control Practice*, 2(6):969 – 977, 1994.

[19] Y. A. Magid, Y. L. Abido, M. A. S. Al-Baiyat, and A. H. Mantawy. Simultaneous stabilization of multi-machine power systems via genetic algorithms. *IEEE Trans. Power Syst.*, 14:1428–1439, 1999.

[20] Y. A. Magid and Y. L. Abido. Optimal multi-objective design of robust power system stabilizers using genetic algorithms. *IEEE Trans. Power Syst.*, 18:1125–1132, 2003.

[21] J. Ackermann. *Robust control*. Springer-Verlag, 1993.

[22] I. R. Petersen, V. Ugrinovskii, and A. V. Savkin. *Robust Control Design using H^∞ Methods*. Springer-Verlag, London, 2000.

[23] Q. Zhao and J. Jiang. Robust controller design for generator excitation systems. *IEEE Transactions on Energy Conversion*, 10(2):210–209, June 1995.

[24] C. A. Desoer and M. Vidyasagar. *Feedback Systems: Input-Output Properties*. Academic Press, New York, 1975.

[25] J. F. Hauer. Robust damping control for large power systems. *IEEE Control*

Systems Magazine, 9(1):12–18, 1989.

[26] Q. Lu and Y. Sun. Nonlinear stabilizing control of multimachine systems. *IEEE Transactions on Power Systems*, 4:236–241, 1989.

[27] J. H. Chow et.al. Robust control design of power system stabilisers using multivariable frequency domain techniques. *Int. Journal of Robust and Nonlinear Control*, 2:123–138, 1992.

[28] D. J. Hill and I. A. Hiskens. Robust, adaptive or nonlinear control for modern power systems. In *Proc. of the 32nd IEEE Conference on decision & control.*, December 1993.

[29] Y. Wang, D. J. Hill, and G. Guo. Nonlinear decentralised control for multimachine power system transient stability enhancement. In *Proc. Int. Sym. on Electric Power Engineering*, pages 435–440, Stockholm, Sweden, 1995.

[30] S. Jain, F. Khorrami, and B. Fardanesh. Decentralized stabilization and control of large-scale power systems with unknown interconnections. *International Journal of control*, 63(3):591–608, February 1996.

[31] Y. Wang, D. J. Hill, and G.Guo. Robust decentralized control for multimachine power systems. *IEEE Transactions on Circuits and Systems-I, Fundamental theory and applications*, 45(3):271–279, March 1998.

[32] N. Sebe. Decentraliased h_∞ controller design. In *Proc. of the 37th IEEE Conference on decision & control.*, pages 2810–2815, December 1998.

[33] G. E. Boukarim, S.Wang, J. H. Chow, G. N. Taranto, and Nelson Martins. A comparison of classical, robust, and decentralized control designs for multiple power system stabilizers. *IEEE Transactions on Power Systems*, 15(4):1287–1292, Nov. 2000.

[34] F. E. Scavoni, A. S. eSilva, A. Trofino, and J. M Campagnalo. Design of robust power system controllers using linear matrix inequalities. In *IEEE Porto Power Tech Conference, 10 -13 September, Porto, Portugal*, 2001.

[35] C. Zhu, R. Zhou, and Y. Wang. A new decentralized nonlinear voltage controller for multimachine power systems. *ICCA '03. Proceedings. 4th International Conference on Control and Automation*, pages 525–530, 2003.

[36] W. Qiu, V. Vittal, and M. Khammash. Decentralized power system stabilizer design using linear parameter varying approach. *IEEE Transaction on Power Systems*, 19(4):1951–1960, November 2004.

[37] D. Bandekas, G. Tsirigotis, P. Antoniadis, and N. Vordos. A robust controller

design for a multimachine power system. *Journal of electrical and electronics engineering; ISSN 1392 - 1215*, 65(1):20–24, 2006.

[38] T. Nan, M. Xiangyang, L. Lin, and W. Xuguang. Robust controller design on uncertain system. In *Proc. of IEEE International Conference on Systems, Man and Cybernetics*, volume 3, pages 1888 – 1891, 2001.

[39] G. E Boukarim, S.Wang, and J. H. Chow. A comparison of classical, robust and decentralised control designs for multiple power system stabilisers. *IEEE Transactions on Power Systems*, 15(4), November 2000.

[40] J. S. Shamma. Gain-scheduled missile autopilot design using linear parameter varying transformations. *Journal of Guidance, Control, and Dynamics*, 16(2), March-April 1993.

[41] J. S. Shamma and M. Athans. Analysis of gain scheduled control for nonlinear plants. *IEEE Transactions on Automatic Control*, 35(8):898–907, August 1990.

[42] W. J. Rugh and J. S. Shamma. Survey paper research on gain scheduling. *Automatica*, 36:1401–1425, 2000.

[43] G. Scorletti and L. Ghaoui. Improved lmi conditions for gain scheduling and related control problems. *Int. J. Robust Nonlinear Control*, 8:845–877, 1998.

[44] C. S. Mehendale and K. M. Grigoriadis. A new approach to LPV gain-scheduling design and implementation. In *Proc. of the 43rd IEEE Conference on Decision and Control*, pages 2942–2947, December 2004.

[45] S. Cui etal. Design of power system stabilizer based on robust gain scheduling control theory. In *Proceedings. Power Con. 2000, Power System Technology*, volume 3, pages 1191 – 1196, 2000.

[46] H. Ukai et al. Stabilising control of multi-machine power systems using gain scheduling control and parameter identification. In *Proc. of Transmission and Distribution Conference and Exhibition 2002*, volume 3, pages 1568 – 1572, 2002.

[47] J. D. Bendtsen, J. Stoustrup, and K. Trangbeak. Multi-dimensional gain scheduling with application to power plant control. In *Proc. of the 42nd IEEE Conference on Decision and Control*, pages 6553–6558, December 2003.

[48] M. C. Turner, N. Aouf, D. G. Bates, I. Postlethwaite, and B. Boulet. Switched control of a vertical/short take-off land aircraft: an application of linear quadratic bumpless transfer. *J. Systems and Control Engineering*, 220(Part

I):157–170, 2006.

[49] A. S. Morse. Supervisory control of families of linear set-point controllers-Part 1: exact matching. *IEEE Trans.Automat.Control*, 41(10):1413–1431, 1996.

[50] E. Skafidas, R.J. Evans, and I.M. Mareels. Optimal controller switching for stochastic systems. In *Proceedings of the 36th Conference on Decision & Control*, pages 200–204, December 1997.

[51] J. H. Frommer, S. R. Kulkarni, and P. J. Ramadge. Controller switching based on output prediction errors. *IEEE Transactions on Automatic Control*, 43(5):3950–3955, May 1998.

[52] M. Zefran and J. W. Burdick. Design of switching controllers for systems with changing dynamics. In *Proc. of 37th IEEE Conference on Decision and Control*, volume 12, pages 2113 – 2118, 1998.

[53] J. P. Hespanha and A. S. Morse. Stability of switched systems with average dwell-time. In *Proceedings of the 38th IEEE Conference on Decision and Control*, pages 2655–2660, December 1999.

[54] G. Zhai, B. Hu, K. Yasuda, and A. N. Michel. Stability analysis of switched systems with stable and unstable subsystems: An average dwell time approach. In *Proceedings of the American Control Conference*, pages 200–204, June 2000.

[55] M. Prandini and M.C. Campi. Logic-based switching for the stabilization of stochastic systems in presence of unmodeled dynamics. In *Proceedings of the 40th Conference on Decision & Control*, pages 393–398, December 2001.

[56] D. Liberzon. *Switching in systems and control*. Birkhauser publications - Systems and Control: Foundations and applications, 2003.

[57] R. Suy, S. Abdelwahedz, and S. Neemaz. A reachability based stability analysis for switching systems. Technical Report ISIS-04-506, Institute for Software Integrated Systems Vanderbilt University, Nashville, Tennessee, 37235, September 2004.

[58] J. Zhao and G. M. Dimirovski. Quadratic stability of a class of switched nonlinear systems. *IEEE Transactions on Automatic Control*, 49(4):574–578, 2004.

[59] S. Mitra and D. Liberzon. Stability of hybrid automata with average dwell time: An invariant approach. In *Poc. of the 43rd IEEE Conference on Decision and Control*, pages 1394–1399, December 2004.

[60] R. Wang, G. M. Dimirovski, and J. Zhao. Output feedback control for uncertain linear systems with faulty actuators: An average dwell-time method. In *Proceedings of the American Control Conference*, pages 5487–5492, 2006.

[61] D. Chatterjee and D. Liberzon. Stability analysis and stabilization of randomly switched systems. In *Proceedings of the 45th IEEE Conference on Decision & Control*, pages 2643–2648, December 2006.

[62] S. Kim, S. A. Campbell, , and X. Liu. Stability of a class of linear switching systems with time delay. *IEEE Transactions on Circuits and Systems*, 53(2):384–393, February 2006.

[63] Mathew C. Turner and Daniel J. Walker. Linear quadratic bumpless transfer. *Journal of Automatica*, 36:1089–1101, 2000.

[64] J. Paxman. *Switching Controllers: Realization, Initialization and Stability.* PhD thesis, Churchill College Control Group Department of Engineering University of Cambridge, October 2003.

[65] L. Zaccarian and A. R. Teel. Brief paper: The L_2 bumpless transfer problem for linear plants: Its definition and solution. *Automatica*, 41:1273–1280, 2005.

[66] J. J. Yame and M. Kinnaert. Research article on bumps and reduction of switching transients in multicontroller systems. Technical Report Volume 2007, Article ID 54212, Mathematical Problems in Engineering, Hindawi Publishing Corporation, 2007.

[67] T. X. Zhu, S. K. Tso, and K. L. Lo. An investigation into the OLTC effects on voltage collapse. *IEEE Transactions on Power Systems*, 15(2):515–521, 2000.

[68] L. Bao, X. Duan, and Y. He. Analysis of voltage collapse mechanisms in state space. *IEE Proceedings on Generation, Transmission, Distribution*, 147(6):395–400, 2000.

[69] C. C. Liu and K. T. Vu. Analysis of tap-changer dynamics and construction of voltage stability regions. *IEEE Transactions on Circuits and Systems*, 36(4):575–590, 1989.

[70] M. Hong, C. Liu, and M. Gibescu. Complete controllability of N-Bus dynamic power system model. *IEEE Transactions on Circuits and Systems-I, Fundamental theory and applications*, 46(6), June 1999.

[71] T. X. Zhu and S. K. Tso. An investigation into OLTC effects on voltage collapse. *IEEE Transactions on Power Systems*, 15(2), May 2000.

[72] Chen-Ching Liu and Khoi T. Vu. Analysis of tap-changer dynamics and construction of voltage stability regions. *IEEE Transactions on Circuits and Systems*, 36(4):575–590, April 1989.

[73] L. Li, V.Ugrinovski, and R. Osri. Decentralised robust control of uncertain Markov jump parameter systems via output feedback. *Automatica*, 43(11):1932–1944, 2007.

[74] Mathew C. Turner and Daniel J. Walker. Linear quadratic bumpless transfer. In *Journal of Automatica*, volume 36, pages 1089–1101, 2000.

[75] CGIRE Task Force 38.01.07 on Power system oscillations. Analysis and control of. *CIGRE Technical Brochure*, (111), Dec. 1996.

[76] IEEE Working group on system oscillations. Power system oscillations. *IEEE Special publication*, (95-TP-101), 1995.

[77] M.A Pai. *Power system stability, Analysis by the direct method of Lyapunov.* North-Holland Publishing Company, 1981.

[78] P.M. Anderson and A.A. Fouad. *Power system control and stability.* IEEE Press, Piscataway, 1994.

[79] I. Horowitz. *Synthesis of feedback systems.* Academic, New York, 1963.

[80] R. M. Canon and E. Schmitz. Initial experiments on the endpoint control of flexible one-link robot. *International Journal of Robotics*, 3(3):62–67, 1984.

[81] B. D. O. Anderson and J. B. Moore. *Optimal control: Linear quadratic methods.* Englewood Cliffs, NJ: Prentice-Hall, 1990.

[82] I. R. Petersen and H. R. Pota. Minimax LQG optimal control of a flexible beam. *Control Engineering Practice*, 11:1273–1287, 2003.

[83] I. R. Petersen. Minimax LQG control. *International Journal of Applied Mathematics and Computer Science*, 16(3):309–323, 2006.

[84] M. Green and D. J. N Limebeer. *Linear Robust Control.* Prentice-Hall, Englewood Cliffs, NJ, 1995.

[85] D. G. Luenberger. *Optimization by vector space methods.* Wiely, NewYork, 1969.

[86] G. A. Leonov A. H. Gelig and V. A. Yakubovich. *Stability of nonlinear systems with nonunique equilibrium.* Nauka, Mascow, 1978.

[87] H. Kwakernaak and R. Sivan. *Linear Optimal Control Systems.* Wiely, 1972.

[88] G. X. Athanasius, H.R. Pota, P. V. Bala Subramanyam, and V. Ugrinovskii.

Robust power system stabiliser design using minimax control approach: Validation using real-time digital simulation. In *46th IEEE Conference on Decision and Control*, pages 2427–2432, 12-14 Dec 2007.

[89] V. Ugrinovskii and H. R. Pota. Decentralized control of power systems via robust control of uncertain Markov jump parameter systems. *International Journal of Control*, 78(9):662–677, June 2005. ISSN 0020-7179.

[90] R. A. Ramos, L. Li, V. Ugrinovskii, and H. R. Pota. Design of switching damping controllers for power systems based on a Markov jump parameter system approach. In *45th IEEE Conference on Decision and Control*, pages 4014–4019, 13-15 December 2006.

[91] M. G Yoon, V.Ugrinovskii, and M. Pszczel. Gain-scheduling of minimax optimal state feedback controllers for uncertain LPV systems. *IEEE Transactions on Automatic Control*, 52(2):311–317, Feb 2007.

[92] T.Basar and P.Bernhard. H^∞ - *optimal control and related minimax design problems: A dynamic game approach*. Birkhauser, Bostan, 2nd edition, 1995.

[93] K. Zhou, J. Doyle, and K. Glover. *Robust and optimal Control*. Prentice-Hall, Upper Saddle River, NJ, 1996.

[94] G. Zhai, K. Yasuda, and M. Ikeda. Decentralized quadratic stabilization of large-scale systems. In *IEEE Proc. 33rd Conf. Decision and Contr.*, pages 2337–2339, Lake Buena Vista, FL, December 1994.

[95] S. Boyd, L. E. Ghaoui, E. Feron, and V. Balakrishnan. *Linear Matrix Inequalities in System and Control Theory*. Society for Industrial and Applied Mathematics, Philadelphia, 1994.

[96] W. Sun, P. P. Khargonekar, and D. Shim. Solution to the positive real control problem for linear time-invariant systems. *IEEE Transactions on Automatic Control*, 39(10):2034–2046, 1994.

[97] Li-Li and V.Ugrinovski. On necessary and sufficient conditions for H^∞ output feedback control of Markov jump linear systems. In *Proc. IEEE CDC, San Diego, CA*, 2006.

[98] D. Liberzon and A. S. Morse. Basic problems in stability and design of switched systems. *IEEE Control Systems Magazine*, 19(5):59 – 70, 1999.

[99] R. DeCarlo, M. Branicky, S. Pettersson, and B. Lennartson. Perspectives and results on the stability and stabilizability of hybrid systems. *Proceedings of IEEE*, 88(7):1069–1082, July 2000.

[100] N. H. McCLamroch and I. Kolmanovsky. Performance benefits of hybrid control design for linear and nonlinear systems. *Proceedings of IEEE*, 8(7):1083–1096, July 2000.

[101] H. Ye, A. Michel, and L. Hou. Stability theory for hybrid dynamical systems. *IEEE Transactions on Automatic Control*, 43(4):461–474, 1998.

[102] M. Athans and P. L. Falb. *Optimal control, an introduction to the theory and its applications*. McGraw-Hill, New York, 1996.

[103] L. Ling, C. Yun-ping S.Nai-qiu, P. Chun-ming, and L. Min. Study on grid-based seamless-link hybrid simulation system for power networks. In *Proceedings IEEE International Conference on Power System Technology*, pages 1–4, 2006.

[104] M. J. Jin, W. Hu, F. Liu, S. W. Mei, and Q. Lu. Nonlinear co-ordinated control of excitation and governor for hydraulic power plants. *IEE Proc.-Gener. Transm. Distrib*, 152(4):544–548, July 2005.

[105] Y. Guo, D. J. Hill, and Y. Wang. Robust decentralized excitation control of multimachine power systems. In *Proceedings of the American Control Conference*, June 1999.

[106] Real time digital simulation documentation, Issued by CPRI, Bangalore, India. *CPRI Documentation*, 2006.

[107] Z. Gajic, D. Karlsson, and M. Kockott. Advanced OLTC control to counteract power system voltage instability. *ABB Power Technologies, Substation Automation, SE-721 59 VSTERS, SWEDEN*, 2006.

[108] P. Kundur, K. Morison, and B. Gao. Practical considerations in voltage stability assessment. *Electrical Power & Energy Systems*, 15(4):205 – 215, 1993.

[109] C. Taylor. *Power System Voltage Stability*. McGraw-Hill, 1994.

[110] T. V. Cutsem. Voltage instability: Phenomena, countermeasures, and analysis methods. *Proceedings of the IEEE*, 88(2):208–227, 2000.

[111] M. A. Pai. *Energy Function Analysis for Power System Stability*. Kluwer Academic Publishers, Boston, 1989.

[112] Felix F. Wu and Chen-Ching Liu. Characterization of power system small disturbance stability with models incorporating voltage variation. *IEEE Transactions on Circuit and Systems*, CAS-33(4):406–417, April 1986.

[113] H. R. Pota, G. X. Athanasius, L. Li, and V.Ugrinovski. Control design for interconnected power systems with OLTCs via robust decentralized robust

control. In *American Control Conference, June 14-16*, 2006.

[114] RTDS User's manual, RTDS Technologies, Canada, issued by CPRI, Bangalore, India.